HYDROLOGICAL MODELLING OF HILLY WATERSHED FOR PLANNING AND MANAGEMENT THROUGH GEOGRAPHIC INFORMATION SYSTEM IN NAGALAND

THESIS SUBMITTED IN PARTIAL FULFILLMENT OF THE REQUIREMENTS FOR THE DEGREE OF DOCTOR OF PHILOSOPHY

By

IMYANGLULA

PhD/ AET/00441

DEPARTMENT OF AGRICULTURAL ENGINEERING & TECHNOLOGY

SCHOOL OF ENGINEERING & TECHNOLOGY, NAGALAND UNIVERSITY, KOHIMA CAMPUS, MERIEMA-797004

MAY, 2026

HYDROLOGICAL MODELLING OF HILLY WATERSHED FOR PLANNING AND MANAGEMENT THROUGH GEOGRAPHIC INFORMATION SYSTEM IN NAGALAND

By

IMYANGLULA and

Dr. CHITRASEN LAIRENJAM

Submitted

In partial fulfillment of the requirements for the Degree of Doctor of Philosophy

In

Agricultural Engineering and Technology

of

Nagaland University

DECLARATION

Nagaland University

May, 2026

I, Imyanglula, hereby declare that the subject matter in this Thesis is the record of work done by me, that the contents of this Thesis did not form the basis of the award of any previous degree to me or to the best of my knowledge to anybody else, and that the Thesis has not been submitted by me for any research degree in any other University/Institute.

This is being submitted to Nagaland University for the degree of Doctor of Philosophy in Agricultural Engineering and Technology.

(IMYANGLULA)

(Prabhakar Sharma)	(Chitrasen Lairenjam)
Head	Supervisor

NAGALAND UNIVERSITY

Kohima Campus

School of Engineering and Technology

Meriema – 797004, Nagaland

Dr. Chitrasen Lairenjam

Associate Professor

Department of Agricultural Engineering

School of Agricultural Sciences

CERTIFICATE – 1

This is to certify that the thesis entitled **"Hydrological Modelling of Hilly Watershed for Planning and Management Through Geographic Information System in Nagaland"** submitted to Nagaland University in partial fulfilment of the requirements for the award of the degree of Doctor of Philosophy in Agricultural Engineering and Technology is the record of research work carried out by Ms. Imyanglula, Registration No. PhD/AET/00441 under my personal supervision and guidance.

The result of the investigation reported in the thesis has not been submitted for any other degree or diploma. The assistance of all kinds received by the student has been duly acknowledged.

Date: (CHITRASEN LAIRENJAM)

Place: Meriema Supervisor

NAGALAND UNIVERSITY

Kohima Campus
School of Engineering and Technology
Meriema – 797004, Nagaland

CERTIFICATE – II

VIVA VOCE ON THESIS OF DOCTOR OF PHILOSOPHY IN AGRICULTURAL ENGINEERING AND TECHNOLOGY

This is to certify that the thesis **“Hydrological Modelling of Hilly Watershed for Planning and Management Through Geographic Information System in Nagaland”** submitted by Ms. Imyanglula, Admission No. PH210102, Registration No. Phd/AET/00441 to the Nagaland University in partial fulfilment of the requirements for the award of the degree of Doctor of Philosophy in Agricultural Engineering & Technology has been examined by the Advisory Board and External examiner on ……………….

The performance of the student has been found to be **Satisfactory/Unsatisfactory.**

Members	**Signature**
1. Dr. Chitrasen Lairenjam (Supervisor)	……………………...
2. Dr. Rajesh Kumar Singh (External examiner)	……………………..
3. HOD, Agricultural Engineering & Technology (Ex – Officio member)	………………………

Members of Advisory Committee

1. Dr. Pramod Chandra Dihingia	...……………………
2. Dr. Hanumant Singh Rathore	………………………
3. Dr. Heisnam Rohen Heisnam	………………………

Head
Department of Agricultural Engineering & Technology

Dean
School of Engineering & Technology

ACKNOWLEDGEMENT

I offer my deepest glory to God Almighty, whose abundant grace and steadfast love have carried me through this journey. He has renewed my strength in moments of weariness and granted me the endurance to complete the work set before me.

I wish to extend my sincere appreciation to my supervisor, **Dr. Chitrasen Lairenjam**, Associate Professor, Department of Agricultural Engineering, SAS, Nagaland University. I am profoundly grateful for his approachable nature, insightful guidance, and constructive feedback that proved instrumental in shaping my academic growth. I am equally indebted to **Prof. Prabhakar Sharma**, Head, Department of Agricultural Engineering, SET, Nagaland University, for his expert advice and the generosity with which he shared his time and commitment to excellence.

My heartfelt thanks go to the members of my Research Advisory Committee: Dr. Pramod Chandra Dihingia, Dr. Hanumant Singh Rathore, and Dr. Heisnam Rohen Singh, for their vital encouragement throughout the research process. I also express my sincere gratitude to Er. Wungshim Zimik for his continuous motivation and the technical assistance that ensured the smooth progress of my work.

I owe my deepest gratitude to my parents, the foundation of my strength. To my father, a true pillar of motivation: thank you for guiding me with quiet strength through every moment of uncertainty. To my mother: thank you for your boundless care, your prayers, and for being the anchor that kept me in good health and spirit.

I also offer a special word of love to my grandmother, whose unceasing prayers have been a wellspring of peace. To my brothers, Imli and Hati, thank you for your constant reassurance; your faith in me gave me the silent strength to persevere with joy. My sincere gratitude goes to Imti for his enduring support and for being a constant source of strength at all times.

My warm appreciation also goes to my friends, Dr. Lochumi Kikon and Dr. Visakhonuo Kuotsu, as well as my batchmates and juniors, for their companionship and emotional support.

I gratefully acknowledge the National Fellowship for Scheduled Tribe (NFST), Ministry of Tribal Affairs, Government of India, for the financial assistance that made this research possible. I also thank the Department of Soil and Water Conservation and the Department of Water Resources, Nagaland, for their cooperation and resources.

Lastly, I offer my heartfelt thanks to everyone, every opportunity, and every experience that has shaped this journey. This work is a testament to God's faithfulness and the collective strength of those who stood by me. As I close this chapter, I trust in His divine plan for the future.

"For I know the plans I have for you," declares the Lord, "plans to prosper you and not to harm you, plans to give you hope and a future." — Jeremiah 29:11

Date:

Place: (IMYANGLULA)

CONTENTS

LIST OF TABLES

LIST OF FIGURES

LIST OF ABBREVIATIONS

˚C	-	Degree Celsius
%	-	Percentage
<	-	Less than
>	-	Greater than
95PPU	-	95% prediction uncertainty
AIC	-	Akaike's Information Criterion
AMC	-	Antecedent Moisture Condition
AR6	-	Sixth Assessment Report
ARS	-	Agricultural Research Service
ASTER	-	Advanced Spaceborne Thermal Emission and Reflection Radiometer
C02	-	Carbon Di Oxide
CanESM5	-	Canadian Earth System Model version 5
CMIP6	-	Coupled Model Intercomparison Project Phase 6
CN	-	Curve Number
CREAMS	-	Chemical Runoff and Erosion from Agricultural Management System
DEM	-	Digital Elevation Model
EPIC	-	Erosion Productivity Impact Calculator
ESGF	-	Earth System Grid Federation
ET	-	Evapotranspiration
FAO	-	Food and Agriculture Organisation
FORTRAN	-	Formula Translation
GCMs	-	Global Climate Models
GIS	-	Geographic Information System
GISS	-	Goddard Institute for Space Studies
GLEAMS	-	Groundwater Loading Effects of Agricultural Management Systems
GLUE	-	Generalized Likelihood Uncertainty Estimation

GRASS	-	Graphical Resources Analysis Support System
HRUs	-	Hydrological Response Units
IDE	-	Integrated Development Environment
IMD	-	India Meteorological Department
IPCC	-	Intergovernmental Panel on Climate Change
KGE	-	Kling Gupta Efficiency
LH	-	Latin Hypercube
LULC	-	Land use/Land Cover
MCMC	-	Markov Chain Monte Carlo
MDL	-	Minimum Description Length
MRI-ESM2-0	-	Meteorological Research Institute Earth System Model version 2.0
NASA	-	National Aeronautics and Space Administration
NCCS	-	NASA Center for Climate Simulation
NetCDF	-	Network Common Data Form
NEX-GDDP	-	NASA Earth Exchange Global Daily Downscaled Projections
NSE	-	Nash Sutcliffe Efficiency
OAT	-	One-factor-at-a-time
Parasol	-	Parameter Solution
PBIAS	-	Percent Relative Bias
PCA	-	Principal Component Analysis
QUAL2E	-	Water Quality Simulation Model
R^2	-	Coefficient of determination
RCP	-	Representative Concentration Pathway
RMSE	-	Root Mean Squared Error
ROTO	-	Routing Outputs to Outlet
RS	-	Remote Sensing
RSR	-	Standardized root mean squared error
SCS	-	Soil Conservation Service
SPI	-	Stream Power Index

SRTM	-	Shuttle Radar Topographic Mission
SSPs	-	Socio-Economic Pathways
STI	-	Sediment Transport Index
SUFI-2	-	Sequential Uncertainty Fitting ver. 2
SWAT	-	Soil and Water Assessment Tool
SWAT-CUP	-	SWAT Calibration and Uncertainty Program
SWPT	-	Sub-Watershed Prioritization Tools
SWRRB	-	Simulator for Water Resources in Rural Basins
TWI	-	Topographic Wetness Index
USDA	-	United States Department of Agriculture
USGS	-	United States Geological Survey
UTM	-	Universal Transverse Mercator
WGEN	-	Weather Generator
WGS	-	World Geodetic System
WSA	-	Weighted Sum Analysis

ABSTRACT

The rapid pace of environmental and anthropogenic transformation in the hilly terrains of Northeast India has critically altered watershed dynamics and resource sustainability. In Nagaland, where steep slopes, fragile soils, and intense monsoonal rainfall dominate, the combined impacts of land-use change, deforestation, and shifting cultivation have intensified soil erosion, runoff generation, and water scarcity. This study aims to assess the morphometric, hydrological, and climatic behavior of three representative hydrological units in Nagaland namely, Dzuza Watershed, Dhansiri river basin, and Khova sub-watershed of Dhansiri river basin, using an integrated Geographical Information System (GIS) and the Soil and Water Assessment Tool (SWAT) framework. The analysis incorporates morphometric evaluation, rainfall–runoff modelling, sensitivity analysis of hydrological parameters, sub-watershed prioritization, and climate change projections (2032–2040) derived from CMIP6 Global Climate Models (GCMs).

The morphometric analysis, conducted using 30 m resolution SRTM Digital Elevation Model (DEM) data, delineated the drainage network, relief, and aerial parameters of the selected hydrological units. The Dzuza watershed, Dhansiri river basin, and Khova sub-watershed were classified as 6th-, 7th-, and 5th-order basins, respectively, exhibiting dendritic drainage patterns that signify homogeneous lithology with minimal structural disturbance. The bifurcation ratio values (4.2–4.3) across the watersheds indicated moderate structural influence, while drainage density ranged from 2.28 to 2.43 km/km², suggesting coarse drainage and moderate infiltration capacity. Relief parameters revealed that Dzuza (2815 m) and Khova (1600 m) possess steep gradients and high relief ratios (0.079 and 0.067), implying greater runoff potential and erosion susceptibility than Dhansiri (1931 m; 0.028). Aerial aspects such as form factor (0.19–0.35) and elongation ratio (0.49–0.67) classified the basins as highly elongated, denoting delayed peak discharge and extended flow duration—key characteristics influencing hydrological response in mountainous regions.

Hydrological modelling using ArcSWAT (2012–2021) was performed with meteorological and discharge datasets obtained from the Department of Water Resources, Nagaland. The model calibration (2014–2018) and validation (2019–2021) phases achieved strong performance statistics, with Nash–Sutcliffe Efficiency (NSE) values between 0.70–0.87 and $R^2 > 0.75$, indicating the reliability of SWAT in data-scarce hilly catchments. The water balance analysis demonstrated that approximately 59–60% of precipitation contributes to total streamflow, of which baseflow constitutes nearly two-thirds, signifying the critical role of subsurface flow in sustaining dry-season discharge. Among the three study areas, Dhansiri exhibited the best calibration results due to its moderate slope and lithological uniformity, while Dzuza and Khova showed higher runoff peaks attributed to steep gradients and reduced infiltration.

A global sensitivity analysis using the SUFI-2 algorithm in SWAT-CUP identified the most influential parameters governing hydrological responses: curve number (CN2), soil hydraulic conductivity (SOL_K), and groundwater parameters (GWQMN, GW_DELAY). Dzuza's streamflow was found to be primarily influenced by infiltration and channel conductivity; Dhansiri's by shallow aquifer and groundwater exchange processes; and Khova's by channel storage and roughness coefficients. These findings confirm that both surface and subsurface hydrological processes play vital roles in regulating streamflow variability across the three basins.

Sub-watershed prioritization using morphometric indices and SWAT-derived hydrological outputs was executed through the Sub-Watershed Prioritization Tool (SWPT) in ArcGIS. The Dzuza sub-watersheds SW1 and SW2 and Dhansiri SW2 and SW4 were classified as high-priority zones requiring immediate soil and water conservation measures, while others fell into moderate and low-priority categories. Such rankings provide a scientifically informed basis for resource allocation, enabling planners to focus conservation efforts where they are most effective—such as check dams, contour bunding, vegetative barriers, and groundwater recharge structures.

To assess future hydrological conditions, bias-corrected CMIP6 climate projections under CanESM5 and MRI-ESM2-0 models were integrated into SWAT simulations for 2032–2040. The MRI-ESM2-0 scenario projected increased early

monsoon peaks and higher flood potential, while CanESM5 indicated reduced monsoon intensity but enhanced post-monsoon flows, reflecting improved groundwater recharge. These diverging projections highlight the uncertainty inherent in climate models but also emphasize the necessity for adaptive watershed management that addresses both flood risks and dry-season water sustainability.

The integrated results reveal that morphometric configuration and climatic variability jointly govern runoff response, erosion risk, and water balance in Nagaland's hilly basins. The elongated basin shapes delay flood peaks, while steep relief and fine drainage texture accelerate soil erosion and surface runoff. Climate-induced shifts in rainfall distribution further modify these dynamics, posing significant challenges for water resource planning. The strong model performance validates the applicability of SWAT and GIS-based approaches in data-limited mountain regions.

This research demonstrates that integrating GIS, Remote Sensing, SWAT, and CMIP6 projections offers a robust framework for understanding and managing the complex hydrological systems of Nagaland. The study not only enhances scientific understanding of morphometric–hydrological interrelations but also provides a practical decision-support base for sustainable watershed management, flood control, and climate adaptation strategies. Future studies are recommended to incorporate high-resolution climate datasets, sediment yield estimation, and machine learning-based prioritization models to improve prediction accuracy and support evidence-based policy formulation for hilly watersheds.

Keywords: GIS, SWAT, Morphometric Analysis, Watershed Prioritization, CMIP6, Climate Change, Nagaland, SUFI-2, Hydrological Modelling

CHAPTER 1

INTRODUCTION

A watershed functions as a natural unit for analysing and managing land–water interactions, particularly in regions where terrain and rainfall strongly influence hydrological behaviour. They act as natural systems regulating water availability, soil fertility, biodiversity, and livelihoods. Hilly watersheds are critical units of fragile mountain ecosystems, acting as natural regulators of hydrological processes, supporting agriculture, and providing essential ecosystem services such as maintaining soil fertility, conserving biodiversity, and ensuring water resource availability (Singh *et al.*, 2021). These watersheds are particularly vital in developing regions, where they serve as the ecological and economic lifelines for rural communities. However, their sustainability is increasingly threatened by land degradation, deforestation, soil erosion, and climate variability.

Nagaland, a north-eastern state of India, is characterized by predominantly undulating hilly terrain. In such hilly terrains, watersheds assume even greater importance due to steep slopes, fragile soils, and heavy dependence on rain-fed agriculture. The physiographic setting, combined with intensive monsoonal rainfall, makes the region highly susceptible to soil erosion, flash floods, and land degradation (Kichu *et al.*, 2022). The region is dominated by rugged topography, elevations ranging from 200 m to more than 3,000 m above mean sea level, and steep slopes often exceeding 45%. Shifting cultivation, deforestation, and the expansion of settlements have accelerated soil erosion and sediment yield (Kichu *et al.*, 2022). Rain-fed agriculture, which forms the backbone of local livelihoods, is vulnerable to rainfall variability and extreme weather (Singh *et al.*, 2021). The combination of high rainfall intensity and fragile geology increases runoff and sediment transport, resulting in land degradation, reduced soil fertility, and declining water quality. Limited hydrological monitoring poses a challenge to the need for a geospatial study of the watershed.

Nagaland is characterized by high monsoonal rainfall, receiving about 1,800–2,500 mm annually, most of which occurs between May and September (NSDMA, n.d.). The steep slopes and fragile soils of the state are therefore highly vulnerable to runoff and soil erosion (Department of Agriculture, Nagaland, n.d.). The agricultural system is predominantly rainfed, and traditional jhum cultivation is still widely practiced due to the hilly terrain, while terrace rice cultivation is also practiced in suitable locations (Kithan, 2014). Because shortened fallow cycles and cultivation on steep lands accelerate soil loss, the interaction of rainfall, land use, and terrain has made soil and water conservation a major concern in the state (Department of Agriculture, Nagaland, n.d.).

Studies worldwide emphasize that morphometric parameters, such as drainage density, bifurcation ratio, elongation ratio, relief ratio, and circularity, serve as indicators of watershed vulnerability to erosion and floods (Das *et al.,* 2016; Dikpal *et al.,* 2017; Singh *et al.,* 2021). In the context of Nagaland, such indices are vital for understanding hydrological behaviour, given the lack of long-term monitoring networks. By integrating morphometric evaluation with hydrological modeling, it is possible to identify critical sub-watersheds and propose conservation strategies suited to the region's physiography.

In recent years, hydrological models have become essential for evaluating how watersheds respond to varying land use and climatic conditions. Among the various models, SWAT (Soil and Water Assessment Tool) is globally recognized for its ability to simulate streamflow, sediment transport, and nutrient dynamics across a range of temporal scales (Arnold *et al.,* 2012). It is a semi-distributed, process-based model capable of simulating streamflow, sediment transport, and nutrient dynamics at daily to decadal scales (Arnold *et al.,* 1993; Arnold *et al.,* 2012). The model discretizes a watershed into sub-basins and Hydrological Response Units (HRUs), allowing detailed representation of soil, slope, and land use variations. Numerous studies across India and abroad have validated the robustness of SWAT in predicting rainfall–runoff relationships (Tripathi *et al.,* 2003; Shrivastava *et al.,* 2004; Jain e*t al.,* 2010). Applications include evaluation of water balance components (Agrawal *et al.,* 2011), sediment yield estimation (Betrie *et al.,* 2011), impact assessment of land use change (Du *et al.,* 2013), and prioritization of critical erosion zones (Kumar *et al.,* 2015). The integration of SWAT with calibration tools such as SWAT-CUP (Calibration and Uncertainty Program) further refines simulation results. The SUFI-2 algorithm, in particular, is widely applied for sensitivity analysis, calibration, and uncertainty assessment of SWAT outputs (Abbaspour *et al.,* 2004; Narsimlu *et al.,* 2015; Hosseini & Khaleghi, 2020). For regions like Nagaland, where field data are limited, the ability of SWAT to incorporate remote sensing inputs, such as DEM (Digital Elevation Model), LULC (Land Use/Land Cover), and soil maps) makes it highly suitable and challenging as well.

Climate change adds a layer of complexity to watershed management. Increasing temperatures, shifting rainfall patterns, and intensifying extreme events affect water availability, runoff generation, and erosion risk. Coupled Model Intercomparison Project Phase 6 (CMIP6) climate models provide multi-decadal projections of precipitation and temperature under different socio-economic pathways (SSPs). When bias-corrected and routed through hydrological models such as SWAT, these projections help assess potential changes in streamflow regimes (Jha *et al.,* 2006; Gosain *et al.,* 2006). Preliminary simulations for Nagaland using two GCMs (Global Climate Models)**,** CanESM5 (Canadian Earth System Model version 5**)** and MRI-ESM2-0 (Meteorological Research Institute Earth System Model version 2.0), project significant variability in monsoonal flows during 2032–2040. While MRI-ESM2-0 indicates earlier and more intense monsoon peaks (raising flood potential), CanESM5 suggests reduced monsoon peaks but enhanced post-monsoon flows, pointing to greater groundwater recharge potential. Such contrasting results underline the uncertainty inherent in climate projections but also highlight plausible hydrological futures that must be incorporated into planning.

Given resource constraints, it is impractical to implement conservation measures uniformly across all sub-watersheds. Prioritization techniques help identify sub-watersheds most vulnerable to degradation. Approaches commonly integrate morphometric indices, hydrological modeling outputs, and multi-criteria decision-making frameworks (Aher *et al.,* 2014; Farhan *et al.*, 2018; Sharma & Mahajan, 2020). More recent studies have applied advanced methods such as Principal Component Analysis (PCA) and Sub-Watershed Prioritization Tools (SWPT) to rank sub-watersheds effectively (Arefin *et al.,* 2020; Pan *et al.*, 2025). For Nagaland, prioritization is vital for targeting interventions such as check dams, afforestation, contour bunding, and groundwater recharge structures in high-risk sub-basins.

Considering these challenges, scientific watershed planning and management in Nagaland is an urgent necessity. Traditional watershed management approaches are often limited by insufficient data, difficult terrain, and localized actions, which may not fully capture the complex interactions between rainfall, runoff, and sediment transport. In this context (Narendra *et al.*, 2013), Geographic Information System (GIS) and Remote Sensing (RS) technologies provide powerful solutions by offering high-resolution spatial data, enabling morphometric analysis, and supporting decision-making in data-scarce regions (Narendra *et al*., 2013). When combined with advanced hydrological simulation models, such as the Soil and Water Assessment Tool (SWAT), GIS, and RS, these tools can simulate rainfall–runoff processes, predict streamflow behavior, and estimate sediment yield under different environmental conditions (Malik *et al*., 2022). This integrated approach helps researchers better understand watershed responses at various spatial and temporal scales and allows planners to develop site-specific soil and water conservation strategies.

Morphometric analysis offers insights into the structural and hydrological features of watersheds, while rainfall–runoff modeling helps evaluate water availability and flood risk potential. Sensitivity analysis of model parameters ensures reliable simulations and highlights the main hydrological factors affecting watershed behavior. Finally, watershed prioritization provides a scientific foundation for targeted actions, aiding the efficient use of limited resources in the most vulnerable areas. Recognizing the importance of an integrated framework for watershed management in hilly terrains, the present research was undertaken in three representative basins of Nagaland: Dzuza, Dhansiri, and Khova. The specific objectives are:

1. To analyze the morphological characteristics of each watershed.
2. To model rainfall-runoff of the watersheds using Soil and Water Assessment Tool in Integrated Geographic Information System.
3. To perform the sensitivity analysis of calibration parameters used in the model.
4. To prioritize the watersheds for effective planning and management.

This research contributes to both scientific understanding and practical management of hilly watersheds:

- It integrates morphometric analysis and SWAT modeling to provide a holistic assessment of watershed hydrology.

- It employs sensitivity and uncertainty analysis, ensuring strong calibration and validation in data-scarce conditions.
- It develops a prioritization framework to guide resource allocation for soil and water conservation.
- It incorporates climate change projections, thereby linking present hydrology with possible future scenarios.

Overall, the study provides a decision-support framework for sustainable watershed management in Nagaland and offers methodological insights applicable to other fragile mountain ecosystems worldwide.

CHAPTER 2

REVIEW OF LITERATURE

A comprehensive literature review has been completed to correlate with the research objectives and to develop an appropriate approach for executing the research. The study provides a literature review categorized as follows:

2.1 Morphometric Analysis of Watershed using Remote Sensing and GIS

2.2 Hydrological Models

2.3 GIS and Remote Sensing in Hydrologic Modelling

2.4 Rainfall-Runoff Modelling

2.5 Calibration, Validation, and Application of the SWAT (Soil and Water Assessment Tool) Model

2.6 Sensitivity Analysis, Calibration, and Validation of the Model using SWAT CUP-SUFI-2 Technique

2.7 Prioritization of Watershed for Development and Management

2.1 Morphometric Analysis of Watershed using Remote Sensing and GIS

Watershed morphometric analysis, utilizing remote sensing and Geographic Information Systems (GIS), is now a crucial method for comprehending river basins' geomorphological and hydrographic features. This methodology provides valuable insights into several key factors, including elevation, valley configurations, inclines, drainage density, and river length, which are crucial for effective water resource management and environmental preservation. By utilizing GIS to analyze fundamental topographic maps and Digital Elevation Models (DEMs), Ivanova *et al.* (2012) pioneered this method, emphasizing how combining various river basins can improve water resource studies. Sujatha *et al*. (2015) enhanced the methodology by specifically examining micro-watersheds. They utilized ASTER DEM data to investigate elongation and relief ratios, crucial factors in developing soil erosion prevention and conservation technologies. As shown by Das *et al*. (2016) and Dikpal *et al*. (2017), Advancements in DEM accuracy and resolution have greatly enhanced morphometric assessments, providing more dependable data for forecasting watershed erosion and strategizing soil conservation. Similarly, Soni (2017) and Kadam *et al*. (2019) used remote sensing and GIS to examine morphometric parameters, providing important frameworks for assessing erosion vulnerability and managing water resources. The approaches employed in recent studies, such as those conducted by Mangan *et al.* (2019) and Prakash *et al.* (2019), have been applied to particular river basins, providing a comprehensive understanding of flood hazards and drainage system development. Sarkar *et al.* (2020) and Singh *et al.* (2021) have advanced our knowledge by integrating morphometric data with flood risk evaluations and sedimentation behavior investigations. Finally, Kichu *et al*. (2022) and Shekar and Mathew (2024) emphasize the need to precisely quantify morphometric characteristics to tackle issues such as soil erosion and watershed management. Together, these studies emphasize the profound influence of combining remote sensing and GIS in morphometric analysis, which leads to the development of better-informed and efficient water resource management plans.

Ivanova *et al.* (2012) conducted a morpho-hydrographic analysis of the Black Sea catchment area in Bulgaria, integrating advanced GIS tools and digital elevation models to evaluate the topographical and hydrological characteristics of the region. The study focused on analyzing drainage networks, watershed boundaries, and elevation data to understand the hydrological dynamics of the area. These morphometric evaluations provide critical insights for flood risk assessment, water resource planning, and soil and water conservation measures prioritization, particularly in regions with diverse topographical features.

Sujatha *et al.* (2015) performed a morphometric analysis of the Palar sub-watershed, which is a component of the Shanmukha watershed in the Amaravati sub-catchment of the Western Ghats, South India, employing Advanced Spaceborne Thermal Emission and Reflection Radiometer Global Digital Elevation Model (ASTER GDEM) data. The research entailed segmenting the sub-watershed into six micro-watersheds and examining several morphometric factors, such as stream order, bifurcation ratio, drainage density, and relief ratio. The results indicated that the sub-watershed is a sixth-order basin characterized by a dendritic drainage pattern, primarily comprising lower-order streams. The average bifurcation ratio of 3.69 indicates structural influence on drainage formation. The relief ratio signifies substantial discharge capacity with restricted groundwater potential. These morphometric assessments are essential for devising soil erosion mitigation and conservation measures in the region.

Das *et al.* (2016) undertook a comparison analysis to assess the efficacy of different Digital Elevation Models (DEMs) in examining drainage morphometric characteristics in the Supin–Upper Tonnes Basin in the Indian Himalayas. The evaluated DEMs comprised ASTER GDEM V2, SRTM V4 (C-Band, 3 arc-second), Cartosat-1 (CartoDEM 1.0), and topographical maps at sizes of 1:250,000 and 1:50,000. The research concentrated on the extraction and analysis of morphometric characteristics, including relief, surface area, basin size, form, and drainage texture from each DEM. Results demonstrated that DEMs obtained from 1:50,000 topographical maps and ASTER GDEM V2 data displayed superior accuracy and consistency in depicting the basin's topological characteristics relative to alternative DEM products. These findings highlight the significance of choosing suitable DEM sources for accurate morphometric analysis in mountainous regions, essential for efficient watershed management and planning.

Dikpal *et al.* (2017) executed an extensive morphometric analysis of the Budigere Amanikere watershed, a tributary of the Dakshina Pinakini River in Karnataka, India, employing Cartosat-1 Digital Elevation Model (DEM) data and Geographic Information System (GIS) methodologies. The research utilized ESRI ArcGIS 10.0 software to derive multiple morphometric parameters, encompassing linear dimensions (e.g., stream order, stream length), aerial characteristics (e.g., drainage density, stream frequency), and relief features (e.g., basin relief, relief ratio). The investigation demonstrated that the watershed displays a dendritic drainage pattern, signifying uniform lithology and limited structural influence. The computed bifurcation ratio indicated a moderate impact of structural disruptions on the drainage network. Furthermore, the drainage density and stream frequency metrics indicated a porous subsurface composition with substantial infiltration capability. Morphometric evaluations are essential for comprehending the hydrological dynamics of the watershed and can anticipate watershed erosion, facilitating the prioritization of soil and water conservation measures.

Soni (2017) conducted an extensive morphometric analysis of the Chakrar watershed in Madhya Pradesh, India, employing GIS methodologies. The study sought to comprehend the geo-hydrological dynamics of the watershed by a quantitative evaluation of its drainage network and associated characteristics. The Chakrar watershed encompasses an area of 415 km² and displays dendritic, parallel, and trellis drainage patterns. It is divided into nine sub-watersheds. The analysis indicated that the watershed is a sixth-order basin, primarily consisting of lower and middle-order streams. A drainage density rating of 2.46 km/km² signifies a landscape characterized by gentle to steep inclines, moderate vegetation density, low soil permeability, and average precipitation levels. The average bifurcation ratio of 4.16 indicates that the drainage networks are developed on uniform rocks with minimal geological structural impact. Furthermore, the values of form factor, circularity ratio, and elongation ratio suggest an elongated basin morphology, which is less susceptible to flooding and exhibits reduced erosion and sediment transport capabilities. The morphometric evaluations are essential for the assessment and management of water resources, as well as for the selection of suitable recharge structures in the region for future water management plans.

Kadam *et al*. (2019) devised a way to pinpoint erosion-prone regions by amalgamating a modified morphometric prioritization approach with sediment production rate (SPR) evaluations, employing remote sensing and GIS technologies. The research concentrated on fourteen sub-watersheds within the basaltic region of the Western Ghats in India. Morphometric data, including drainage density, bifurcation ratio, and relief characteristics, were evaluated by Weighted Sum Analysis (WSA) to rank sub-watersheds according to their erosion vulnerability. The prioritization was confirmed by comparing the results with observed SPR data, revealing a robust link between the WSA-derived priorities and real sediment yields. This comprehensive method serves as an essential instrument for watershed management, facilitating the identification of key regions for soil conservation interventions.

Mangan *et al*. (2019) used remote sensing and GIS to analyze the Nanganji River Basin in Tamil Nadu, India, morphometrically. The study examined the basin's drainage to inform water resource management and soil conservation. High-resolution satellite photos and digital elevation models were used to extract stream order, bifurcation ratio, drainage density, and relief characteristics. The Nanganji River Basin has dendritic drainage, indicating similar lithology and low structural control. The drainage network was moderately affected by structural problems, according to bifurcation ratios. Additionally, drainage density and stream frequency indicated a porous subsurface material with good infiltration. The study used a correlation matrix and component analysis to understand morphometric parameter correlations. This statistical method distilled the dataset into key parameters that significantly affect the basin's hydrology. Morphometric characteristics like drainage density and stream frequency affect the basin's runoff potential and erosion risk. These morphometric evaluations help prioritize soil and water conservation efforts by understanding the hydrological behavior of the Nanganji River Basin and predicting watershed degradation. Remote sensing and GIS helped comprehend the basin's morphometry, which is crucial for sustainable watershed management.

Prakash *et al.* (2019) performed a comprehensive morphometric investigation of the Karmanasa River basin in North Central India, employing Shuttle Radar Topography Mission (SRTM) data and Geographic Information System (GIS) methodologies. The study sought to evaluate the drainage characteristics of the basin to guide water resource management and soil conservation methods. The researchers derived the drainage network from SRTM data, uncovering a trellis structure in the upstream regions and a dendritic pattern in the intermediate and downstream sections. The computed drainage density varied between 0.34 and 0.44 km/km^2, signifying extremely permeable subsurface and thick vegetation. Elevated roughness number and relief ratio indicate that the Karmanasa basin is susceptible to soil erosion. Morphometric evaluations are essential for comprehending the hydrological dynamics of the basin and can anticipate watershed erosion, facilitating the prioritisation of soil and water conservation measures.

Sarkar *et al.* (2020) performed a morphometric investigation of the Nagar River Basin in the Indo-Bangladesh Barind Tract, employing Shuttle Radar Topography Mission (SRTM) Digital Elevation Model (DEM) data and Geographic Information System (GIS) methodologies. The study sought to evaluate the drainage characteristics of the basin to guide water resource management and soil conservation methods. The researchers derived the drainage network using SRTM-DEM data, uncovering a dendritic drainage pattern, which suggests uniform lithology and limited structural influence. The computed drainage density and stream frequency data indicate a permeable subsurface material with substantial infiltration capacity. Morphometric evaluations are essential for comprehending the hydrological dynamics of the basin and can act as indicators of watershed erosion, facilitating the prioritization of soil and water conservation measures.

Singh *et al*. (2021) undertook a morphometric investigation of the Dudhnai Watershed, a sub-basin of the Brahmaputra River in Assam, India, to evaluate its susceptibility to soil erosion. The study employed remote sensing and GIS technologies to analyze several morphometric characteristics, such as bifurcation ratio, drainage density, drainage intensity, channel maintenance constant, infiltration number, and roughness number. The results demonstrated that the Dudhnai Watershed is well analyzed, exhibiting a minimal danger of flooding and soil erosion. High infiltration and roughness numbers indicate diminished infiltration capability, resulting in heightened surface runoff and probable soil erosion. The research indicated that channel erosion is more significant than sheet erosion inside the basin. The prioritization of sub-watersheds indicated the Chil sub-watershed as the most vulnerable area, requiring specific soil and water conservation interventions. This study highlights the significance of morphometric analysis in pinpointing key regions within a watershed susceptible to soil erosion. The study employs remote sensing and GIS to offer a cost-effective and efficient method for watershed management, enabling the execution of focused conservation initiatives.

Kichu *et al.* (2022) used Shuttle Radar Topography Mission (SRTM) DEM data in a GIS framework to quantify the morphology of the Dzumah watershed in Nagaland, India's Upper Dhansiri region. Research shows that the Dzumah watershed is a fifth-order drainage basin covering 65.55 km^2 and containing 228 stream segments totalling 130.71 km. The drainage density of 1.99 km/km^2 indicates a coarse texture, promoting infiltration and permeability. The watershed is extended, according to aerial form factor, circularity ratio, and elongation ratio measurements. A steep and irregular topography was indicated by the relief features' heights of 328 m to 2,345 m above mean sea level, relief ratio of 0.14, and roughness number of 4.02. These properties suggest that steep topography and high precipitation may increase surface runoff and soil erosion despite low drainage density's permeability. This thorough morphometric analysis of the Dzumah watershed's hydrological dynamics highlights soil erosion-prone areas and guides soil and water conservation.

Shekar and Mathew (2024) carried out a thorough review of the morphometric analysis of watersheds, highlighting the necessity of objectively assessing morphometric parameters such as relief, linear, and areal characteristics. This study emphasises the importance of these analyses for comprehending and managing watersheds, which is essential for hydrological research. The authors observe that although these parameters are crucial, there is an absence of standardized classification and explicit implications for each parameter in certain research publications. This review highlights the need for standardized methodologies and classifications in morphometric analysis to improve the precision and relevance of watershed management strategies.

2.2 Hydrological Models

Hydrologic models are most commonly used to simulate or predict flows, either on a continuous or event-specific basis. Models depicting water flows, water quality, and ecology are being developed and applied in more significant numbers and varieties. Hydrology and water quality investigations are integral components of the watershed management scheme. A watershed hydrological model is a set of mathematical descriptions of several hydrological cycle components (Singh and

Woolhiser, 2002). Recently, mathematical models have taken over the most significant duties in hydrological problem-solving (Beran and Rodier, 1985). Resolving scale problems in models, improving data collection, developing comprehensive decision support systems incorporating the most advanced technologies, and developing an efficient approach to characterizing parameter uncertainty in models are all challenging research issues in hydrologic and water quality modeling requiring additional attention. Aside from this, proper processes for testing, calibrating, and validating hydrologic and water quality models for various hydrometeorological circumstances are critical research topics (Tim, 1995).

Rainfall-runoff models were developed in the middle of the nineteenth century to estimate maximum flow for problems like drainage system design, flood flow exits, and sewage systems (Gosain *et al.* 2009). Mulvaney (1851) described what is now known as the "rational formula" in a paper to the Institution of Civil Engineers of Ireland and developed the concept of a rational method for peak discharge estimation from precipitation measurement, which is the earliest and simplest hydrologic model but is limited to small urban catchments. Further, the methodology was adjusted for large and homogeneous basins to consider the impact of non-uniform rainfall distribution and the geographic variability of watershed characteristics. The modified rational formula, the original transfer function model, was founded on the idea of isochrones, or lines with equal journey times. Every day, mathematical models are required, primarily to help with decision-making difficulties. The rational formula modeling approach has been a hydrological model since its inception. This is the numerical representation of flood flow rates for relatively small catchments in connection to precipitation and watershed areas. The technique was founded on the "time of concentration," or the time needed for water to go from the area's most remote point to its outflow. Sherman (1932) created the superposition-based unit hydrograph modeling idea. Many presumptions went into this superposition notion, such as the catchments acting as a linear, dynamic, time-variable causal system for transforming precipitation into runoff.

The systems approach was used to analyze complicated dynamic systems in the 1950s. After input and output data were analyzed, the response function was determined and expressed mathematically. The systems method was utilized to analyze complicated dynamic systems in the 1960s and 1970s (Lewarne, 2009). After input and output data were analyzed, the response function was determined and expressed mathematically. The response function has no bearing on the system's physical characteristics. Computers started to become more commonly available and robust enough to aid in the modeling process at this time. Numerous hydrological techniques exist, and they can be categorized according to the pollutants they address, the complexity of the sources of the pollutants, whether the model is dynamic or steady state and the period they simulate. Whether a model is lumped or distributed—that is, able to forecast various sites within a river is also crucial in choosing the right one.

Numerous alternative methods were explored in the 1960s to provide a more tangible understanding of the rainfall-runoff process and numerous conceptual, lumped models of the process were released. The majority of hydrological models are deterministic. Hydrological models fall into three categories: conceptual, black-box, and physically based. Singh and Frevert (2002), Cunderlik (2003), and Daniel *et al.* (2011). Subsequently, numerous models emerged, including Dawdy and O'Donnell (1965), the Stanford Watershed Model, also known as SWM/Hydrologic Simulation package-Fortran IV (HSPF) (Crawford and Linsley, 1962; Crawford and Linsley, 1966; Bicknell *et al.* 1993; Burnash *et al.* (1973), and the precipitation-runoff modeling system, or PRMS (Leavesley *et al*. (1984). These models' core operation is governed by the drainage system's processes, which depict the interrelated subsystems differently. An optimization process is used to estimate the parameters. These models are shown to be helpful, but they are not helpful for catchments that are not gauged because there is no long-term data available for these catchments to be calibrated (Gosain *et al.* 2009). A review of the application of watershed models (Borah and Bera, 2004; Migliaccio and Srivastava, 2007), a review of the sediment and nutrient models (Borah *et al*. 2006), and a review of the erosion models (Merritt *et al.* 2003) are some more citations that may be of interest. Hydrologic models are crucial for analyzing the effects of climate change and the equilibrium of water resources. Thus, they value the many outcomes of choices while allowing the assessment of water resources and aiding in their management.

2.2.1 International Studies on Hydrological Models

Wagener *et al*. (2001) proposed an analytical framework for the development and application of hydrological models, highlighting the necessity for models that reconcile complexity with data availability and modeling aims. They promote a multi-objective strategy for model calibration and analysis, seeking to attain suitable degrees of model complexity by available data, hydrological system attributes, and modeling objectives. This framework offers instruments to maximize the utilization of available data for identifying model structure and parameters, hence enabling a comprehensive investigation of model behavior. The objective is to create models that are both succinct and proficient in precisely depicting the relevant hydrological processes.

Amatya *et al.* (2008) utilized the Soil and Water Assessment Tool (SWAT) hydrologic model to establish a Total Maximum Daily Load (TMDL) for the Chapel Branch Creek watershed in South Carolina. This watershed spans roughly 1,555 hectares and features a variety of land uses, such as urban, residential, agricultural, and forested areas, which collectively contribute to nonpoint source pollution. The research focused on evaluating nutrient loading and determining effective management practices to address water quality concerns in the creek. The researchers employed SWAT to assess nutrient loading and allocations through source area identification and proposed best management practices for the watershed. The model's predictions were validated with observed data, confirming its efficacy in simulating streamflow and nutrient concentrations. The research emphasized the significance of combining hydrologic modelling with TMDL development to guide water quality management decisions. The research identified critical source areas and evaluated the potential effectiveness of various BMPs, offering valuable insights for stakeholders seeking to enhance water quality in the Chapel Branch Creek watershed.

Praskievicz and Chang (2009) performed an extensive assessment of hydrological modeling at the basin scale, emphasizing the effects of climate change and urban development on water resources. They highlighted the essential function of hydrological models in evaluating the impact of these factors on water availability, quality, and distribution. The review indicated that climate change is anticipated to modify precipitation patterns, resulting in a heightened frequency and severity of extreme hydrological events, including floods and droughts. Urban growth, marked by the proliferation of impermeable surfaces, leads to elevated surface runoff and diminished infiltration, intensifying flood risks and compromising water quality. The scientists observed that the synergistic effects of climate change and urbanization might substantially affect water supplies, with the extent of these effects differing according to regional attributes and particular scenarios. They determined that including climate change forecasts and urban development scenarios in hydrological models is crucial for efficient water resource management and planning.

Daniel *et al.* (2011) conducted a review of watershed modeling, highlighting its significance for water resource management. They emphasized significant trends: The increasing application of artificial intelligence (AI) techniques, such as artificial neural networks and genetic algorithms, to enhance hydrological simulations. The challenge of scaling hydrological systems across spatial and temporal dimensions, impacts model precision. The impact of data resolution on model precision, wherein high-resolution data improves model correctness. The review offers insights into enhancing watershed modeling methodologies.

Liu *et al.* (2012) examined the integration of a sub-grid topographic index into a conceptual, distributed hydrological model to improve streamflow simulations. They developed two parameterization schemes for soil moisture storage capacity: the grid-parameterization scheme, applied within a distributed model framework, and the catchment-averaged scheme, used in a semi-distributed model framework. The study applied both models to the Jiangwan experimental catchment in Zhejiang Province, China, using streamflow data from 1971 to 1986. The results showed that as the grid scale increased, the mean and variation of the topographic index and soil moisture storage parameter decreased significantly. While both models produced similar streamflow simulations, the semi-distributed model slightly outperformed the distributed model when using only outlet streamflow data for comparison. Furthermore, the distributed model effectively represented the variable source area concept, supported by field experiment data.

Du *et al.* (2013**)** investigated and quantified the hydrological processes in the quickly urbanizing Qinhuai River basin, one of China's most rapidly urbanizing areas, utilizing the SWAT model. Alterations in land use and land cover (LULC) within a watershed are acknowledged as significant determinants influencing hydrological processes and water supplies. Modeling the hydrological impacts of land-use change is essential not only for retrospective studies but also for comprehending and forecasting the prospective hydrological repercussions of current land-use practices. A diverse parameterization technique was created in the study by creating regression equations using designated SWAT parameters as dependent variables and catchment impermeable area as the independent variable. The efficacy of the newly created variable parameterization method was evaluated against the traditional fixed parameterization method in modeling hydrological processes amid land use and land cover changes. The suggested modeling approach may serve as a crucial reference for evaluating the effects of land use and land cover changes on hydrology in different locations.

Najmaddin *et al.* (2017) modeled rainfall runoff for the lesser Zab catchment, Iraq, using remotely sensed rainfall data. The study suggested that the soil moisture balance principally controlled runoff dynamics in the catchment and that groundwater dynamics and snowmelt made relatively small contributions to the shape and magnitude of the hydrograph (although snowmelt is predicted to be significant in spring and baseflow is essential in dry seasons). However, considerable uncertainty exists in the model simulation reported, manifested as equifinality. The component of this uncertainty was quantified using Generalised Likelihood uncertainty estimation (GLUE), which defined uncertainty bounds on predicted flows (resulting, in part, from poorly constrained calibration). Still, epistemic uncertainty was unknown and likely to be significant.

2.2.2 National Studies on Hydrological Models

Gajbhiye (2015) used the CN method to estimate the surface runoff in the Kanhaiya Nala watershed in the Satna district of Madhya Pradesh. The total area of the watershed was 19.53 km2. Land use, soil map, and slope map were generated in the ArcGIS environment. Since the curve number method was used as a distributed model, information regarding many sub-catchments in the basin is highly crucial. Direct runoff in a catchment depends on soil type, land cover, and rainfall. Out of the available methods, SCS-CN was the most popular method for estimating rainfall runoff. The study's thematic layers, like soil maps, elevation maps, rainfall maps, and land cover maps, were created in Arc View 3.1. The findings concluded that runoff varied from 1196.93 mm. to 1551.17 mm in the study area.

Chouhan *et al*. (2016) tried to set a rainfall-runoff model for the Shipra River basin using the AWBM RRL Model. Weighted daily rainfall, evapotranspiration, and observed runoff data of 11 years from 1996 -2006 were used to set up the model. The model was calibrated for the first six years and was validated for the remaining five years. The result showed that the value of the coefficient of determination, Nash-Sutcliffe efficiency index, root mean square error, and the correlation coefficient was acceptable.

Aherwar and Aherwar (2018) employed the SCS-CN model to simulate rainfall-runoff in the Shipra River basin, Madhya Pradesh, India. The model exhibited strong performance, evidenced by favourable statistical metrics: Nash-Sutcliffe Efficiency (72%), Coefficient of Determination (R^2 = 0.616), and Coefficient of Correlation (0.78), indicating its efficacy in predicting runoff. The research validates the model's relevance in areas with insufficient data for hydrological assessment.

Aherwar and Aherwar (2019) researched the Shipra basin using the rainfall-runoff model and the SCS-CN method. They compared the results with those obtained using the MIKE NAM model for the Shipra river basin. Ten years of meteorological data were taken for modeling, and the model was calibrated using 2/3rd of the observed data, and validation was done for the rest 1/3rd of the observed data. The results indicated that the NAM model performed better for the basin and proved comparatively faster, more accurate, and easier to operate.

2.2.3 North East India Studies on Hydrological Models

Hydrological modeling in Northeast India has garnered attention owing to the region’s distinctive physiographic and meteorological characteristics. The area experiences intense monsoonal precipitation, rugged terrain, and fragile ecosystems, presenting significant challenges for flood management and sustainable water-resource planning.

Among the limited modeling studies conducted in this region, Pervez and Henebry (2015) assessed the impacts of climate and land-use/land-cover changes on freshwater availability in the Brahmaputra River Basin using the Soil and Water Assessment Tool (SWAT). Their study demonstrated that alterations in land cover and climatic variables substantially influence streamflow dynamics, water yield, and surface runoff in the basin. They reported that deforestation and agricultural expansion increase surface runoff and reduce groundwater recharge, intensifying seasonal water imbalances. The research emphasized the critical role of hydrological modeling in understanding the combined effects of anthropogenic and climatic changes in data-scarce, monsoon-dominated basins such as those in Northeast India.

This study underscores the need for expanded application of GIS- and remote-sensing-based hydrological models in Northeast India to enhance the understanding of runoff processes, sediment dynamics, and future climate-change impacts in complex terrain.

2.3 GIS and Remote Sensing in Hydrologic Modelling

Hydrologic modeling has undergone significant advancements, from incorporating spatial data software to using geographical information systems (GIS), which has become commonplace in preparing data intended for use in a hydrologic model. GIS has dramatically expedited the analysis of watersheds of all sizes and proved to be very adaptive to the needs of the hydrologic model.

2.3.1 International Studies on GIS *and Remote Sensing in Hydrologic Modelling*

Adham *et al.* (2010) carried out a study utilizing GIS and remote sensing methods to examine the groundwater recharge capability of Bangladesh's Rajshahi District Barind Tract. Software like ERDAS IMAGINE and ESRI's Arc View, Landsat 7 ETM, SPOT, and aerial photographs that underwent various treatment processes were employed. The degree of influence was examined for each element to calculate the total groundwater recharge capacity of the two groups (reasonable to small). The generated map indicated that the potential for groundwater recharge was moderate in the remaining 85% of the region, while it was low in the remaining area.

2.3.2 National Studies on GIS and Remote Sensing in Hydrologic Modelling

Hashmi (2005) used HEC-GeoHMS and HEC-HMS for rainfall-runoff modeling in the Kaha Hill Torrent watershed D.G. Khan District. The HEC-HMS model was calibrated using daily historical rainfall data from the Murange rain gauge station, and it was compared well with the observed flood peak at the Darraha gauging station.

Agarwal *et al.* (2013) conducted a study using a GIS and remote sensing technique to determine the location of artificial recharge. They identified the recharge sites for water conservation measures using groundwater depth data, the SCS-CN model, and morphological factors. For the watershed analysis, the water resource plan was recommended to be enhanced by constructing runoff storage facilities like test dams, percolation tanks, and Nala packages. The primary instrument for storing, analyzing, and integrating spatial and attribute data for such type studies was GIS, which was utilized to analyze and integrate groundwater fluctuation, slope, ripple, drainage, and morphometric features.

Narendra *et al.* (2013) performed a study using GIS and remote sensing to find potential groundwater zones in the Visakhapatnam area of the Narava Basin, Andhra Pradesh. This article discussed using GIS and remote sensing methods to identify potential groundwater zones in the Narava basin in the Visakhapatnam district. To identify possible groundwater zones, thematic maps of drainage density, geomorphology, slope, linear density, geology, and LULC were made. The Weighted Index Overlay (WIO) method was employed to determine the number of unique opportunities and evaluate the appropriateness granted to every unit by its corresponding weight. Different groundwater prospect zones, including very good (18.9% of the area), good (26.4% of the area), moderate (17.1% of the area), and poor (37.6 of the study area), were displayed on the integrated research area map.

Singh *et al*. (2014**)** used GIS and remote sensing to assess drainage and extract their relative parameters for the Orr watershed Ashok Nagar district, M.P. The study showed large-scale watershed analysis using GIS, remote sensing data, and a digital elevation model (DEM). DEM has efficient tools for understanding terrain parameters such as bedrock, infiltration capacity, surface runoff, *etc*., which help better understand the status of landform and their processes, drainage management, and evolution of groundwater potential for watershed planning and management.

Thakur *et al*. (2017) showed the integration of remote sensing (RS), geographic information systems (GIS), and global positioning systems (GPS) as an emerging research area in the field of groundwater hydrology, resource management, environmental monitoring, and emergency response. Recent advancements in RS, GIS, GPS, and higher levels of computation will help provide and handle an extensive range of data simultaneously in a time- and cost-efficient manner.

2.3.3 ***North East India Studies on*** **GIS and Remote Sensing in Hydrologic Modelling**

Kusre (2016) conducted a GIS-based morphometric analysis of the Diyung Watershed in the Kopili River Basin, Assam, to facilitate flood management. Topographic and DEM-derived data, including drainage density (3.24 km/km^2) and stream frequency (5.26 km^{-2}), indicated a significant potential for runoff formation. The research illustrated how morphometric assessment utilizing GIS can measure flood vulnerability in data-deficient, mountainous regions.

Gupta and Dixit (2022) assessed rainfall-induced surface runoff in the Assam Valley utilizing remote sensing and GIS to extract hydrological parameters under monsoonal conditions. The methodology demonstrated efficacy in runoff estimation in areas with sparse gauge networks, highlighting the promise of GIS-based hydrologic modeling in intricate Northeast Indian landscapes.

2.4 Rainfall-Runoff Modelling

The models of rainfall and runoff can be categorized as follows: physically based (white-box), conceptual, black-box, or empirical models; lumped models to distributed models; and deterministic to stochastic models. Integrated watershed models provide a detailed depiction of the hydrologic processes. Several integrated watershed models exist; however, researchers have found SWAT to be the most computationally efficient and promising.

2.4.1 *International Studies on Rainfall-Runoff Modelling*

Shamseldin (1997) used different types of input information, such as rainfall, historical seasons, and nearest neighbor information, to test the chosen form of neural network. The technique is applied to data from six catchments for four input situations, each including some or all of these input kinds. The technique's performance is compared to that of models that use identical input data, such as the simple linear model (SLM), seasonally based linear perturbation model (LPM), and nearest neighbor linear perturbation model (NNLPM). The findings reveal that the neural network has much promise in rainfall-runoff modeling but also has many flaws, as do all models of this type.

Tokar and Johnson (1999) used Artificial Neural Network (ANN) methodology to anticipate daily runoff as a function of daily precipitation, temperature, and snowmelt. The results from the ANN rainfall-runoff model were superior to those produced using existing techniques such as statistical regression and a basic conceptual model. The ANN model takes a more systematic approach, minimizes the length of calibration data, and cuts down on model calibration time. It represents an enhancement over current forecast accuracy and adaptability methods.

Liden and Harlin (2000) employed the HBV-96 model for model calibration and parameter assessments, and automated and Monte Carlo techniques were used. Because of a cleaner water balance and more climatic variability in drier locations, performance declined, and calibration period length requirements rose as watershed dryness increased. When analyzing runoff alone, the results showed that it might not matter if parameter values are not unique as long as the model application is inside the same flow regime.

Bates and Campbell (2001) used the Metropolis-Hastings algorithm and the Markov chain Monte Carlo (MCMC) method. Model parameters subject to non-negative constraints and interval, equality, and order constraints are updated using single-site and block-updating strategies. The results indicate that the recommended solutions for dealing with model parameter restrictions are compelling; the likelihood function chosen affects the model parameters. When the CRRM complexity surpasses the limits of the rainfall-runoff data available, careful implementation of the MCMC technique is required. Trustworthy results will be challenging to get.

Chen and Adams (2006) propose a hybrid rainfall-runoff model incorporating artificial neural networks (ANNs) and conceptual models. Constructing a semi-distributed form of conceptual rainfall-runoff models based on this integrated method may explore the spatial variation of rainfall, the variety of watershed characteristics, and their impacts on runoff. Based on the selection of three different types of conceptual rainfall-runoff models, the feasibility of this innovative technique was proved in the study. The verification results from the three conceptual models reveal that the approach provided in this research of merging artificial neural networks with conceptual models shows potential in rainfall-runoff modeling.

Nourani *et al.* (2011) employed wavelet analysis in conjunction with artificial neural networks to examine the rainfall-runoff dynamics of the Ligvanchai watershed in Tabriz, Iran. The principal time series of two variables, rainfall and runoff, were decomposed into several multi-frequency time series utilizing the wavelet approach, which were subsequently employed as input data for the ANN to forecast runoff discharge one day in advance. The proposed model uses a multi-scale time series of rainfall and runoff data as input for the ANN, indicating its capability to predict both short- and long-term runoff discharges.

Jeong *et al.* (2010) presented the construction and testing of a sub-hourly rainfall-runoff model in SWAT. SWAT algorithms for infiltration, surface runoff, flow routing, impoundments, and surface runoff lagging have been tweaked to allow flow simulations with sub-hourly time intervals as short as one minute. According to statistical analysis, the improvement in model performance with sub-hourly time intervals is primarily attributable to better prediction of high flows. Although further work on water quality modeling is needed, the sub-hourly version of SWAT is a potential tool for hydrology and non-point source pollution assessment research.

Daniel *et al.* (2011) clarified the watershed model idea. According to their statement, watershed models measure the impact of human activity on these processes and imitate the natural processes occurring in every given watershed. Using simulations to mimic these natural processes is essential to solving issues about water, money, and environmental resources.

Grimaldi *et al.* (2012) suggest that the automated DEM-based geomorphic characterization of runoff dynamics in barely monitored river basins in a parsimonious hydrological modeling approach. Case studies are offered to evaluate model performance, compare simulated and observed hydrographs of 25 flood occurrences, and examine discrepancies with the geomorphological instantaneous unit hydrograph

(GIUH) model results. Using the concentration-time to calibrate the WFIUH channel flow velocity parameter provides intriguing insights for using such an approach for hydrological prediction in ungauged basins.

Chau (2017) demonstrates that the management of water resources, utilizing meta-heuristic methodologies in rainfall-runoff modeling, is gaining popularity. These strategies can enhance forecasting precision by calibrating data-driven rainfall-runoff models. This special issue of the journal Water seeks to address the literature gap by presenting articles on recent advancements in the use of meta-heuristic tools to rainfall-runoff simulation. The data and analysis can facilitate the development and implementation of precise hydrological forecasts, hence enabling appropriate preventative measures.

Najmaddin *et al*. (2017) revealed that the soil moisture balance is primarily responsible for the size and shape of the hydrograph, with only a minor contribution from groundwater dynamics and snow melt (although base flow and snow melt are expected to be significant in the dry season and spring, respectively). Generalized Likelihood Uncertainty Estimation (GLUE), which establishes uncertainty boundaries on projected flows (partially because of inadequately restricted calibration), can be used to calculate some of this uncertainty; however, epistemic uncertainty is unknown and probably significant.

2.4.2 *National Studies on Rainfall-Runoff Modelling*

Chavare and Shinde (2013) performed a morphometric study to examine and determine the drainage pattern and character of the Urmodi River basin using topographical maps, SRTM data, and geospatial methods. The study area was 412.29 km2 and included the Urmodi river basin, one of the Krishna River basins of Satara district, Maharashtra. This work also computed morphometric parameters to understand the research topic better.

2.5 Calibration, Validation, and Application of the SWAT (Soil and Water Assessment Tool) Model

In the early 1990s, the conceptual, physically based, continuous simulation watershed model SWAT was developed (Arnold et al., 1993). The Simulator for Water

Resources in Rural Basin (SWRRB) model is the origin of the initiative. The SWAT model is widely utilized in hydrology. Hydrological modeling, assessments of land use change effects, water quality research, predictions of optimum management practices, and numerous other applications have been employed.

The model comprises components such as weather, hydrology, erosion and sedimentation, plant growth, nutrients, pesticides, agricultural management, stream routing, and pond/reservoir routing. The model's semi-distributed structure divides the watershed into multiple sub-basins known as hydrological response units (HRUs). It runs on a daily time interval. Surface runoff, including runoff over frozen soils, percolation, lateral subsurface flow, groundwater flow, snowmelt, evapotranspiration, transmission losses, irrigation water transfer, and ponds, make up the hydrology component of the model. ArcSWAT, the updated concept version, has a graphical user interface. Additionally, it has a semi-distributed character. Thus, it separates the watershed into sub-basins with similar land cover, soil, climate, and management techniques.

2.5.1 International Studies on Application of SWAT

Arnold *et al.* (1998) employed the SWAT model to model the hydrology, soil erosion, and sediment movement in the Texas Trinity River basin's Richland-Chambers watershed. The GIS was used to prepare the input data for the SWAT, including the DEM, soil map, and land use map. Monthly stream flows, land erosion, and sediment transfer were all satisfactorily predicted using SWAT.

Srinivasan *et al.* (1998) utilized the SWAT model to simulate hydrological processes in the Richland-Chambers watershed of the Trinity River basin in Texas. The streamflow was calibrated and validated for the watershed. The calibration conducted in the study indicated that the monthly streamflow rates predicted by SWAT were well aligned with the observed values, demonstrating minimal differences.

Romanowicz *et al.* (2005) assessed the sensitivity of the SWAT model to the pre-processing of soil and land use data to replicate the rainfall-runoff dynamics in Belgium's Thyle watershed. Thirty-two unique soil and land use parameterization approaches were developed and evaluated to investigate this sensitivity. The results indicate that the quality of soil and land use data significantly influences the sensitivity of the SWAT model. The resolution and fragmentation of the original map items are significantly affected. The catchment size threshold value (CSTV) is a critical determinant.

Jha *et al.* (2006) employed SWAT to evaluate the impact of climate change sensitivity on stream flows in the Upper Mississippi River Basin. Monthly stream flows during 1968–1987 and 1988–1997 were used for SWAT calibration and validation, respectively. For the calibration period, the computed values of R^2 and Nash-Sutcliffe simulation efficiency were 0.74 and 0.69, respectively, while for the validation period, they were 0.82 and 0.81. These values were used in the monthly comparisons. After that, the results of six climate change scenarios and nine 30-year (1968–1997) sensitivity runs were examined to a scenario baseline. The average annual streamflow increased by 36% when atmospheric CO_2 was doubled to 660 ppmv (all other climate variables remained constant). In contrast, average annual flow changes of -49, -26, 28, and 58% were predicted for scenarios involving precipitation changes of -20, -10, 10, and 20 percent, respectively.

Gassman *et al.* (2007) analyzed the historical development, applications, and prospective research domains of the SWAT model. This model is developed by the USDA Agricultural Study Service. Numerous worldwide conferences on SWAT, hundreds of SWAT-related papers presented at various scientific gatherings, and dozens of articles published in peer-reviewed journals demonstrate that SWAT has achieved international recognition as a strong transdisciplinary watershed modeling tool. Numerous federal and state agencies in the United States, including the USDA via the Conservation Effects Assessment Project, are utilizing the model, which has also been incorporated into the Better Assessment Science Integrating Point and Nonpoint Sources (BASINS) software package from the Environmental Protection Agency. Approximately 250 peer-reviewed articles have been published that detail SWAT applications, assessments of SWAT components, or other studies connected to SWAT. A multitude of peer-reviewed articles is summarized according to relevant application categories, encompassing streamflow calibration and related hydrologic analyses, the impact of climate change on hydrology, pollutant load evaluations, model comparisons, and sensitivity analyses and calibration techniques. The model's merits and drawbacks are examined, and recommendations for additional SWOT research are proposed.

Wu and Johnston (2007) claimed that to ensure the process-based hydrological models accurately matched reality, they were often calibrated before being used. Various hydrological processes and climate variations may impact model validation and calibration. A comparative analysis was conducted on a 901 km^2 watershed in northern Michigan to evaluate the impact of calibrating the SWAT model using distinct sets of climate data representing average and drought conditions.

Rostamian *et al*. (2008). applied the SWAT model to estimate runoff and sediment in two mountainous basins in central Iran, showing its effectiveness in simulating complex hydrological processes. The model demonstrated good performance with statistical metrics such as Nash-Sutcliffe Efficiency (0.72) and Coefficient of Determination (R^2 = 0.616). SWAT has been widely used in various regions for hydrological modeling, with studies by Arnold *et al.*, (1998) and Gassman *et al.*, (2007) confirming its versatility. Despite its advantages, studies like White and Letcher (2005) highlight the need for accurate data and proper calibration, especially in data-scarce regions.

Githui *et al.* (2009) employed the Soil and Water Assessment Tool (SWAT) to evaluate the effects of land-cover alterations on runoff in the Nzoia River watershed in Kenya. The model was calibrated utilizing measured daily discharge data, and land-cover changes were analyzed via satellite image classification. Their research indicated that from 1973 to 2001, agricultural land expanded from 39.6% to 64.3%, whilst forest cover diminished from 12.3% to 7.0%. Analysis of runoff between 1970-1975 and 1980-1985 revealed that alterations in land cover contributed to a 55% to 68% variation in surface runoff between these intervals. Furthermore, their land-cover scenarios demonstrated that, relative to the 1980-1985 runoff, the optimal scenario yielded a 16% reduction, whereas the pessimistic scenario resulted in a 30% augmentation of runoff. This study emphasises the substantial impact of land-cover alterations on hydrological processes, underscoring the necessity of sustainable land management techniques to alleviate negative consequences on water supplies.

Simić *et al.* (2009) provided an extensive analysis of the Soil and Water Assessment Tool (SWAT) for simulating rainfall-runoff dynamics in intricate catchment regions. They elaborated on the model's architecture, highlighting its hydrodynamic elements, and delineated the numerical methodologies employed in its implementation. The paper is a significant resource for comprehending SWAT's basic principles and practical use in hydrological modeling.

Easton *et al.* (2010) adapted the Soil and Water Assessment Tool (SWAT) to forecast runoff and sediment loss in Ethiopia's Blue Nile Basin. Their improved model integrated a daily water balance and topographic wetness index to mimic saturation-excess runoff, consistent with known basin dynamics. The model, calibrated over various subbasins, attained Nash-Sutcliffe Efficiencies ranging from 0.53 to 0.92, signifying dependable performance. Research indicated that early-season upland erosion substantially facilitated sediment delivery, whereas channel mechanisms prevailed after vegetation was formed. This study highlights the significance of focused erosion management in particular landscape regions to safeguard water supplies.

Reungsang *et al.* (2010) utilized SWAT for the Chi River Sub-basin II in northern Thailand. The calibration and validation of the SWAT output entailed juxtaposing projected stream flows with actual in-stream data from four gauging stations. Over the course of the watershed from 2000 to 2003. Statistical analyses of the simulated results versus the empirical data for the calibration year revealed a commendable alignment, indicated by the monthly coefficient of determination (r^2) and the Nash-Sutcliffe Coefficient (E), with values spanning from 0.77 to 0.88 and 0.55 to 0.79, respectively. The validation findings demonstrated reduced r^2 and E values, varying from 0.23 to 0.77 and -7.98 to 0.66, respectively.

Asres and Awulachew (2010) utilized the Soil and Water Assessment Tool (SWAT) to forecast runoff and sediment output in the Gumera watershed of Ethiopia's Blue Nile Basin. Their research sought to determine the spatial distribution of sediment yield and evaluate the efficacy of watershed management strategies in mitigating sediment load from important regions. The findings revealed that among 30 sub-watersheds, 18 exhibited a mean annual sediment yield between 11 and 22 t ha^{-1} yr^{-1}, predominantly situated in the upstream regions. Conversely, the lower slope and wetland regions demonstrated reduced sediment yields, varying from 0 to 10 t ha^{-1} yr^{-1}. The research determined that the implementation of vegetation filter strips of varying widths might markedly diminish sediment generation from essential micro-watersheds.

Chiang *et al.* (2010) utilized the Soil and Water Assessment Tool (SWAT) to assess the effects of land use changes and pasture management on water quality in a Conservation Effects Assessment Project (CEAP) watershed. They incorporated pertinent management strategies into the SWAT model by examining land use data from 1992 to 2004. Their findings demonstrated that changes in land use led to increased overall sediment and nitrogen losses, particularly in subwatersheds experiencing urban development. Conversely, variations in pasture management strategies mostly influenced total nitrogen losses in pasture-centric areas. The study underscores the importance of separately evaluating the impacts of land use changes and conservation measures to accurately determine water quality outcomes in variable watersheds.

Tibebe and Bewket (2011) employed the Soil and Water Assessment Tool (SWAT) to evaluate surface runoff and soil erosion in the Keleta watershed, situated in the Awash River basin of Ethiopia. Their research aimed to quantify runoff and identify areas vulnerable to erosion, laying the groundwork for targeted soil and water conservation efforts. The SWAT model was calibrated and evaluated using actual hydrological data, demonstrating notable effectiveness in simulating runoff and sediment yield. The results indicated that certain sub-basins within the watershed exhibited increased runoff and erosion rates, highlighting the need for priority intervention in these areas. This study underscores the efficacy of SWAT in facilitating sustainable watershed management in data-scarce regions.

Agrawal *et al.* (2011) performed a hydrological analysis of the Chhokranala watershed in India utilising the Soil and Water Assessment Tool (SWAT) model in conjunction with a weather generator. Their study concentrated on modelling runoff and sediment output in this minor agricultural watershed. The research indicated that the SWAT model, when properly calibrated and validated, accurately forecasts hydrological responses, even with simulated rainfall data. This method is especially advantageous for areas with limited meteorological data, as it facilitates dependable hydrological modelling crucial for efficient watershed management and conservation strategies.

Betrie *et al.* (2011) employed the Soil and Water Assessment Tool (SWAT) to simulate soil erosion in Ethiopia's Upper Blue Nile Basin, to pinpoint erosion-prone regions and assess the efficacy of Best Management Practices (BMPs) in diminishing sediment output. The research indicated that the application of Best Management Practices, including filter strips, stone bunds, and reforestation, substantially reduced sediment production at both sub-basin and basin levels. The SWAT model exhibited commendable performance, with a Nash-Sutcliffe efficiency exceeding 0.83 for daily sediment concentration calculations. These findings highlight the model's effectiveness in informing sediment management practices in the region.

Luo *et al.* (2011) used Geographic Information System (GIS) methodologies to designate watersheds for the Soil and Water Assessment Tool (SWAT) model on flat polders. They employed digital elevation models (DEMs) to delineate watershed boundaries, stream networks, and sub-basins, thereby enabling the configuration of the SWAT model for hydrological simulations. This method is especially advantageous in flat, low-lying regions where conventional techniques may be less efficacious. The research underscores the need to combine GIS with hydrological modeling to improve the precision and effectiveness of watershed management in these areas.

Oeurng *et al.* (2011) evaluated hydrology, sediment, and particulate organic carbon (POC) yield in the Save catchment (1110 km²) in southwestern France utilizing the SWAT model. They modeled daily discharge and sediment transport from January

1999 to March 2009, including data on agricultural management methods like crop rotation, planting dates, fertilizer use, and irrigation. The model effectively replicated the hydrological processes, aligning with the daily discharge, sediment, and POC data. The findings revealed that, on average, 726 mm of precipitation was allocated as follows: 78.3% to evapotranspiration, 14.1% to groundwater recharge, and 7.1% to surface runoff. The research also pinpointed sites susceptible to erosion, with yearly sediment output fluctuating geographically from 0.1 to 6 t ha^{-1}, contingent upon slope and agricultural practices. The findings underscore the SWAT model's efficacy in simulating hydrological and sediment transport processes in agricultural catchments, offering critical insights for soil and water management methods.

Yu *et al.* (2011) investigated streamflow simulation in large arid basins with limited rain gauge data by combining the Soil and Water Assessment Tool (SWAT) with multiple precipitation sources. They combined rain gauge data with Tropical Rainfall Measuring Mission (TRMM) satellite data to spatially allocate precipitation inputs for the SWAT model. Their research conducted in the Manas River basin in northwestern China showed that the integration of radar data with rain gauge data improved the accuracy of streamflow estimates compared to using only rain gauge data. This approach is particularly beneficial in arid regions with sparse rain gauge networks, as it enhances the precision of hydrological modeling and water resource management.

Park *et al.* (2011) evaluated the possible effects of climate change on hydrology and stream water quality within the 6,642 km^2 mountainous Chungju Dam watershed in South Korea, employing the Soil and Water Assessment Tool (SWAT). The research employed downscaled climate data from the MIROC3.2 HiRes and ECHAM5-OM models based on the Special Report on Emissions Scenarios (SRES) A2, A1B, and B1 scenarios. The results demonstrated that, within the A1B scenario, prospective climate circumstances may result in a 4.8°C rise in temperature and a 34.4% augmentation in precipitation by the 2080s relative to 2000 levels. As a result, evapotranspiration, groundwater recharge, and streamflow are anticipated to rise by 23.1%, 28.1%, and 39.8%, respectively. In contrast, sediment loads are anticipated to diminish under the A2, A1B, and B1 emission scenarios. These findings highlight the necessity of integrating climate change forecasts into watershed management policies to tackle possible issues related to water supply and quality.

Shi *et al.* (2011) assessed the efficacy of the Soil and Water Assessment Tool (SWAT) for hydrological modeling in the Xixian River Basin, situated at the source of the Huaihe River in China. They evaluated SWAT's performance against the Xinanjiang (XAJ) model, which is extensively utilized in China. The investigation revealed that both models exhibited commendable performance, with a percentage of bias (PBIAS) below 15%, a Nash-Sutcliffe efficiency (NSE) exceeding 0.69, and a coefficient of determination (R^2) greater than 0.72 for both calibration and validation phases at the four stream stations. Both SWAT and XAJ effectively simulated surface runoff and baseflow contributions. For flood forecasting and runoff modeling, XAJ, which required minimal input data preparation, was favored. Conversely, the intricate, process-oriented SWAT model can concurrently simulate both water quantity and quality, while assessing the impacts of land use alterations and anthropogenic activities, rendering it advantageous for sustainable water resource management in the Xixian watershed, characterized by intensive agricultural practices.

Arnold *et al.* (2012) present a thorough examination of the Soil and Water Assessment Tool (SWAT), emphasizing its application, calibration, and validation methodologies. They underscore the necessity of performing sensitivity analysis to ascertain critical parameters that substantially affect model outputs. The authors examine diverse calibration techniques, encompassing both human and automated methods, and emphasize the importance of verifying the model with independent datasets to guarantee its predicted precision. They also tackle the problems related to model calibration, including the necessity for precise input data and the consideration of parameter uncertainty. This publication is a great resource for scholars and practitioners aiming to properly employ SWAT for hydrological modeling and water quality evaluations.

Qiu et *al.* (2012) assessed the Soil and Water Assessment Tool (SWAT) for modeling runoff and sediment transport in a small watershed located in China's loess hilly-gullied region. SWAT successfully reproduced runoff and sediment yield, accurately representing the region's intricate terrain and soil erosion dynamics. Nonetheless, obstacles were the necessity for precise input data and the model's susceptibility to parameter selection. The research emphasized the necessity of calibrating SWAT with regional data to improve its forecast precision in these areas.

Lirong and Jianyun (2012) employed the Soil and Water Assessment Tool (SWAT) to evaluate the hydrological response of the Beijiang River Basin to climate change. Their simulations demonstrated that SWAT accurately represented streamflow fluctuations in the basin. The study forecasted that climate change will result in heightened runoff and diminished water availability, underscoring the imperative for adaptive water resource management measures to tackle these expected alterations.

Mengistu and Sorteberg (2012) used SWAT to assess the Eastern Nile River basin streamflow's climate change response. Simulations showed that the Abbay, BaroAkobo, and Tekeze subbasins lost roughly 60% of their mean annual precipitation to evaporation, with runoff coefficients of 0.24, 0.30, and 0.18, respectively. Research showed that annual streamflow responses to precipitation and temperature fluctuations varied among basins and were not linearly connected with their severity. With temperature constant, the Abbay subbasin had a 19% annual streamflow response to a 10% precipitation change, the BaroAkobo subbasin 17%, and the Tekeze subbasin 26%. The Abbay subbasin had a mean annual streamflow response of -4.4%, the BaroAkobo subbasin -6.4%, and the Tekeze subbasin -1.3% to a 1°C temperature rise with constant precipitation. It was found that climate models predicted different magnitudes and orientations of future precipitation changes, underscoring the need to use many models to anticipate future streamflow fluctuations.

Principe and Blanco (2012) used remote sensing, GIS, and SWAT to estimate climate change impacts on Cagayan River Basin River discharge. Digital elevation modeling was done using SRTM data and Landsat images for land cover classification. The study predicted that climate change would boost basin sediment yield. To prevent sedimentation and improve water quality, the scientists suggested land cover changes including plant cover and soil protection.

Baker and Miller (2013) applied the Soil and Water Assessment Tool (SWAT) to assess the impact of land use alterations on water resources in an East African watershed. Their research indicated that SWAT proficiently modeled streamflow and sediment transport, accurately reflecting the effects of diverse land use scenarios. The results emphasized the significance of accounting for land use alterations in water resource management and the effectiveness of SWAT in guiding sustainable practices.

Da Silva *et al.* (2013) assessed erosivity, surface runoff production, and soil erosion rates for the Mamuaba catchment, a sub-catchment of the Gramame River basin in Brazil, utilizing the AvSWAT model. The model was calibrated and tested regularly, effectively simulating surface runoff and soil erosion with high accuracy. The projected soil erosion rates were credible, and consistent with field observations and findings from prior research in the catchment area. The research illustrates that the AvSWAT model is a proficient instrument for evaluating soil erosion and facilitates sustainable land management strategies in northeastern Brazil.

Koch *et al.* (2013) employed the SWAT model to assess the impact of tile drainage systems on stream flow composition within the largely tile-drained Warnow catchment in northeastern Germany, focussing on a subbasin scale. Furthermore, the model's performance was evaluated after Omitting tile drainages from the calibrated model configuration. Sensitivity analysis identified the greatest sensitivities for parameters related to evapotranspiration, soil properties, and groundwater flow, exhibiting significant diversity in sensitivity rankings throughout the subbasins. Nash-Sutcliffe efficiencies (NSE) exhibited significant variability throughout the subbasins in the tile-drained model configuration, ranging from 0.22 to 0.81 during calibration and from −0.81 to 0.66 during the validation period.

Kushwaha and Jain (2013) utilized the Soil and Water Assessment Tool (SWAT) to evaluate runoff and analyze the sensitivity of model parameters in the Dabka watershed, primarily a forested region in the Kumaun portion of the Himalayas. The model was calibrated at an upstream gauging station, and a sensitivity analysis was conducted on 13 input variables, emphasizing water supply, surface runoff, and baseflow. The research indicated that the model exhibited commendable performance, with a Root Mean Square Error (RMSE) of 0.242 during calibration and 0.81 during validation, alongside Nash-Sutcliffe Efficiency (NSE) values of 0.77 and 0.73 for the calibration and validation periods, respectively. The characteristics most significantly influencing water yield were CN2, GWQMN, and SOL_Z. The sensitivity ranking for streamflow was CN2, SOL_K, and SOL_AWC, whereas for baseflow, the most sensitive factors were SOL_AWC, SOL_Z, and GWQMN.

Lubini and Adamowski (2013) applied the Soil and Water Assessment Tool (SWAT) to assess the possible effects of four climate change scenarios on the discharge of the Simiyu River in Tanzania, located within the Lake Victoria watershed. The research entailed the calibration and validation of the SWAT model with historical streamflow data from 1970 to 1971 and 1973 to 1976. The model exhibited adequate performance, with Nash-Sutcliffe Efficiency (NSE) values of 0.52 and 0.66, and correlation coefficients (R^2) of 0.72 and 0.70 for daily and monthly intervals, respectively. The climate change scenarios included elevated CO_2 levels, resulting in seasonally specific modifications to baseline temperature and precipitation. In all scenarios, the discharge of the Simiyu River increased by 24–45%, with the most pronounced increase occurring during the rainy season (March to May). The research determined that discharge was more responsive to alterations in precipitation than to fluctuations in temperature. The findings indicate that climate change may result in elevated river flows, hence heightening the risk of floods and its detrimental impacts on infrastructure, human health, and the ecosystem within the watershed.

Santra and Das (2013) applied the ArcSWAT model to evaluate runoff in the western catchment of Chilika Lake, India. The model was calibrated with observed streamflow data and its performance was assessed using statistical criteria. The research demonstrated that the model accurately predicted runoff, achieving Nash-Sutcliffe Efficiency (NSE) values of 0.75 and 0.72 during the calibration and validation phases, respectively, alongside R^2 values of 0.80 and 0.78. Modeling results suggested that approximately 60 % of rainfall is allocated to runoff water, which transports a substantial sediment load and contributes to Chilika Lake.

Khoi and Suetsugi (2014) examined the effects of climate and land-use alterations on hydrological processes and sediment output in the Be River watershed, Vietnam, utilizing the SWAT model. The Sensitivity Analysis, model calibration, and validation demonstrated that the SWAT model could effectively replicate the hydrology and sediment yield within the catchment. The findings demonstrated that deforestation augmented the annual flow by 1.2 percent and the sediment load by 11.3 percent, whereas climate change substantially elevated the annual streamflow by 26.3 percent and the sediment load by 31.7 percent. Due to the effects of interconnected climate and land-use alterations, the annual streamflow and sediment load rose by 28.0 percent and 46.4 percent, respectively. Overall, between 1978 and 2000, climate change had a more significant impact on the hydrological processes in the Be River basin than land use change.

Lee *et al.* (2014) evaluated the impact of watershed slopes on recharge/baseflow and soil erosion in the Haean-myeon watershed in South Korea. This study proposed and evaluated an approach for enhancement. the adaptive capacity of a river system inside a steep watershed. This study calibrated the Soil and Water Assessment Tool (SWAT) to evaluate runoff and sediment, and measured alterations in hydrologic responses, including groundwater recharge rate, soil erosion, and baseflow, based on two scenarios including adjustments to the watershed slope (from steep to mild). The findings indicate that a decrease in watershed slope enhanced groundwater recharge and baseflow while reducing silt levels.

Manaswi and Thawait (2014) utilized the SWAT 2010 model for runoff modeling in the Karam River basin in Madhya Pradesh, India. The model's capacity was evaluated over 38 years (1976-2012). Sub-watershed boundaries, drainage network, slope, land use map, and soil map were developed using ArcGIS. The model simulated annual rainfall for 10 years and was compared with real observed results. The SWAT CUP was utilized for the calibration of the period from 2000 to 2010. The findings of this investigation indicated that the SWAT model can create yearly average rainfall and produce runoff that closely approximates the reported values.

Shivhare *et al.* (2014) utilized the Soil and Water Assessment Tool (SWAT) to model surface runoff in the upper Tapi sub catchment of the Burhanpur watershed in India. They employed diverse input data, encompassing the Digital Elevation Model (DEM), land use/land cover (LULC), soil data, and temporal data for temperature and precipitation. The model operated from 1992 to 1997, and the simulated monthly runoff values were juxtaposed with observed data. The coefficient of determination (R^2) for monthly runoff values from 1992 to 1996 was recorded as 0.82, 0.68, 0.92, and 0.69, signifying a commendable degree of precision in modeling surface runoff.

Fukunaga *et al.* (2015) applied the Soil and Water Assessment Tool (SWAT) to assess its efficacy in simulating daily streamflows in the upper Itapemirim River basin in Brazil. The model was calibrated and validated with data from 1993 to 2000. The calibration method indicated that SWAT exhibited significant sensitivity to baseflow, the principal calibration variable. Validation analyses produced statistical metrics demonstrating adequate performance: Nash-Sutcliffe Efficiency (NS) of 0.67, logarithmic Nash-Sutcliffe Efficiency (NSlog) of 0.68, Percent Bias (PBIAS) of 22%, and the Ratio of the Root Mean Square Error to the Standard Deviation of measured data (RSR) of 0.57. The results indicate that SWAT is a dependable instrument for hydrological modeling in tropical watersheds, offering significant insights into water resource management.

Narsimlu *et al.* (2015) employed the Soil and Water Assessment Tool (SWAT) for streamflow prediction in the Kunwari River Basin, India. They employed the Sequential Uncertainty Fitting (SUFI-2) method for model calibration and uncertainty assessment. The study attained commendable calibration and validation outcomes, exhibiting Nash-Sutcliffe Efficiency (NSE) values of 0.74 and 0.69, respectively, alongside R^2 values of 0.77 and 0.71. The p-factor and r-factor during calibration were 0.82 and 0.76, respectively, whereas during validation, they were 0.71 and 0.72. These results highlight the efficacy of SWAT in hydrological modelling and the significance of uncertainty analysis in water resource management.

Tibebe *et al.* (2015) executed an extensive investigation on the hydrology and water requirements of the Holetta River in Ethiopia's Awash Subbasin, utilizing the

Soil and Water Assessment Tool (SWAT) and CropWat models. They modeled the rainfall-runoff dynamics of the watershed and evaluated water requirements for primary consumers, including the Holetta Agricultural Research Centre, Tesdey Farm, and local agriculturalists. The research demonstrated that the SWAT model proficiently mimicked hydrological processes, as evidenced by performance indicators like the coefficient of determination (R^2) and Nash-Sutcliffe Efficiency (NSE), which indicated strong model efficacy. The analysis identified a water demand deficit throughout the dry season, especially in February, March, and April, underscoring the necessity for integrated water resource management measures to mitigate seasonal water scarcity.

Vilaysane *et al.* (2015) utilised the Soil and Water Assessment Tool (SWAT) to assess its efficacy in predicting streamflow within the Xedone River Basin in Laos. The research employed the Sequential Uncertainty Fitting (SUFI-2) method for model calibration and uncertainty assessment. The findings demonstrated that the SWAT model accurately replicated daily streamflow, with Nash-Sutcliffe Efficiency (NSE) and R^2 values surpassing 0.70 throughout both calibration and validation phases. Monthly simulations exhibited robust performance, with NSE and R^2 values over 0.80. The sensitivity analysis revealed 230 Hydrological Response Units (HRUs) within the basin, and the 95% prediction uncertainty (95PPU) intervals closely aligned with the observed discharge data. The findings indicate that SWAT is a dependable instrument for hydrological modelling in the Xedone River Basin, offering significant insights for water resource management and planning.

Yesuf *et al.* (2015) applied the Soil and Water Assessment Tool (SWAT) to simulate sediment yield in the Maybar gauged watershed located in northeast Ethiopia. The model was calibrated and verified using observed streamflow and sediment data, yielding Nash-Sutcliffe Efficiency (NSE) values of 0.75 and 0.71, and R^2 values of 0.80 and 0.74, respectively. The research pinpointed essential erosion zones within the watershed, offering significant insights for sustainable land management and erosion mitigation measures.

Gholami *et al.* (2016) performed hydrological streamflow modeling in the Talar catchment, situated in the middle region of the Alborz Mountains in northern Iran, with the SWAT model. They concentrated on parameterization and uncertainty analysis utilizing SWAT-CUP (Calibration and Uncertainty Program), a program intended to evaluate the uncertainty in model parameters and simulations. The research sought to assess the precision of stream flow forecasts and the influence of model errors on hydrological outcomes. The investigation encompassed the calibration and validation of the model utilizing observed streamflow data during a designated time frame. The research additionally assessed the efficacy of diverse parameters and the model's sensitivity to distinct hydrological processes in the area. The results elucidated the hydrological dynamics of the catchment and pinpointed the most significant characteristics, enhancing the reliability of water resource management in the region.

Sahu *et al.* (2016) utilized the SWAT model for hydrological modeling of the Mahi basin, concentrating on the simulation of streamflow and water balance in the area. The research entailed the calibration and validation of the SWAT model utilizing observed discharge data to evaluate the basin's hydrological response to diverse precipitation and land use scenarios. The study enhanced comprehension of the basin's water resource dynamics through the simulation of long-term runoff. The findings were used to discern essential hydrological processes, and the model's efficacy was assessed using statistical techniques to verify its dependability. This modeling methodology offers significant insights into water management and sustainable land use techniques for the Mahi basin.

Ha *et al.* (2017) employed the SWAT-CUP method to calibrate regionally distributed hydrological processes and evaluate ecosystem services in a Vietnamese river basin. The research utilized remote sensing data to improve the model's precision in simulating hydrological dynamics. The calibration procedure utilized observed hydrological data, and the model's efficacy was assessed according to multiple criteria. The research moreover concentrated on assessing ecosystem services, encompassing water availability and soil erosion, throughout various land use and climate change scenarios. This methodology enhanced comprehension of hydrological processes within the basin and yielded significant insights for water resource management and land-use planning in the area.

Khatun *et al*. (2018) simulated the SWAT model to simulate surface runoff in a section of the Satluj Basin, emphasising parameterization and global sensitivity analysis utilising SWAT-CUP. The research sought to enhance the model's precision through the calibration and validation of hydrological parameters using empirical data. A global sensitivity analysis was performed to determine the critical parameters affecting the model's performance. The study revealed that particular parameters substantially influenced runoff forecasts, enhancing the model for improved runoff forecasting. This method illustrated the efficacy of SWAT-CUP in improving hydrological modeling for extensive river basins and offered insights for efficient water resource management.

Hosseini and Khaleghi (2020) evaluated the efficacy of the Soil and Water Assessment Tool (SWAT) model in modeling sediment loads in dry and semi-arid areas. The model was calibrated and its uncertainty was evaluated using the Sequential Uncertainty Fitting version 2 (SUFI-2) algorithm. The research concentrated on modeling water resources, agricultural production, and water quality at the Hydrological Response Unit (HRU) level using monthly intervals. Notwithstanding various uncertainties, the SWAT model demonstrated commendable performance during the validation phase. The research discerned three critical sensitive parameters—CN2, SOL_BD, and USLE_P—utilizing SWAT-CUP. The study underscores the efficacy of the SWAT model in simulating sediment loads and its capability for evaluating the effects of climate change on soil erosion.

El Harraki *et al.* (2021) seek to investigate the sensitivity of streamflow predictions generated by the SWAT model to the spatial resolution of land use data. The impact of land use quality was analyzed using a low-resolution global dataset (ESA-CCI at 300-meter resolution) and a revised dataset identified from Sentinel-2 satellite photos (20-meter resolution). Two models were constructed successfully. Utilizing ArcSWAT and SWAT-CUP software, which underwent calibration and validation following sensitivity and uncertainty studies. The recorded precipitation in the Bine El Ouidane dam catchment was utilized for model calibration and validation. Snowmelt parameters were initially calibrated before assessing the sensitivity of flow parameters and calibrating the most sensitive ones. The calibration and validation performance for both models were quite satisfactory, as evidenced by statistical coefficients, graphical assessments, and parameter uncertainty within the 95 PPU band. The findings indicated marginally superior Nash-Sutcliffe efficiency coefficients, root mean square errors, and R2 values for the SWAT-CCI model compared to the SWAT-Sentinel-2 model (during calibration, NSE was approximately 0.85 for the former and 0.76 for the latter, while in validation, NSE was 0.70 and 0.61, respectively). This study revealed that the accuracy of streamflow assessment using the SWAT model was not improved by utilizing better spatial resolution land use data, nor was it directly correlated with the increase in the number of delimited hydrological response units (HRUs).

Bennour *et al.* (2022) created and implemented a novel method for utilizing dispersed geographic remote sensing data to calibrate hydrological models. A year's worth of remote sensing data on actual evapotranspiration (ETa) spatially distributed over the 37 sub-basins of the Lake Chad Basin in Africa was used to calibrate the Soil and Water Assessment Tool (SWAT) model. Global sensitivity analysis used the Sequential Uncertainty Fitting Algorithm–version 2 (SUFI–2) from the SWAT-Calibration and Uncertainty Programme (SWAT-CUP) to determine influential model parameters. This process reduces the number of unknowns while maintaining spatial variability. It is intended to handle spatially variable parameters and estimates multiplicative or additive adjustments applicable to the entire model domain. Fifteen significant parameters were found through the sensitivity analysis and were chosen for calibration. Based on high Nash–Sutcliffe Efficiency (NSE), Kling–Gupta Efficiency (KGE), and determination coefficient (R2), the optimized parameters provided the highest model performance.

Aloui *et al*, (2023) conducted a review of SWAT applications in Mediterranean catchments, assessing the tool's feasibility, applications, and potential future directions. The study explored how SWAT has been utilized in hydrological modeling across Mediterranean regions, focusing on its adaptability to diverse climatic and land-use conditions. The review also identified key challenges, such as data availability and model calibration, and suggested areas for future research to enhance SWAT's utility in managing water resources and addressing environmental issues in Mediterranean watersheds.

Khaleghi *et al*. (2024) sought to evaluate the efficacy of the SWAT model and SWAT-CUP software for hydrological simulation and uncertainty assessment in runoff estimation. The watershed was segmented into 12 sub-basins and 294 hydrological response units (HRUs). Calibration and uncertainty analysis was conducted utilizing the Sequential Uncertainty Fitting (SUFI-2) algorithm for two intervals: 2000–2006 and 2007–2010. The sensitivity analysis pinpointed critical elements influencing runoff, namely the USLE_P soil protection factor, wet soil density (SOL_BD), and the SCS-CN (Curve Number), with SCS-CN exhibiting the highest sensitivity. The model exhibited subpar performance during calibration, with R^2, bR^2, and Nash–Sutcliffe efficiency (NS) values recorded at 0.75, 0.59, and 0.67, respectively. During the validation phase, these values fell to 0.46, 0.24, and 0.42, signifying subpar model performance. This may be due to constraints in accessible regional data, especially about upstream water collection and springs, resulting in uncertainty during calibration. Notwithstanding these constraints, the model demonstrated promise for application in arid and semiarid areas of Iran with comparable data accessibility. Nevertheless, owing to data limitations, the uncertainty associated with future runoff forecasts was not assessed.

2.5.2 National Studies on Application of SWAT

Tripathi *et al.* (2003) demonstrated that key sub-watersheds may be successfully identified and prioritized for management objectives using the SWAT model. The minor watershed Nagwan, situated in the Upper Damodhar Valley Corporation in the Hzaribagh district of Bihar, India, was calibrated and validated using the SWAT model. To develop an efficient management plan, they used the calibrated and validated SWAT model based on daily rainfall, runoff, and sediment yield data spanning seven years (1992–1998). They also prioritized critical sub-watersheds based on the average annual sediment yield and nutrient losses over three years (1996–1998). The crucial sub-watersheds were determined using the erosion rates and their classes as a criterion.

Shrivastava *et al.* (2004) employed GIS technology and satellite data to assess the hydrology of a minor watershed named "Chhokeranala" in eastern India. They produced many maps delineating the boundaries of watersheds and sub-watersheds, the drainage network, land use and cover, and soil texture. The SWAT model was evaluated daily and monthly to quantify surface runoff and sediment yield. The results indicate a robust association between the simulated and observed runoff and sediment yield throughout the research. The model's capacity to generate precipitation was evaluated throughout a decade (1992–2001). A robust correlation exists between the model-simulated and observed daily precipitation. The researchers determined that the SWAT model can effectively replicate daily and monthly precipitation, runoff, and sediment generation.

Tripathi *et al.* (2004) used the rainfall generated from the SWAT model to calculate the sediment production and runoff for hydrological modeling of a small agricultural watershed in eastern India. The model's ability to produce rainfall was assessed over sixteen years (1981–1998). The study's findings showed that the SWAT model can satisfactorily provide monthly average rainfall, which can produce monthly average values of sediment output and surface runoff that are close to the actual values. Therefore, it can be said that the crucial erosion-prone sections of a small watershed could benefit from a multi-year management plan developed using the SWAT model.

Tripathi *et al.* (2006) investigated how watershed subdivision affected the water balance components' modeling for the Nagwan watershed in eastern India using SWAT. The watershed was divided geographically into three sub-watershed decomposition schemes: one, twelve, and twenty-two. The study's findings demonstrated that, for all decomposition strategies, the Nagwan watershed had an ideal water balance. According to the results, the quantity and size of sub-watersheds do not significantly impact surface runoff. Variations were noted in the other components of the water balance, such as evapotranspiration (5 to 48%), percolation (2 to 26%), and soil water content (0.30 to 22%), even though the runoff component of the water balance varied very little in the three examples. They concluded that, aside from surface runoff, watershed subdivision significantly affects other water balance components.

Gosain *et al.* (2006) used SWAT to analyze the impact of climate change on the hydrology of Indian river basins as part of the National Communication (NATCOM) project, which was carried out by the Ministry of Environment and Forests, Government of India, . The spatiotemporal water availability in the river systems is ascertained by the study using the HadRM2 daily meteorological data. Using 40 years of simulated weather data (20 years for control, or the present, and 20 years for GHG (Greenhouse Gas), or the future climate scenario), a simulation covering 12 river basins across the nation was created. The preliminary investigation has shown that the severity of droughts and the intensity of floods may worsen throughout the nation under the GHG scenario. Furthermore, under the GHG scenario, a general decrease in accessible runoff has been projected.

Agrawal *et al*. (2009) evaluated SWAT on a monthly and seasonal basis to formulate management scenarios for the important sub-watersheds of a small agricultural watershed in Chhattisgarh. The watershed and sub-watershed boundaries, drainage networks, slope, and soil texture maps were produced utilizing GIS. A supervised classification method was employed for land use or land cover categorization utilizing satellite images. The model was calibrated for the monsoon seasons of 2002 and 2003, then validated for 2004 and 2005. The results indicated that the model well predicted monthly and seasonal surface runoff and sediment output.

Jain *et al.* (2010) utilized the SWAT model to simulate runoff and sediment output in a watershed in the Himalayas. Their research highlighted the model's potential to depict hydrological processes in hilly regions with intricate topographies. Calibration and validation were conducted with observed data, yielding satisfactory performance metrics for the model, including Nash-Sutcliffe Efficiency and Coefficient of Determination values. The results emphasized the influence of land-use patterns and soil types on runoff and sediment production, illustrating SWAT's effectiveness in forecasting hydrological responses across diverse environmental situations. The study corroborates prior research illustrating SWAT's efficacy in watershed management and erosion forecasting. Arnold et al. (1998) and Gassman et al. (2007) highlighted the model's resilience across several geographical contexts.

Kannan *et al* (2007) emphasize that precise input data and calibration are essential for dependable conclusions, especially in data-deficient areas such as the Himalayas. This research provides significant insights into using SWAT for sustainable watershed management and soil conservation strategies.

Sahoo (2013) evaluated the suitability of the Soil and Water Assessment Tool (SWAT) for hydrological modeling in the Bandu River Basin of India. The research included 12 years of daily precipitation data (1997–2008) and 5 years of daily streamflow data (2004–2008) for calibration and validation purposes. The SWAT model accurately predicted surface runoff and streamflow, achieving Nash-Sutcliffe Efficiency (NSE) values of 0.75 for calibration and 0.72 for validation, along with R^2 values of 0.80 and 0.78, respectively. The results demonstrate that SWAT is a dependable instrument for hydrological modeling in the Bandu River Basin, offering significant insights into water resource management.

Khare *et al.* (2014) conducted hydrological simulations utilising the SWAT model to analyse runoff in the Barinallah watershed, situated in the western hills of Chamba district, Himachal Pradesh. The model was Calibrated utilising field-measured discharge data from the watershed during two years (2002 to 2003), with validation conducted for the year 2004. The monthly simulated runoff of the Barinallah watershed during the calibration and validation periods exhibited a strong correlation with the measured discharge values, yielding coefficients of determination (R^2) of 0.9385 and 0.9361, respectively. The model's simulated daily runoff was validated by commendably high Nash–Sutcliffe simulation coefficients of 0.8958 and 0.8229, a high index of agreement (d) of 0.9755 and 0.9600, and low root mean square errors of 0.1477 and 0.2589 during the calibration and validation periods, respectively. The results of this investigation demonstrate that the model's effectiveness in simulating overflow is exceptional.

Kumar *et al.* (2015) employed the Soil and Water Assessment Tool (SWAT) to pinpoint major erosion-prone basins in the Damodar catchment, India, to improve reservoir lifetime. The model was calibrated and verified utilizing observed runoff and sediment yield data from two watersheds and two reservoir inflows. The verified model pinpointed essential erosion zones that corresponded closely with the erosion map created by the Soil Conservation Department of the Damodar Valley Corporation.

Simulations revealed that sedimentation rates in the Konar and Panchet reservoirs were 1.12 million cubic meters per year and 3.65 million cubic meters per year, respectively, during the study period from 1997 to 2001. Conservation measures in the designated important watersheds decreased sedimentation rates to 0.98 and 1.80 million cubic meters annually, consequently prolonging the reservoirs' usable life by 8 and 85 years, respectively. This work illustrates the efficacy of distributed hydrological modeling in pinpointing crucial erosion zones and formulating management measures to mitigate soil erosion, decrease reservoir sedimentation, and enhance reservoir longevity.

Malik *et al.* (2022) concentrated on streamflow modeling to facilitate soil conservation planning, water resource management, and long-term management methods. The SWAT 2012 model was employed to simulate streamflow in the Linder catchment, situated in southeast Kashmir Valley, for the period from 2007 to 2015. The Sequential Uncertainty Fitting 2 (SUFI-2) approach from SWAT-CUP was employed for multi-site model calibration and validation using monthly intervals. The research pinpointed critical sensitive parameters, such as the initial SCS curve number (CN2), snow melt factor (SFTMP), temperature lapse rate (TLAPS), and snowfall temperature (SMTMP). The study underscores the necessity of comprehending hydrological processes and identifying critical factors for the creation of a dependable hydrological model.

2.5.3 Application of SWAT Model in Forest Watersheds

Although the Soil and Water Assessment Tool (SWAT) was originally developed for agricultural watersheds, its application has expanded considerably to forest-dominated and mountainous watersheds owing to its capability to simulate major hydrological processes such as surface runoff, evapotranspiration, infiltration, percolation, lateral flow, groundwater flow, and sediment transport. In forest watersheds, hydrological processes are strongly controlled by vegetation cover, canopy interception, infiltration characteristics, subsurface flow, and groundwater contribution. Therefore, SWAT has been increasingly used to evaluate the hydrological behaviour of forested basins under varying climatic, topographic, and land-use conditions.

Kushwaha and Jain (2013) utilized the Soil and Water Assessment Tool (SWAT) to evaluate runoff and analyze the sensitivity of model parameters in the Dabka watershed, primarily a forested region in the Kumaun portion of the Himalayas. The model was calibrated at an upstream gauging station, and sensitivity analysis was conducted on 13 input variables, emphasizing water yield, surface runoff, and baseflow. The study reported satisfactory model performance and identified groundwater and soil-related parameters as highly influential in runoff simulation. This study demonstrated the suitability of SWAT for simulating hydrological processes in forest-dominated mountainous watersheds.

Park *et al.* (2011) evaluated the possible effects of climate change on hydrology and stream water quality within the mountainous Chungju Dam watershed in South Korea using the SWAT model. The study showed that SWAT successfully simulated the hydrological response of the watershed and projected significant changes in evapotranspiration, groundwater recharge, and streamflow under future climate scenarios. The results highlighted the usefulness of SWAT in understanding the hydrological dynamics of steep forested watersheds and their response to climatic variability.

Lee *et al.* (2014) assessed the influence of watershed slope on groundwater recharge, baseflow, and soil erosion in the Haean-myeon watershed in South Korea using SWAT. The study demonstrated that watershed slope conditions significantly affect recharge and baseflow processes in steep terrain, and that reducing slope gradient increased groundwater recharge and baseflow while decreasing sediment yield. These findings confirm that SWAT can effectively represent the interaction between topography, groundwater processes, and runoff generation in hilly and forested watersheds.

Karki *et al.* (2023) developed the SWAT-3PG framework by integrating a process-based forest growth model with SWAT to improve forest growth and hydrological simulation in forested watersheds. The study showed that improved representation of forest dynamics enhanced the simulation of evapotranspiration, biomass growth, and watershed hydrology, thereby demonstrating the continuing advancement of SWAT for forest ecosystem applications. This work is particularly important because it indicates that SWAT is being further refined for better applicability in forest-dominated basins.

Pachac-Huerta *et al.* (2024) investigated the spatio-temporal hydrological dynamics of a mountainous basin using SWAT and reported that the model was effective in representing streamflow, evapotranspiration, and groundwater recharge under complex terrain conditions. Their findings emphasized that SWAT can successfully capture the spatial variability of hydrological processes in mountainous watersheds, making it suitable for watersheds with rugged topography and heterogeneous land cover.

Karki *et al.* (2023) evaluated the performance of SWAT-3PG in simulating hydrologic and water quality processes in a forested watershed and found that the integrated model improved the estimation of forest hydrology and associated watershed processes. The study confirmed that the enhanced SWAT framework is suitable for evaluating both hydrological and ecological responses in forest environments.

2.6 Sensitivity Analysis, Calibration, and Validation of the Model using SWAT CUP-SUFI-2 Technique

Hydrologic models are increasingly utilized by hydrologists and resource managers to comprehend and regulate natural and anthropogenic influences on watershed systems. The efficacy of a hydrologic model is contingent upon the quality of its calibration (Duan *et al*. 1992). Hydrologic models, even physically-based models, frequently incorporate factors that cannot be directly tested because to limitations in measurement and scale (Beven, 2012). These parameters must be determined by an inverse method through calibration to ensure that observed and expected output values align. Before the extensive accessibility of high-speed computers, hydrologic professionals relied on their understanding of the watershed and experiential knowledge of the model to manually alter parameters through a trial-and-error approach (Gupta *et al.* 1999). This calibrating method is subjective and labor-intensive. In recent years, automatic calibration methods, characterized by their objectivity and ease of implementation with high-speed computers, have gained popularity (Vrugt *et al.* 2003). Numerous physically-based watershed models have been effectively utilized in real hydrologic modeling challenges. Nevertheless, due to the time-intensive nature of executing these models, it is virtually infeasible to evaluate the optimization techniques for the intricate models. This study selected the complex distributed hydrologic model, Soil and Water Assessment Tool (SWAT) (Arnold *et al.* 1998), for calibration and validation in the Manasgaon micro-watershed. Model calibration is a demanding and meticulous procedure that relies on the number of input parameters, the complexity of the model, and the number of iterations (Vanrolleghem *et al.* 2003). Sensitivity Analysis and Uncertainty Analysis are critical methods for mitigating the uncertainties arising from modifications in model parameters and structure (Gupta *et al.* 2006; Wagener and Gupta, 2005). Recent advancements in calibration and uncertainty analysis methodologies for watershed models encompass: the MCMC (Markov Chain Monte Carlo) method (Vrugt *et al.* 2008), GLUE (Generalised Likelihood Uncertainty Estimation) (Beven and Binley, 1992), ParaSol (Parameter Solution) (Yang *et al*. 2008), and SUFI-2 (Sequential Uncertainty Fitting) (Abbaspour *et al.* 2004). The approaches (GLUE, Parasol, SUFI-2, and MCMC) are associated with the SWAT model via the SWAT-CUP algorithm (Abbaspour *et al*. 2007), facilitating sensitivity analysis (SA) and uncertainty analysis (UA) of model parameters and structure (Rostamian *et al.* 2008). Research on model calibration and uncertainty analysis has highlighted and validated that the SWAT model is an efficient instrument for water resource management (Tang *et al.* 2012). Abbaspour *et al.* 2004 and Yang *et al.* 2008 utilized the SUFI-2 methodology to assess the SWAT model. The SUFI-2 technique requires a minimum number of model runs for the assessment of the SWAT model. The SUFI-2 methodology requires a small number of model runs to get superior calibration and uncertainty outcomes (Yang *et al.* 2008).

2.7 Prioritization of Watershed for Development and Management

2.7.1 International Studies on Prioritization of Watershed

Fallah *et al*. (2016) conducted a study on the prioritizing of watersheds for the implementation of soil and water conservation methods. The research focused on identifying critical watersheds where conservation efforts will effectively reduce soil erosion and manage water supplies. The study utilized various criteria, including hydrological, topographical, and land use factors, to assess the susceptibility of watersheds to erosion and their potential for sustainable development. The researchers prioritized watersheds using GIS technologies and multi-criteria decision analysis (MCDA) to evaluate their vulnerability and conservation potential. This method finds areas appropriate for the deployment of soil and water conservation strategies to improve agricultural output and reduce environmental deterioration.

Farhan *et al.* (2018) executed a study to rank sub-watersheds in a substantial semi-arid drainage basin in southern Jordan employing morphometric analysis, GIS, and multivariate statistics. The research sought to evaluate the hydrological attributes of multiple sub-watersheds to inform land and water management strategies. They analyzed the spatial distribution of these parameters using GIS techniques and morphometric indices, including drainage density, slope, and elongation ratio. The findings indicated that sub-watersheds exhibiting elevated drainage density and steeper gradients were more susceptible to erosion and runoff, whilst those with diminished values were more conducive to sustainable land management methods. The research emphasized the efficacy of integrating GIS and statistical techniques to prioritize sub-watersheds for conservation initiatives in semi-arid areas.

Arefin *et al*. (2020) sought to prioritize watersheds for soil and water conservation in the northern elevated region of Bangladesh utilizing GIS, remote sensing, and a Principal Component Analysis (PCA)-based methodology. The research employed diverse morphometric and land use factors, derived from remote sensing data and analyzed via GIS methodologies. Principal Component Analysis (PCA) was utilized to diminish data dimensionality and ascertain the most significant components influencing watershed dynamics. The methodology facilitated the identification of sub-watersheds most vulnerable to erosion and degradation, hence allowing for the precise targeting of conservation measures. The results facilitated enhanced sustainability in land and water management within the region.

Khan and ElKashouty (2023) performed a watershed prioritization and hydro-morphometric analysis for the prospective development of the Tabuk Basin in Saudi

Arabia. The research employed multivariate statistical analysis in conjunction with remote sensing (RS) and GIS methodologies to evaluate and rank watersheds according to diverse morphometric criteria, including basin area, slope, and drainage density, among others. The investigation sought to facilitate sustainable development and land management by pinpointing regions most susceptible to erosion, flooding, and degradation. The findings highlighted the significance of RS-GIS integration in watershed prioritization, essential for efficient resource management in arid areas such as Saudi Arabia.

Tavosi *et al.* (2024) concentrated on sub-watershed prioritization grounded in hydrological security through the application of diverse multi-criteria decision-making (MCDM) methodologies. The study sought to evaluate the hydrological security of various sub-watersheds, encompassing the assessment of runoff, sedimentation, water quality, and ecosystem health. Various MCDM strategies were employed to prioritize the sub-watersheds based on their susceptibility and management requirements. The study incorporated multiple factors to produce a thorough prioritization that could enhance resource management and conservation efforts. The findings are crucial for informing efficient water resource planning and management amid escalating environmental issues. Raj *et al.* (2024) investigated the applications of sophisticated technology for watershed prioritization. The authors emphasized the significance of contemporary technology, including remote sensing (RS), geographic information systems (GIS), and sophisticated data analytics, in improving watershed management. They examined how these technologies facilitate the effective prioritization of watersheds according to hydrological and environmental criteria. The research highlighted that these technological applications enhance prioritization accuracy, enabling improved decision-making in conservation, water resource management, and land use planning. These improvements are essential for sustainable growth and alleviating environmental degradation.

Halder *et al.* (2024) concentrated on essential watershed prioritization utilizing multi-criteria decision-making (MCDM) methodologies combined with geographical information systems (GIS) for efficient watershed management. The study's authors published in Sustainability examined how the integration of MCDM with GIS facilitates the evaluation of several aspects, including hydrological, environmental, and socio-economic elements. This comprehensive strategy improves decision-making by pinpointing critical areas requiring urgent focus for conservation, water management, and sustainable development. The research promotes the implementation of these sophisticated techniques to tackle issues in watershed management, guaranteeing enduring sustainability and resilience against environmental stressors.

2.7.2 National Studies on Prioritization of Watershed

Vittala *et al.* (2008) devised a comprehensive methodology for the prioritization of sub-watersheds, emphasizing sustainable development and natural resource management. They integrated remote sensing, GIS, and socio-economic data to evaluate and prioritize sub-watersheds according to criteria such as land use, soil properties, water availability, and socio-economic conditions. The study sought to identify sub-watersheds most conducive to resource management actions. The results informed the formulation of conservation strategies, land management, and resource allocation, highlighting the necessity of incorporating environmental and socio-economic considerations in watershed management. This method established a thorough structure for prioritizing areas necessitating urgent focus for sustainable development.

Aher *et al*. (2014) concentrated on quantifying morphometric characterization and prioritization for management planning in the semi-arid tropics of India, employing remote sensing and GIS methodologies. The study sought to evaluate the physical characteristics of watersheds to facilitate land and water management. It employed several morphometric metrics, including basin shape, drainage density, slope, and additional topographical features, to assess watershed characteristics. The researchers included these factors into a GIS-based decision-making framework to prioritize watersheds according to their management planning suitability. The research emphasized the significance of morphometric analysis in identifying locations most vulnerable to erosion and other environmental issues in semi-arid settings, hence facilitating sustainable watershed management.

Ahirwar *et al.* (2019) executed a study to rank sub-watersheds for soil and water conservation within segments of the Narmada River basin, employing morphometric analysis alongside remote sensing and GIS. The research examined the spatial attributes of the watershed, encompassing drainage patterns, slope, and area, to assess their potential for soil erosion and water conservation requirements. The morphometric study pinpointed critical sub-watersheds that exhibited heightened susceptibility to erosion and deterioration. Remote sensing and GIS methodologies were employed to delineate land use, topography, and hydrological characteristics, subsequently integrated to inform conservation planning. The results offered critical insights for directing soil and water conservation initiatives in the area.

Sharma and Mahajan (2020) performed GIS-based sub-watershed prioritization research in the outer Himalayan area of India utilizing morphometric analysis. The research sought to identify and rank sub-watersheds most vulnerable to soil erosion and degradation, employing morphometric factors such as drainage density, slope, and stream order. Geographic Information System approaches were utilized to map and analyze these metrics, offering a geographical comprehension of the watershed characteristics. The study determined that the prioritization strategy is useful for directing conservation efforts and managing natural resources sustainably in the region, especially in areas susceptible to erosion and land degradation.

Kumar *et al.* (2021) performed a study on the prioritization of watersheds utilizing remote sensing (RS) and geographic information system (GIS) methodologies. The study sought to pinpoint the most susceptible regions within a watershed for efficient soil and water conservation strategies. The research employed multiple spatial data layers, such as topography, land use, soil type, and hydrological characteristics, to assess and categorize sub-watersheds according to their susceptibility to erosion, runoff, and other ecological variables. The study's results provide insights into identifying priority regions for watershed management and sustainable development, highlighting the importance of RS-GIS integration for effective environmental planning and resource management.

Pan *et al.* (2025) prioritized sub-watersheds in the Shilabati River Basin, West Bengal, India, employing a multi-analytical framework integrating morphometric analysis, principal component analysis (PCA), land use/land cover (LULC) assessment, hypsometric analysis (HA), and the Sub-Watershed Prioritization Tool (SWPT). Published in the *Journal of Water and Climate Change*, the study identified erosion- and flood-prone areas by combining RS-GIS technologies with advanced statistical approaches, ultimately categorizing 23 sub-watersheds into high, medium, and low priority classes. This holistic methodology provides actionable insights for soil and water conservation, enabling targeted management interventions to mitigate erosion, enhance flood resilience, and promote sustainable watershed management.

2.8 Critique

A literature review was conducted on watershed prioritization and hydrological modelling utilizing the Soil and Water Assessment Tool (SWAT), Geographic Information Systems (GIS), and remote sensing methodologies, emphasizing runoff estimation, sediment yield, and watershed management. The evaluated research emphasized SWAT model in modelling hydrological processes across diverse land use and meteorological scenarios. Researchers such as Hosseini and Khaleghi (2020) and Malik *et al.* (2022) underscored the necessity of calibrating and testing the SWAT model with methods such as SUFI-2 to enhance simulation precision. The integration of GIS and sophisticated techniques for morphometric analysis improves the spatial comprehension of watershed attributes. The reviewed literature indicated that morphometric analysis and GIS integration are essential for prioritizing sub-watersheds and pinpointing erosion-prone regions. Nevertheless, numerous studies predominantly depend on morphometric measures, failing to sufficiently incorporate socio-economic or cultural aspects, hence constraining the comprehensive applicability of the results. Moreover, although sensitivity and uncertainty studies have been extensively performed, issues such as inadequate data quality and restricted field validation frequently undermine the dependability of these models. Limited efforts have been undertaken to assess the effects of climate change and prospective land use scenarios on runoff and sediment output. Although certain studies recognise the importance of these aspects, they predominantly depend on historical data, neglecting to consider the long-term consequences for watershed sustainability. The absence of standardized criteria and procedures, as emphasized in research such as Halder *et al.* (2024), obstructs the comparison of outcomes across different locations. Despite the tremendous improvements in watershed prioritization techniques due to breakthroughs in remote sensing and GIS, their implementation frequently differs in scale and resolution, affecting the precision of results. Furthermore, whereas technical methodologies for watershed prioritization are extensively documented, the conversion of these findings into practical policy recommendations and effective conservation strategies is insufficient. Therefore, it is essential to perform regional studies that incorporate SWAT modelling, socio-economic factors, and high-resolution data for effective watershed management. Future research must prioritize the integration of climate change projections, the enhancement of data accuracy, and the alignment of research findings with policy frameworks to improve the sustainability of water resources and land management.

CHAPTER 3

MATERIALS AND METHODS

This chapter describes the study area, data collection procedures, and data processing techniques. It explains how to create soil maps, LULC (Land use/Land Cover) maps, DEMs (Digital Elevation Models), and morphometric parameters using ArcGIS. A detailed overview of the process used by ArcSWAT (Soil and Water Assessment Tool) to automatically define watershed and sub-watershed boundaries with DEM is provided. Additionally, methods for breaking down sub-watersheds into several Hydrological Response Units (HRUs) using land use, land cover, soil maps, and slope classes through overlay techniques are discussed. A summary and clear explanation of the ArcSWAT model's functions and limitations are included, along with details of the input and output files used to evaluate the model. This chapter also explains how to calibrate and validate the model with SWATCUP (Soil and Water Assessment Tool Calibration and Uncertainty Program), including the criteria for assessing its performance. The process of identifying key HRUs and sub-watersheds in the study area and how to prioritize their management is covered.

Lastly, this chapter encompasses the climate change impact assessment conducted utilizing CMIP6 (Coupled Model Intercomparison Project Phase 6) datasets and Shared Socioeconomic Pathway (SSP) scenarios. Climate projections for temperature and precipitation were incorporated into the SWAT model to assess potential future variations in runoff and water supply. The research employs an entropy-based weighting technique to identify the most dependable Global Climate Models (GCMs), thereby guaranteeing an accurate depiction of future climatic conditions in the Dhansiri Basin.

3.1 Description of the Study Area

The study area is located in the Indian state of Nagaland (26.1584° N, 94.5624° E), where the Dzuza watershed, Dhansiri river basin, and Khova sub-watersheds were chosen to determine the applicability and performance of the SWAT models in evaluating runoff. **Figure 3.1** shows the location map of the study area. Nagaland, with an area of 16,579 km², features severe topography, steep slopes, and mountainous terrain, which profoundly influences the region's hydrology and land use patterns. In Nagaland, agriculture is mostly practiced on hillside slopes and is mostly dependent on rain-fed systems. Though the region's varied heights and distinct climatic conditions support a variety of agroecosystems, they also make it susceptible to land degradation and soil erosion. As a result, good watershed management is vital for sustaining agricultural output and protecting natural resources.

The Dzuza watershed is a hilly catchment of the river Dzuza (also known as Rengma- Zubza River) where the outlet point is situated at latitude N 25°54'19.7" and longitude E 93°58'4.2". The River Dzuza is a major tributary of the river Dhansiri and receives numerous small tributaries from the hill through which it makes its way. The Dzuza River basin spans the Kohima and Dimapur districts, covering approximately 349.647 km² (SWAT generated area). The catchment is 'Dhansiri to Lohit confluence', and the watershed is the Rengma watershed. This watershed is essential for sustaining local communities by supplying water for domestic use, agriculture, and many activities.

On the other hand, the hydrological framework of the region is further complicated by the Dhansiri River basin, encompassing the districts of Peren and Dimapur, located at latitude N 25°54'45.6" and longitude E 93°44'36.0". This basin covers an area of 1696.01 km², with the Chathe and Dzuza rivers contributing to its flow. The Dhansiri River is a significant tributary of the Brahmaputra River in Northeast India. It originates from the Laisang peak located at the Peren district of Nagaland, situated at an elevation of around 800 m above mean sea level. Subsequently, the Dhansiri River flows northeast for approximately 76 km until it reaches the city of Dimapur in Nagaland. Beyond Dimapur, the river alters its trajectory and proceeds in a northern direction. It maintains its northern trajectory for over 240 km before converging with the Brahmaputra River on its southern bank near Dhansirimukh in Assam. The overall length of the Dhansiri River, from its source at Laisang Peak to its confluence with the Brahmaputra River, is roughly 352 kilometres. The Dhansiri River is the principal watercourse traversing the Golaghat region of Assam and Dimapur city in Nagaland. This basin is a significant hydrological resource that influences the region's ecological health and adds to the total water supply.

The Khova sub basin is recognized locally as a minor tributary of the Dhansiri river basin, which ultimately merges with the Brahmaputra system. Its geographical coordinates are N 25°46'51.6" E 93°43'37.8" (Dimapur District, Nagaland), covering an area of 110.45 km^2. Overall, the unique topography and hydrology of Nagaland, especially in the Dzuza watershed, Dhansiri river basin, and Khova sub-watershed, require a detailed understanding of watershed dynamics. This research aims to illuminate these dynamics to support the development of sustainable management strategies that protect the region's agricultural livelihoods and water resources in a biodiverse and culturally rich area. The detailsof the location of the three weather stations are shown in **Table 3.1**.

Table 3.1 Location details of meteorological stations

S. No.	Latitude	Longitude	Location
1	N 25°54'19.7"	E 93°58'4.2"	Dzuza
2	N 25°54'45.6"	E 93°44'36.0"	Dhansiri
3	N 25°46'51.6"	E 93°43'37.8"	Khova

3.2 Data Acquisition

3.2.1 Meteorological Data

Historical daily rainfall data from 2012 to 2021 were collected from the Department of Water Resources, Nagaland, which were measured at the Dzuza, Dhansiri, and Khova outlets. It also provided information on wind speed, relative humidity, maximum and minimum air temperatures, recorded at the outlet stations.

3.2.2 Hydrological Data

Data on daily discharge for the Dzuza, Dhansiri, and Khova were gathered from the Department of Soil and Water Conservation, Nagaland, over 11 years (2012–2021).

3.2.3 Soil and Land Use Data

The soil map of the area was extracted from the Digital Soil Map of the World compiled by the Food and Agriculture Organisation (FAO). The land use land cover map of the area was created from the land cover imagery of the area acquired from the Living Atlas database

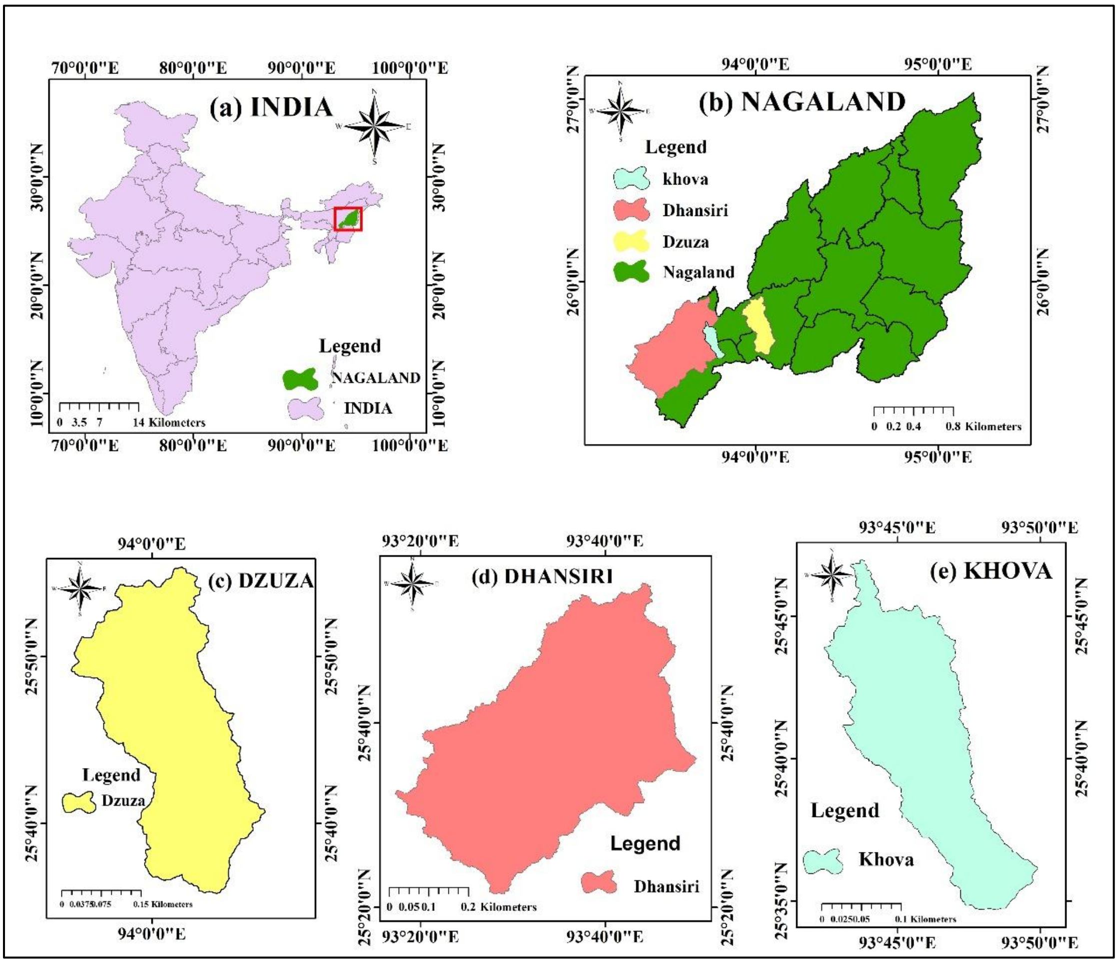

Figure 3. 1: (a) Geographical position of Nagaland on the map of India (b) Map of the Dzuza, Dhansiri, and Khova in Nagaland (c) Dzuza watershed, (d) Dhansiri river basin, (e) Khova sub-watershed

3.2.4 Digital Elevation Model

The Shuttle Radar Topographic Mission (SRTM) Digital Elevation Model (DEM) was obtained from the radar system, which is less impacted by weather conditions than the optical ASTER (Advanced Spaceborne Thermal Emission and Reflection Radiometer) DEM. However, regardless of the data source or the method used to process the data, all DEMs contain errors (Forkuor & Maathuis, 2012). The remote sensing data were acquired from the United States Geological Survey (USGS) website (https://earthexplorer.usgs.gov/) with a spatial resolution of 30 m. The DEM is used to delineate watersheds, which is the first phase of the simulation. The flow accumulation, stream network, and stream linkages will be built based on the elevation (**Figure 3.2**).

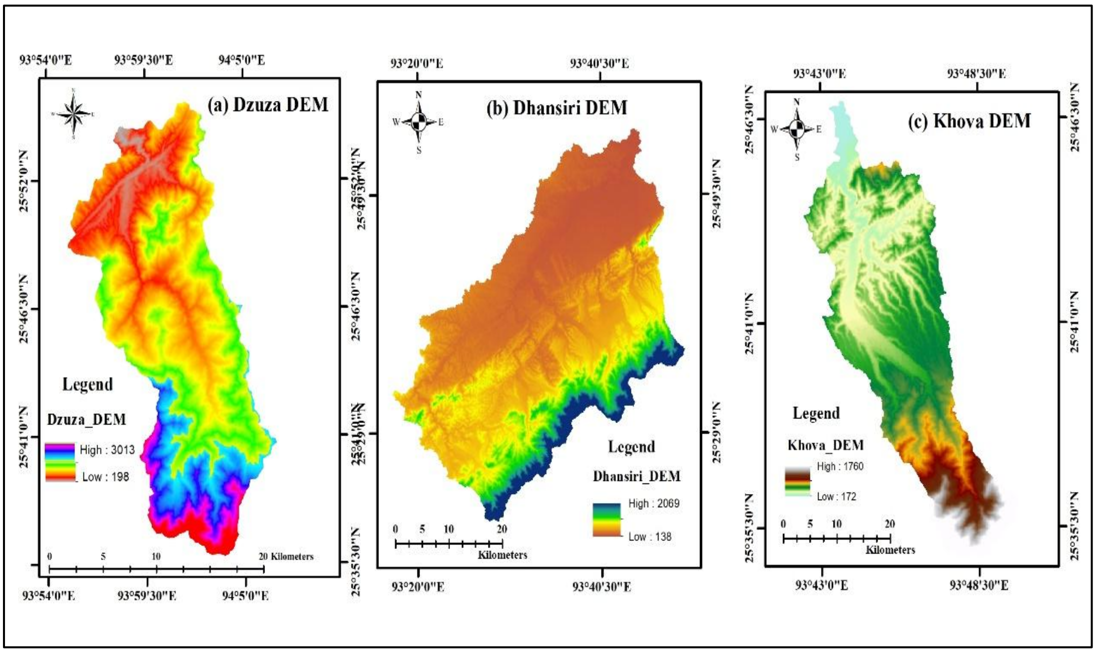

Figure 3. 2: (a) Dzuza DEM, (b) Dhansiri DEM, (c) Khova DEM

3.2.5 Software Used

For this study, a variety of software and tools were employed. ArcGIS/IGis was used for watershed delineation, DEM processing, geospatial analysis, HRU creation, and dataset preparation. Google Earth supported visual interpretation, land use/land cover validation, and geo-referencing. ArcSWAT facilitated hydrological modeling and runoff simulation within the ArcGIS environment. At the same time, SWAT-CUP 2012 was applied for model calibration, validation, sensitivity, and uncertainty analysis using the SUFI-2 (Sequential Uncertainty Fitting ver. 2) algorithm. Python (Spyder IDE) was utilized to download and preprocess rainfall, temperature, and NetCDF (Network Common Data Form) data. The Morphometric Toolbox enabled automated extraction of linear, areal, and relief morphometric parameters, and the SWPT Toolbox was employed for sub-watershed prioritization based on morphometric and hydrological parameters.

3.3 Morphometric Analysis of the Watershed

Table 3.2: Calculation methods for various morphometric parameters

Morphometric Parameters	Methods	References
LINEAR ASPECTS		
Stream Order (U)	Hierarchical order	Strahler (1964)
Stream Length (Lu)	Length of the stream	Horton (1945)
Mean Stream Length (L_{sm})	$L_{sm} = L_u/Nu$, where L_u = Stream length of order "U" N_u = Total number of stream segments of order "U"	Horton (1945)
Stream Length Ratio (R_l)	$R_l = L_u/L_{u-1}$, where L_u = total Stream length of order "U"; L_{u-1} = Stream length of next lower order	Horton (1945)
Bifurcation Ratio (R_b)	$R_b = N_u/N_{u+1}$, where N_u = Total Number of stream segments of order U, N_{u+1} = Number of stream segments of next higher order	Schumm (1956)
RELIEF ASPECTS		
Basin Relief (B_h)	Basin relief is the vertical distance between the lowest and highest points of the watershed.	Schumm (1956)
Relief Ratio (R_h)	$R_h = Bh/L_b$, where B_h = Basin Relief; L_b = Basin Length	Schumm (1956)
Ruggedness Number (R_n)	$Rn = B_h \times D_d$, where B_h = Basin Relief; D_d = Drainage density	Schumm (1956)
Height of basin mouth (z), m	GIS analysis/DEM	
Maximum height of the basin (Z), m	GIS analysis/DEM	
Total basin relief (H), m	$H = Z - z$	Strahler (1952)
Relative relief ratio (R_{hp})	$R_{hp} = H \times 100/P$	Melton (1957)
Gradient ratio (G_r)	$G_r = (Z - z)/L_b$	Sreedevi (2005)
Melton ruggedness number (MRn)	MRn = H/A0.5	Melton (1957)
AERIAL ASPECTS		
Drainage Density (D_d)	$D_d = L/A$, where L = Total length of streams; A = Area of watershed	Horton (1945)
Drainage Texture (T)	$T = F_s*D_d$, where F_s = Stream frequency; D_d = Drainage density	Horton (1945)

Table 3.2 (continued)

Form Factor (R_f)	$R_f = A/(L_b)^2$, where A = Area of watershed; Lb = Basin Length	Horton (1945)
Circularity Ratio (R_c)	$R_c = 4\pi A/P^2$, where A = Area of watershed; P = Perimeter of watershed; $\pi = 3.14$	Miller (1953)
Elongation Ratio (R_e)	$Re = 2\sqrt{(A/\pi)}/L_b$, where A = Area of watershed; L_b = Basin Length; $\pi = 3.14$	Schumm (1956)
Length of Overland Flow (L_{of})	$L_{of} = 1/2D_d$, where D_d = Drainage density	Horton (1945)
Constant Channel Maintenance (C)	$C = 1/D_d$, where D_d = Drainage density	Horton (1945)
Infiltration number (I_f)	$I_f = F_s \times D_d$	Faniran (1968)
Basin area (A), km^2	GIS software analysis	Schumm (1956)
Basin perimeter (P), km	GIS software analysis	Schumm (1956)
Fitness ratio (R_f)	$Rf = Cl/P$	Melton (1957)

3.3.1 Morphometric Parameters

3.3.1.1. Linear aspect

3.3.1.1.1. Stream Order (U)

The notion of stream order, initially proposed by Strahler (1964), functions as a crucial instrument in the examination of drainage basin geomorphology. This method offers a hierarchical structure to outline the branching configuration of streams in a watershed. The most diminutive headwater channels are designated as first-order streams in the Strahler system. The confluence of two first-order streams marks in a second-order stream; likewise, the merging of two streams of identical order elevates the order by one (Shekar & Mathew, 2024). This classification aids in quantifying the structure and complexity of a basin's drainage network. The merger of two first-order streams produces a second-order stream (Shekar & Mathew, 2024). The union of two second-order streams generates a third-order stream—this leads to the creation of higher-order streams as more branches merge. The Strahler ordering system develops the resolution of representing stream order with the letter "U" or an underscore below the numerical value (Shekar & Mathew, 2024).

3.3.1.1.2. Mean Stream Length (L_{sm})

The drainage network, and its adjacent surfaces posses a distinctive quality (Strahler, 1964). The cumulative lengths of all watercourses in each order were aggregated and divided by the number of streams in each order (Shekar & Mathew 2024). It is denoted by L_{sm}.

The subsequent formula is employed to compute L_{sm}:

$$L_{sm} = {}^{L_u}/_{N_u} \tag{3.1}$$

Where, Nu = stream number and Lu = stream length.

3.3.1.1.3. Stream Length Ratio (R_I)

The stream length ratio (R_I) shows the average length of streams of a certain order compared to the average length of streams of the next lower order (Horton, 1945; Strahler, 1964). In general, this ratio goes up as the stream order goes up, which shows that there is a systematic geometric relationship in the drainage network. But a decreasing stream length ratio frequently means that the land is uneven or wavy, with many short tributaries and complicated drainage patterns. In some circumstances, higher-order streams may be shorter than predicted because of local topography or geology, which makes the R_I value for those orders larger. This form is frequently found in ranges with substantial runoff, leading to erosion risks (Shekar & Mathew 2024).

R_I is calculated using the formula shown below:

$$R_I = \left(\frac{L_u}{L_u - 1}\right) \tag{3.2}$$

3.3.1.1.4. Bifurcation Ratio (R_b)

Horton (1945) introduced the bifurcation ratio (R_b) as a fundamental metric for evaluating landscape relief and degree of dissection. Subsequent research by Strahler (1957) suggested that, barring significant geological influences, these values remain remarkably consistent across diverse environments. Furthermore, Nag

(1998) observed that lower R_b values are typically characteristic of watersheds that possess stable drainage patterns and minimal structural deformation. The ratio is calculated using the following equation:

$$R_b = \frac{N_u}{N_u + 1} \tag{3.3}$$

R_b will not be precisely uniform between successive orders due to possible differences in lithology and catchment morphology; however, they often remain stable. A watershed exhibiting a diminished bifurcation ratio is expected to have seen fewer structural disruptions and a drainage pattern that remains unaffected by such disturbances. The bifurcation ratio (R_b) shows the overall morphology and structural regulation of a drainage basin. Generally, reduced R_b levels correlate with more circular or less elongated basins, indicating less geological disruption and a cohesive drainage pattern. Conversely, elevated R_b values frequently arise in extended basins, where structural or lithological factors impact stream orientation. An R_b value under 3 is typically seen as indicative of an optimal or natural drainage system that has evolved without considerable structural alteration (Strahler, 1964; Schumm, 1956).

Within the range of 3 to 5, the basin's drainage pattern is mostly unaffected by geological structures, though there is a notable rise in branching complexity (Shekar & Mathew 2024). A bifurcation ratio greater than 5 signifies an elongated basin where geological formations substantially influence the basin's morphology (**Table 3.3**), leading to a pronounced level of branching density.

Table 3.3: Significance and range of bifurcation ratio (Strahler, 1964)

Significance	Range
Theoretical basin	< 3
The basin’s drainage pattern is not distorted by the geologic features	3 to 5
The basin is elongated, and geological structures control the basin	>5

3.3.1.2. Relief Aspects

3.3.1.2.1. Basin Relief (B_h)

Relief denotes the difference in elevation present within a certain watershed area. It measures the disparity between the maximum and minimum elevations within that region. This topographical factor significantly affects the slope features of a basin. The topographic gradient significantly influences a terrain's vulnerability to soil erosion. Regions with elevated relief values generally have steeper gradients and more elevation variability, hence augmenting runoff velocity and erosive capacity. Thus, areas with significant topographical variation are typically more prone to erosion than flatter terrains (Horton, 1945). Conversely, diminished relief values specify more gradual elevation changes, resulting in smoother slopes and a likely decrease in erosion susceptibility. The watershed is believed to be increasingly susceptible to erosion as basin relief increases (Shekar & Mathew, 2024). It is represented as B_h.

The relief was calculated as:

$$B_h = H - h \tag{3.4}$$

Where H = maximum elevation, h = minimum elevation.

3.3.1.2.2. Relief Ratio (R_h)

The relief ratio (R_h), established by Schumm (1956), denotes the relation of the entire basin relief to its maximum basin length, as measured along the principal drainage line. This indicator is a significant indicator of the basin's overall gradient and topographic variance. A larger relief ratio indicates steeper topography and increased probability for erosion and runoff intensity, whereas lower values signify milder slopes and diminished erosive activity. Consequently, the relief ratio offers significant insight into the geomorphological configuration and erosional processes of a watershed (Ratnam *et al.,* 2005).

The relief ratio was calculated using the formula:

$$R_h = \frac{B_h}{L_b} \tag{3.5}$$

Where B_h is relief and L_b is the basin length.

3.3.1.2.3. Ruggedness Number (R_n)

The ruggedness number (R_n), introduced by Strahler (1964), is determined by multiplying drainage density (D_d) by the maximum basin relief. This dimensionless indicator integrates the impacts of slope steepness and surface dissection, representing the total terrain roughness of a watershed. Elevated R_n values signify regions with steep, intricately dissected slopes, suggesting increased vulnerability to erosion and runoff, whereas diminished values represent more gentle, less rugged terrains. The ruggedness number is the product of drainage density and relief (Strahler 1957). Alterations in either quantity affect erosion variables, gradient steepness, and length.

R_n is determined using the formula presented below:

$$R_n = B_h \times D_d \tag{3.6}$$

3.3.1.2.4. Height of Basin Mouth/Uutlet (z)

The height of the basin mouth/outlet is the lowest point of elevation on the watershed or the outlet of the watershed.

3.3.1.2.5. Total Basin Relief (H)

The total relief of a drainage basin denotes the vertical distance between its greatest elevation and the lowest point on the valley floor or basin outflow. This measurement indicates the total elevation range and energy potential of the watershed, which subsequently affects slope formation, runoff characteristics, and erosion severity (Schumm, 1956).

3.3.1.2.6. Relative Relief Ratio (R_{hp})

The notion of relative relief (R_{hp}), proposed by Melton (1957), employs watershed perimeter and total relief to assess local elevation fluctuation within a basin. It denotes the variation in elevation within a specified region in relation to a local base level, offering a more nuanced comprehension of the terrain's slope attributes and geomorphic processes (Melton, 1957). Relative relief, encompassing both vertical and areal components, effectively indicates landform development and morphogenetic procedures within a region (Bhunia *et al.,* 2018).

The parameter is computed via the expression:

$$R_{hp} = \frac{H \times 100}{P} \tag{3.7}$$

Where H = Maximum elevation and P = perimeter.

3.3.1.2.7. Gradient Ratio (G_r)

Gradient ratio quantifies the slope of the main channel by comparing the elevation change from source to mouth (a-b) against the stream's longitudinal distance (L_s) within the watershed boundaries (Strahler, 1964). Following the approach outlined by Sreedevi *et al*., 2005, the ratio was computed as follows:

$$G_r = \frac{(a - b)}{L_s} \tag{3.8}$$

3.3.1.2.8. Melton Ruggedness Number (MRn)

A slope indicator called the Melton Ruggedness Number (MRn) uniquely represents the relief ruggedness within a watershed.

3.3.1.3. Aerial Aspects

3.3.1.3.1. Drainage Density (D_d)

The total length of all stream segments divided by the total area of the basin serves as a primary indicator of landscape connectivity and hydrological behavior. According to Shekar & Mathew (2024), D_d not only reflects the spacing of the drainage network but also provides an indirect assessment of the underlying lithology. This measure is particularly vital when identifying potential groundwater recharge zones (Shekhar & Mathew 2024). Generally, low D_d values are found in permeable, heavily vegetated regions with minimal relief (Vittala *et al.,* 2004). In contrast, high D_d measurements typically signify impermeable surfaces, sparse vegetation, and rugged topography (Nautiyal, 1994)

The subsequent formula was employed to obtain D_d:

$$D_d = \frac{L_u}{A} \tag{3.9}$$

Where L_u = total stream length, A = watershed area.

The texture of a watershed elucidates the idea of drainage density by detailing the spatial arrangement and distribution of stream channels within a basin (Horton, 1945). It indicates the extent of division and the structure of a landscape, hence representing the proximity of channel spacing (Schumm, 1956). A fine texture, with a drainage density surpassing 4.97, signifies severely dissected terrain characterized by tightly packed streams, resulting in a complicated drainage network (Shekar & Mathew, 2024). These basins are generally linked to steep gradients and swift runoff, typical of regions with restricted infiltration and significant erosive capacity (Horton, 1945). A fine texture, associated with drainage densities ranging from 3.73 to 4.97 (**Table 3.4**), indicates relatively lower yet still dense drainage patterns, typically observed in moderately steep terrains with well-established stream systems (Shekar & Mathew, 2024). The moderate texture, characterized by drainage densities ranging from 2.49 to 3.73, indicates gentle slopes and a sparsely distributed channel network, implying diminished terrain roughness and intermediate runoff potential (Strahler, 1964). The coarse texture, characterized by drainage densities ranging from 1.24 to 2.49, signifies subdued terrain and widely dispersed streams, typically linked to less erosive environments (Schumm, 1956). A notably coarse texture (D_d < 1.24) defines flat or low-relief areas with sparsely scattered channels and inadequately integrated drainage networks (Shekar & Mathew, 2024). Consequently, drainage texture serves as a significant morphometric indicator for evaluating terrain subdivision, slope conditions, and hydrological responses within a watershed (Horton, 1945).

Table 3.4: Drainage density-based watershed texture

Drainage density	Textures
> 4.97	Very fine
3.73——4.97	Fine
2.49——3.73	Moderate

Table 3.4 (continued)

1.24——2.49	Coarse
<1.24	Very coarse

3.3.1.3.2. Stream Frequency (F_s)

It is defined as the total number of stream segments per unit area (Horton, 1945). This step is primarily governed by the lithological properties of the catchment and the overall geometry of the drainage system (Horton, 1945). High F_s values typically correlate with elevated surface runoff, impermeable or resistant bedrock, and stream frequencies are characteristics of watersheds with minimal relief and highly permeable surface materials (Obi *et al.,* 2002). **Table 3.5** illustrates that F_s is characterized into five distinct classes.

The following formula was used to get F_s:

$$F_s = \frac{\sum N_u}{A} \quad (3.10)$$

Where, N_u = total watershed stream numbers, and A = watershed area.

In areas designated with a “Very High” stream frequency, there are generally 20 to 25 streams per km^2 (Horton 1945). These regions are distinguished by a condensed network of rivers, signifying a substantial degree of hydrological movement (Shekar & Mathew 2024). Descending the spectrum, regions designated as “High” stream frequency display a little reduced density, with roughly 15 to 20 streams per km^2 (Schumm 1956). Despite being regarded as relatively compact, these places may possess fewer streams than those designated as “Very High” (Strahler 1964). The "Moderately High" stream frequency category includes areas with 10 to 15 streams per square kilometer (Shekar & Mathew, 2004). These places exhibit a moderate concentration of streams, signifying a notable presence of waterways, albeit less evident than the preceding groups (Strahler 1964). Areas with a "Moderate" stream frequency show a density of 5 to 10 streams per square kilometer (Shekar & Mathew, 2024). Although exhibiting a significant presence of streams, these regions demonstrate a relatively modest degree of hydrological action relative to the higher classifications. Regions characterized by a “Low” stream frequency demonstrate the minimal stream density, ranging from 0 to 5 streams per km^2 (Shekar & Mathew, 2004). These regions may have a reduced number of streams or a more scattered pattern of streams, signifying a diminished amount of hydrological movement. Comprehending the stream frequency distribution per square kilometer yields critical insights for diverse applications, including land supervision, environmental evaluations, and water resource planning.

Table 3.5: Stream frequency distribution based on square kilometers of streams

Stream frequency	Number of streams per square kilometer
Very High	20-25
High	15-20
Moderately high	10-15
Moderate	5-10
Low	0-5

3.3.1.3.3. Drainage Texture (D_t)

Horton (1932) initially defined drainage texture as the aggregate of all stream segments across all orders within a specified border. It is denoted by D_t (Horton 1932). Various natural elements, such as flora, precipitation, geology, climate, infiltration capacity, soil classifications, developmental stage, and topography, influence drainage texture (Smith, 1950). D_t classification is synonymous with drainage density classification. Horton characterized drainage texture as comprising drainage density and stream frequency, and recognized infiltration capacity as the paramount factor influencing Dt. **Table 3.6** shows five categories of drainage texture.

D_t is calculated using the formula shown below:

$$D_T = \frac{\sum N_u}{P} \tag{3.11}$$

Where N_u = stream numbers, P = watershed perimeter.

The texture of drainage is essential for comprehending and evaluating the attributes of a drainage system. It pertains to the dimensions of particles or substances within the system (Horton 1932). Very fine drainage texture encompasses bigger particles with a size above 08 units. Fine drainage texture comprises relatively tiny particles, ranging from 06 to 08 units (Shekar & Mathew, 2004). Restrained drainage texture denotes particles of intermediate size, varying from 0.4 to 0.6 units. Finally, coarse drainage texture consists of bigger particles measuring between 02 and 04 units. It is crucial to acknowledge that the particular unit of measurement is not delineated in the provided table. In discussions about drainage texture, it is essential to specify the units to fully comprehend the dimensions of particles or constituents inside a drainage system (Shekar & Mathew, 2024).

Table 3.6: Drainage texture and range

Drainage Texture	**Range**
Very fine	>8
Fine	06- 08
Moderate	04- 06
Coarse	02- 04
Very coarse	< 02

3.3.1.3.4. Form Factor (R_f)

The form factor (R_f) is a dimensionless parameter defined by Horton (1932) as the ratio between the basin area and the square of its length. This indicator is instrumental in categorizing watershed morphology, with values for more elongated shapes (Rai *et al.*, 2017). Geometrically, a circular basin is prone to intense, short-duration peak flows, while an elongated system tends to distribute runoff over a more extended period, resulting in muted peak discharges (Chandrashekar *et al.*, 2015).

The subsequent formula was used to get the Form factor:

$$R_f = \frac{A}{L_b^2} \tag{3.12}$$

3.3.1.3.5. Circularity Ratio (R_c)

The circularity ratio (R_c) serves as a quantitative measure of a basin's shape by comparing its total area to that of a circle with a matching perimeter (Miller, 1953). This metric typically ranges between 0-1, reflecting the complex interplay of a watershed's topographic relief, climatic conditions, and geological structures (Bali *et al.*, 2012). Furthermore, R_c is sensitive to variations in stream frequency, channel length, and land-use patterns within the catchment (Shekar & Mathew, 2024). The value is derived using the following formula:

$$R_c = \left(\frac{4\pi A}{P^2}\right) \tag{3.13}$$

Where π = 3.14, P = Watershed perimeter, and A = watershed area.

3.3.1.3.6. Elongation Ratio (R_e)

It is defined as the ratio of the diameter of a circle with an area equal to the basin and the maximum length of that basin (Horton 1945). **Table 3.7** (Shekar & Mathew, 2024) delineates five classes of drainage texture. The analysis of basin morphology is a vital indicator that offers perception into the hydrological composition of a drainage basin. An elongated basin is less efficient at discharging runoff compared to a circular basin.

The elongation ratio was determined utilizing the formula:

$$R_e = \frac{(2(A/\pi)^{0.5})}{L_b} \tag{3.14}$$

If the elongation ratio is below 0.5, the shape is seen as more elongated. Shapes within the range of 0.5 to 0.7 are classified as elongated (Schumm 1956). While they exhibit some elongation, it is less prominent than that of the "more elongated" category (Strahler 1964). Shapes with elongation ratios ranging from 0.7 to 0.8 are considered minimally elongated. Finally, geometries with elongation ratios between 0.8 and 0.9

are classified as oval (Pareta & Pareta, 2012). The major and minor axes in this range exhibit similar lengths, yielding a more rounded or oval configuration.

Table 3.7: Elongation ratio and shape range

Watershed	**Shape Ratio**
More elongated	Less than 0.5
Elongated	Between 0.5 and 0.7
Less elongated	Between 0.7 and 0.8
Oval	Between 0.8 and 0.9
Circular	Between 0.9 and 0.1

3.3.1.3.7. Length of Overland Flow (L_o)

The phrases "overland flow" and "surface runoff" denote two separate types of water movement. Overland flow denotes precipitation that traverses the land surface, ultimately entering stream channels, whereas surface runoff pertains to the movement of water inside the stream channels that departs the watershed (Shekar & Mathew, 2024). The prevalence of overland flow fluctuates according to watershed size, with smaller watersheds exhibiting a more pronounced impact of overland flow. Horton (1945) noted that overland flow generally displays laminar properties, categorized by a shallow depth and limited distance. The extent of overland flow significantly influences the hydrological and physiographic evolution of drainage watersheds. It functions as an autonomous variable affecting various methods. Overland flow can be estimated by calculating the reciprocal of D_d divided by two, signifying an inverse correlation with the mean slope of the channel (Chow *et al.*, 1988). This variable is intricately linked to the length of sheet flow and is denoted by the sign L_o.

L_o is calculated using the formula provided below:

$$L_o = \left(1/_{(2D_d)}\right) \tag{3.15}$$

Where "D_d" is the drainage density.

3.3.1.3.8. Constant Channel Maintenance (C_{cm})

The parameter known as the constant of stream maintenance is the inverse of D_d (Schumm, 1956). As this constant, measured in km^2/km, possesses the measurement of length, its magnitude increases with the size of the landform unit (Shekar & Mathew, 2024). It is represented by C_{cm}.

The calculation for the Constant channel maintenance utilized the formula:

$$C_{cm} = \left({}^{1}/_{D_d}\right) \tag{3.16}$$

The most erosion-resistant channels exhibit superior resilience to erosion and necessitate less maintenance to preserve stability (Schumm 1956). They can efficiently manage sediment under a threshold of less than 0.5. The erodibility of these channels is marginally higher than that of the most resistant classification; however, they have commendable stability (Bali *et al.*, 2012). These channels can contain sediment within the range of 0.4 to 0.5, signifying their capacity for moderate sediment transmission (Strahler 1964). Moderately low erodible channels reveal a moderate degree of erodibility, situated between the low erodible and moderate erodible classifications (Shekar & Mathew, 2024). They can carry sediment within a range of 0.2 to 0.3, signifying an elevated risk for erosion and sediment displacement (**Table 3.8**). Channels with greater erodibility are the most susceptible to erosion. They have the highest erodibility and can transfer sediment over a range exceeding 0.2. These channels necessitate meticulous management and maintenance measures to alleviate erosion and preserve their functionality (Shekar & Mathew, 2024).

Table 3.8: Constant channel maintenance and range (Schumm, 1964)

Constant channel maintenance	Range
Least erodible	Less than 0.5
Low erodible	Between 0.4 and 0.5
Moderately low erodible	Between 0.3 and 0.4
Moderate erodible	Between 0.2 and 0.3
More erodible	More than 0.2

3.3.1.3.9. Infiltration Number (I_f)

As established by Faniran (1968), higher infiltration numbers (I_f) correlate with diminished infiltration rates and intensified surface runoff. This parameter serves as a critical proxy for a watershed's hydrological efficiency, revealing a strong negative correlation with subsurface water retention (Horton, 1945). Research by Rai *et al.*, 2017 confirms that I_f measurements consistently signal lower infiltration potential and higher drainage discharge.

The calculation for I_f is as follows:

$$I_f = (F_s \times D_d) \qquad (3.17)$$

3.3.1.3.10. Basin Area (A)

The spatial dimensions of a watershed and the cumulative length of its channels are fundamental parameters in both geomorphology and hydrology (Horton, 1945). Schumm (1964) established that a significant relationship exists between the contributing area of a catchment (A) and the total length of its constituent streams. This principle suggests that larger drainage basins generally support more complex and extensive stream networks (Strahler, 1964). Understanding this link is crucial for environmental modelling, as it provides a window into the structural complexity and hydrological behavior of a specific region (Shekar & Mathew 2024)

3.3.1.3.11. Basin Perimeter (P)

The basin perimeter (P) is defined as the total linear measurement of the boundary around a catchment region (Strahler, 1964). This measure delineates the boundary between neighbouring watersheds and serves as a crucial indicator of a basin's geometric and spatial arrangement (Horton, 1945). Shekar & Mathew (2024) assert that the perimeter offers critical information regarding the watershed's configuration, which subsequently affects sediment movement and the conversion of precipitation into discharge. Moreover. Schumm (1956) underscores that the analysis of P is essential for evaluating drainage connectivity and the efficacy of surface runoff channels

3.3.1.3.12. Length of Basin (L_b)

Basin length is the longest dimension of a basin parallel to the main drainage line (Schumm, 1956).

3.3.1.3.13. Fitness Ratio (R_f)

The fitness ratio is a statistic used in hydrology and geomorphology to assess the topographic efficiency of a river network within a catchment area (Horton 1945). The computation entails dividing the total length of the primary channel(s) within a specific watershed by the perimeter of that catchment (Schumm 1956). The fitness ratio is predicated on the notion that a well-established river system will have a greater ratio of channel length to its catchment periphery. It assesses the extent to which a network of streams can optimize its drainage effectiveness by reducing the extent of its primary channels in relation to the magnitude of the adjacent catchment area (Pareta & Pareta, 2012). An elevated fitness ratio signifies a better effective drainage framework, as the primary channel(s) encompass a greater amount of the catchment periphery (Shekar & Mathew, 2024). This indicates that water discharge from the watershed is effectively directed through the river system, minimizing flood risk and optimizing flow capacity. The fitness ratio is an effective tool for analyzing river network evolution, catchment hydrology, and understanding the relationship between topography and drainage trends. It offers insights into the efficiency and operation of river systems, facilitates environmental planning, and assists in flood prediction and river management (Shekar & Mathew, 2024).

3.4 Hydrological Modelling Using SWAT

Input data, such as digital elevation maps, soil maps, and landuse maps, were obtained from the GIS database, meteorological data, and hydrological data from the Department of Water Resources, Nagaland, and the Department of Soil and Water Conservation, Nagaland. The GIS data include: DEM, LULC maps, and soil maps. Climate data includes precipitation, maximum and minimum air temperature, relative humidity, solar radiation, and wind speed. The runoff data were required to calibrate and validate the model. The SWAT model version 2012 was applied to simulate runoff, and the model was calibrated and validated by the SWAT-CUP software. The flow diagram of the execution of the SWAT model is shown in **Figure 3.3**.

3.4.1 Overview of the SWAT Model

SWAT 2012 is a comprehensive, physically based, continuous simulation watershed model. It can replicate surface runoff, sediment output, and nutrient losses from small, medium, and large watersheds. The framework is distributed, deterministic, computationally feasible, and can simulate continuously over extended periods (Arnold *et al*., 1998). Instead of using regression equations to connect input and output variables, SWAT requires specific data about weather, topography, soil properties, vegetation, and land administration practices within the basin (Gassman *et al.,* 2007). It has eight main modules: hydrology, climate, sedimentation, agricultural management, water quality, land cover, water bodies, and main channel processes, as shown in **Figure 3.4**.

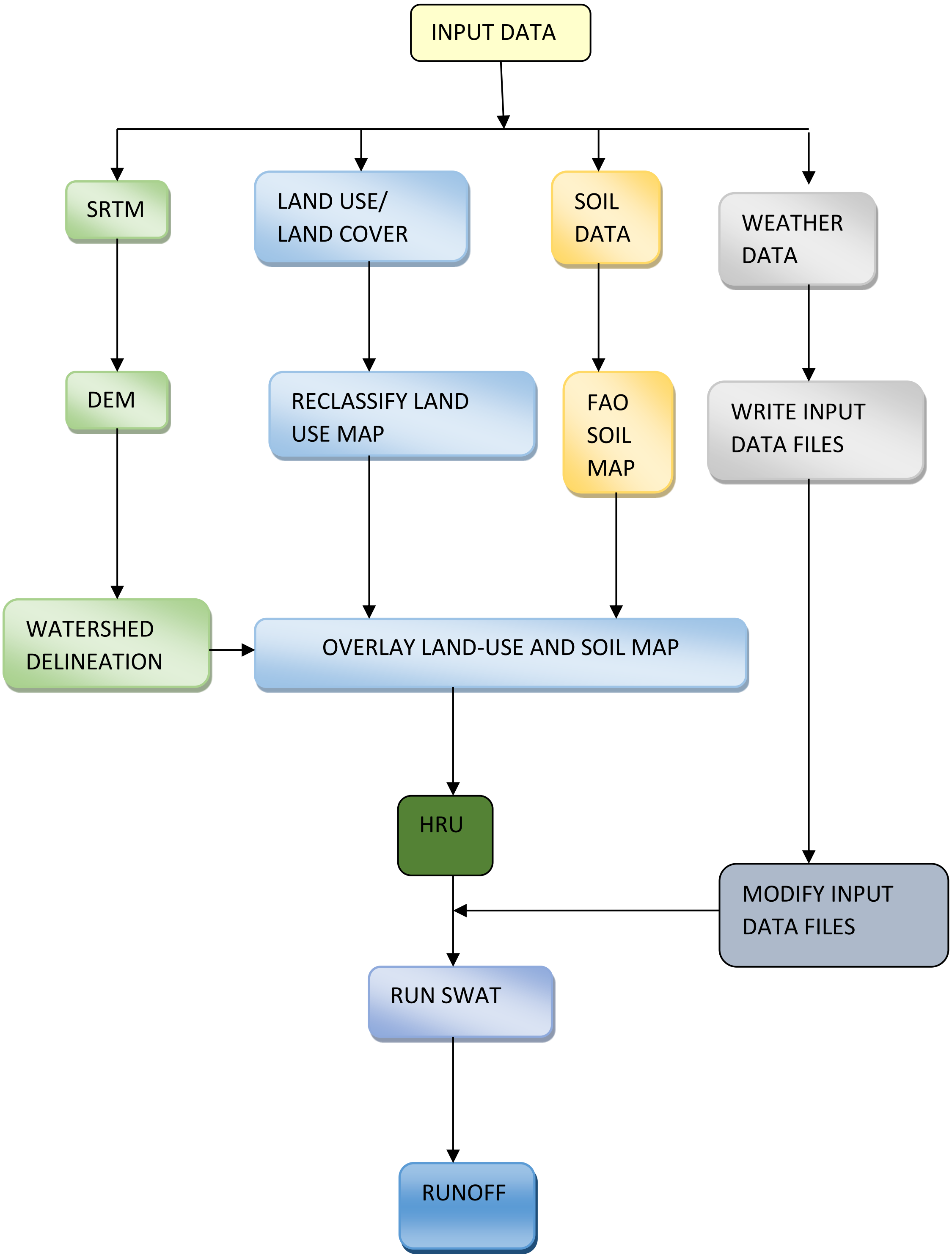

Figure 3.3: Flow diagram of execution of SWAT model

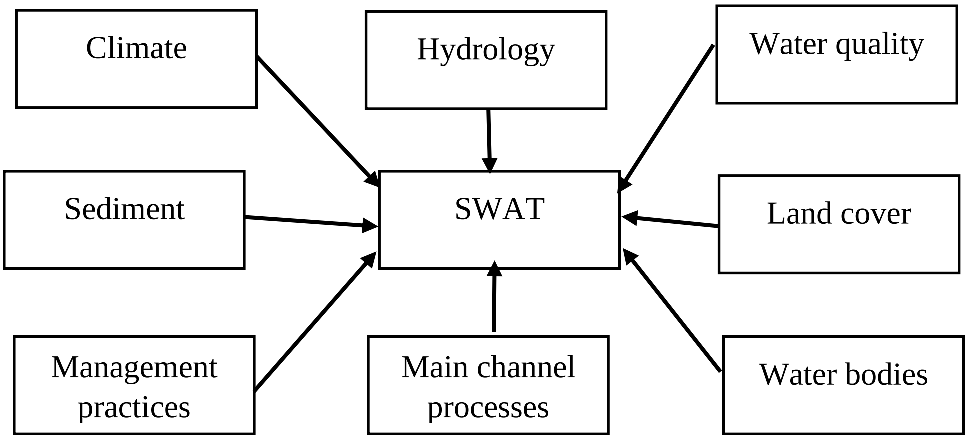

Figure 3.4: Modules of SWAT model

3.4.2 Model Development

SWAT, the Soil and Water Assessment tool, is a watershed-scale model developed by the United States Department of Agriculture (USDA) – Agricultural Research Service (ARS), Grassland, Soil and Water Research Laboratory in Temple, Texas (Arnold *et al*., 1998). The current version of the SWAT, known as SWAT 2012, is the result of the combined effort of many researchers over the last three decades. The SWAT model has evolved from the SWRRB (Simulator for Water Resources in Rural Basins) model, which was created to evaluate the effects of management on water and sediment transport for ungauged rural watersheds. A significant improvement was achieved in the augmentation of the surface runoff component and improved catchment representation for as many as ten sub-watersheds, to predict watershed water yield. additional enhancements encompassed an optimized peak runoff rate methodology, the computation of transmission losses and the addition of various new components, notably groundwater return flow (Arnold *et al.*, 1993), reservoir retention, the EPIC (Erosion Productivity Impact Calculator) crop growth sub model, a weather generator, and sediment transport, pesticide fate component, optional USDA-SCS (United States Department of Agriculture- Soil Conservation Service) technology for determining peak runoff values and freshly formulated sediment yield formulas. These adjustments enhanced the model's capability to address a diverse range of watershed water quality management problems. Arnold *et al*. (1998) created the Routing Outputs to Outlet (ROTO) model in the early 1990s to evaluate an assessment of the downstream effects of water management. SWRRB and ROTO were consolidated into the unified SWAT model. SWAT has experienced continued evaluation and enhancement of its capabilities since it was created in the early 1990s. Significant enhancements for earlier iterations of the model (SWAT 94.2, 96.2, 98.1, 99.2, and 2000) are explained below (Arnold & Fohrer, 2005; Steven *et al.*, 2005). **Figure 3.5** shows the schematic depiction of the SWAT developmental history.

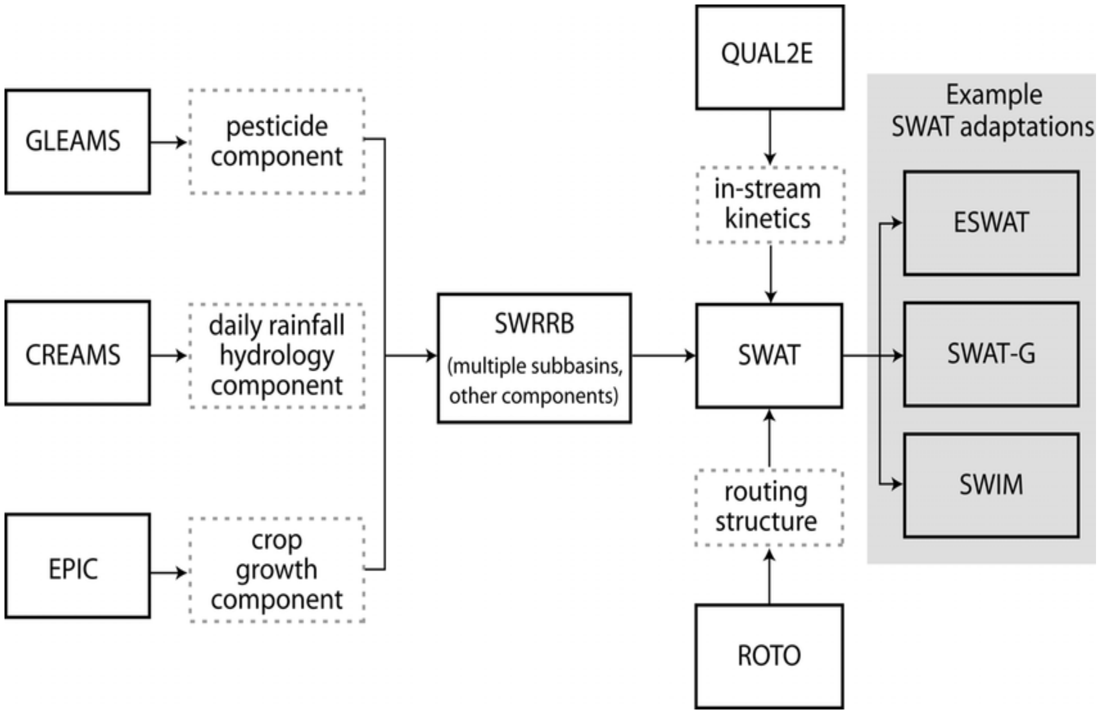

Figure 3. 5: Schematic representation of SWAT developmental history

SWAT is written in FORTRAN (Formula Translation) 90 and consists of 220 subroutines and just over 40,000 lines of code. GIS interface has been developed for SWAT using both GRASS (Graphical Resources Analysis Support System) and ArcGIS. The developed interfaces automatically subdivide a watershed (grids or sub-watersheds) and then extract model input data from map layers and associated relational databases for each sub-watershed. Soil, land use, weather, management, and topographic data are collected and written to the appropriate model input files. The output interface enables users to display output maps and graph output data by selecting a sub-watershed from the GIS map. SWAT is capable of simulating a number of different physical processes occurring in a watershed. For modeling purposes, a watershed is separated into numerous sub-watersheds that are categorized by main land use, soil type, and management, which are further subdivided into hydrologic response units (HRUs) that consist of homogeneous land use, management, and soil characteristics. The use of sub-watersheds in a simulation is mainly valuable when diverse areas of the watershed are subject to land uses or soils different enough in properties to effect hydrology. By partitioning the watershed into sub-watersheds, the user can reference different areas of the watershed to one another spatially. Input information for each sub-watershed is clustered or organized in the various categories, viz., climate; hydrologic response units (HRUs); ponds/wetlands; groundwater, and the main channel or the reach draining the sub-watershed. HRUs are lumped land areas within the sub-watershed that are comprised of unique land cover, soil, and management blends.

3.4.3 Description of the SWAT Model

According to Arnold *et al*., 2012, SWAT is a daily time-step river basin model that is physically based, semi-distributed, and process-based. SWAT works well for watershed discretization since the delineation procedure divides a huge watershed into several smaller sub-basins. Based on the local land use and soil profile, these sub-basins are further subdivided into even smaller areas known as hydrological response units (HRUs). In essence, all feasible combinations of soil and land use data result in the formation of HRUs. Thus, as the name implies, HRUs are the result of several hydrological components, such as runoff and sediment production, responding to specific combinations of soil properties and land use. It is possible to categorize the SWAT model into two main parts: the routing phase and the land phase. The eight main characteristics that are addressed by the land phase component of SWAT are agricultural management, hydrology, weather, sedimentation, soil temperature, crop growth, nutrients, and pesticides. The movement, channel flow, and modifications of all the parameters related to the land phase component of SWAT are under the purview of the routing phase component of the organization.

According to Arnold *et al.*, 1998, the SWAT model has the following benefits:

1. It is a physically based distributed model that is rather easy to use, incorporates readily available inputs, and is basic.

2. Operating on a large basin in a large basin is computationally efficient.
3. It permits a great deal of spatial detail.
4. It is not constrained by the spatial scale and may simulate different land management situations.
5. Because it is a continuous-time model, it can simulate the long-term effects of management changes.

According to Arnold *et al.,* 1998, the SWAT model has the following drawbacks:

1. It ignores the precipitation intensity, which is a far more important aspect in runoff estimation, and only accounts for the amount of precipitation in the form of daily or sub-daily precipitation.
2. Because of the high reliance on data for its functioning, runoff estimation can be significantly erroneous when relying just on the data from a single station to represent a whole watershed or when attempting to "spatially weight" the precipitation for a watershed. This is especially true for data related to precipitation.
3. Since SWAT simulates continuous time rather than event-based flooding and sediment movement, it lacks detail.
4. For long-term simulations, the relatively basic sediment equations that are employed may be unrealistic since they assume that the channel's dimensions remain constant throughout the simulation period.

3.4.3.1 Hydrological Component of SWAT

Replication of the hydrology of a watershed is done in two discrete components. The first one is the land phase of the hydrologic cycle that controls the water movement on and in the land and determines the water, sediment, nutrients, and pesticides that will be loaded into the main stream. Hydrological components modeled in the terrestrial phase of the hydrological cycle are canopy storage, infiltration, redistribution, evapotranspiration, lateral subsurface flow, surface runoff, ponds, and tributary channels return flow (Arnold *et al.,* 1998). The second component is the routing phase of the hydrologic cycle, in which water is routed in the channel network of the watershed, carrying the sediment, nutrients, and pesticides to the outlet. In the land phase of the hydrologic cycle, SWAT models the hydrological cycle with the water balance equation and incorporates key hydrological processes like precipitation, evapotranspiration, overland flow, lateral flow, baseflow, and soil water storage (Arnold *et al.*, 1998) as shown in **Eq.3.18**. The water balance for the soil component of each HRU is expressed as;

$$SW_f = SW_i + \sum_{i=1}^{t}(R_{day} - ET_a - Q_{sur} - Q_1 - W_p + CR) \tag{3.18}$$

Where, SW_f= Final soil water content of the soil layer (mm),

SW_i= Initial soil water content of the soil layer on day i (mm),

t= Time (days),

R_{day}= Amount of precipitation on day *i* (mm),

ET_a= Amount of evapotranspiration on day *i* (mm),

Q_{sur}= Amount of surface runoff on day *i* (mm),

Q_1= Lateral flow on day *i* (mm),

W_p= Amount of water percolating to the underlying soil layer on day *i* (mm), and

CR= Upward movement of water from the shallow aquifer on day *i* (mm).

The contribution to runoff from each HRU (assuming a single soil layer) can be represented by **Eq. 3.19**

$$Q = R_{day} - ET_a - Q_{sur} - Q_1 - W_p - CR - Q_{gws} - Q_{gwd} \tag{3.19}$$

Q= Runoff leaving the HRU on day *i* (mm),

Q_{gws}= Base flow from the shallow aquifer on day *i* (mm),

Q_{gwd}= Groundwater flow lost to the deep aquifer on day *i* (mm)

The total amount of water that runs off the watershed is the sum of the Q contributions from each HRU. The following are explanations of the several hydrologic parts of SWAT modelling:

3.4.3.2 Precipitation

The key component in watershed modeling is precipitation, which can be either rain or snow. The accuracy of the input greatly influences the model's reliable output.

Therefore, precipitation is the most crucial factor in watershed modeling. In humid regions, rain is the primary source of precipitation, while in cold areas, snow generally serves as the main source. This distinction clarifies the surface and subsurface hydrological cycle, as shown in **Figure 3.6.** Precipitation can be categorized as either rain or snow based on the average daily temperature (Beven, 2012). In the SWAT model, the critical temperature used to differentiate snow from rain is set by the user (Arnold *et al.*, 2012). If the average daily air temperature falls below this critical temperature, the precipitation is classified as snow. Snowfall accumulates on the ground as snowpack, and the water stored within the snowpack is measured as snow water equivalent (Beven, 2012). The snowpack grows with additional snowfall and decreases through snowmelt or sublimation. In the SWAT model, snowmelt is calculated based on air temperature, snowpack temperature, a melting factor, and snow cover. The melted snow, represented by snow water equivalent, is then added to the precipitation to determine surface runoff and percolation (Arnold *et al.,* 2012).

Due to the limited availability of rainfall stations within the study area, spatial variability in rainfall was addressed using the best available combination of observed and gridded data. In the Dzuza watershed, only one rainfall station was available, so rainfall input was taken from that station. In the Dhansiri river basin, two observed rainfall stations along with IMD gridded rainfall data were used to better represent the spatial distribution of rainfall. Since the Khova watershed is a sub-basin of the Dhansiri river basin, it was represented using the same rainfall data framework. The use of both station observations and gridded rainfall data helped account for spatial variability more effectively in this data-scarce region.

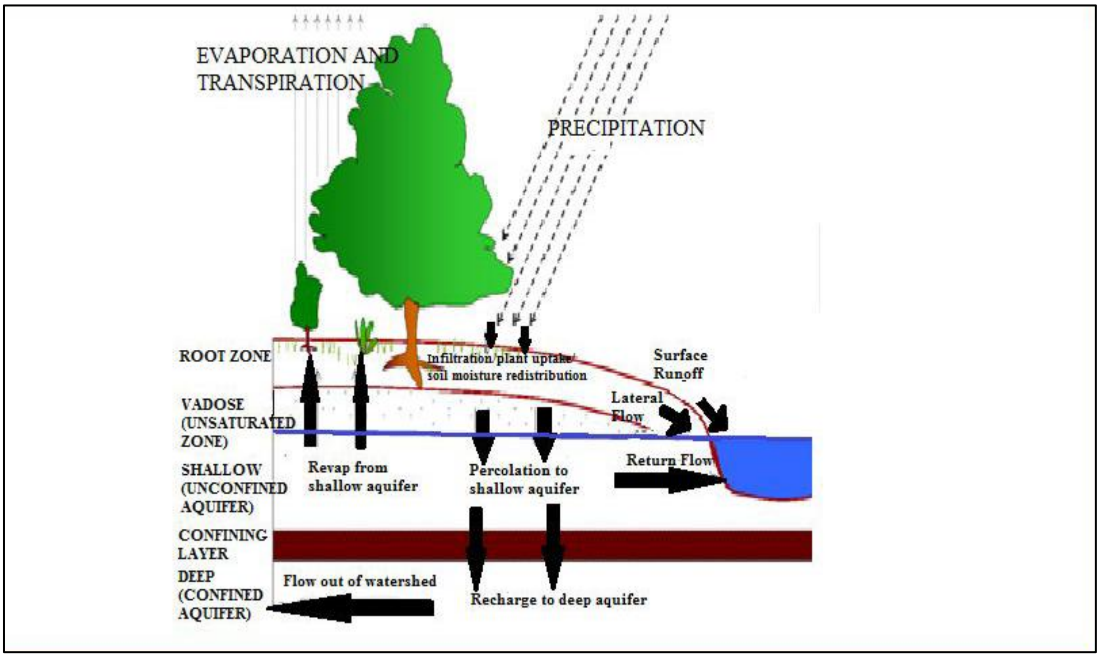

Figure 3. 6*:* Schematic representation of various components of hydrologic cycle

3.4.3.3 Evapotranspiration

Evapotranspiration (ET) constitutes a fundamental element of the hydrologic cycle (Beven, 2012). It influences the water balance from the moment water is deposited on the land as precipitation until the residual flows into the ocean. ET includes evaporation of water from land and water surface, and transpiration by vegetation. Evapotranspiration from vegetative surface is the result of several processes, like radiation exchange, vapor transport, and biological growth operating within a system involving the atmosphere, plant, and soil. The model provides three alternatives for calculating potential evapotranspiration (ET)-Penman-Monteith, Hargreaves, and Priestley-Taylor methods (Gassman *et al.,* 2007). The Priestley-Taylor method necessitates solar radiation and air temperature as inputs, whereas the Hargreaves approach requires simply air temperature. The Hargreaves or Priestley-Taylor methods provide options that give realistic results in most cases (Arnold *et al*., 1998). In the present study, Hargreaves' method was used for estimating the evapotranspiration.

3.4.3.4 Surface Runoff

Surface runoff constitutes a significant element of the hydrologic cycle within the SWAT model. It denotes the segment of precipitation that traverses the land surface and enters streams and rivers, instead of infiltrating into the soil or being absorbed by vegetation. The volume of surface runoff in the SWAT model is affected by various factors, including the intensity and duration of the precipitation event, the antecedent soil moisture conditions, the slope of the land, the length of the slope of the watershed, land cover of the watershed, and the existence of impervious surfaces (such as roads and buildings), which can exacerbate runoff. The SWAT model simulates surface runoff through various methods and equations that take consider these factors. For example, the model uses the Soil Conservation Service Curve Number (SCS-CN) approach to quantify the runoff generated by a given precipitation event, taking into account soil type, land use, and antecedent moisture conditions of the watershed. The volume and timing of surface runoff in the SWAT model can substantially affect water quality and quantity, since it can convey sediment, nutrients, and other contaminants from the land into streams and rivers. Therefore, precise modelling of surface runoff is essential for comprehending and managing the hydrology of a watershed.

This study employed the Soil Conservation Service method (SCS)-Curve Number (CN) approach for surface runoff estimation in the SWAT model, with a daily time step. The equation for the SCS curve number is:

$$Q_{surf} = \frac{(R_{day} - I_a)^2}{R_{day} + I_a + S} \qquad 3.20$$

Where,

Q_{surf} = accumulated runoff (mm)

I_a = daily rainfall depth (mm)

R_{day} = initial abstraction which includes surface storage, interception and infiltration before runoff (mm)

S = potential maximum retention

The potential maximum retention parameter exhibits spatial variability as a result of fluctuations in soil water content. The projected potential maximum retention is:

$$S = (\frac{25400}{CN} - 254) \qquad 3.21$$

Where,

CN = Curve number

The initial abstraction is commonly approximated as 0.2S in the above equation.

$$Q_{surf} = \frac{(R_{day} - 0.2I_a)^2}{R_{day} + 0.8S} \quad 3.22$$

For R_{day} > 0.2S

The SCS-CN is affected by soil properties, land use/land cover (LULC), and Antecedent Moisture Condition (AMC). The curve number was ascertained utilizing a land use map, a soil map, and sub-watershed maps. These maps were superimposed in ArcGIS, and statistical analysis was conducted on the data, including pixel counts for various land uses and soil textures. The weighted average curve numbers for each sub-watershed were computed utilizing this information as input for computational techniques.

In the SWAT model, surface runoff is estimated using the SCS Curve Number method, in which the default assumption for initial abstraction is Ia = 0.2S. This formulation is embedded in the standard SWAT runoff routine and has been widely used in SWAT applications worldwide, including studies from India (Neitsch *et al.*, 2011; Arnold *et al.,* 2012). However, hydrological studies in India have reported that, for many Indian watersheds, Ia = 0.3S may provide better runoff estimation under local conditions (Mishra & Singh, 2013). Since the present study used the standard SWAT structure without modifying the initial abstraction ratio, runoff from the study watersheds was computed using the default Ia = 0.2S assumption. Therefore, the runoff estimation in this study follows the standard SWAT methodology, although alternative values such as Ia = 0.3S have been suggested in the Indian literature for specific regional applications.

Overland flow is categorized into two portions: infiltration excess overland flow and saturation excess overland flow (Beven, 2012). When it rains hard enough that the soil can't absorb it entirely, it causes infiltration, overflow, and runoff. The saturation surplus runoff mechanism may manifest in the following scenarios: (1) in regions with elevated antecedent soil moisture levels; (2) where a thin soil layer restricts storage capacity; and (3) in places characterized by low permeability and little slope (Beven, 2012). Hence, surface runoff depends upon the infiltration capacity and degree of saturation of underlying soil layers. It also depends upon the vegetation cover of the ground as well as the degree of ground slope (Shekar & Mathew, 2024). To compute surface runoff in the SWAT model, either the SCS curve number method or the Green & Ampt infiltration equation (Green & Ampt, 1911) can be used. Before utilizing either method, the entire catchment basin is divided into several sub-basins. Thereafter, the overland flow for each sub-basin is predicted separately and routed through a channel system to calculate the total watershed surface runoff.

Surface runoff volume was estimated by the model using the Soil Conservation Service (SCS) curve number technique (USDA, 1972). The SCS curve number equation used in the model is as follows:

$$Q = \frac{(R - 0.2S)^2}{R + 0.8S} \quad 3.20$$

$$CN = \frac{25400}{245 + 8} \quad 3.21$$

Where Q is the daily runoff, R denotes the daily rainfall, and S signifies a retention parameter. The retention parameter, S, fluctuates (a) within sub-basins due to differences in soils, land use, management, and slope, all of which vary, and (b) over time as a result of alterations in soil water content. The parameter s is associated with the curve number (CN) by the SCS equation (USDA, 1972). Consequently, R and Q are represented in mm. CN represents the curve number for antecedent moisture condition (AMC) II. The values of the curve number for various land use circumstances and hydrologic soil groups are given in **Table 3.9**. These values are applied to AMC II only, *i.e.*, for average conditions. **Eq. 3.20** provides the runoff value (Q) expressed in depth units.

Table 3.9 Runoff curve numbers (AMC-II) for the Indian conditions

S. No	Landuse	Treatment/Practices	Hydrologic	Hydrologic Soil Groups			
				A	B	C	D
1.	Cultivated	Straight Row	-----	76	86	90	93
		Contour	Poor	70	79	84	88
			Good	65	75	82	86
		Contour & Terraced	Poor	66	74	80	82

Table 3.9 (continued)

			Good	62	71	77	81
		Bunded	Poor	67	75	81	83
			Good	59	69	76	79
		Paddy	-----	95	95	95	95
2.	Orchards	With under stony cover	--	39	53	67	71
		Without under stony cover	---	41	55	69	73
3.	Forest	Dense	-----	26	40	58	61
		Open		28	44	60	64
		Shrubs		33	47	64	67
4.	Pasture		Poor	68	79	86	89
			Fair	49	69	79	84
			Good	39	61	74	80
5.	Waste Land		---	71	80	85	88
6.	Hard surface		----	77	86	91	93

3.4.3.5 Infiltration

The infiltration has a vital function in supplying water for plant development and in recharging the groundwater aquifers. The rate of infiltration is affected by the soil's physical qualities, the amount of vegetation on the ground, the soil's initial water content, the temperature of the soil, and the amount of rain or snowmelt (Shekar & Mathew 2024). In the SWAT model, the amount of water infiltrating into the soil profile is estimated indirectly because the surface runoff is computed directly using either of the previously mentioned methods (Neitsch *et al*., 2011). Hence, the infiltrated water was determined as the difference between the volume of rainfall and the volume of surface runoff.

3.4.3.6 *Percolation*

The percolation component of SWAT employs a storage routing methodology integrated with a crack-flow model to forecast flow across each soil layer. When water infiltrates beneath the root zone, it is lost from the watershed, either into groundwater or appears as return flow in downstream basins. The storage routing technique is predicted on the equation:

$$SW_i = SW_{oi}e^{\frac{-\Delta t}{TT_i}} \tag{3.22}$$

where, SW_{oi} and SW_i are the soil water contents at the beginning and end of the day in mm, Δt is the time interval (24 h), and TT_i is the travel time through layer i in h. The percolation is computed as under:

$$O_i = SW_i\left[1 - SWe^{\frac{-\Delta t}{TT_i}}\right] \tag{3.23}$$

Where, O is the percolation rate in mmd^{-1}.

The travel time, TT_i, is computed for each soil layer with the linear storage equation:

$$TT_i = \frac{SW_i - FC_i}{H_i} \tag{3.24}$$

where, H_i is the hydraulic conductivity in mmh^{-1} and FC_i is the field capacity for layer i in mm. The hydraulic conductivity varied from the saturated conductivity value at saturation to near zero at field capacity.

3.4.3.7 *Lateral Subsurface Flow*

Lateral subsurface flow, or interflow, arises beneath the ground surface yet above the saturated soil and bedrock layer (Beven, 2012). It contributes to runoff within the watershed. In the SWAT model, interflow is computed using the redistribution phenomenon, characterized as the continuous movement of water through soil profiles (Neitsch *et al.,* 2011). The redistribution component is computed in SWAT using a kinematic storage model developed by Sloan & Moore 1984. Since the redistribution phenomenon is influenced by soil temperature, the SWAT model does not allow redistribution from the soil layer with a temperature of 0°C or below (Arnold *et al.,* 2012).

3.4.3.8 Return Flow

A segment of the input precipitation ultimately recharges groundwater aquifers after percolating through various soil layers. Return flow, or baseflow, is the water that originates from groundwater and contributes to streamflow (Beven, 2012). In the SWAT model, groundwater is divided into two aquifer systems: (1) shallow aquifer, and (2) deep aquifer. A shallow aquifer is an unconfined aquifer that contributes to the baseflow of the stream within the watershed, while a deep aquifer is a confined aquifer that supplies baseflow to the stream outside the delineated watershed (Arnold *et al.,* 1993). Therefore, water recharging the deep aquifer does not contribute to runoff within the watershed boundary. To estimate the amount of water percolating through each soil layer, the SWAT model employs a storage routing mechanism combined with a crack-flow routine. Using this method, the contribution of water to recharge either the shallow or deep aquifer can be determined.

3.4.4 Runoff Modelling using SWAT

SWAT simulates surface runoff volumes for each HRU using either of the two methods: the SCS Curve Number (CN) procedure and the Green-Ampt infiltration method. Later requires sub-daily precipitation data, thus restricting its use. The SCS-CN equation is an empirical model involving rainfall-runoff relationships from small rural watersheds, and the model predicts the amount of surface runoff under varying land-use and soil types. The SCS-CN equation is:

$$Q_{surf} = \frac{(R_{day} - I_a)^2}{R_{day} - I_a + S} \tag{3.25}$$

Where, Q_{surf}= Accumulated runoff or rainfall excess (mm),

R_{day}= Rainfall depth of the day (mm),

I_a= Initial abstractions, which include surface storage, interception, and infiltration before runoff (mm), and

S= Retention parameter (mm).

The retention parameter, S, varies spatially due to changes in soils, land use, management, and slope, and temporally due to changes in soil water content, and is defined by the equation as:

$$S = 25.4 + (\frac{100}{CN} - 10) \quad (3.26)$$

Where, CN= Curve number for the day

The initial abstraction I_a is estimated as $0.2S$ and

Thus, **Eq 3.26** becomes:

$$Q_{surf} = \frac{(R_{day} - 0.2S)^2}{R_{day} + 0.8S} \quad (3.27)$$

Runoff will occur when $R_{day}>I_a$

The curve number depends on the soil's permeability, land use, and previous soil water conditions. Soil can be classified into one of four groups based on its runoff potential: A, B, C, and D. As you move from A to D, the runoff potential increases, with 'A' having the lowest and 'D' the highest. Besides soil properties and land use, antecedent soil moisture conditions also influence the curve number. The SCS defined three antecedent moisture conditions (AMC): I – dry (wilting point), II – average moisture, and III – wet (field capacity). In SWAT, the curve number for AMC II is used as a default; the model then adjusts the CN based on antecedent moisture, which is derived from daily rainfall data. The retention parameter can vary depending on the water content within the soil profile.

3.4.5 Input Data Preparation

The SWAT model requires high data input but can deliver quality outputs after specifying basic input variables and calibrating them. The necessary ArcSWAT spatial datasets include the SRTM Digital Elevation Model (DEM), LULC, and soil map.

3.4.5.1 Digital Elevation Model

The SRTM-DEM was used to meet the topographic data needs of SWAT. SRTM data have a resolution of 30 m, and the dataset was downloaded from the USGS website. The DEM was used to calculate percent slope values, automatically delineate watershed boundaries, define stream networks, and identify gage outlets.

3.4.5.2 Slope Map

The slope attributes of the three watersheds were obtained from the Soil and Water Assessment Tool (SWAT), which employs Digital Elevation Model (DEM) data to categorize and examine terrain gradients. Slope is a vital parameter in SWAT, as it affects surface runoff, infiltration, soil erosion, and sediment yield processes. This study classified slope distribution into five categories: 0–10%, 10–20%, 20–30%, 30–50%, and greater than 50%. The area statistics for various slope classes in the Dzuza, Dhansiri river basin, and Khova sub-basin are displayed in **Tables 3.10, 3.11**, and **3.12**.

The Dzuza watershed is mostly defined by steep to very steep inclines. The predominant portion of the basin is categorized within the 30–50% slope range, encompassing 129.245 km² (36.92%), succeeded by slopes exceeding 50%, which constitute 91.201 km² (26.05%) of the watershed area (**Table 3.10**). Gentle slopes (0–10%) are restricted, covering merely 12.444 km² (3.55%). The slope distribution indicates the hilly and rough topography of the Dzuza watershed, rendering it very vulnerable to runoff, landslides, and significant erosion risks, while providing little potential for extensive agricultural growth (**Figure 3.7 (a)**).

Table 3.10: Area statistics of different slopes in Dzuza Watershed

Sl. No.	Slope Name	Area (km^2)	Per cent of Watershed Area
1	0-10	12.4441	3.554998
2	10-20	42.6541	12.18531
3	20-30	74.50076	21.28318
4	30-50	129.245	36.92237
5	50-9999	91.20125	26.05413

The Dhansiri river basin, by comparison, displays a very mild topography relative to Dzuza. The 0–10% slope class predominates the basin, including 667.754 km² (39.33%), succeeded by the 10–20% category with 391.108 km² (23.04%) (**Table 4.6**). Moderate to steep slopes (20–30% and 30–50%) comprise around 31.53%, whilst very steep slopes (>50%) cover merely 103.617 km² (6.10%). The distribution indicates that the Dhansiri river basin possesses advantageous circumstances for agriculture and habitation in its low-lying regions, whilst the steeper parts necessitate soil conservation strategies to prevent erosion (**Figure 3.7 (b)**).

Table 3.11: Area statistics of different slopes in Dhansiri river basin

Sl. No.	Slope Name	Area (km^2)	Per cent of Watershed Area
1	0-10	667.7535	39.32883
2	10-20	391.1082	23.03519
3	20-30	268.1219	15.79164
4	30-50	267.2722	15.74159
5	50-9999	103.6169	6.102747

The Khova sub-watershed exhibits a more even slope distribution across all classifications (**Table 4.7**). The 30–50% slope category encompasses the most extensive area at 31.817 km² (29.23%), succeeded by the 0–10% slopes (22.045 km², 20.25%) and the 20–30% slopes (21.057 km², 19.34%). Extremely steep slopes (>50%) encompass 14.568 km² (13.38%), whilst the 10–20% gradient class spans 19.373 km² (17.80%). This combination of gentle, moderate, and steep inclines signifies a fairly rough landscape, necessitating land use planning to balance agricultural viability in flatter regions with conservation strategies in steeper sections (**Figure 3.7 (c)**).

Slope analysis utilizing SWAT indicates that the Dzuza watershed is characterized by steep and very steep slopes, rendering it more susceptible to erosion and hydrological extremes. The Dhansiri river basin features a predominance of mild to moderate slopes, which are conducive to agriculture and human settlement. The Khova watershed exhibits a uniformly distributed slope profile, necessitating comprehensive land and water management measures to reconcile profitable land use with soil conservation.

Table 3.12: Area statistics of different slopes in Khova sub-watershed

Sl. No.	SlopeName	Area (km^2)	Per cent of Watershed Area
1	0-10	22.0455	20.25122
2	10-20	19.3729	17.79615
3	20-30	21.05667	19.34288

Table 3.12 (continued)

4	30-50	31.81709	29.22751
5	50-9999	14.56792	13.38224

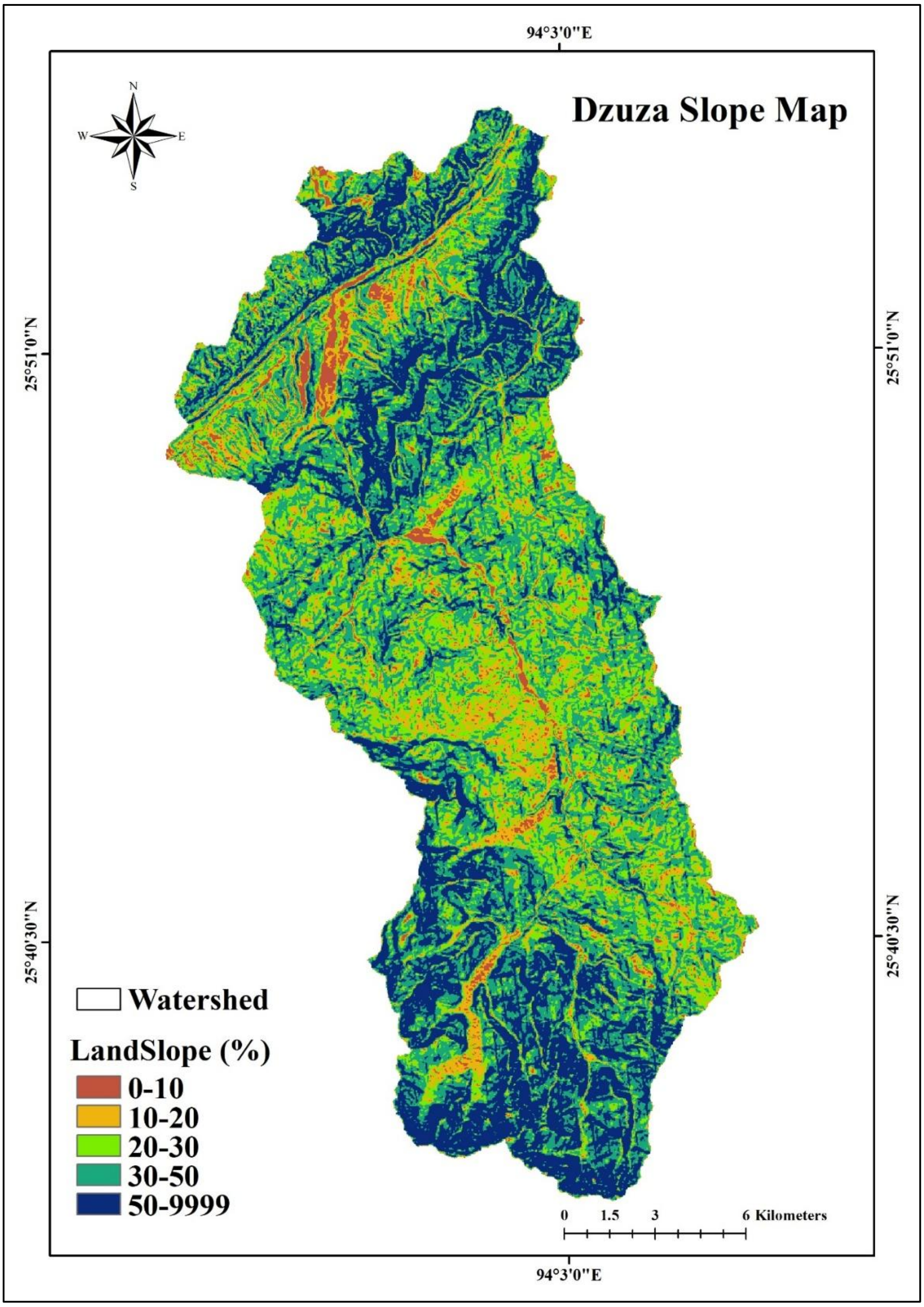

Figure 3.7 (a): Slope map of the Dzuza watershed

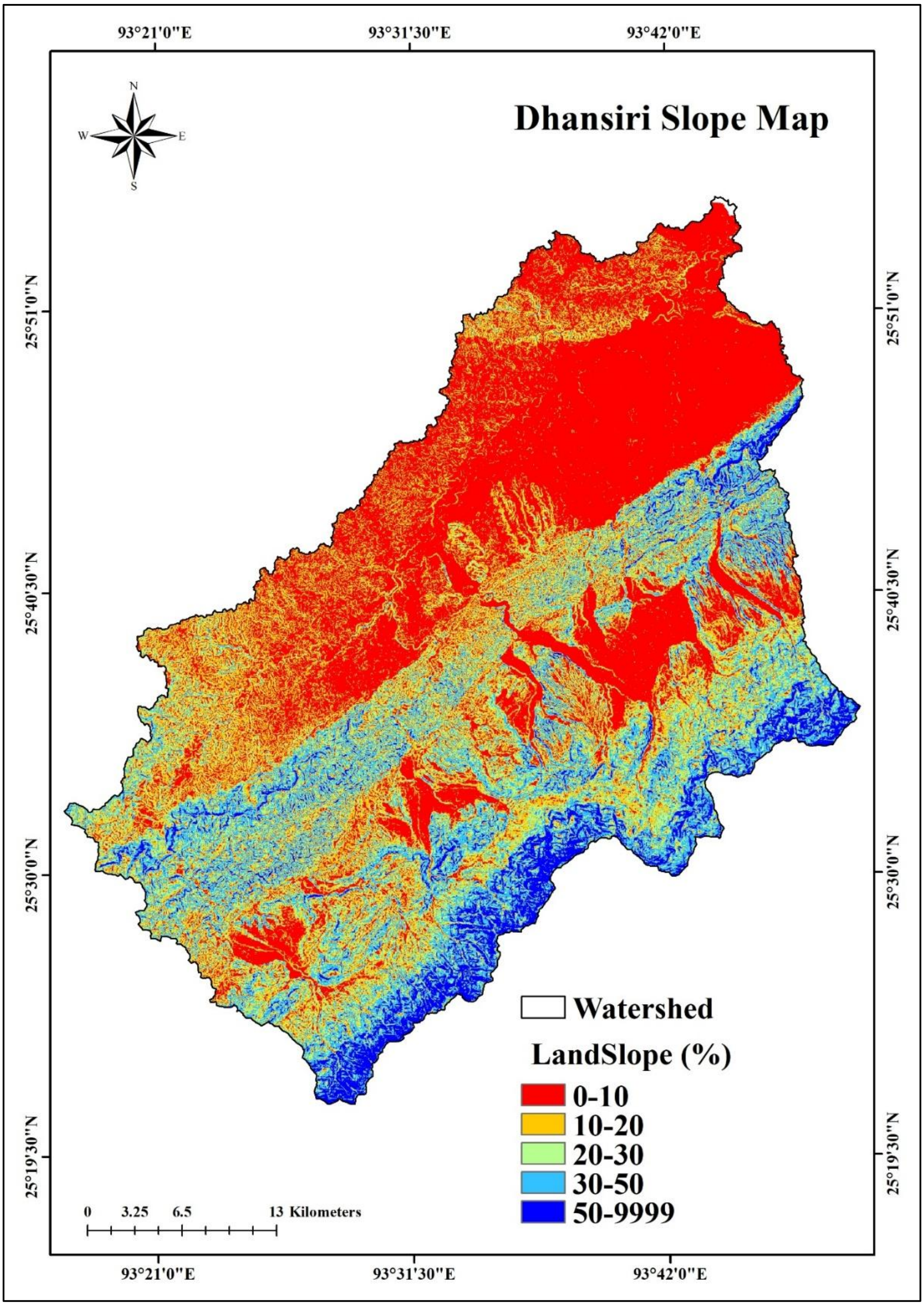

Figure 3.7 (b): Slope map of the Dhansiri river basin

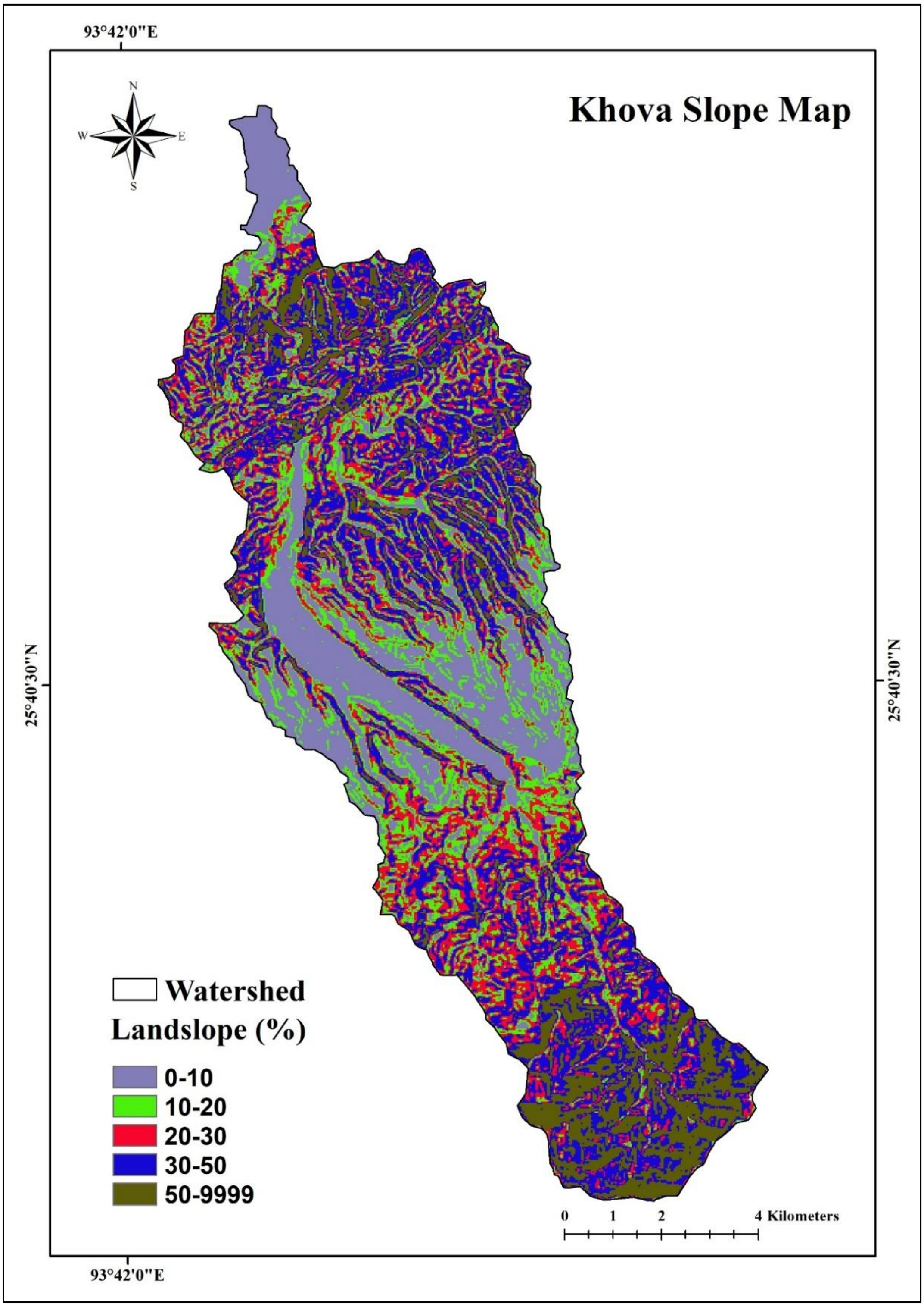

Figure 3.7 (c): Slope map of the Khova sub-watershed

3.4.5.3 *Land Use/Land Cover Map*

The land use and land cover map of the region was created from land cover imagery sourced from the Living Atlas database. The Dzuza watershed area was categorized into five land use and land cover classes: Agricultural Land-Generic, Forest-Mixed, Range-Grasses, Residential-Med/Low Density, and Water, coded as AGRL, FRST, RNGE, URML, and WATR, respectively. The area statistics are provided in **Table 3.13.** The total area of the selected watershed is 351.46 km². The largest portion of the watershed is covered by forest (92.76%), followed by urban land (5.02%), rangeland (2.01%), agricultural land (0.16%), and water (0.05%). The spatial distribution of different land uses within the Dzuza watershed is shown in **Figure 3.8 (a).**

The Dhansiri basin area was divided into six land use and land cover classes: Agricultural Land-Generic, Forest-Mixed, Range-Grasses, Residential-Med/Low Density, Water, and Wetlands-Mixed, coded as AGRL, FRST, RNGE, URML, WATR, and WETL, respectively. The area statistics are provided in **Table 3.14.** The total area of the selected watershed is 1697.12 km²**.** The largest portion of the watershed is covered by forest (82.20%), followed by agricultural land (8.81%), urban land (6.38%), rangeland (2.35%), water (0.26%), and wetland (0.002%). The spatial distribution of different land uses within the Dhansiri basin is shown in **Figure 3.8 (b)**

The Khova sub-basin area was divided into five land use and land cover classes: Agricultural Land- Generic, Forest- Mixed, Range- Grasses, Residential-Med/Low Density, and Water, coded as AGRL, FRST, RNGE, URML, and WATR, respectively. The area statistics are provided in **Table 3.15**. The total area of the selected watershed is 108.75 km²**.** The largest portion of the watershed is covered by forest (90.83%), followed by agricultural land (4.12%), rangeland (2.63%), urban land (2.40%), and water (0.002%). The spatial distribution of different land uses within the Khova sub-watershed is shown in **Figure 3.8 (c)**

Although SWAT was originally designed for agricultural watersheds, its application has greatly expanded to forest-dominated and mixed land-use basins because it is a process-based model capable of simulating key components of the hydrological cycle under different land-use conditions. The model considers the effects of topography, soil, climate, and land cover on watershed hydrology, making it suitable not only for agricultural areas but also for watersheds with significant forest cover. Recent review studies have also emphasized the wide applicability of SWAT across various watershed environments. Since more than 82% of the land in the three selected watersheds is covered by forests, using SWAT in this study remains scientifically justified, especially for evaluating watershed hydrological behavior when supported by appropriate input data, calibration, and validation (Janjić & Tadić, 2023; Zhao *et al.*, 2024).

Table 3.13: Land use/land cover area statistics of Dzuza watershed.

Sl. No.	SWAT_CLASS	Area (km^2)	Percent of watershed area
1	AGRL	0.56	0.16
2	FRST	326.00	92.76
3	RNGE	7.06	2.01
4	URML	17.65	5.02
5	WATR	0.18	0.05
	Total=	**351.46**	

Table 3.14: Land use/land cover area statistics of Dhansiri river basin

Sl. No.	SWAT_CLASS	Area (km^2)	Percent of watershed area
1	WATR	4.39	0.26
2	FRST	1395.02	82.19
3	WETL	0.033	0.002
4	AGRL	149.6	8.81
5	URML	108.34	6.38
6	RNGE	39.87	2.35
	Total =	**1697.12**	

Table 3.15: Land use/land cover area statistics of Khova sub-watershed

Sl. No.	SWAT_CLASS	Area (km^2)	Percent of watershed area
1	WATR	0.02	0.02
2	FRST	98.78	90.83
3	AGRL	4.48	4.12
4	URML	2.61	2.39
5	RNGE	2.86	2.63
	Total =	**108.75**	

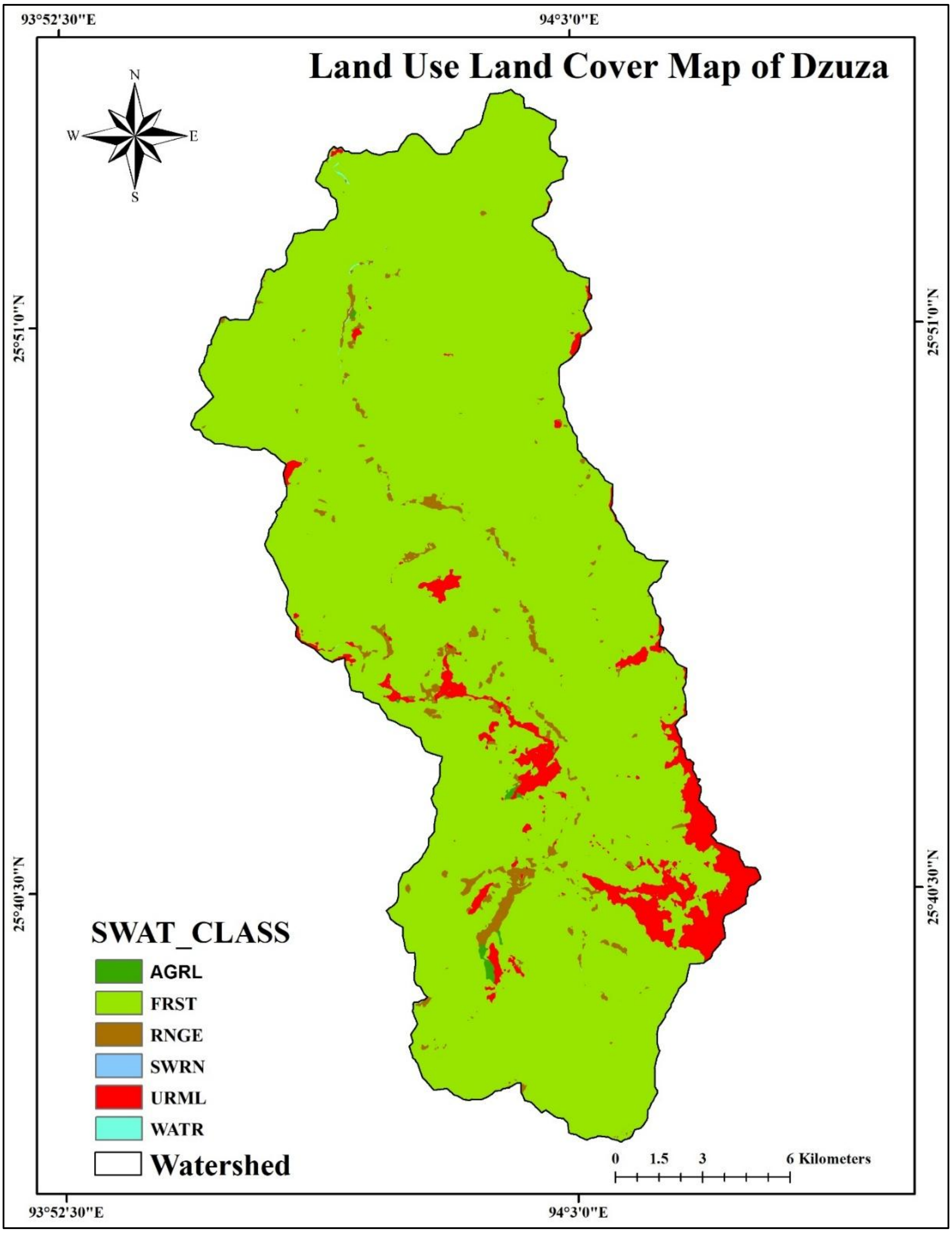

Figure 3.8 (a): Land use land cover map of the Dzuza watershed

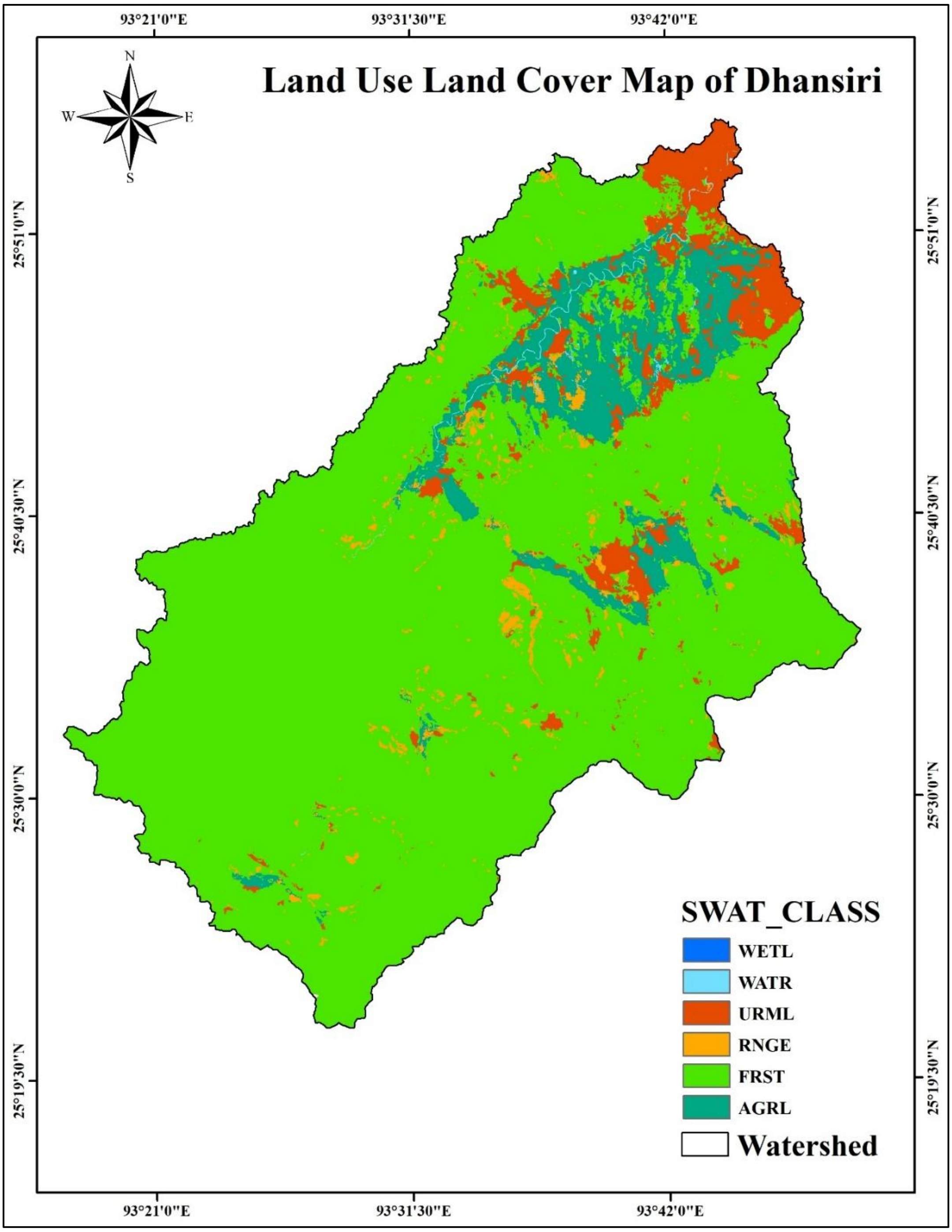

Figure 3.8 (b): Land use land cover map of the Dhansiri river basin

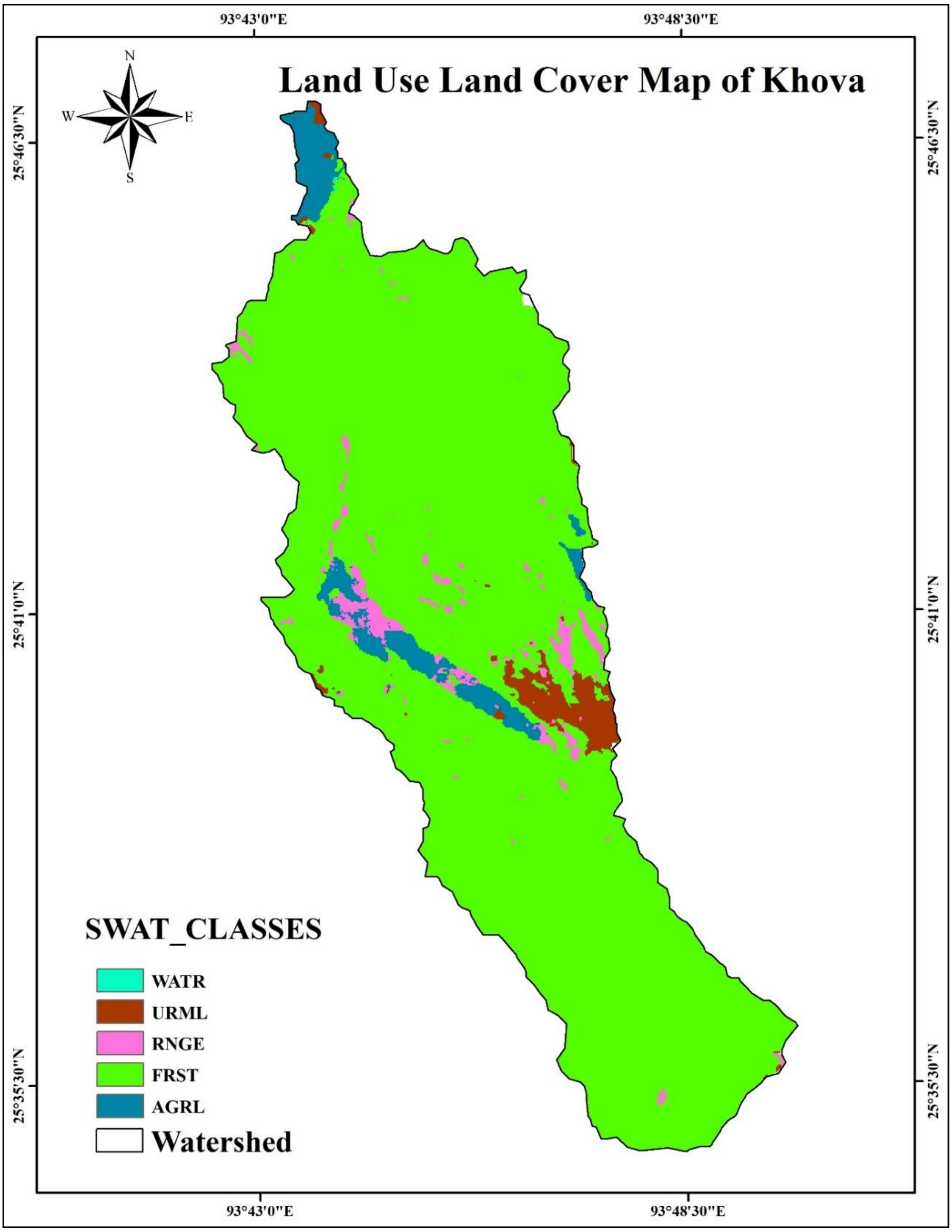

Figure 3.8 (c): Land use land cover map of the Khova sub-watershed

3.4.5.4 Soil Map

The FAO soil map of India has been taken as a reference map, which was geo-referenced and clipped to the catchment area. This map was categorized based on the SWAT code, and soil properties extracted from the soil database were stored in the SWAT database through the soil data input interface. These properties were stored layer by layer for each soil type. A lookup table was prepared to link the soil map to the database.

The soil map of the research regions was developed utilizing the FAO Soil Map of India, which offers a consistent classification of soil types nationwide. These maps facilitate comprehension of the geographical distribution of soil texture and composition within the designated watersheds, which are essential for hydrological modeling, erosion evaluation, and land management strategies. The Dzuza watershed is characterized by a single soil type. The entire basin consists solely of clay loam, classified by the FAO as Ao76-2-3c-4276 (**Figure 3.9 (a)**). The dominance of this soil type indicates a very uniform soil texture throughout the watershed, which greatly affects infiltration, runoff, and soil erosion processes. The clay loam texture has moderate permeability and excellent water retention capabilities, making it suitable for agriculture; however, it is prone to erosion during heavy rainfall if not properly managed.

The Dhansiri river basin exhibits a more diverse soil composition characterized by three distinct FAO soil groups. The first soil type is Af48-2ab-3637 (sandy clay loam), mainly found in the northern part of the basin. This soil type contains a balanced mix of sand, silt, and clay, which promotes moderate drainage conditions. The second dominant soil type is Ao76-2-3c-4276 (clay loam), located in the central and southeastern areas of the watershed. This soil is somewhat fine-textured, showing a higher water-retention capacity but lower infiltration rates, which influences runoff generation. The third soil type, Af47-2b-4255 (sandy clay loam), is primarily located in the southwestern part of the watershed. Similar to Af48-2ab-3637, it offers moderate drainage and structural stability but may be prone to erosion on steep slopes. The presence of these three soil types (**Figure 3.9 (b)**) highlights the Dhansiri basin's varied soil profile, which greatly impacts land use planning, hydrological response, and soil conservation efforts. The Khova watershed consists entirely of clay loam, classified under the FAO soil classification Ao76-2-3c-4276 (**Figure 3.9 (c)**). Similar to the Dzuza watershed, having a single homogeneous soil type throughout the watershed makes it easier to assess soil-related hydrological processes. The clay loam provides excellent fertility and moisture retention, making it beneficial for agriculture; however, there is a significant risk of erosion after heavy rainfall and poor land management practices. Consistent clay loam soils characterize the Dzuza and Khova watersheds, but the Dhansiri basin is distinguished by its heterogeneity, comprising both sandy clay loam and clay loam soils. The heterogeneity in Dhansiri adds significant complexity to hydrological modeling, soil erosion forecasting, and land management techniques, in contrast to the more similar soil profiles of Dzuza and Khova.

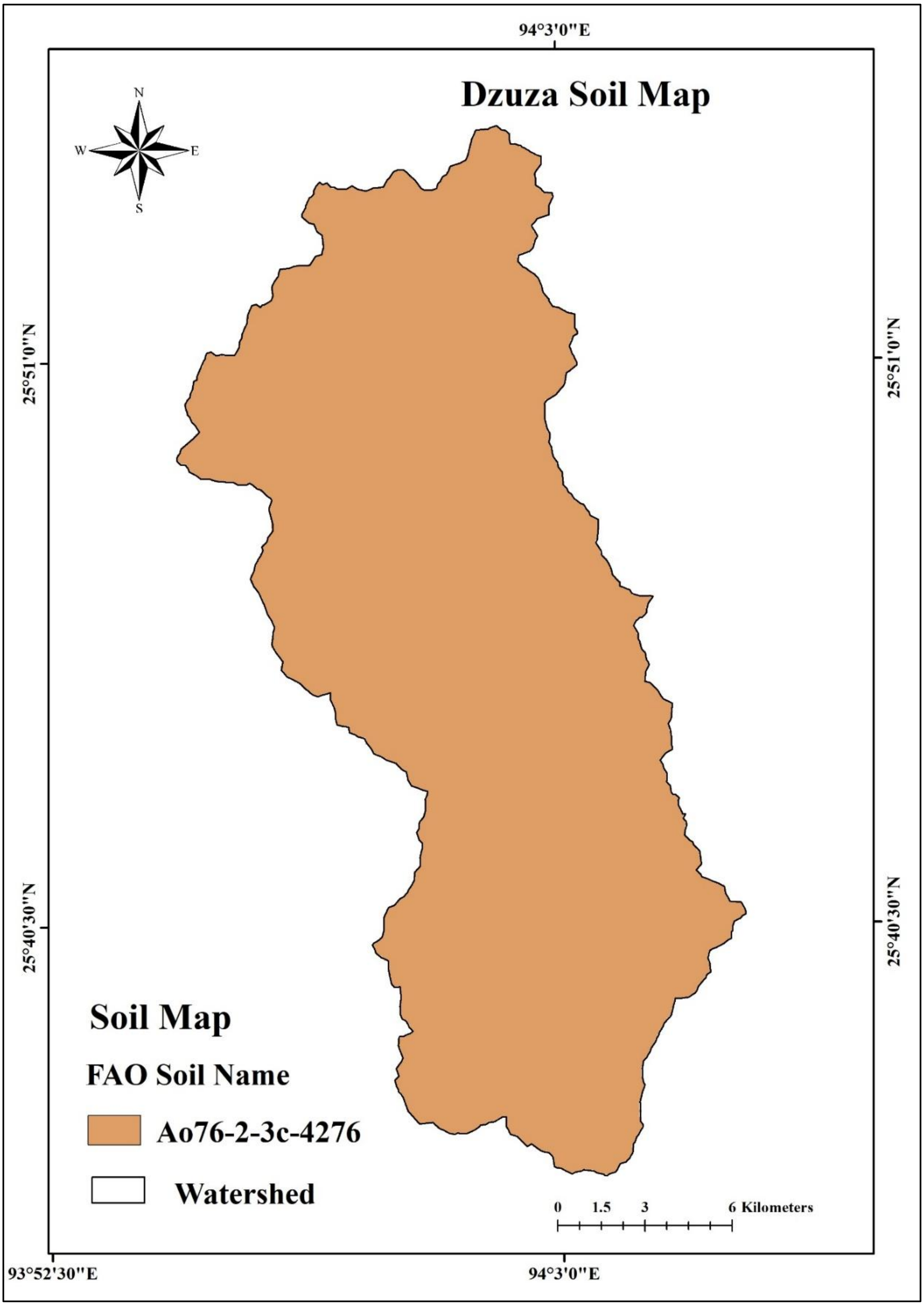

Figure 3.9 (a): Soil map of Dzuza watershed

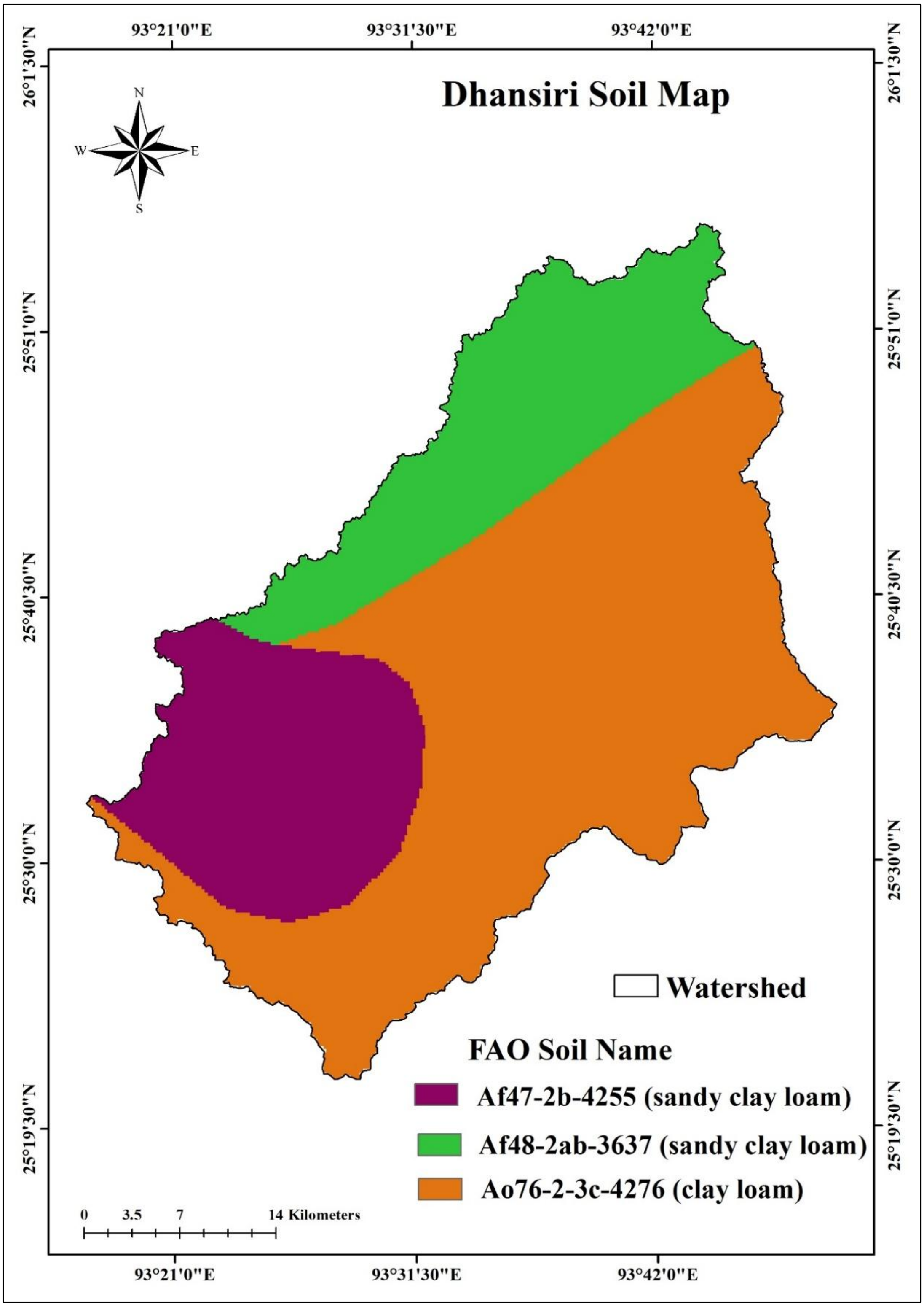

Figure 3.9 (b): Soil map of Dhansiri river basin

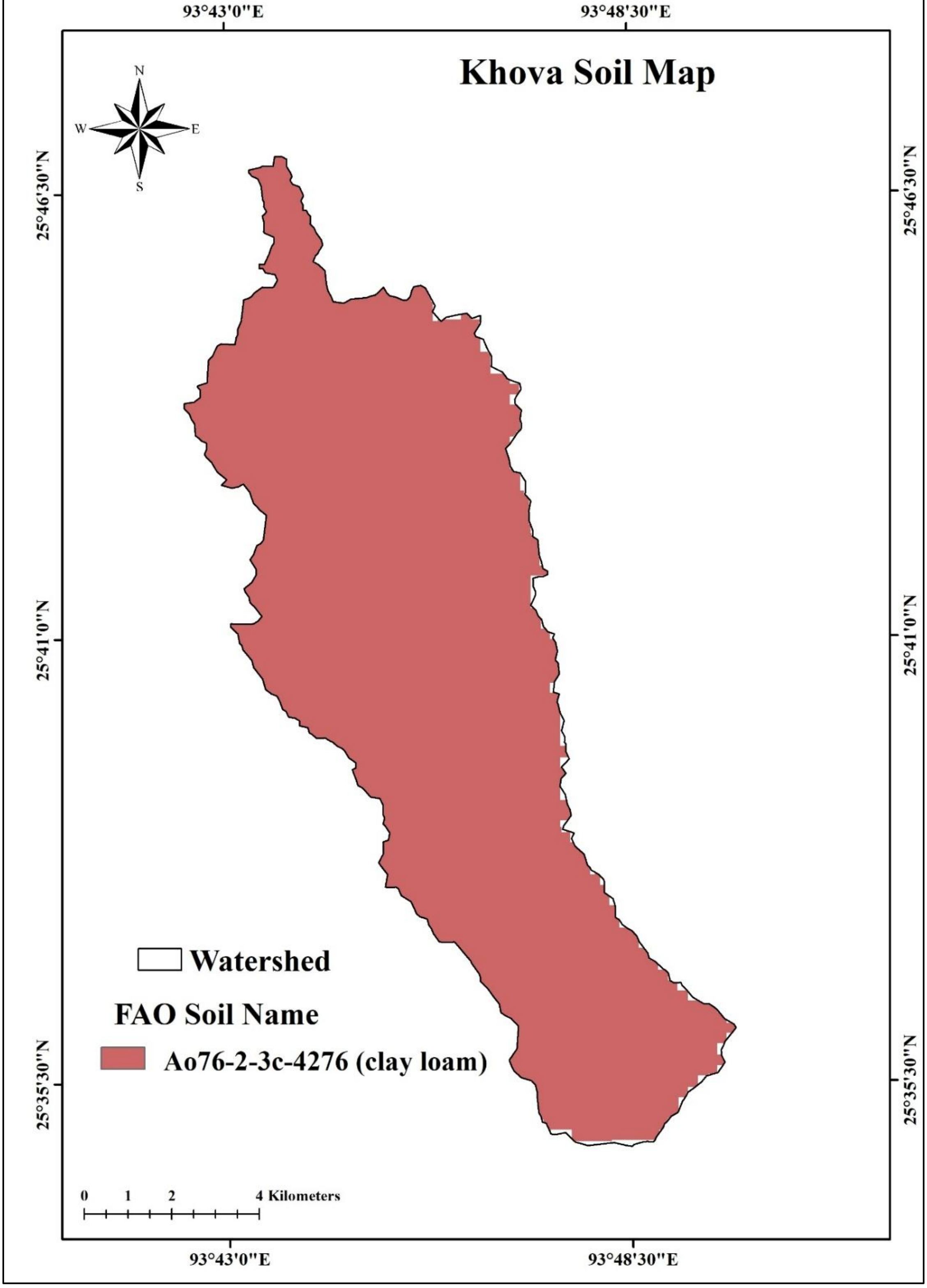

Figure 3.9 (c): Soil map of Khova sub-watershed

3.4.5.5 Arc SWAT Model Setup

Initially, the setup for the new SWAT project was completed. SRTM data (30 m resolution) with a geographic coordinate system were converted into a projected coordinate system (WGS (World Geodetic System)1984 Northern Hemisphere 46N). After subsetting the SRTM data, it was imported into the SWAT project to begin watershed delineation.

3.4.5.5.1 Watershed Delineation

ArcSWAT used DEM data to automatically delineate the watershed into multiple hydrologically connected sub-watersheds. The first step in watershed delineation involved importing the accurately estimated Digital Elevation Model (DEM). A mask was generated over the DEM around the study region to reduce GIS processing time. A polyline stream network database was incorporated into the SWAT sub-basin reaches to match the designated stream reaches. Incineration within a stream network enhances hydrological segmentation and sub-watershed delineation. After loading the DEM grid and overlaying the stream networks, the DEM map grid was processed to eliminate non-draining areas (Luo *et al.,* 2011).

The 3-river basin was delineated using USGS Earth Explorer digital elevation model (DEM) data in ArcGIS. Various geoprocessing techniques were employed to outline the river basin. The step-by-step geoprocessing methods required for delineating the 3-river basin, such as fill basin, flow direction, flow accumulation, basin raster, and basin raster to feature, are shown in **Figure 3.10** (Dzuza), **Figure 3.11** (Dhansiri), and **Figure 3.12** (Khova). The geoprocessing results in ArcGIS 10.5 will generate a polygon that is separated from other polygons through the clipping technique.

Stepwise Delineation of Dzuza watershed, Dhansiri river basin, and Khova sub-basin in the Arc GIS Environment- Open ArcMap and create a new blank map document. Use the Add Data button from the toolbar menu for adding the DEM and shape file of the study area. The spatial coordinate system of World Geodetic System (WGS 1984) UTM (Universal Transverse Mercator) 46N was given and used for all the layers in the entire study.

1) Fill DEM

The fill tool in the hydrology toolbox of the spatial analyst tool is employed to remove any inadequacies in the DEM. **Figure 3.10 (b)** illustrates the filled Digital Elevation Model (DEM) of the Dzuza watershed, **Figure 3.11 (b)** depicts the filled DEM of the Dhansiri River basin, and **Figure 3.12 (b)** presents the filled DEM of the Khova sub-basin. The input surface raster is set as DEM, and the output raster is set as fill in the working directory.

2) Flow Direction

A flow direction grid allocates a value to each cell of the DEM to specify the direction of flow, i.e., the direction that water will flow from that specific cell based on the topography of the landscape. **Figure 3.10 (c)** illustrates the flow direction of the Dzuza watershed. The flow direction of the Dhansiri River basin is illustrated in **Figure 3.11 (c),** whereas the flow direction of the Khova sub-basin is depicted in **Figure 3.12 (c).**

3) Flow Accumulation

The flow accumulation tool analyses the flow into each cell by recognizing the upstream cells that drain into each downstream cell. This process also depends on the landscape geography of the area. The flow accumulation of the Dzuza watershed is shown in **Figure 3.10 (d),** the Dhansiri River basin in **Figure 3.11 (d),** and the Khova sub-basin in **Figure 3.12 (d).**

4) Stream Order

Stream order assigns a numeric order to segments of a raster representing branches of a linear network. Set raster calculator as input for stream raster, flow direction as the input for flow direction raster, and name the output raster as stream order. The Strahler method for stream ordering was utilized, with the outcomes for the Dzuza watershed illustrated in **Figure 3.10 (e),** the Dhansiri River basin depicted in **Figure 3.11 (e),** and the Khova sub- basin shown in **Figure 3.12 (e).**

5) Stream to Feature

It converts a raster representing a linear network to features(polyline) representing the linear network. The DEM was processed using the hydrology tool. The input is set as stream order, flow direction as input for flow direction raster, and output as Stream polygon. The values of different morphological parameters are found in the attribute table of this output file. The stream to Feature for the Dzuza watershed is represented in **Figure 3.10 (f),** the Dhansiri River basin is portrayed in **Figure 3.11 (f),** and the Khova sub- basin is shown in **Figure 3.12 (f).**

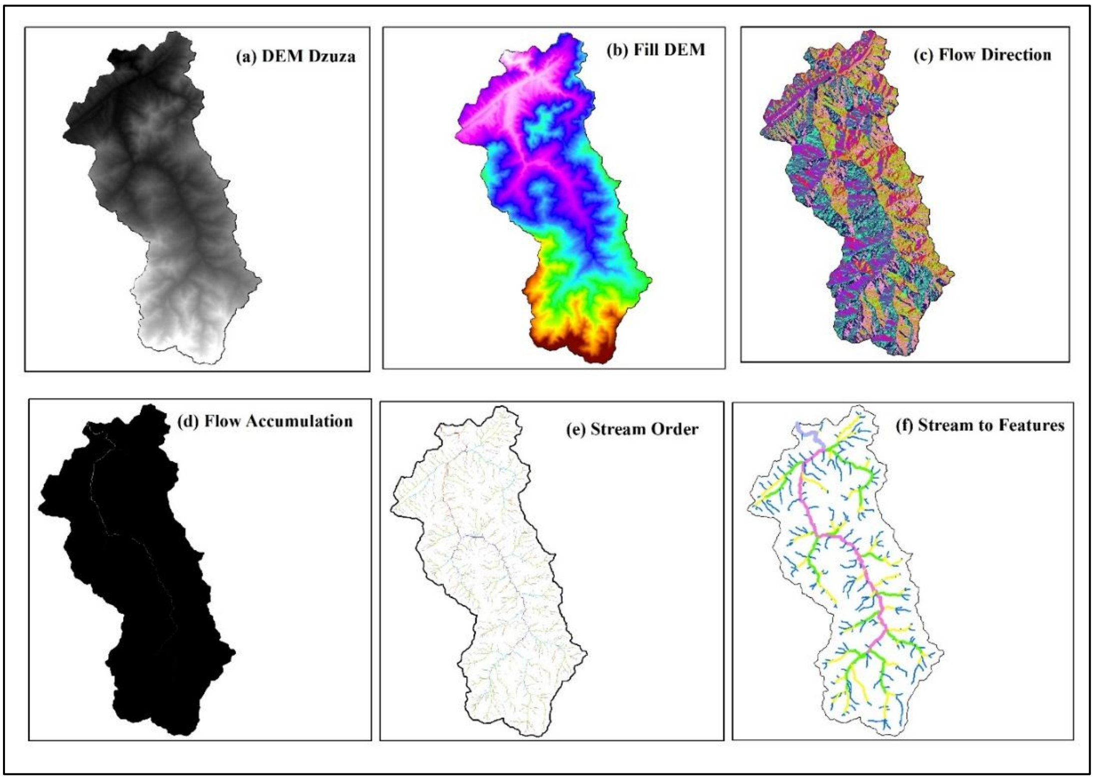

Figure 3.10: Stepwise delineation of Dzuza watershed in Arc GIS environment

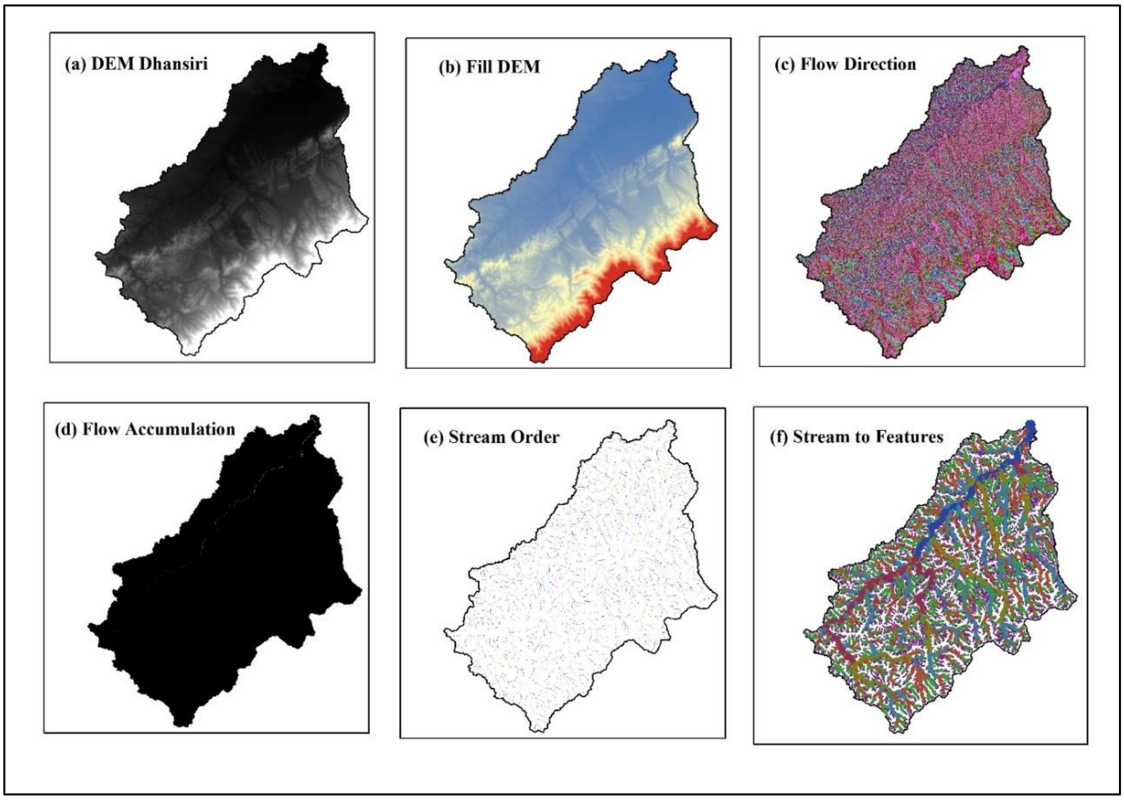

Figure 3.11: Stepwise delineation of Dhansiri river basin in Arc GIS environment

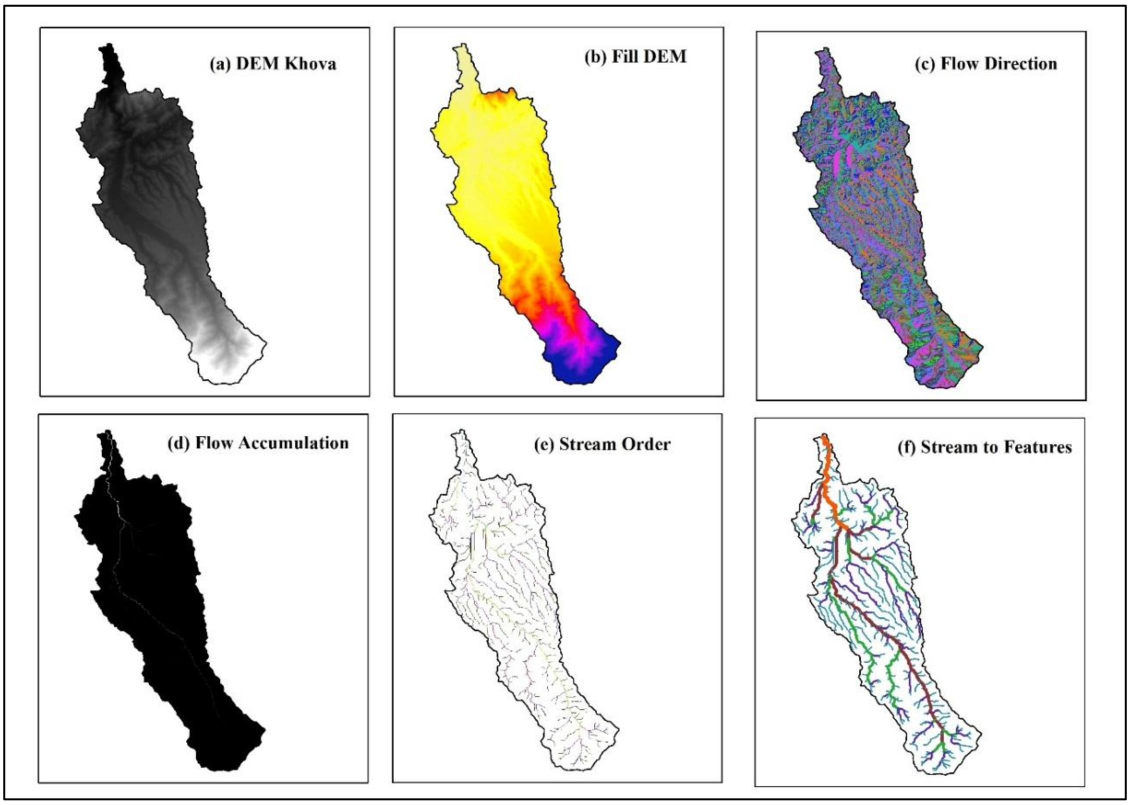

Figure 3.12: Stepwise delineation of Khova sub watershed in Arc GIS environment

3.4.5.5.2 *Stream Definition*

This section defines the original stream network and sub-basin outlets. It offers the capability to establish streams according to a drainage area threshold or to import predefined watershed boundaries and streams. Subsequently, the flow direction and accumulation were computed.

3.4.5.5.3 *Outlet and inlet definition*

This section provided a clear definition of the watershed demarcation by specifying the discharge outlet points for both the sub-basins and the entire watershed. Sub-watershed outlets were the locations in the drainage network where stream flow departed from the sub-watershed region. The outlet for the entire watershed was delineated manually. The sub-basin region was reduced from its previously stated extent upon the identification of the outlet, and this information was recorded in the "Monitoring Points" layer. The final phase in delineating the watershed was calculating watershed metrics, including geomorphic parameters. The section on the calculation of sub-watershed parameters includes functions for determining geomorphic properties and reaches, as well as identifying the sites of reservoirs, if present within the watershed. A topographic report was generated, summarising and detailing the distribution of discrete land surface elevations throughout the sub-watersheds.

3.4.5.5.4 *Hydrologic Response Unit Analysis*

Hydrologic Response Units (HRUs) are aggregated land areas inside a sub-watershed, characterized by distinct combinations of land cover, soil types, and slope gradients. HRUs allow the model to represent variations in evapotranspiration and other hydrological variables across diverse land covers, soils, and slopes. Runoff was estimated for each HRU and then routed to calculate the overall runoff for the watershed. This approach enhances the precision of flow calculation and provides a significantly improved physical representation of the water balance. Land use and soil data in a projected grid file format were imported into the ArcSWAT interface to calculate the area and hydrologic parameters of each land-soil-slope category simulated inside each sub-watershed. Land cover categories were established using the lookup table. A lookup table was created to associate the 4-letter SWAT codes with various categories of land use/land cover (LULC), thereby linking grid values to SWAT land cover/land use classifications. After assigning the SWAT land use code to all map categories, the area encompassed by each land use was calculated and subsequently reclassified. The soil layer in the map was associated with the user soil database by importing the soil lookup table and applying reclassification.

The land slope classes were incorporated into the description of the hydrologic response units. The DEM data utilized in the watershed delineation were also employed for slope categorization. Subsequently, land use, soil, and slope grids were superimposed. The final phase of the HRU analysis involved defining the HRU. The distribution of HRUs in this study was established by allocating numerous HRUs to each sub-watershed. A threshold level was employed in the multiple HRU definition to exclude minor land uses, soils, and slope classes within each sub-watershed. Land uses, soils, or slope classes that fell below the threshold level were excluded, and the area of the remaining land use, soil, or slope class was redistributed to ensure that 100% of the land area in the sub-watershed could be modelled.

3.4.5.5.5 Weather Data Definition

The climate of a watershed supplies the moisture and energy necessary to regulate the water balance and ascertain the significance of various components of the water cycle (Zhang 2008). The meteorological variables necessary for SWAT, including daily precipitation, maximum and minimum temperatures, solar radiation, wind speed, and relative humidity, were formatted into a suitable database structure. Weather data were supplied as inputs to the model via the "write input tables" command in SWAT. This study utilized WGEN (Weather Generator) USER as the customized weather database. The placements of meteorological stations allocate climate data to sub-watersheds and specific Hydrologic Response Units (HRUs). The approach employed for possible evapotranspiration was Penman-Monteith.

3.4.5.5.6 Creating SWAT Input Datasets

The "Write commands" are activated once the weather data has been successfully loaded. These commands were activated sequentially and must be executed just once for a project. Two methods existed to establish the initial values: activating the Write All command or utilizing the individual Write commands from the Write Input Tables menu. The initial option was chosen in this investigation.

In hilly watersheds, subsurface flow and baseflow often constitute a substantial proportion of total streamflow. However, in the present study, only total observed streamflow data were available at the outlet of each watershed, while separate observations of surface runoff and baseflow were not available. As a result, explicit separation of baseflow and surface runoff was not undertaken in the data processing stage. Instead, calibration and validation of the SWAT model were conducted utilizing total streamflow data. This is because SWAT simulates streamflow as the combined effect of surface runoff, lateral flow, and groundwater contribution (baseflow) within the watershed system. Such an approach is commonly adopted in SWAT applications where observed discharge data are available only in aggregated form. Therefore, the use of total streamflow data for model calibration and validation was considered scientifically justified in this study (Zhao *et al.,* 2024).

3.4.5.5.7 SWAT Simulation

The primary components of the SWAT simulation conducted on the watershed are enumerated below:

- Output time step: monthly
- Simulation period: ten years (2012–2021)
- Rainfall distribution: skewed normal
- Runoff Generation: SCS-CN Method

The data regarding watershed characteristics was extracted from an output text file stored within the MS Excel database.

3.4.6 Model Calibration and Validation

Since SWAT is a theoretical model, the results from its simulation might not fully match observed values due to some uncertainties in prediction. Therefore, calibration and validation are essential to make the model more practical and suitable for field use. Calibration is an effort to better parameterize a model to a given set of local conditions, thereby reducing the prediction uncertainty (Arnold *et al.,* 2012). With the knowledge of various parameters influencing the hydrology of the study area, along with an idea of the degree of influence, and based on previous similar studies conducted, the model input parameters are assigned a specific range of values that are used for the calibration of the parameters.

After calibration of the model, it is validated for the desired hydrologic component (streamflow, sediment yield, etc.). Model validation is the procedure of establishing that a given site-specific model can provide sufficiently accurate simulations, although “sufficiently accurate” may differ according to project objectives (Refsgaard, 1997). The process entails executing the model with the calibrated parameters as model input and comparing the results with an observed dataset that has not been used in calibration.

3.4.6.1 SWAT-CUP

SWAT-CUP, which stands for Soil and Water Assessment Tool-Calibration and Uncertainty Procedures, is a publicly available computer program developed by the Swiss Federal Institute of Aquatic Science and Technology (Eawag) for calibration, validation, sensitivity, and uncertainty analysis of SWAT models. The performance of the model in simulating runoff and sediment outflow was evaluated using the SWAT Calibration and Uncertainty Program (SWAT-CUP). SWAT-CUP provides a decision-making framework that incorporates a semi-automated approach, Sequential Uncertainty Fitting-2 (SUFI2), employs both manual and automatic calibration, along with sensitivity and uncertainty analysis. Users can iteratively modify parameters and ranges between auto-calibration runs. Parameter sensitivity analysis helps focus the calibration, and uncertainty analysis provides statistics for goodness-of-fit. The manual aspect of the calibration process helps users gain a better understanding of overall hydrologic processes (such as baseflow ratios, ET, sediment sources and sinks, crop yields, and nutrient balances) and parameter sensitivity. By integrating these tools into the calibration process, SWAT-CUP offers a effective approach to watershed calibration. Designed to integrate various calibration and uncertainty analysis programs for SWAT through a different interface, SWAT-CUP can currently run SUFI2; Generalized Likelihood Uncertainty Estimation (GLUE) (Beven & Binley, 1992); Parameter Solution (ParaSol) (van Griensven & Meixner, 2006); Particle Swarm Optimization (PSO); and Markov Chain Monte Carlo (MCMC) procedures. In this study, the SUFI2 procedure was employed for the calibration and validation of the model.

3.4.6.2 SWAT-CUP Model Parameterization

The parameterization of a watershed concept presents a complex challenge due to the extensive range of possibilities involved. The parameters utilized in the calibration were selected through a one-at-a-time sensitivity analysis, which involved varying a single parameter while maintaining the constancy of all other parameters, as well as a global sensitivity analysis that assessed the variation of all parameters concurrently. The objective of sensitivity analysis is to quantify the variation in the output of a model in relation to alterations in model input. The program SWAT-CUP, coupling various programs to SWAT, has the general concept shown in **Figure 3.13**. The steps were: 1) calibration program writes model parameters in the model; 2) swat_edit.exe edits the SWAT's input files, inserting the new parameter values; 3) the SWAT simulator is run; and 4) the swat_extract.exe program extracts the desired variables from SWAT's output files and writes them to the model out. The procedure operates as mandated by the calibration program.

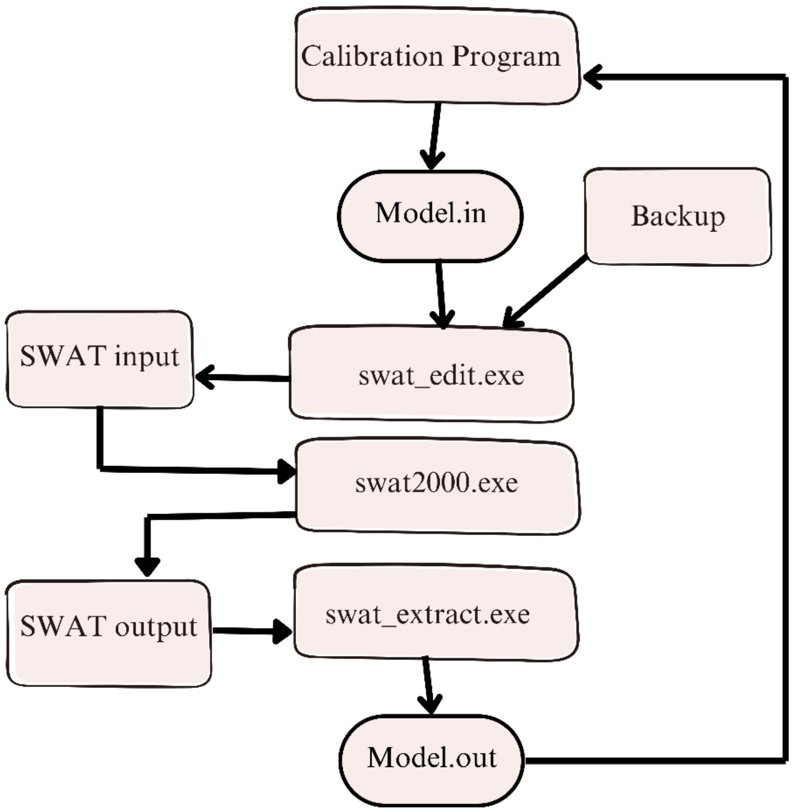

Figure 3. 13: Interaction between a calibration program and SWAT in SWAT-CUP

3.4.6.3 SUFI-2 Algorithm

The program Sequential Uncertainty Fitting ver. 2 (SUFI-2) was used for a combined sensitivity, calibration, uncertainty analysis, and validation. In any hydrological/sediment modeling work, there are uncertainties in input (e.g., rainfall), in the conceptual model, in model parameters, and in the measured data (e.g., runoff/ sediment yield) (Abbaspour *et al*., 2007). SUFI-2 maps the aggregated uncertainties to the parameters and aims to obtain the smallest parameter uncertainty ranges. The parameter uncertainty leads to uncertainty in the output, which was quantified by the 95% prediction uncertainty (95PPU) calculated at the 2.5% (L95PPU) and the 97.5% (U95PPU) levels of the cumulative distribution obtained through Latin hypercube sampling. The extent to which all uncertainties are considered for is quantified by a metric known as the p-factor, representing the percentage of observed data encompassed by the 95% prediction uncertainty (95PPU). The best parameter values were selected based on whether the width of the uncertainty band (r-*factor)* was close to zero and the p-*factor* was close to 1. Starting with large but physically meaningful parameter ranges that bracket 'most' of the measured data within the 95PPU, SUFI-2 decreases the parameter uncertainties iteratively. New and narrower parameter uncertainty ranges were calculated following each iteration, where the more sensitive parameters find a larger uncertainty reduction than the less sensitive parameters (Schuol *et al.,* 2008).

3.4.6.4 Calibration and Validation using SUFI2

Model calibration aims to optimize a model's parameters for a specific set of local conditions, hence diminishing prediction uncertainty. Model calibration involves the meticulous selection of input parameter values within their uncertainty ranges, contrasting model predictions (outputs) under specified conditions with observed data under the identical conditions (Arnold *et al.,* 2012). Model validation is the procedure of establishing that a given site-specific model can produce adequately precise predictions. This implies the application of the calibrated model without changing the parameter values that were set during the calibration, when simulating the response for a period other than the calibration period (Refsgaard, 1997).

The model calibration and validation process were conducted in this research using the SWAT CUP (SWAT Calibration and Uncertainty Program) tool. SWAT CUP is a computer program for automatic calibration of SWAT models. It was developed by Eawag Swiss Federal Institute, to analyze the prediction uncertainty of SWAT model calibration and validation results. It provides the user to choose between several algorithms to perform the calibration such as SUFI-2 (Sequential Uncertainty Fitting ver.2), GLUE (Generalized Likelihood Uncertainty Estimation), MCMC (Markov Chain Monte Carlo), Parasol (Parameter Solution), In this study SUFI-2 has been used as the calibration algorithm since it has been widely used popular calibration tool and has achieved good calibration and uncertainty results. In SUFI2, the uncertainty in parameters portrays all sources of uncertainty, like uncertainty in parameters, conceptual model, driving variables (e.g., rainfall), and measured data.

SUFI2 (Sequential Uncertainty Fitting ver.2) procedure of calibration expresses the uncertainty in parameters as uniformly distributed ranges while taking into consideration various kinds of uncertainties, namely, driving variables uncertainties (e.g., rainfall), the conceptual model uncertainties, model parameters uncertainties, and uncertainties in observed data. Due to the existence of these uncertainties in the input parameters, which result in uncertainties in the model output, which are henceforth expressed as the 95% probability distributions, which is regarded as the 95% prediction uncertainty or 95 PPU. These 95 PPUs are considered the model outputs, which are obtained in the form of an envelope of good solutions and not as a single signal representing the model output (Abbaspour, 2015). **Figure 3.14** shows the process involved in the calibration of parameters using the SUFI2 algorithm.

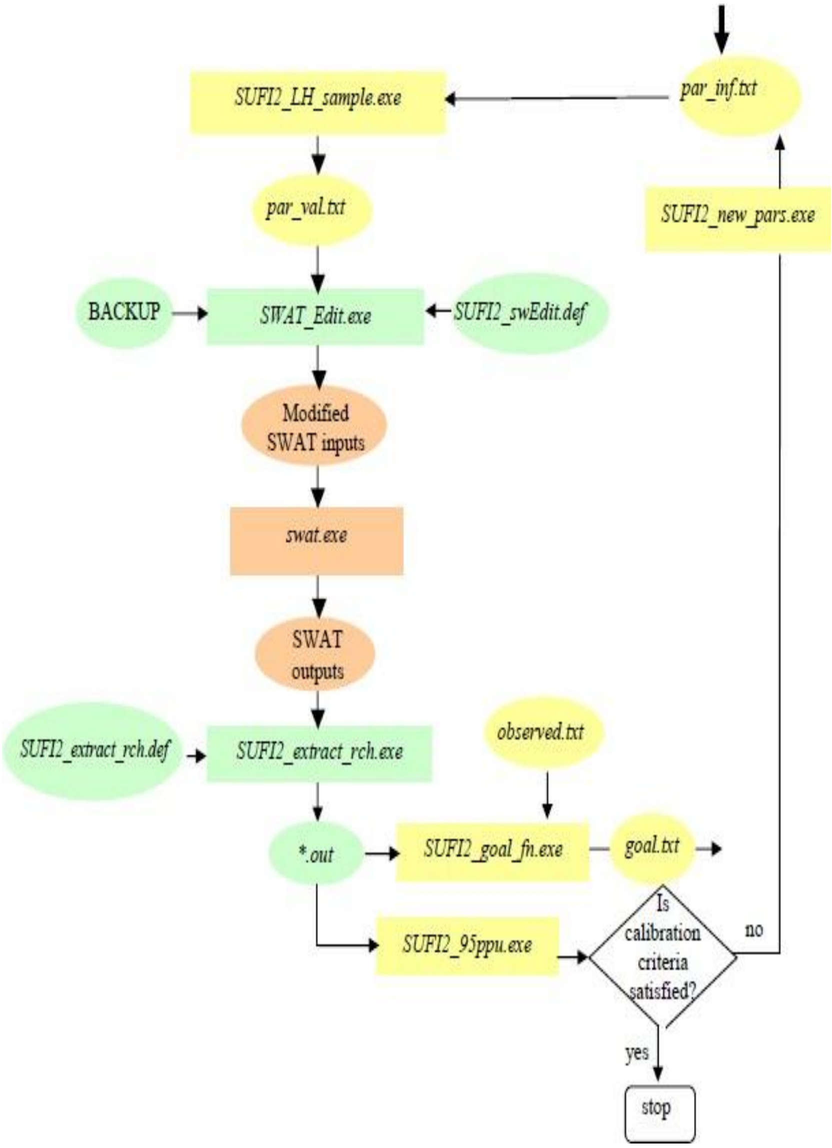

Figure 3.14: Flow diagram for step-wise calibration using SUFI2

3.4.6.5 *Calibration Inputs*

Par_inf.txt: This file contains the input parameters that need to beoptimized. All the parameters that are present in SWAT are available here to be edited bythe user. Depending upon the knowledge of the study area, required parameters can be added with a suitable range of values they can take with a certain qualifier (relative, replace, or absolute) as a mathematical operation to optimize the value. The replace qualifier (v_) replaces the available parameter value with the assigned value. The absolute qualifier (a_) adds the assigned value to the available parameter value. The replace qualifier (r_) multiplies the available parameter value by (1 + assigned value). It also contains the number of simulations to be run in every iteration. For applying parameter qualifiers, the changes made to the parameters should have physical meanings and should reflect the physical factors such as land use, soil, elevation, etc., hence the following scheme has been suggested (Abbaspour *et al*., 2015). A minimum of 500 simulations is required in each iteration to get satisfactory results. However, for low-performing devices, 200-300 simulations in each iteration could be acceptable. Usually, amaximum of 4 iterations is enough to obtain decent results.

SUFI2_swEdit.def: This is a SWAT–CUP file that contains the beginning and the ending simulation years. Here, the beginning year of the simulation should be such that it excludes the warm-up period given during the simulation because SWAT, thoughsimulating the warm-up period, doesn't print the output for those years, and hence, SWAT-CUP neglects that period.

File.cio: This is a SWAT file, which is basically a summary of the input commands used in SWAT. The rows to look out for here are the simulation years and the number of warm-up years. Generally, it is recommended to have a warm-up period of 2-3years.

Absolute_SWAT_Values.txt: This file contains most of the parameters availablein SWAT with their absolute minimum and maximum values, i.e., the range in which they operate in SWAT - CUP.

Observation: In this file, the observed dataset is added to three different files, namely, output.rch, output. hru and output.sub, depending upon the observed dataset and simulated variables. However, the latter two files do not appear in SWAT–CUP.

Extraction: This contains two types of files, namely Var_file_rch.txt and SUFI2_extract_rch.def. The first file just involves the editing of the name of the output file for the simulated variable(s) and their respective sub-basin numbers. The second file is a link between the SWAT output tables and the variable(s) that are to be calibrated in SWAT–CUP. Both of these files are self-explanatory.

Objective function: This file is where an appropriate objective function for the evaluation of model performance is selected, besides the addition of the observed dataset and naming the SWAT–CUP output file again, as done in the Observation and Extraction steps. If an acceptable value of the objective function is obtained, the model can be considered properly calibrated. Otherwise, the calibration process is repeated with a new set of parameter values obtained at the end of the previous calibration.

3.4.7 Model Evaluation

To evaluate the performance of the model, two approaches were applied, viz., visual or graphical and statistical index methods. As a means of graphical comparison, hydrographs and scatter plots were used. It helps to compare the timing and magnitude of the predicted runoff to the observed runoff. Additionally, the peak flows and the shape of the recession curves of the predicted and observed runoff help to visualize the goodness-of-fit of the simulated data. In this study, monthly runoff hydrographs were plotted for the calibration and validation periods. A scatter plot helps to facilitates the relationship between two variables. In addition, it is easier to view the outlier data with the help of a scatter diagram. In the present study, scatter plots of monthly observed versus simulated values were plotted. Statistical method provides a quantitative measure of the goodness-of-fit of the predicted values to the observed values. The calibration and validation results were assessed according to statistical criteria such as Nash Sutcliffe Efficiency (NSE), Coefficient of determination (R^2), Standardized root mean squared error (RSR), PBIAS (%), pfactor and r-factor, Root Mean Squared Error (RMSE), Normalized mean squared error (NMSE), Correlation coefficient (r), Percent error, Akaike's Information Criterion (AIC), and Minimum Description Length (MDL). The model performance coefficients, which were used in the present study, are described below:

3.4.7.1 Coefficient of Determination (R^2)

The goodness of fit of a dataset into a statistical model is indicated by the coefficient of determination. The coefficient of determination, R^2, ranges from 0 to 1, where an $R^2 = 1$ signifies a perfect fit, whereas an $R^2 = 0$ indicates no fit at all. The coefficient of determination can be computed using the subsequent formula:

$$R^2 = \frac{[\sum_i (Q_{m,i} - \overline{Q_m})(Q_{s,i} - \overline{Q_s})]^2}{\sum_i (Q_{m,i} - \overline{Q_m})^2 \sum_i (Q_{s,i} - \overline{Q_s})^2} \tag{3.28}$$

Where,

R^2 = Coefficient of determination

Q = Output variable (e.g., discharge, sediment, nutrient etc.)

m = Measured

s = Simulated

i = i^{th} measured or simulated data

Although R^2 is often utilized for model evaluation, it is over-sensitive to high extreme values (outliers) and insensitive to additive and proportional differences between model predictions and observed data (Legates & McCabe, 1999). The nearer the values of E and R^2 are to 1, the better the model performs. The model performance is considered to be acceptable or satisfactory when the E value and R^2 surpasses 0.5 and 0.6, respectively (Moriasi *et al.,* 2007).

3.4.7.2 Nash-Sutcliffe Efficiency (NSE)

Nash and Sutcliffe (1970) came up with a coefficient to assess the predictive power of a hydrological model. The Nash-Sutcliffe efficiency (NSE) is a standardized metric that assesses the relative amount of the residual variance ("noise") relation to the measured data variance ("information") (Nash and Sutcliffe, 1970). NSE examines the degree to which the plot of observed vs simulated data aligns with the 1:1 line. The Nash-Sutcliffe efficiency varies from -∞ to 1 where NSE = 1 signifies an ideal match (Gupta *et al.,* 1999 and Moriasi *et al.,* 2007) between simulated output and observed data, NSE = 0 suggests that the model estimations are accurate as the mean of the observed data, whereas NSE < 0 points to the mean of the observed data being a superior predictor compared to the model. NSE is recommended for use by ASCE (1993), Legates & McCabe (1999), and it is very commonly used, which provides extensive information on reported values. (Servat & Dezetter, 1991) identified the NSE as the most effective function for accurately representing the overall fit of a hydrograph. The NSE performance rating as given by Moriasi *et al*. (2007) is given in

Table 3.16. Also, the performance ratings for NSE reported by different researchers are given in **Table 3.17**. The Nash-Sutcliffe Efficiency can be calculated using the following formula:

$$NSE = 1 - \left[\frac{\sum_i (Q_m - Q_s)^2}{\sum_i (Q_{m,i} - \overline{Q}_m)^2}\right] \quad (3.29)$$

Where,

NSE = Nash-Sutcliffe Efficiency

Q = Output variable (e.g., discharge, sediment, nutrient etc.)

m = Measured

s = Simulated

i = i^{th} measured or simulated data

Table 3.16: Performance rating of NSE (*Moriasi et al., 2007*)

Sl. No.	Performance Rating	NSE value
1	Very Good	0.75 ≤NSE ≤ 1
2	Good	0.65 < NSE ≤ 0.75
3	Satisfactory	0.50 < NSE ≤ 0.65
4	Unsatisfactory	NSE ≤ 0.50

Table 3.17: Reported performance ratings for NSE (Moriasi *et al.,* 2007)

Model	Value	Performance Rating	Modeling Phase	Reference
SWAT	0.54 to 0.65	Adequate	Calibration and Validation	Saleh *et al.,* (2000)
SWAT	>0.50	Satisfactory	Calibration and Validation	Santhi *et al.,* (2001); adapted by Bracmort *et al*., (2006)
SWAT and HSPF	>0.65	Satisfactory	Calibration and Validation	Singh *et al.,* (2005); adapted by Narasimhan *et al.,* (2005)

3.4.7.3 Percent Relative Bias (PBIAS)

It measures the average tendency of the simulated data to be larger or smaller than their observed counterparts. The optimal value of PBIAS is 0.0, with low-magnitude values indicating an accurate model simulation. Positive values indicate model underestimation bias, and negative values indicate model overestimation bias (Moriasi *et al*., 2007). PBIAS is calculated as shown below:

$$PBIAS = \left[\frac{\sum_{i=1}^{n}(O_i - P_i)}{\sum_{i=1}^{n}(O_i)}\right] \times 100 \tag{3.30}$$

The reported values of performance ratings for PBIAS are given in **Table 3.18**.

Table 3.18: Reported performance ratings for PBIAS (Moriasi *et al*., 2007)

Model	Value	Performance Rating	Modeling Phase	Reference
SWAT	< 15%	Satisfactory	Flow calibration	Santhi *et al.,* (2001)
SWAT	< 20%	Satisfactory	For sediment after flow calibration	Santhi *et al.,* (2001)
SWAT	< 25%	Satisfactory	For nitrogen after flow and sediment calibration	Santhi *et al.,* (2001)
SWAT	20%	Satisfactory	Calibration and validation	Bracmort *et al.,* (2006)
SWAT	< 10%	Very good	Calibration and validation	Van Liew *et al.,* (2007)
SWAT	< 10% to 15%	Good	Calibration and validation	Van Liew *et al.,* (2007)
SWAT	< 10% to < 25%	Satisfactory	Calibration and validation	Van Liew *et al.,* (2007)

SWAT	25%	Unsatisfactory	Calibration and validation	Van Liew *et al.,* (2007)

3.4.7.4 Standardized Root Mean Squared Error (RSR)

RSR standardized RMSE (root mean squared error) using the observations' standard deviation, and it combines both an error index and includes a scaling/normalization factor as recommended by Singh *et al.*, (2013). RSR is calculated as the ratio of the RMSE and standard deviation of measured data, as:

$$RSR = \frac{\sqrt{\sum_{i=1}^{n}(O_i - P_i)^2}}{\sqrt{\sum_{i=1}^{n}(O_i - \overline{O}_i)^2}} \tag{3.31}$$

where, RSR = standardized root mean squared error

n= number of observations

O_i= ith observed value

P_i= ith simulated value

$\overline{O}_i$= mean of the observed value

The criteria for rating the performance of hydrological models are presented in **Table 3.19.**

Table 3.19: General performance ratings for recommended statistics for a monthly time step (Moriasi *et al.*, 2007)

Sl. No.	Performance Rating	RSR	PBIAS for Stream flow	R^2
1	Very Good	0.00 ≤ RSR ≤0.50	PBIAS ≤ ± 10	0.7 - 1.0
2	Good	0.50 ≤RSR ≤0.60	± 10 ≤PBIAS ≤ ±15	0.6 - 0.70
3	Satisfactory	0.60 ≤RSR ≤0.70	15 ± ≤ PBIAS ≤ ± 25	0.5 – 0.6
4	Unsatisfactory	RSR >0.70	PBIAS ≥±	<0.5

General reported ratings for coefficient of determination, Nash-Sutcliffe efficiency, Root Mean Square Error, and Mean Relative Bias for calibration and validation process of ArcSWAT as suggested by Rossi *et al.*, (2008) are presented in **Table 3.20**

Table 3.20: SWAT evaluation parameters

Parameter	Value	Rating
Coefficient of determination (R^2)	>0.50	Satisfactory
Nash-Sutcliffe efficiency (NSE)	>0.65	Very good
	0.54 to 0.65	Adequate
	>0.50	Satisfactory
Root mean square error (RMSE)	≤0.5	Very good
	0.5 to 0.6	Good
	0.6 to ≤0.7	Satisfactory
	≥0.7	Unsatisfactory
Percent relative bias (PBIAS)	<±20%	Good
	±20% to 40%	Satisfactory
	>40 %	Unsatisfactory

In order to assess how well the model performed, Green & van Griensven (2008) used standards of NSE > 0.4 and R^2> 0.5. Moriasi *et al.*, 2007 suggested that model simulation can be judged as satisfactory if NSE > 0.50 and RSR ≤ 0.70, and if PBIAS ± 25% for stream flow for a monthly time step.

3.4.7.5 Mean Squared Error (MSE)

The mean squared error (MSE) is used to measure the prediction accuracy. It always produces positive values by squaring the errors. The MSE is zero for a perfect fit, and increased values indicate higher discrepancies between predicted and observed values. The Mean Squared Error between observed and predicted values is determined by the following equation:

$$MSE = \frac{\sum_{i=1}^{n}(O_i - P_i)^2}{n} \qquad (3.32)$$

where, n = number of observations

3.4.7.6 Kling Gupta Efficiency (KGE)

This goodness-of-fit measure was developed by Gupta *et al.,* 2009 to provide a diagnostically interesting decomposition of Nash-Sutcliffe efficiency (and hence MSE), which facilitates the analysis of the relative importance of its different components (correlation, bias, and variability) in the context of hydrological modeling. A revised version of this index was proposed to ensure that bias and variability ratios are not cross-correlated. The values of KGE vary between -∞ to 1, while its optimal value is 1

$$KGE = 1 - \sqrt{(r-1)^2 + (\beta-1)^2 + (\gamma-1)^2} \tag{3.33}$$

where, r= Pearson correlation coefficient

γ= term representing the variability of prediction errors

β= bias term

3.4.8 Uncertainty Analysis Performance Indicators (p-factor and r-factor)

Abbaspour *et al.,* 2007 suggested two measures referred to as the p-factor and the r-factor to evaluate the strength of calibration and uncertainty measures. The p-factor is the percentage of measured data bracketed by the 95 percent prediction uncertainty, often referred to as 95PPU, which was used to quantify all the uncertainties associated with the SWAT model (Arnold *et al.,* 2012). This index provides a measure of the model's ability to capture uncertainties. As all the "true' processes are reflected in the measurements, the degree to which the 95PPU does not bracket the measured data indicates the prediction error (Abbaspour *et al.,* 2015). The 95PPU is calculated at the 2.5 % and 97.5 % levels of the cumulative distribution obtained through Latin hypercube sampling, disallowing 5 % of the very bad simulations. Ideally, the p-factor should have a value of 1, indicating 100 per cent bracketing of the measured data, hence capturing or accounting for all the correct processes.

The r-factor, on the other hand, is a measure of the quality of the calibration and indicates the thickness of the 95PPU and is the average width of the 95PPU band divided by the standard deviation of the measured variable, and varies in the range 0–1 (Abbaspour *et al.*, 2007). Its value should ideally be near zero, hence coinciding with the measured data. The combination of p-factor and r-factor together indicates the strength of the model calibration and uncertainty assessment (Arnold *et al.*, 2012). The p- and r-factors are closely related to each other, which indicates that a larger p-factor can be achieved only at the expense of a higher r-factor. After balancing these two factors, and at an acceptable value of the r- and p-factors, the calibrated parameter ranges can be generated (Yang *et al.*, 2008). The r-factor is given by **Eq. 3.21**

$$r - factor = \frac{\frac{1}{n}\sum_{t_{i=1}}^{n}(y_{t_i,97.5\%}^{M} - y_{t_i,2.5\%}^{M})}{\sigma_{obs}} \quad (3.34)$$

3.5 Sensitivity Analysis

The objective of the sensitivity analysis is to identify which parameters require more attention and research to reduce output uncertainty, which parameters influence output variability more, which parameters are less significant and don't require calibration, and which parameters are highly correlated with model output (Hamby, 1994; Hsu *et al.*, 1995). The influence of different parameters on the simulation result, i.e., the response of the output variable to a change in the input parameter, is evaluated through sensitivity analysis (White & Chaubey, 2005). It is often challenging to determine which parameters to calibrate so that they accurately reflect the field parameters as closely as possible. In such situations, sensitivity analysis helps to identify and rank the parameters that have a noteworthy effect on specific model outputs of interest (Saltelli *et al.*, 2000). SUFI-2 calibration and uncertainty algorithm, which is linked with SWATCUP-2012 version 5.1.6, was used to perform a sensitivity analysis of parameters. One-factor-at-a-time (OAT) design, with a combination of Global Sensitivity Analysis, was used to conduct sensitivity analysis. After an initial iteration run of the model, the most sensitive parameters were identified, and only those parameters were adjusted so that the calibration efficiency could be improved and calibration variances could be minimized in the study area.

3.5.1 Global Sensitivity Analysis

The global sensitivity analysis is carried out by resolving the subsequent multiple regression system that reverses the parameters produced by the sampling of the Latin Hypercube (LH) associated with the values of the objective function. The relationship is depicted through **Eq. 3.35.**

$$g = \propto + \sum_{i=1}^{m} \beta_i b_i \tag{3.35}$$

Subsequently, the outcome of each parameter (bi) is calculated using the t-test. Estimates of the average number of changes in the objective occupation corresponding to the changes in each parameter are the sensitivities acquired accordingly. In this analysis, the sensitivities of parameters are transactions in terms of t-stat and p-value. A high t-stat value and a low p-value value suggest a highly sensitive parameter and vice versa.

3.5.2 Uncertainty Analysis

SWAT models of the river basin scale suffer from the problem of high model uncertainties. These can be classified as theoretical model uncertainty, input uncertainty, and parameter uncertainty. Here, many processes might be taking place in the river basin, which are not added into the model either deliberately or inadvertently, resulting in large uncertainties. Uncertainties are able to also occur due to simplifications in the conceptual model. Using P-factor and R-factor, quantification of uncertainties is prepared. The P-factor is the percentage of observed data expressed by the outcome of the simulation, and the R-factor is the depth of the 95PPU envelop. Despite the fact that there is no ideal information for the values of these factors, a P-factor > 0.7 and an R-factor < 1 has been suggested by Abbaspour *et al.*, 2015 as an adequate limit of uncertainty for runoff simulation.

3.6 Watershed Prioritization

Watershed prioritization has become a crucial framework for identifying regions vulnerable to environmental degradation and developing effective conservation strategies. This process allows for the efficient use of limited resources to tackle soil erosion, sedimentation, and hydrological issues, which are vital for sustainable natural resource management (Shrimali *et al.,* 2001; Vittala *et al.,* 2004). The importance of this methodology lies in its ability to combine geomorphological, hydrological, and land use data to determine priority areas for soil and water conservation efforts (Mishra & Nagarajan, 2010). Effective watershed management is key to reducing environmental degradation, encouraging balanced development, and maintaining long-term ecosystem health (Kudnar & Rajasekhar, 2020).

The morphometry of a watershed is a crucial component of hydrological analysis, as it provides a quantitative understanding of topographic relief, drainage patterns, and sediment transport dynamics (Das & Das, 2024a, 2024b). Morphometric parameters, such as drainage density, bifurcation ratio, and stream frequency, play a crucial role in assessing flood susceptibility and soil erosion potential (Sreedevi *et al.*, 2009; Maddamsetty & Pawar, 2023). Recent advancements in remote sensing (RS) and geographic information systems (GIS) have revolutionized watershed analysis by enabling the rapid and accurate assessment of morphometric attributes across diverse landscapes (Grohmann, 2004; Kouli *et al.,* 2007; Kaya *et al*., 2019; Yadav *et al*., 2024). These tools have become indispensable for delineating watershed boundaries, extracting drainage networks, and prioritizing sub-watersheds based on their vulnerability to environmental stress (Patel *et al.,* 2016; Dey *et al.*, 2025). The study utilized a multi-analytical framework to prioritize sub-watersheds within the study areas based on morphometric and topohydrological characteristics.

3.6.1 Arc-SWPT Analysis

The SWPT is an automated extension (Rahmati *et al.*, 2019) within ArcGIS software that prioritizes sub-watersheds for soil and water conservation based on 12 factors, including morphometric, topographic, and hydrological parameters, using rational methods (Abdulkareem *et al.*, 2018). The SWPT tool generates 12 key parameters—stream frequency (Fs), bifurcation ratio (Rb), form factor (Rf), elongation ratio (Re), circularity ratio (Rc), drainage density (D), texture ratio (Rt), compactness coefficient (Cc), constant of channel maintenance (C), topographic wetness index, stream power index, and sediment transport index (STI)—from a high-resolution DEM. SWPT employs an automated weighted sum analysis (WSA) to rank hydrological units, assigning weights based on statistical correlations to determine each factor's importance (**Figure 3.15**). The prioritization formula (Aher *et al.*, 2014) is defined as follows.

$$Prioritization = \sum_{i=1}^{n} W_i \times X_i \tag{3.36}$$

where W_i is the weight of each parameter and $X_i$is the corresponding value. SWPT offers efficient and accessible analysis of data, avoiding shortcomings of the traditional methods. Sub-watersheds are ranked by Cp values, with lower values indicating higher susceptibility (Rahmati *et al.*, 2019). This data can be used with machine learning algorithms for prioritization and sustainable management practices.

3.6.2 DEM-Derived Hydrological Indices

To incorporate terrain-based hydrological processes into watershed prioritization, three widely used indices were derived from the Digital Elevation Model (DEM): the Topographic Wetness Index (TWI)**,** Stream Power Index (SPI)**,** and Sediment Transport Index (STI)**.** These indices represent soil moisture distribution, flow erosivity, and sediment transport potential, respectively.

1. Topographic Wetness Index (TWI)

$$TWI = \ln(\frac{A_s}{\tan\beta}) \tag{3.37}$$

A_s= upslope contributing area per unit contour length (m²/m)
β= local slope angle (radians)
TWI reflects the tendency of a location to accumulate water, thereby identifying potential zones of soil saturation (Beven & Kirkby, 1979).

2. Stream Power Index (SPI)

$$SPI = A_s \times \tan\beta \tag{3.38}$$

SPI quantifies the erosive power of flowing water and highlights areas susceptible to high runoff energy (Moore & Wilson, 1992).

Sediment Transport Index (STI)

$$STI = (\frac{A_s}{22.13})^m \times (\frac{\sin\beta}{0.0896})^n \quad (3.39)$$

m,n = empirical constants (commonly *m*=0.4, *n*=1.3).

STI is a measure of the potential for sediment detachment and deposition, providing insight into erosion vulnerability (Moore *et al.*, 1991).

Together, these indices were computed within the GIS environment and subsequently integrated into the Sub-Watershed Prioritization Tool (SWPT) framework for ranking sub-watersheds based on erosion susceptibility.

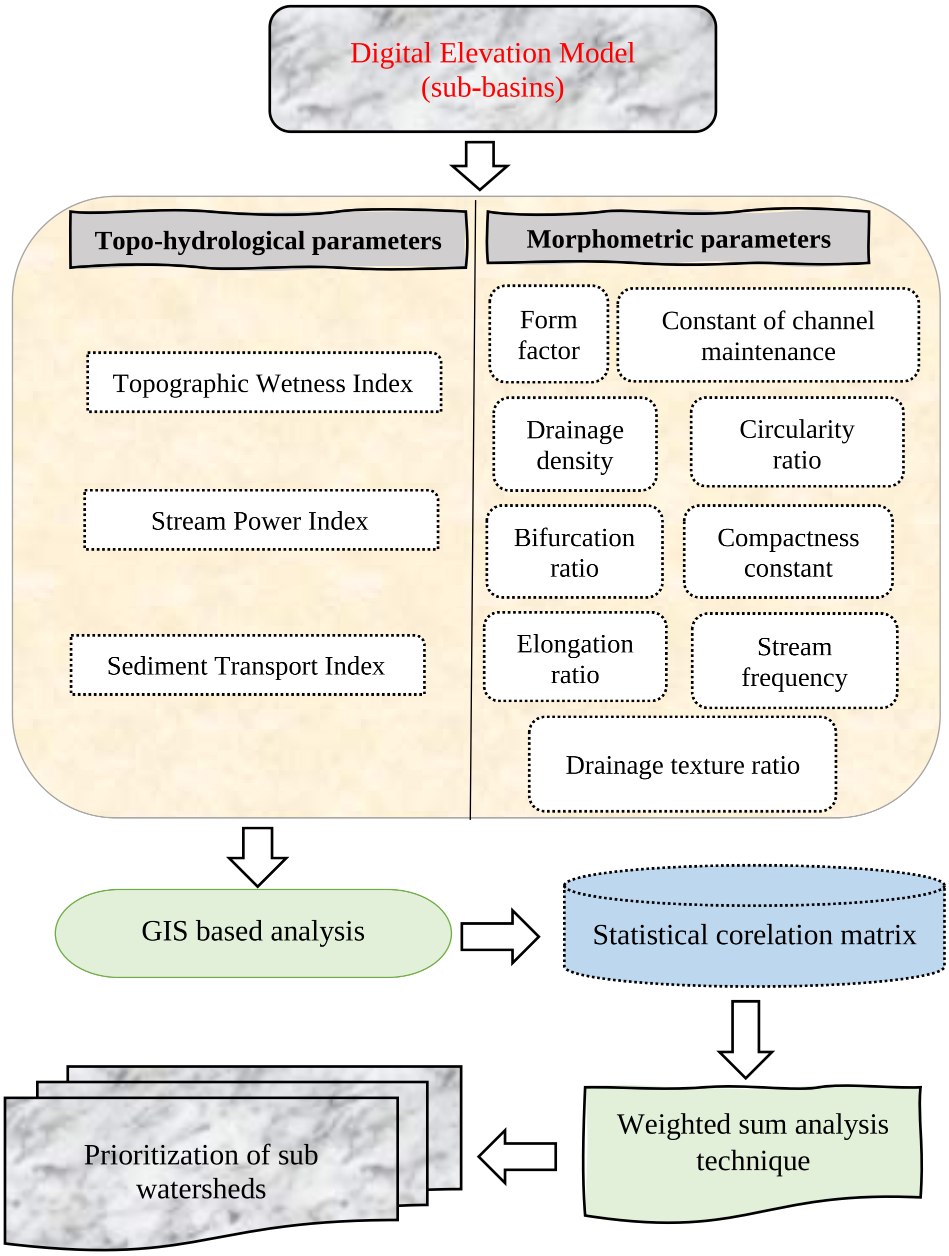

Figure 3.15: A conceptual framework for prioritizing sub-watersheds using SWPT.

3.7 Climate Change Impacts Assessment

Climate change affects hydrologic cycle by changing the water flow in various systems through decreasing/increasing precipitation and creating adverse climate for biota (Shrestha *et al.*, 2016). Climate change has become a major concern for our planet, and it is crucial to understand its impacts on natural resources and ecosystems.

3.7.1 Coupled Model Intercomparison Project Phase 6 (CMIP 6)

One of the key components of CMIP6 is the use of SSPs, which are scenarios that describe possible future socioeconomic developments and their impacts on the climate system. CMIP6 provides an outline for climate models to be compared and used for climate change research. By incorporating CMIP6 data into SWAT, researchers can better understand how climate change will affect agriculture and natural resources at the local and regional scales. By understanding the potential impacts of climate change, researchers/water managers can develop strategies to mitigate its effects and adapt to a changing climate. The precipitation and temperature data in the SWAT model are varied based on the projected values. This process is applied for the present situation and the optimum situation to assess the effect of change in climate conditions on runoff rate in the future watershed situation, instead of continuing the present condition. The future condition of climatic variables can be predicted by different Institutes' GCMs. These data are included in AR6 (Sixth Assessment Report) (IPCC (Intergovernmental Panel on Climate Change) Six Assessment Report) SSPs scenarios that vary based on radiative forcing, shown in **Figures 3.16** and **3.17**. These scenarios mainly focus on providing the concentration of greenhouse gases and radiative forcing according to time passage (Shrestha *et al.*, 2016).

There are five SSP scenarios used in CMIP6, ranging from a sustainable future (SSP1-1.9) to a future with high greenhouse gas emissions and limited environmental policy (SSP5-8.5). The SSP scenarios are designed to capture a range of possible future socioeconomic and environmental conditions, allowing researchers to explore how different drivers of change may impact the climate system.

This research utilizes historical data on precipitation and temperature from the recently released CMIP6 GCMs. In the CMIP6 phase, the previous RCP (Representative Concentration Pathway) scenarios (RCP 2.6, RCP 4.5, RCP 6.0, and RCP 8.5) from CMIP5 have been updated to new shared socio-economic pathways (SSPs), namely SSP1-

1.9, SSP2-4.5, SSP3-7.0, SSP4-6.0, and SSP5-8.5, each considering radiative forcing levels for the year 2100. These SSPs were established by the climate change research community to facilitate integrated analyses of future climate vulnerabilities, impacts, adaptation, and mitigation, as outlined by Riahi *et al.*, 2017. The details about the different SSPs are given below:

3.7.1.1 SSP1-1.9 (Sustainable Development)

This scenario represents a future in which sustainable development is achieved through strong global cooperation, improved governance, and investments in education, health, and infrastructure. It assumes rapid technological progress and low population growth.

3.7.1.2 SSP2-4.5 (Middle of the Road)

This scenario represents a future in which current trends continue, with moderate population growth, gradual improvements in economic development, and limited environmental policy. It assumes a mix of fossil fuels and renewable energy sources.

3.7.1.3 SSP3-7.0 (Regional Rivalry)

This scenario represents a future with high regional inequality, slow economic growth, and fragmented international cooperation. It assumes a reliance on fossil fuels and limited environmental policy.

3.7.1.4 SSP4-6.0 (Inequality)

This scenario represents a future in which rapid economic development occurs sustainably, with a focus on renewable energy and global cooperation. It assumes low population growth and rapid technological progress.

3.7.1.5 SSP5-8.5 (Fossil-fueled Development)

This scenario represents a future with high greenhouse gas emissions and limited environmental policy, driven by a focus on economic growth and a lack of international cooperation. It assumes a continued reliance on fossil fuels.

These SSP scenarios provide a useful framework for exploring how different socioeconomic and environmental conditions may impact the climate system. By using these scenarios in combination with climate models, researchers can better understand the potential impacts of climate change and develop strategies to mitigate its effects.

One way to study climate change is by using the SWAT, which is a hydrological parameter-based model that simulates the impact of land use, climate change, and other factors on water resources and soil quality. Recent studies have used SWAT to investigate the impacts of climate change on water resources and crop yield, using data from the CMIP6 (Turconi *et al.*, 2020; Kumar *et al.*, 2022, 2024). The results of these studies have shown that climate change is likely to have significant impacts on water resources and crop yield in many regions of the world. For example, some regions may experience increased precipitation, leading to flooding and erosion, while others may experience droughts and reduced crop yield. These impacts will have significant implications for food security, water management, and other aspects of human and ecosystem well-being.

In climate change research, GCMs are used to simulate and predict future climate scenarios. However, with numerous GCMs available, it can be challenging to determine which models are the most reliable and accurate. To address this issue, a recent review was conducted to select the best GCM models for climate change research for Indian conditions. The review analyzed various GCM models and their performance in simulating past climate conditions, as well as their ability to predict future climate scenarios. After careful analysis, the review identified 13 GCM models that were deemed to be the most reliable and accurate for climate change research. These models were selected based on their ability to accurately simulate past climate conditions, as well as their robustness and consistency in predicting future climate scenarios across different regions and time periods.

The climate model datasets used in this study were obtained from the NASA Center for Climate Simulation (NCCS) via their Climate Data Portal. The data consist of CMIP6 outputs, including variables such as temperature, precipitation, and related climate parameters, covering the period from 2030 to 2040 for the Dhansiri Basin. These datasets were employed to analyze future climate scenarios relevant to this research.

The NEX-GDDP-CMIP6 (NASA Earth Exchange Global Daily Downscaled Projections) dataset, created to aid in climate change impact studies at local to regional scales, is available for download. This dataset comprises downscaled climate scenarios from Global Climate Model (GCM) runs. NASA's GISS (Goddard Institute for Space Studies) has contributed various model configurations to the CMIP6 model data repository through the Earth System Grid Federation (ESGF). The data is useful for studying climate change impacts.

For studying the major forcing climate extremes related to food and water resources in this study, SSP2-4.5 was used (Mishra *et al.*, 2020). The selection of the best model among these 13 GCM models provides a useful framework for climate change research, as it allows researchers to focus on the most reliable and accurate models for predicting future climate scenarios. By using these models, researchers can better understand the potential impacts of climate change and develop strategies to mitigate its effects.

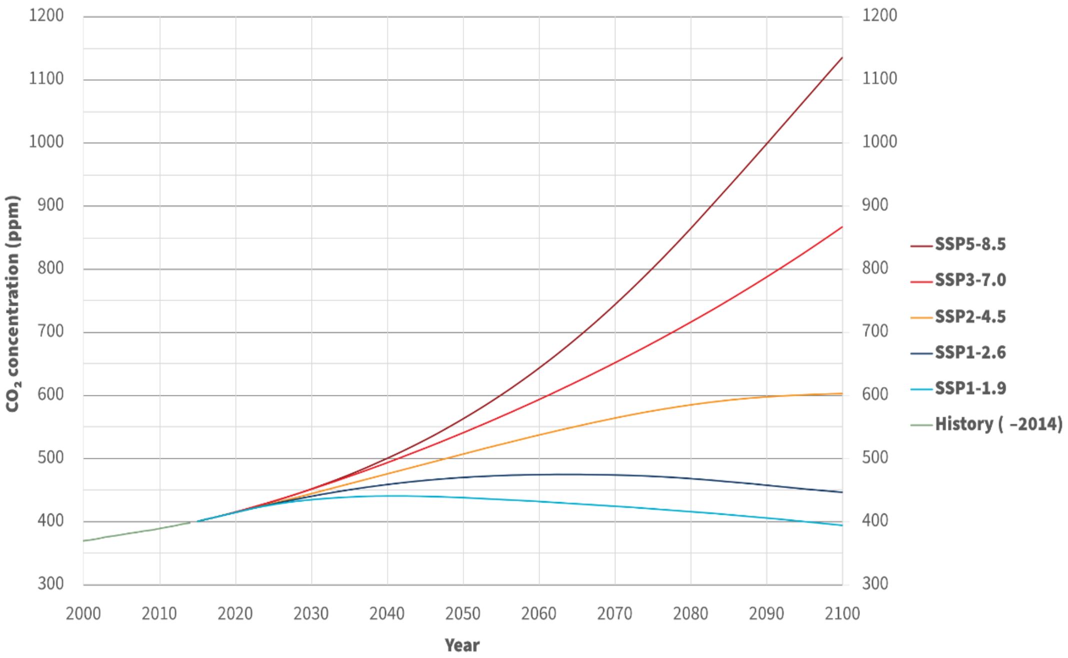

Figure 3. 16: Carbon Di Oxide (C02) concentration in different SSPs (IPCC, 2016)

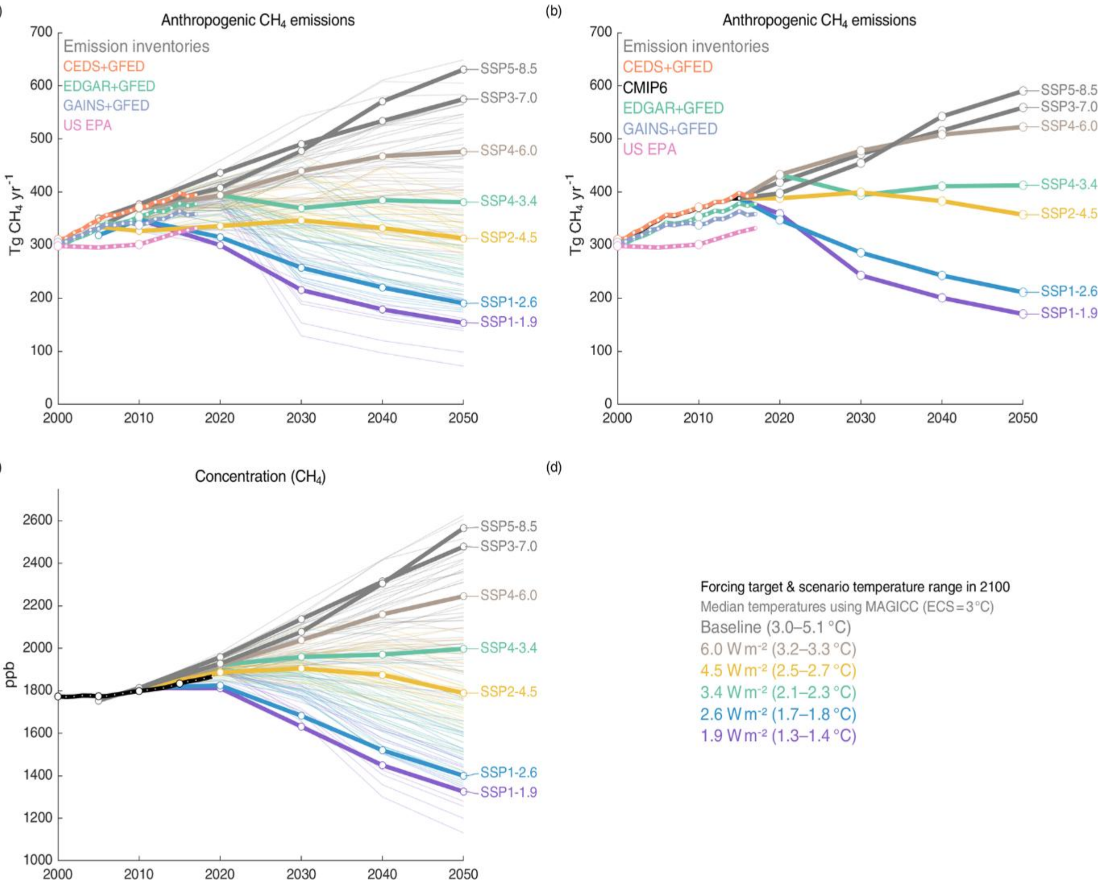

Figure 3. 17 (a)Anthropogenic Methane (CH4) emission inventories in different GCM, (b)Anthropogenic CH4 emission inventories in different GCM with CMIP 6, (c)concentration of CH4 in different SSPs, and (d) forcing target & scenario temperature range of SSPs (IPCC report)

3.7.2 Entropy Based Weight Method for Best Model Selection

Entropy originally emerged as a thermodynamic concept, employed to characterize the irreversible changes in the state of motion. Subsequently, in the realm of information, entropy found application in gauging the uncertainty associated with various phenomena. The determination of entropy weight involves the utilization of a judgment matrix. In the context of information, entropy serves as a tool to quantify the extent of valuable information present in a given problem. The relationship is such that a higher quantity of information corresponds to lower levels of uncertainty and entropy, and conversely.

GCM model selection is of paramount importance when it comes to making complex decisions, especially in the field of multi-criteria decision-making (MCDM). The choice of the most suitable GCM model can have a significant impact on the accuracy and reliability of decision outcomes. This is where the entropy weight method comes into play, offering a systematic and objective approach to evaluate and rank different GCM models based on their performance and suitability for a given decision problem. By considering various criteria and their respective weights, the entropy weight method ensures a comprehensive and unbiased selection process, leading to more informed and robust decisions.

3.7.2.1 Performance Indicator

The criteria used for entropy weight calculation for GCM model selection include the evaluation of different performance indicators such as root mean square error, mean absolute error, and correlation coefficient, etc. These indicators provide quantitative measures of the model's ability to accurately simulate various climate variables. Additionally, the weighting criteria may also consider the model's ability to capture extreme events, such as heatwaves or heavy precipitation, as these events are crucial for understanding the impacts of climate change. The entropy weight method takes into account the relative importance of each criterion to assign weights that reflect their significance in the overall model selection process. (Sepehri *et al.*, 2019; Zhu *et al.*, 2020; Li *et al.*, 2021). Various researchers concluded that the correlation coefficient, BIAS, PBIAS, NSE, RMSE, KGE, and coefficient of determination were good to check the performance of each selected GCM model's historical data with respect to IMD gridded data to assess the performance of the GCM model. Out of these, R^2, NSE, and KGE were used to decide model performance with respect to the IMD (India Meteorological Department) gridded dataset. R^2 (**Eq.3.28**), NSE (**Eq. 3.29**), and KGE (**Eq. 3.33**) were defined earlier.

3.7.2.2 Entropy Weight Method (EWM) Procedure

In this approach, the evaluation involves setting m indicators and n samples, where the measured value of the i^{th} indicator in the j^{th} sample is denoted as xij. The initial step is standardizing the measured values, with the standardized value of the ith index in the j^{th} sample represented as P_{ij}. The calculation method for P_{ij} is determined as follows:

$$P_{ij} = \frac{X_{ij}}{\sum_{i=1}^{n} X_{ij}} \tag{3.40}$$

In practical EWM evaluations, it is common to set a threshold when $P_{ij} = 0$ for the sake of computational convenience. Within the EWM framework, the entropy value E_i associated with the i^{th} index is specifically defined as:

$$E_i = \frac{\sum_{j=1}^{n} P_{ij}.\ln P_{ij}}{\ln n} \tag{3.41}$$

The range of entropy value E_i is [0, 1]. The larger the E_i is, the greater the differentiation degree of index *i* is, and more information can be derived. Hence, higher weight should be given to the index.

The entropy value E_i ranges from 0 to 1, where a larger E signifies a higher degree of differentiation for index i, yielding more extractable information. Consequently, a higher weight is assigned to the index. In the EWM, the calculation method for weight is determined based on this principle:

$$W_i = \frac{1 - E_i}{\sum_{i=1}^{m}(1 - E_i)} \tag{3.42}$$

Where,

W = Final weight

E_i = Entropy value

CMIP6 aims to improve our understanding of future climate conditions through enhanced emissions data, land-use scenarios, improved physical processes, and model parameterization, as described by Eyring *et al.* (2016) and O'Neill *et al.* (2016).

In this research, 5 sets of historical Global Climate Models (GCMs) of precipitation, maximum and minimum temperatures, sourced from the CMIP6 database spanning the period from 2030 to 2040 selected. This timeframe aligns with the data availability of CMIP6 GCMs, which extends up to 2040 and corresponds to the 10-year baseline period used in CMIP6. The selection criteria for GCMs were based on the presence of at least one SSP projection for the future, common GCMs across precipitation and temperature variables, and relevance to the study area. It's noteworthy that CMIP6 incorporates various ensemble members such as r1i1l1f1, r2i1l1f1, and r3i1l1f1, signifying different aspects of the models like realization, initialization, and model physics. This code is justified as:

The code "r1i1l1f1" in the context of CMIP6 refers to specific attributes of a model ensemble member. Each component in the code has a distinct meaning:

(i) r1: Realization

This indicates the realization number. In climate modelling, multiple runs or realizations of the same model may be conducted with slightly different initial conditions or parameter settings to account for inherent variability.

(b) i1: Initialization

This represents the initialization number. Similar to realizations, different initial conditions may be used to capture the range of possible outcomes.

(c) l1: land use initialization

This signifies the land use initialization number. Land use data can have an impact on climate simulations, and different initializations may be employed to explore this variability.

(d) f1: model physics

This corresponds to the model physics number. Climate models may incorporate different parameterizations or formulations for physical processes (e.g., cloud physics, radiation), and varying these settings can lead to different model outputs.

In summary, "r1i1l1f1" represents the first realization, first initialization, first land use initialization, and first model physics setting within a particular ensemble of a CMIP6 climate model. The use of multiple realizations and initializations allows researchers to assess the range of possible climate outcomes and uncertainties associated with a specific model.

For our investigation, emphasis was placed on the first ensemble members, r1i1l1f1, ensuring an unbiased comparison. Further details regarding the selected CMIP6 GCMs are outlined in **Table 3.21**.

Table 3.21: Selected GCM models for study

S No.	CMIP6 model name	Institution, country	Resolution (lon. by lat. in degrees)
1	ACCESS-CM2	Australian Community Climate and Earth System Simulator, Australia	1.9° × 1.3°
2	BCC-CSM2-MR	Beijing Climate Center, China	1.1° × 1.1°
3	CANESM5	Canadian Centre for Climate Modelling and Analysis, Canada	1.9° × 1.9°
4	MPI-ESM1-2-HR	Max-Planck-Institut für Meteorologie, Germany	2.5° × 1.3°
5	MRI-ESM2-0	Meteorological Research Institute, Japan	1.1° × 1.1°

CHAPTER 4.

RESULTS AND DISCUSSION

This chapter presents the findings derived from the comprehensive morphometric, hydrological, and modeling assessments performed on the Dzuza watershed, Dhansiri river basin, and Khova sub-watershed. The research was conducted in five principal segments. First, a comprehensive morphometric and hydrological investigation of the three watersheds was conducted utilizing GIS techniques. Morphometric characteristics were extracted from DEM datasets, and hydrological analysis was performed to comprehend watershed dynamics regarding drainage, slope, and runoff potential. Second, the SWAT model was developed, calibrated, and validated with 10 years of daily meteorological and hydrological data from 2012 to 2021. The first two years (2012–2013) functioned as a warm-up period, data from 2014–2018 were utilized for calibration, and 2019–2021 for validation. The model's performance was assessed using statistical indices including Nash Sutcliffe Efficiency (NSE), Coefficient of determination (R^2), Percent Relative Bias (PBIAS), Standardized root mean squared error (RSR), and p- and r-factors, along with graphical and scatter plot assessments. Third, a sensitivity study of SWAT model parameters was performed using SWAT-CUP to determine the most significant parameters influencing streamflow, thereby enhancing model robustness and reliability. Fourth, the Sub-Watershed Prioritization Tool (SWPT) in ArcGIS facilitated the prioritization of sub-watersheds, allowing for the identification of essential sub-basins that necessitate urgent soil and water conservation interventions. Finally, future climate projections were evaluated utilizing CMIP6 climate datasets for the Dhansiri river basin, offering insights into the anticipated effects of climate change on future flow and sediment dynamics. This chapter offers a thorough assessment of watershed processes, model efficacy, parameter sensitivity, and prospective hydrological scenarios through five components, establishing a foundation for efficient watershed management methods in the studied area.

4.1 Morphometric Parameters

For morphometric characteristics, the measurements were carried out using DEM having a 30m resolution. The basic morphometric parameters were calculated very precisely to avoid any misinterpretations, as these values are directly proportional to other parameters and can affect most of the other parameters. For exporting the watershed boundary and stream network in vector format, ArcGIS 10.5 software was used. The watershed delineation was carried out to generate information on basic morphometric parameters such as area, perimeter, stream order, and stream length, which was further used to calculate other linear, areal, and relief parameters of the drainage basin. The results of these calculations are summarized in **Table 4.1** for all three study areas.

4.1.1 Linear Aspects

Table 4.1 displays the outcomes of the linear characteristics, including the stream order (U), stream length (Lu), mean stream length (Lsm), stream length ratio (RL), and bifurcation ratio (Rbm).

4.1.1.1 Stream Order (U)

The Dzuza watershed has been determined to be a 6th-order trunk stream. It exhibits the highest stream order frequency in first-order streams, followed by second-order streams, third-order streams, and ultimately, the highest-order stream. The basin contains 1061 first-order streams, 248 second-order streams, 53 third-order streams, 13 fourth-order streams, two fifth-order streams, and one sixth-order stream (**Figure 4.1 (a)**). The Dhansiri River Basin has a stream order of seven, including 5055 first-order streams, 1073 second-order streams, 240 third-order streams, 58 fourth-order streams, 14 fifth-order streams, three sixth-order streams, and one seventh-order stream (**Figure 4.1 (b)**). The Khova sub-watershed has a stream order of 5, including 309 first-order streams, 61 second-order streams, 17 third-order streams, 4 fourth-order streams, and one fifth-order stream (**Figure 4.1 (c)**).

4.1.1.2 Stream Length (Lu)

Stream orders 1, 2, 3, 4, 5, and 6 have respective lengths of 433.45, 192.90, 77.99, 58.42, 31.19, and 5.63 km for the Dzuza watershed. The stream length of the

Dzuza, Dhansiri, and Khova was 799.58 km, 4116.50 km, and 266.22 km, respectively.

4.1.1.3 Mean Stream Length (Lsm)

The mean stream lengths of the Dzuza watershed, Dhansiri river basin, and Khova sub-watershed are 133.26 km, 588.07 km, and 53.24 km

4.1.1.4 Stream Length Ratio (RI)

Dzuza watershed exhibited a stream length ratio of 0.46 on average. The stream length ratios ranged from 0.18 for the sixth/fifth order to 0.53 for the fifth/fourth order, 0.75 for the fourth/third order, 0.40 for the third/second order, and 0.44 for the second/first order. In the Dzuza watershed, RI values exhibit an unpredictable declining trend, reflecting fluctuations in slope and lithology alongside moderate basin maturity. The Dhansiri river basin displays more stable ratios, indicating homogenous lithological influence and a well-established drainage system. Conversely, the Khova sub-watershed exhibits uneven RI patterns, indicating structural influence and underdeveloped drainage systems.

4.1.1.5 Bifurcation Ratio (Rb)

The bifurcation ratio for the Dzuza watershed transitioned from the sixth to fifth order was 2, from fifth to fourth was 6.5, from fourth to third was 4, from third to second was 4.6, and from second to first order was 4.2, resulting in an average value of 4.3. The basin displays a prolonged shape and a slight impact on the structure. The average Rb ratio of the studied basin provides insight into how the structural and lithological factors influence the drainage system's ongoing development in the investigated area. The bifurcation ratio for the Dhansiri river basin transitioned from the seventh to sixth order was 3, from sixth to fifth was 4.6, from fifth to fourth was 4.1, from fourth to third was 4.1, from third to second order was 4.5, and from second to first order was 4.7, resulting in an average value of 4.2. The average bifurcation ratio of the Khova sub-watershed is 4.2.

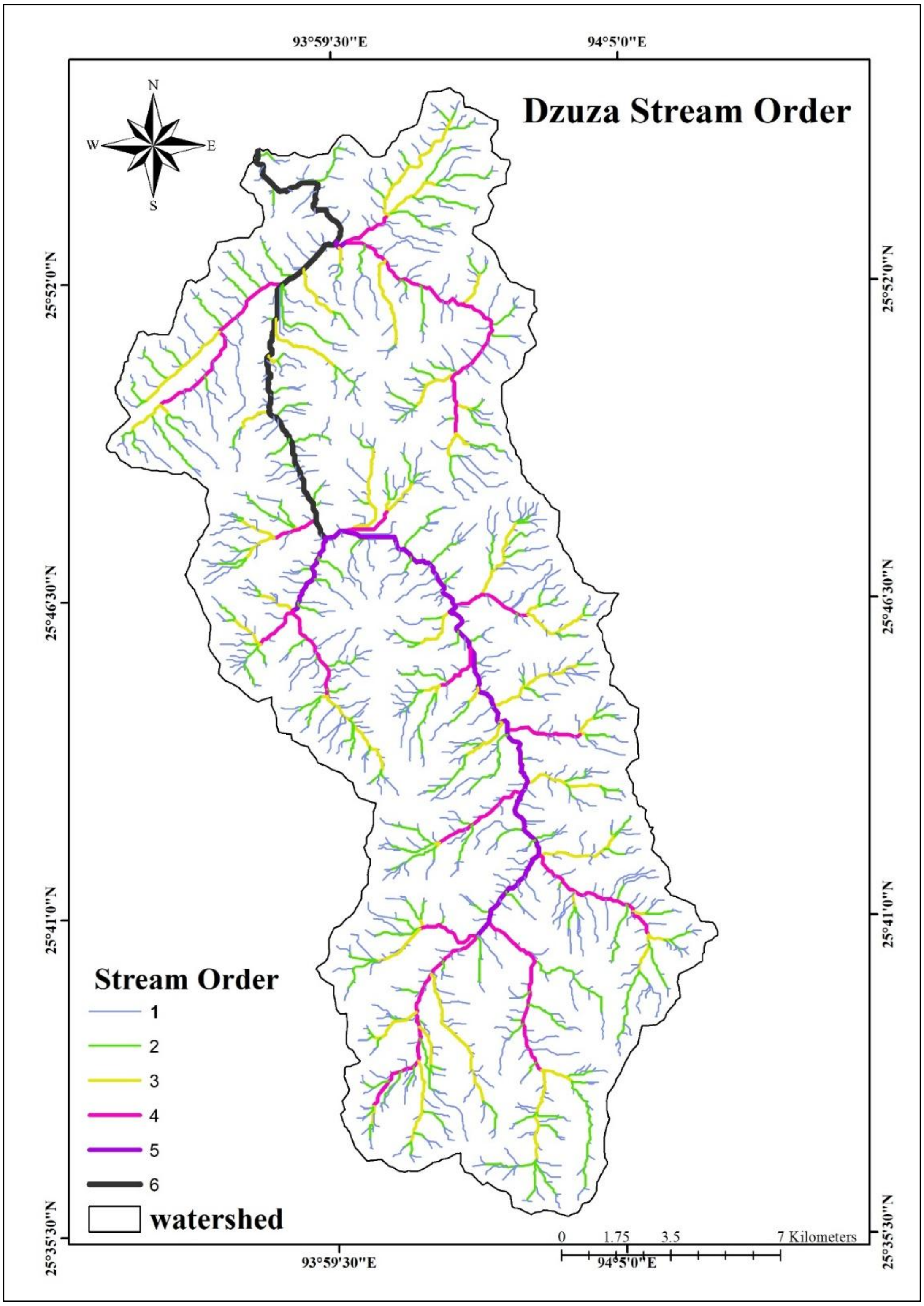

Figure 4.1 (a): Stream order map of Dzuza watershed

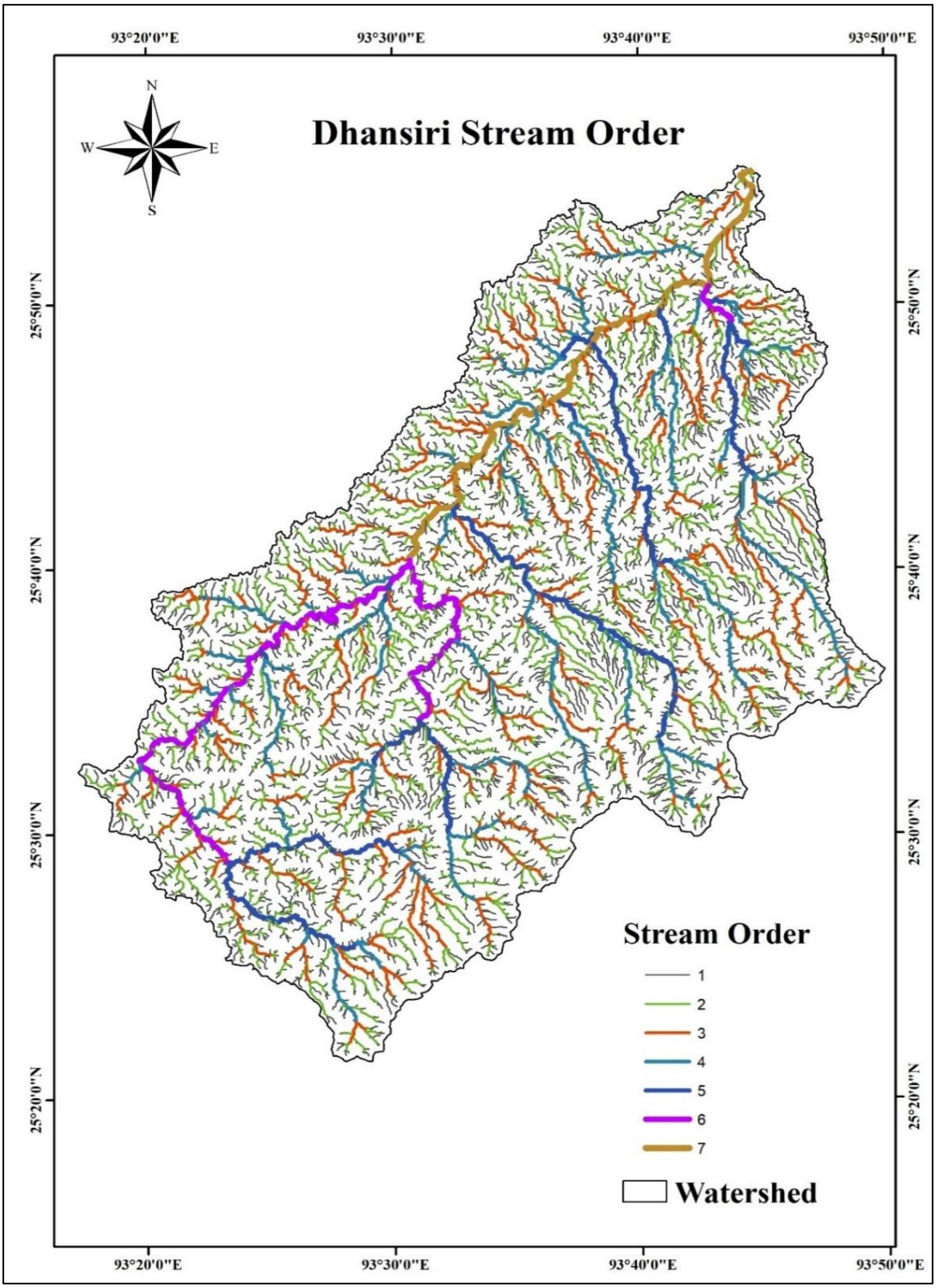

Figure 4.1 (b): Stream order map of Dhansiri river basin

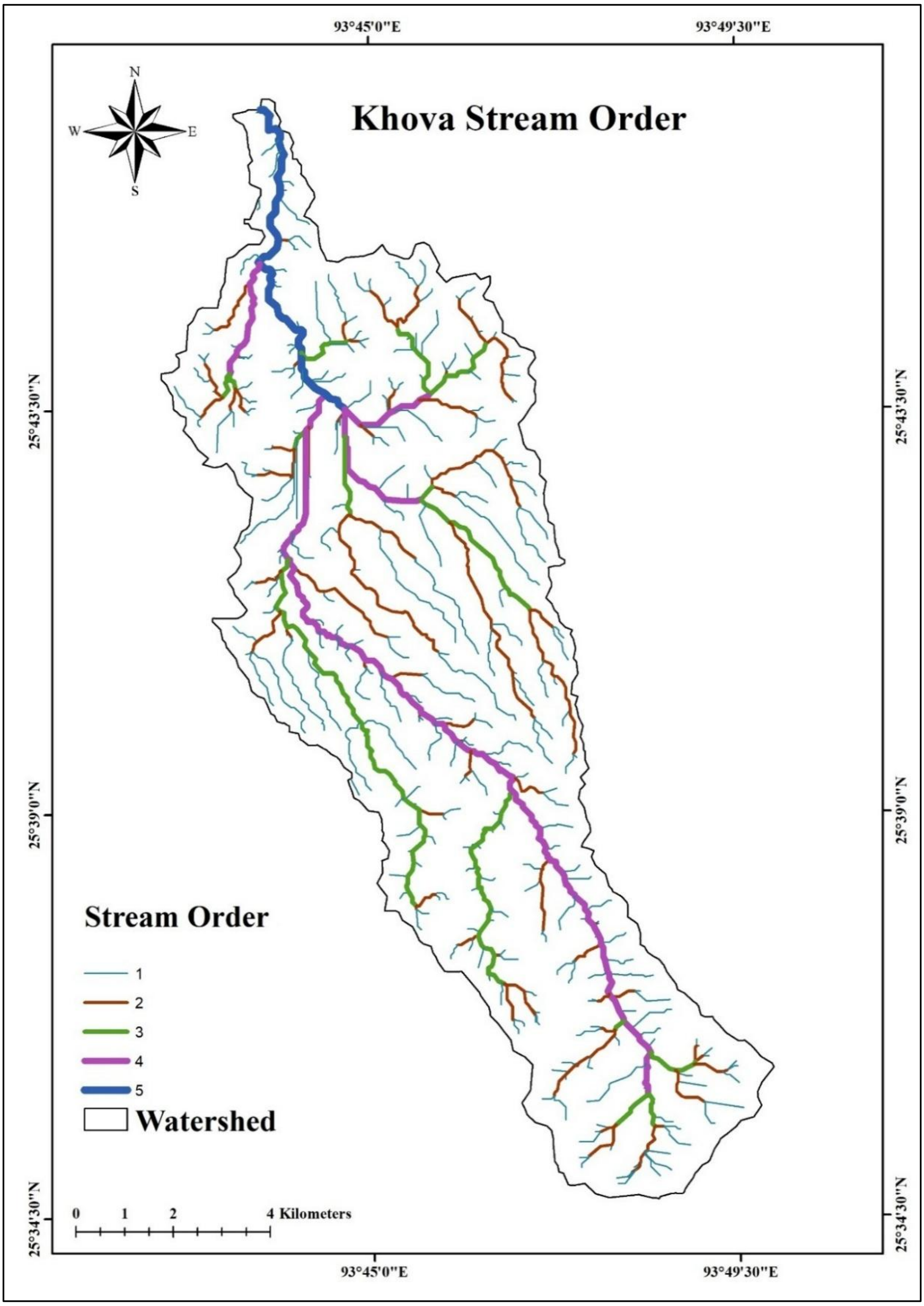

Figure 4.1 (c): Stream order map of Khova sub-watershed

4.1.2 Relief Aspects

The relief aspect encompasses the examination of various factors, including basin relief (Bh), relief ratio (Rh), ruggedness number (Rn), height of basin mouth/outlet (z), maximum height of the basin (Z), total basin relief (H), relative relief ratio, gradient ratio, and Melton ruggedness number (MRn). **Table 4.1** presents a comprehensive list of the values.

4.1.2.1 Basin Relief (Bh)

The Dzuza watershed exhibits a basin relief of 2,815 meters, indicating a rolling landscape and considerable water movement, which leads to extensive soil erosion. The Dhansiri river basin and Khova sub-watershed have basin relief of 1,931 meters and 1,600 meters, respectively.

4.1.2.2 Relief Ratio (Rh)

The relief ratios of the Dzuza watershed, Dhansiri river basin, and Khova sub-watershed have been determined to be 0.079, 0.028, and 0.067, respectively.

4.1.2.3 Ruggedness number (Rn)

The research region of Dzuza, Dhansiri, and Khova has a ruggedness number of 6.44, 4.69, and 3.86, respectively.

4.1.2.4 Height of Basin Outlet (z)

The research areas of the Dzuza watershed, Dhansiri river basin, and Khova sub-watershed have an elevation of 198.0 m, 138 m, and 167, respectively.

4.1.2.5 Maximum Height of the Basin (Z)

In the case of the Dzuza watershed, Dhansiri river basin, and Khova sub-watershed, these measurements were recorded as 3.013 km, 2.067 km, and 1.767 km, respectively.

4.1.2.6 Total Basin Relief (H)

The Dzuza watershed, Dhansiri river basin, and Khova sub-watershed have a total difference in elevation of 2815 m, 1931 m, and 1600 m, respectively.

4.1.2.7 *Relative Relief Ratio (R_{hp})*

The relief ratios in the Dzuza watershed, Dhansiri river basin, and Khova sub-watershed are 2.567, 0.761, and 2.286, respectively.

4.1.2.8 *Gradient Ratio (G_r)*

The current study found that the gradient ratio for the Dzuza watershed was 0.079, indicating a relatively low value. This suggests a flat riverbed with sluggish water flow capable of carrying only limited amounts of very fine particles. The Dhansiri river basin's gradient ratio was 0.028, and the Khova sub-watershed's gradient ratio was 0.067, both of which are also very low.

4.1.2.9 *Melton Ruggedness Number (MRn)*

The MRn values for the research areas of the Dzuza, Dhansiri, and Khova were 150.54, 46.88, and 152.24, respectively.

4.1.3 Aerial Aspects

4.1.3.1 *Drainage Density (Dd)*

The Dd value of the Dzuza watershed was discovered to be 2.287(**Figure 4.2 (a)**), indicating a coarse drainage basin; the Dhansiri basin's Dd value is 2.427(**Figure 4.2 (b)**), and the Khova sub-watershed's Dd value is 2.410 (**Figure 4.2 (c)**), indicating coarse drainage density.

4.1.3.2 *Stream Frequency (Fs)*

The computed stream frequency (Fs) value for the Dzuza watershed was 3.941 (>3), suggesting that the watershed has a coarse texture, experiences significant runoff, and has moderate to high elevation differences with limited permeability. Stream frequency (Fs) values for the Dhansiri basin and Khova sub-watershed were 3.799 and 3.594, which can be attributed to high relief and low infiltration capacity.

4.1.3.3 *Drainage Texture (T)*

Findings suggest that the drainage texture of the Dzuza watershed was quantified as 12.569, suggesting an extraordinarily fine texture. Whereas the drainage texture of the Dhansiri basin was 25.387, indicating an extremely fine texture. The Khova sub-watershed was 4.608, which is a moderate texture.

4.1.3.4 Form Factor (Rf)

The Dzuza watershed, Dhansiri river basin, and Khova sub-watershed have a form factor value of 0.340, 0.356, and 0.192, which signifies their highly elongated shape.

4.1.3.5 Circularity Ratio (Rc)

The circulation ratio of 0.6, 0.33, and 0.283 in the Dzuza watershed, Dhansiri river basin, and Khova sub-watershed indicates that the basin is substantial.

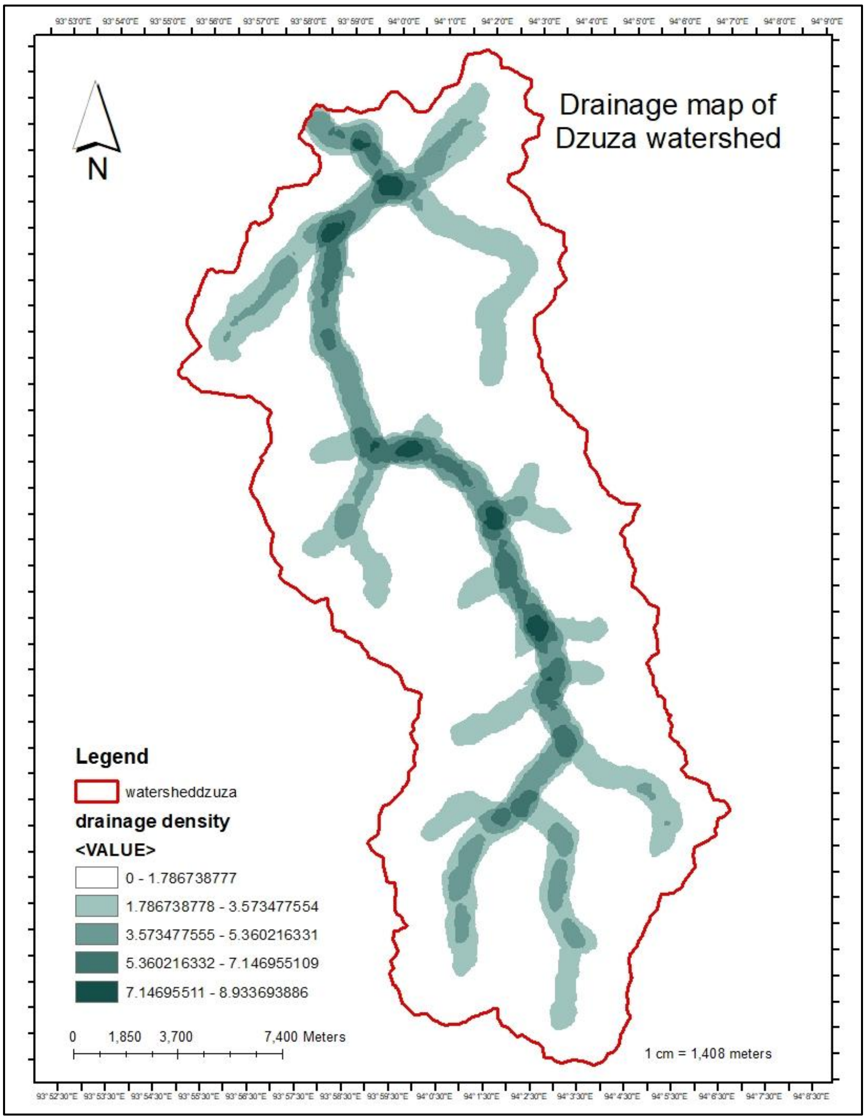

Figure 4.2 (a): Drainage density map of Dzuza watershed

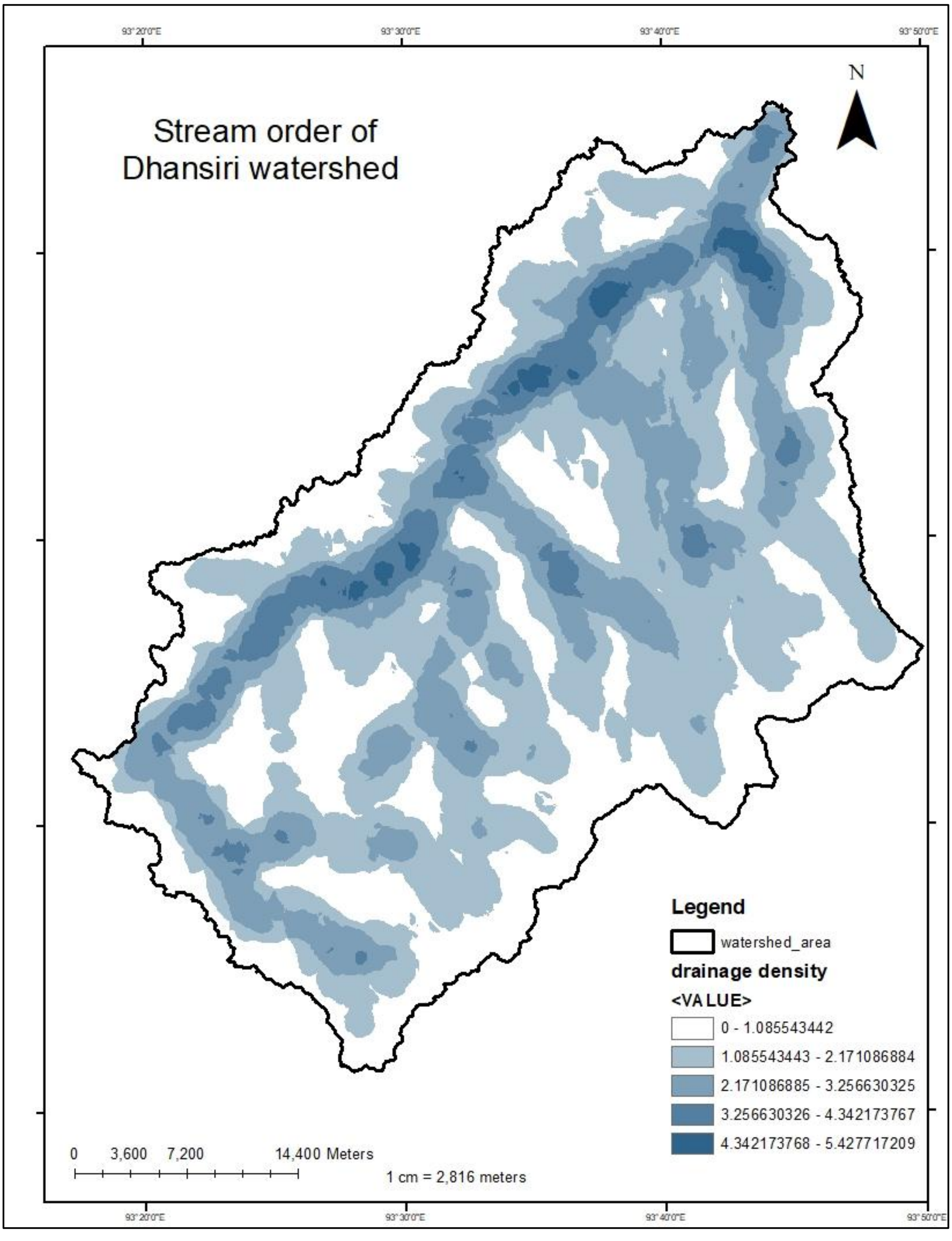

Figure 4.2 (b): Drainage density map of Dhansiri river basin

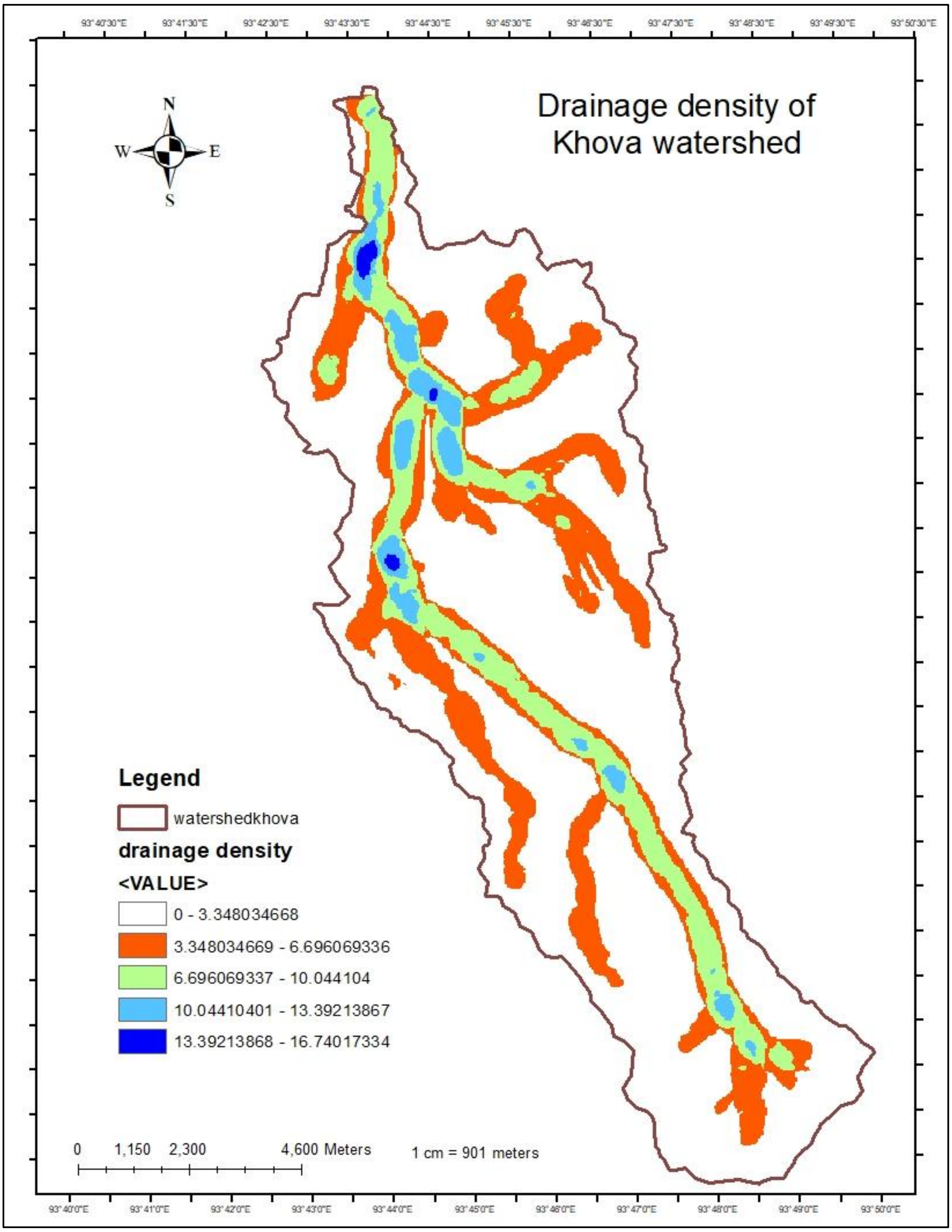

Figure 4.2 (c): Drainage density map of Khova sub-watershed

4.1.3.6 Elongation Ratio (Re)

The Dzuza watershed, Dhansiri river basin, and Khova sub-watershed have an elongated shape, as indicated by their elongation ratio of 0.594, 0.673, and 0.495, respectively.

4.1.3.7 Length of Overland Flow (Lof)

The length of overland flow values is categorized into three groups: low value (0.2), moderate value (0.2-0.3), and high value (>0.3). The overland flow length (Lof) in the research area measured 0.219, 0.219,0.206, and 0.207 for the Dzuza watershed, Dhansiri river basin, and Khova sub-watershed respectively, indicating a landscape with moderate to high elevation variations, significant water runoff, and noticeable water infiltration into the ground.

4.1.3.8 Constant Channel Maintenance (C)

The channel maintenance constant is determined by permeability, rock type, relief, vegetation, and length of rainfall. The constant channel maintenance in the watersheds was found to be 0.437, 0.412, and 0.415, respectively.

4.1.3.9 Infiltration Number

As Horton (1964) suggested, higher infiltration numbers suggest a decrease in infiltration capability and an increase in runoff. The basin's infiltration number (If) was 9.013, 9.222, and 8.663, for the Dzuza, Dhansiri, and Khova respectively, indicating a reduced capacity for infiltration and increased runoff.

4.1.3.10 Basin Area (A)

The region holds the same importance as the total length of the stream in terms of statistical significance. The Dzuza, Dhansiri, and Khova areas were 351.4594, 1697.116, and 108.7512 km^2, respectively.

4.1.3.11 Basin Perimeter (P)

The basin's perimeter of Dzuza, Dhansiri, and Khova is calculated using Geographic Information System (GIS) tools, revealing a measurement of 109.6, 253.8, and 69.9 kilometers, respectively.

4.1.3.12 Length of Basin (Lb)

The basin length refers to the most significant dimension of a basin that runs along the main drainage line, as defined by Schumm in 1956. The basin of the research areas Dzuza, Dhansiri, and Khova has a length of 35.5, 69.0, and 23.9 kilometers, respectively.

4.1.3.13 Fitness Ratio (Rf)

The topographic fitness metric is defined as the fitness ratio proposed by Melton in 1957. The fitness ratios for the Dzuza watershed, Dhansiri river basin, and Khova sub-watershed were 0.428, 0.438, and 0.430, respectively.

Table 4.1: Findings of the morphometric parameters in the study areas

Morphometric Parameters	Dzuza	Dhansiri	Khova
Linear Aspects			
Stream Order (U)	1-6	1-7	1-5
Stream Length (Lu), km	799.58	4116.50	266.22
Mean Stream Length (Lsm)	0.58	0.64	0.67
Stream Length Ratio (Rl)	2.18	1.99	2.12
Bifurcation Ratio (Rb)	4.31	4.19	4.19
Relief Aspects			
Basin Relief (Bh), m	2815.0	1931	1600
Relief Ratio (Rh)	0.079	0.028	0.067
Ruggedness Number (Rn)	6.44	4.69	3.86
Height of basin mouth (z), m	198.0	138	167
Maximum height of the basin (Z), m	3013	2069	1767
Total basin relief (H), m	2815	1931	1600
Relative relief ratio (Rhp)	2.57	0.76	2.29
Gradient ratio (Rg)	0.079	0.028	0.067
Melton ruggedness number (MRn)	150.54	46.89	152.24
Aerial Aspects			
Drainage Density (Dd)	2.29	2.43	2.41
Stream Frequency (Fs)	3.94	3.79	3.59
Drainage Texture (T)	12.57	25.39	5.67
Form Factor (Rf)	0.34	0.36	0.19
Circularity Ratio (Rc)	0.6	0.33	0.28
Elongation Ratio (Re)	0.59	0.67	0.49
Length of Overland Flow (Lof)	0.219	0.21	0.21
Constant Channel Maintenance (C)	0.44	0.41	0.41
Infiltration number (If)	9.01	9.22	8.66
Basin area (A), km^2	351.46	1697.12	108.75
Basin perimeter (P), km	109.6	253.83	69.97
Fitness ratio (Rf)	0.43	0.44	0.43

4.2 Model Application

The sequential technique for model construction outlined in Chapter III encompasses the preprocessing of input data, namely, daily records of precipitation, streamflow, and temperature. Additional pertinent parameters and the formulation of a digital elevation model (DEM), land use map, and soil map in accordance with the specified formats of the SWAT model. With the provision of these inputs, the model was prepared to execute.

4.2.1 Watershed Delineation

Watershed delineation was conducted with a digital elevation model (DEM) with a resolution of 30 m x 30 m. Based on this criterion, the delineation of the Dzuza, Dhansiri, and Khova watersheds resulted in one basin for Dzuza and three sub-basins, with sub-basin number 2 in Dhansiri identified as the Khova watershed, as illustrated in **Figure 4.3**. The total area of the watershed determined through delineation was 351.4594, 1697.116, and 108.751 km² for the three basins. The watershed outlet was manually identified using the edit option in the SWAT model.

4.2.2 Hydrologic Response Units (HRU)

Table 4.2 shows the area and percent distribution of Hydrologic Response Units (HRUs) by LULC and slope class in the Dzuza Watershed. Forest (FRST) HRUs were dominant across the watershed, regardless of slope classification, on soil type Ao76-2-3c-4276, covering areas from 3,635.54 ha (10–20% slope) to 12,323.90 ha (30–50% slope), with steep forested areas (>50% slope) totaling 8,993.81 ha. Urban land (URML) appeared in smaller, fragmented patches, covering 569.77 ha on slopes of 20–30%, and 99.93 ha on slopes above 50%, while water bodies (WATR) were mostly confined to small patches under 10 ha, spread across slopes of 0–50%. Rangeland (RNGE) HRUs were mainly found on moderate to steep slopes, with the largest unit (30–50%) covering 158.38 ha. Agricultural land (AGRL) HRUs were limited to specific low-slope areas, with the largest being 30.89 ha on 10–20% slopes. The HRU framework highlighted the importance of slope in creating watershed heterogeneity: gentle slopes (0–10%) support agriculture, urban development, and small forest patches; moderate slopes (10–30%) are mostly forest and rangeland; and steep slopes (30–50% and >50%) are primarily forest and rangeland, making them critical for soil erosion.

Table 4.2: Area and percent distribution of Hydrologic Response Units (HRUs) by LULC and slope class in Dzuza watershed

LULC	Slope Class	Area (ha)	Percent within LULC	Percent watershed
AGRL	0-10	9.71	17.38	0.03
AGRL	10-20	30.89	55.29	0.09
AGRL	20-30	6.44	11.53	0.02
AGRL	30-50	6.44	11.53	0.02
AGRL	50-9999	2.38	4.26	0.01
FRST	0-10	968.19	2.96	2.75
FRST	10-20	3635.54	11.13	10.33
FRST	20-30	6740.77	20.64	19.16
FRST	30-50	12323.9	37.73	35.04
FRST	50-9999	8993.81	27.53	25.57
RNGE	0-10	136.31	19.32	0.39
RNGE	10-20	184.68	26.18	0.52
RNGE	20-30	145.93	20.68	0.41
RNGE	30-50	158.38	22.45	0.45
RNGE	50-9999	80.25	11.37	0.23
URML	0-10	104.26	6.02	0.29
URML	10-20	392.85	22.68	1.12
URML	20-30	569.77	32.89	1.62
URML	30-50	565.27	32.63	1.61
URML	50-9999	99.93	5.77	0.28
WATR	0-10	7.15	38.57	0.02
WATR	10-20	4.41	23.81	0.01
WATR	20-30	2.74	14.76	0.01
WATR	30-50	2.29	12.38	0.01
WATR	50-9999	1.94	10.48	0.01

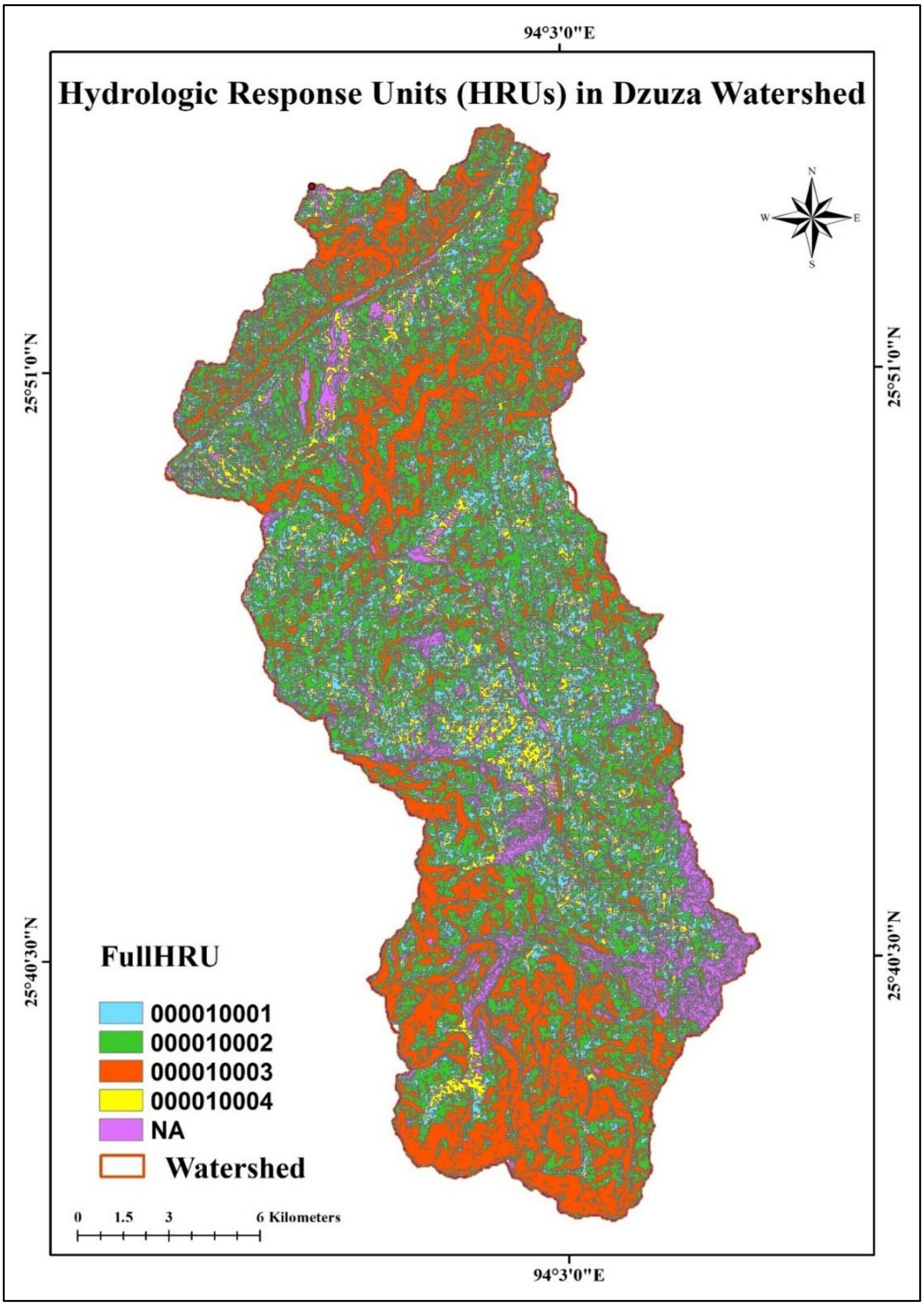

Figure 4.3: HRU map of the Dzuza watershed.

The HRU Land Use/Soils Report generated by SWAT indicates that the Dhansiri watershed comprises 25 HRUs distributed across three sub-basins (**Figure 4.4**). At the watershed level, forest land use (FRST) covers a total of 169,957.93 hectares. **Table 4.3** shows that the soils are mainly made up of Ao76-2-3c-4276

(58.38%), followed by Af47-2b-4255 (25.34%) and Af48-2ab-3637 (16.28%). Regarding slope distribution, about 56% of the watershed features mild to moderate slopes (0–20%), while severe slopes (30–50%) account for 18.95%, and extremely steep slopes (>50%) make up 6.45%. Sub-basin 1 has the highest number of Hydrologic Response Units, showing a variety of soil and slope combinations. For example, HRU 1 (FRST–Af47-2b-4255–0–10%) covers 10,411.03 hectares (6.76% of the sub-basin area), while HRU 9 (FRST–Ao76-2-3c-4276–10–20%) spans 20,119.15 hectares (13.06%). Sub-basins 2 and 3 are somewhat smaller, with fewer HRU pairings. Sub-basin 2 is defined solely by the Ao76-2-3c-4276 soil class, which includes five slope-based Hydrologic Response Units. The largest HRU is FRST–Ao76-2-3c-4276–30–50%, covering 3,465.31 hectares (31.89% of the sub-basin), followed by the 20–30% slope category at 20.88%. Sub-basin 3 has a smaller area; however, it shows greater variability in Hydrologic Response Units. It contains both Af47-2b-4255 and Ao76-2-3c-4276 soil types, spread across various slope categories. The main HRUs are FRST–Ao76-2-3c-4276 20–30% (1,138.42 hectares, 22.57%) and FRST–Ao76-2-3c-4276–30–50% (1,132.60 hectares, 22.46%), together making up about half of the sub-basin area.

Table 4.3: Hydrological Response Units (HRUs) for the Dhansiri river basin

Sub basin	HRU No.	Soil	Slope	Area (ha)	Percent Subbasin
1	1	Af47-2b-4255	0-10	10411.03	6.76
1	2	Af47-2b-4255	10-20	13833.98	8.98
1	3	Af47-2b-4255	20-30	9759.13	6.34
1	4	Af47-2b-4255	30-50	8542.63	5.55
1	5	Af48-2ab-3637	10-20	8585.23	5.57
1	6	Af48-2ab-3637	0-10	19075.99	12.38
1	7	Ao76-2-3c-4276	0-10	18120.33	11.76
1	8	Ao76-2-3c-4276	30-50	18970.43	12.31
1	9	Ao76-2-3c-4276	10-20	20119.15	13.06
1	10	Ao76-2-3c-4276	50-9999	8712.56	5.66
1	11	Ao76-2-3c-4276	20-30	17959.44	11.66

Table 4.3 (continued)

2	12	Ao76-2-3c-4276	50-9999	1587.09	14.6
2	13	Ao76-2-3c-4276	20-30	2268.99	20.88
2	14	Ao76-2-3c-4276	10-20	1998.54	18.39
2	15	Ao76-2-3c-4276	30-50	3465.31	31.89
2	16	Ao76-2-3c-4276	0-10	1499.73	13.8
3	17	Af47-2b-4255	10-20	179.9	3.57
3	18	Af47-2b-4255	30-50	103.07	2.04
3	19	Af47-2b-4255	20-30	139.14	2.76
3	20	Af47-2b-4255	0-10	99.91	1.98
3	21	Ao76-2-3c-4276	50-9999	660.05	13.09
3	22	Ao76-2-3c-4276	30-50	1132.6	22.46
3	23	Ao76-2-3c-4276	10-20	1118.93	22.18
3	24	Ao76-2-3c-4276	20-30	1138.42	22.57
3	25	Ao76-2-3c-4276	0-10	476.34	9.44

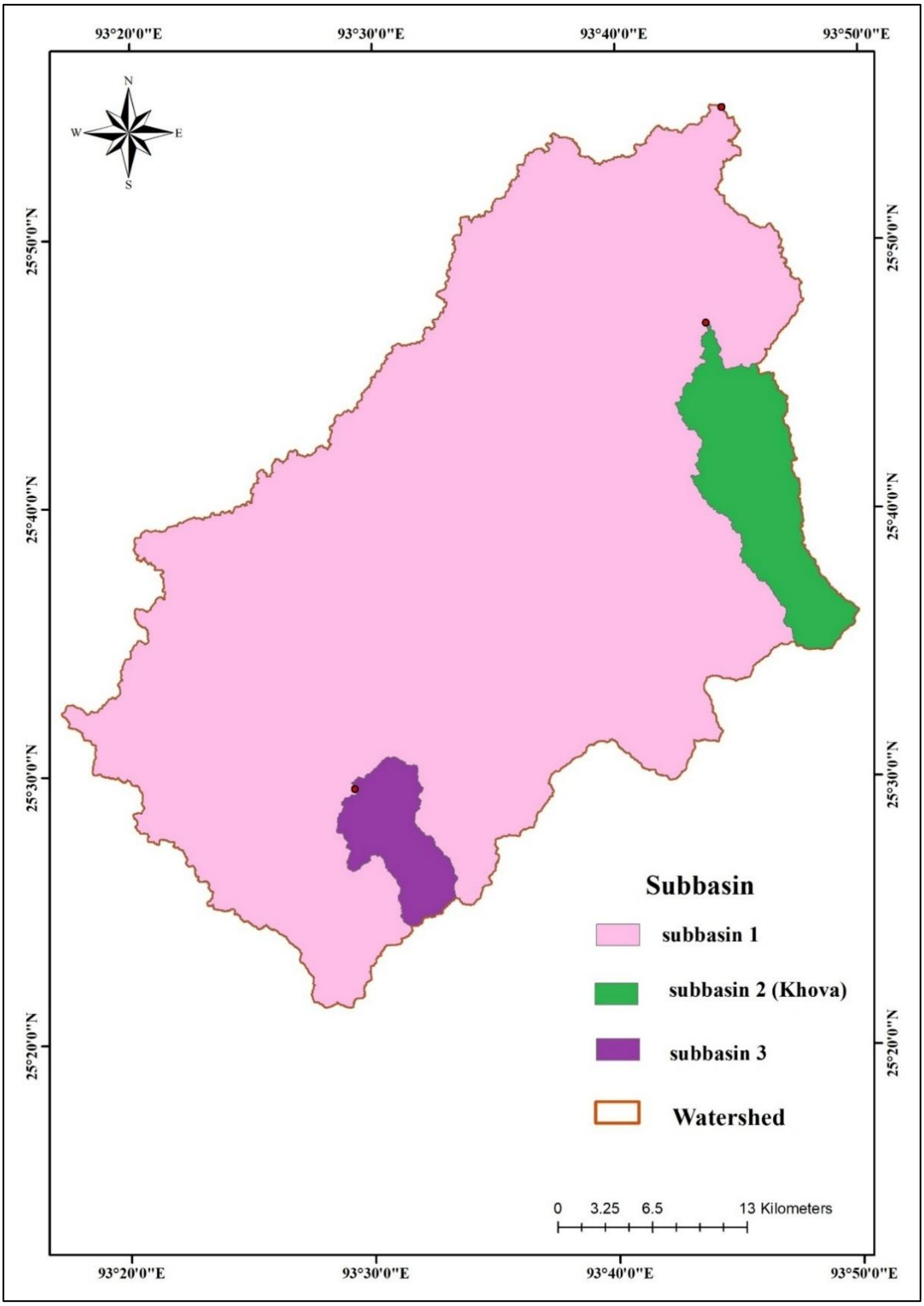

Figure 4.4: Sub-basin map of Dhansiri river basin

4.3 Sensitivity Analysis

Hydrologic models consist of many parameters with default values determined for certain hydro-climatic conditions. As physical and meteorological conditions evolve, parameter-output connections likewise alter. Screening parameters prior to calibration aids in (i) concentrating efforts on the most significant factors, (ii) reducing computing expenses, and (iii) elucidating predominant processes.

Consequently, we conducted two complementary sensitivity analyses for the Dzuza watershed, Dhansiri river basin, and Khova sub-watershed, using daily discharge at the outlets (FLOW_OUT) as the response variable.

One At a Time (OAT) sensitivity: One parameter was varied individually within a physically feasible range while others remained constant, and sensitivity was assessed based on alterations in event peaks, timing, hydrograph form, and recessions in relation to observations. This stage was employed to identify key controls and to formulate a process-oriented calibration sequence.

Global Sensitivity Analysis (GSA): We utilized a SUFI-2 within SWAT-CUP to capture joint effects and parameter interactions. For each basin, thousands of parameter sets were sampled utilizing the model's "R/A/V" update rules (R: multiplicative, A: additive, V: replacement). The significance of parameters was subsequently graded using t-statistics and p-values, offering a quantifiable hierarchy to inform calibration and showing which parameters could be maintained at baseline levels. The OAT diagnostics (mechanistic insight) and the GSA rankings (statistical proof) collectively established the definitive calibration technique for all three basins.

4.3.1 OAT Sensitivity Analysis of Dzuza Watershed (FLOW_OUT_1) (Table 4.4)

Most influential controls

- *Formation and timing of runoff*: SURLAG primarily controlled peak timing and sharpness; lower values produced earlier, sharper peaks. OV_N showed only minor effects in this basin.
- *Infiltration–storage partitioning:* CN2, SOL_K, SOL_AWC, SOL_BD governed event volumes and early recessions (↑CN2 or ↓SOL_K/↓SOL_AWC ⇒ larger peaks and higher runoff ratios).

    - *Groundwater feedback:* REVAPMN, GWQMN, GW_DELAY, RCHRG_DP altered low-flow persistence and late recessions via shallow-aquifer interactions.
    - *Routing:* CH_N2 (high) and CH_K2 (moderate) controlled channel attenuation and in-channel leakage.
    - *Energy-balance polishers*: ESCO (moderate) and EPCO (low) influenced inter-event ET and thus low-flow levels.
- *Sediment parameters*: USLE_K and USLE_P were held constant for flow calibration.

Recommended calibration sequence:

1. CN2, SOL_K, SOL_AWC (get volumes right)
2. SURLAG (fix peak timing/shape) + CH_N2 if more attenuation is needed
3. REVAPMN, GWQMN, GW_DELAY, RCHRG_DP (recessions/baseflow)
4. CH_K2 (routing losses, if needed)
5. ESCO/EPCO (inter-event losses)

4.3.2 OAT Sensitivity Analysis of Dhansiri River Basin (FLOW_OUT_1) (Table4.5)

Most influential controls

- *Hillslope hydraulics:* OV_N and SURLAG distinctly influence peak time and sharpness; elevated values result in broader and delayed peaks.
- *Runoff partitioning:* CN2, SOL_K, and SOL_AWC predominantly influenced the infiltration–runoff distribution and event volumes; higher CN2 combined with lower SOL_K/SOL_AWC resulted in larger, more rapid peaks.
- *Groundwater exchange:* REVAPMN and RCHRG_DP (deep percolation fraction) altered inter-event persistence; increased values diminished shallow-aquifer feedback and decreased post-storm flow.

  Recommended calibration sequence:

  1. CN2, SOL_K, SOL_AWC
  2. OV_N, SURLAG
  3. REVAPMN, RCHRG_DP (recessions/baseflow)

4.3.3 OAT Sensitivity Analysis of Khova Sub-Watershed (FLOW_OUT_2) (Table 4.6)

Most influential controls

- *Channel routing and leakage:* CH_N2 (channel Manning's n) and CH_K2 (channel alluvium conductivity) exhibited significant sensitivity—decreasing CH_N2 intensified peaks, while increasing CH_K2 augmented channel losses and diminished peaks.
- *Bank storage and groundwater timing:* ALPHA_BNK, GW_DELAY, and GWQMN influenced the volume and timing of baseflow; reduced GW_DELAY and GWQMN resulted in more rapid and substantial baseflow contributions.
- *Hillslope partitioning:* CN2, SOL_K, and SOL_AWC governed event volumes, similar to the other basins.
- *Shallow aquifer exchange and prolonged leakage:* REVAPMN, GW_REVAP (where applicable), and RCHRG_DP provide inter-event flow thresholds.
- *Energy-balance polishers:* ESCO and EPCO influenced ET and consequently low-flow dynamics.

Recommended calibration sequence:

1. CN2, SOL_K, SOL_AWC (quantities)
2. CH_N2, CH_K2 (peak morphology/attenuation)
3. ALPHA_BNK, GW_DELAY, GWQMN (baseflow time)
4. REVAPMN / GW_REVAP / RCHRG_DP
5. ESCO/EPCO (optimization of losses).

The OAT screening significantly optimized calibration. Dzuza has a linked hillslope-groundwater interaction with significant evapotranspiration feedback; Dhansiri is primarily influenced by hillslope runoff and shallow-aquifer exchange; Khova incorporates substantial routing and bank-storage regulation. Concentrating on the aforementioned ranked subsets enhanced efficiency, diminished equifinality, and elucidated process interpretation across all three basins.

Table 4.4: Sensitive parameters of Dzuza watershed

Parameter	Sensitivity level	Hydrologic role	Calibration notes
CH_N2	High	Channel roughness (Manning's n)	Affects peak attenuation and travel time in channels.
CN2	High	Runoff generation (curve number)	Controls event runoff; higher CN2, higher peaks, shorter lag.
GWQMN	High	Baseflow threshold	Sets groundwater contribution start; alters low flows/peaks sustain.
GW_DELAY	High	GW response time	Controls timing of baseflow response and recession limbs.
RCHRG_DP	High	Deep-aquifer percolation fraction	Redistributes water to deep aquifer; reduces quick flow, boosts baseflow.
REVAPMN	High	Revap threshold (shallow aquifer)	Affects evap from GW to soil; tweaks low flows and inter-event water.
SOL_K	High	Soil saturated hydraulic conductivity	Infiltration vs runoff partitioning; changes peak size and timing.
SURLAG	High	Surface runoff lag time	Shifts/attenuates peaks; larger SURLAG smooths and delays hydrograph.
CH_K2	Moderate	Channel alluvium conductivity	Influences in-channel losses; affects peak attenuation & baseflow.
ESCO	Moderate	Soil evaporation compensation	(Energy-balance polisher) Modulates soil evaporation; tunes inter-event losses.

Table 4.4 (continued)

SOL_AWC	Moderate	Soil available water capacity	Buffers quick runoff; affects peak rounding and recession.

Table 4.5: Sensitive parameters of Dhansiri river basin

Parameter	Sensitivity level	Hydrologic role	Calibration notes
CN2	High	Runoff generation	Controls event runoff; higher CN2, higher peaks, shorter lag.
SURLAG	High	Surface runoff lag	Shifts/attenuates peaks; larger SURLAG smooths and delays the hydrograph.
GWQMN	High	Baseflow threshold	Sets groundwater contribution start; alters low flows/peaks sustain.
GW_DELAY	High	GW response time	Controls the timing of baseflow response and recession limbs.
CH_N2	High	Channel roughness	Affects peak attenuation and travel time in channels.
SOL_K	High	Soil conductivity	Infiltration vs runoff partitioning; changes peak size and timing.
RCHRG_DP	Moderate	Deep recharge frac	Redistributes water to the deep aquifer; reduces quick flow, boosts baseflow.
REVAPMN	Moderate	Revap threshold	Affects evap from GW to soil; tweaks low flows and inter-event water.
SOL_AWC	Moderate	Soil water holding	Buffers quick runoff; affects peak rounding and recession.
CH_K2	Moderate	Channel conductivity	Influences in-channel losses; affects peak attenuation & baseflow.

Table 4.5 (continued)

OV_N	Moderate	Overland roughness	Changes overland travel time/peaks during events.
ALPHA_BF	Moderate	Baseflow recession	Controls groundwater recession rate and tail of hydrograph.
SOL_BD	Moderate	Soil bulk density	Indirectly affects infiltration/storage; moderate influence on peaks.

Table 4.6: Sensitive parameters of Khova sub-watershed

Parameter	Sensitivity level	Hydrologic role	Calibration notes
2_CN2	High	Runoff generation	Primary control on storm runoff and peak magnitude.
2_RCHRG_DP	High	Deep recharge fraction	Shifts water between quickflow and baseflow.
2_GW_DELAY	High	GW response time	Alters the timing and damping of baseflow response.
2_GWQMN	High	Baseflow threshold	Controls the onset of groundwater contribution to the stream.
2_SOL_K	High	Soil conductivity	Infiltration/runoff split; strong effect on peaks.
2_CH_N2	High	Channel roughness	Peak attenuation & celerity in the channel network.
2_SOL_AWC	Moderate	Soil water holding	Buffers event runoff; rounds peaks.
2_SOL_BD	Moderate	Soil bulk density	Influences infiltration via porosity/compaction.
2_CH_K2	Moderate	Channel conductivity	In-channel losses affect attenuation & low flows.

Table 4.6 (continued)

2_ALPHA_BNK	Moderate	Bank storage alpha	Controls temporary bank storage; modulates recession.
2_OV_N	Moderate	Overland roughness	Event travel time & peak sharpness.
2_GW_REVAP	Moderate	Revap coefficient	Controls upward flux to soil; tweaks low flows.

4.3.4 Global Sensitivity Analysis of Dzuza Watershed

Global sensitivity was evaluated using SWAT-CUP (SUFI-2) by employing the t-statistic and p-value to measure the impact of each parameter on simulated discharge. The ranking unequivocally positions soil and runoff generation controls as the foremost priority. SOL_K (soil saturated hydraulic conductivity) is the most significant parameter (**Figure 4.5**), exhibiting a t-value of 8.74 and a p-value approximately equal to 0.00 (**Table 4.7**), thereby affirming its predominant influence on infiltration capacity and its effect on event runoff and recession dynamics. CN2 (SCS curve number) is ranked second ($t = 5.72$, $p \approx 0.00$), underscoring the significance of runoff partitioning for peak magnitude and event volumes.

Subsequently, routing and groundwater time will be addressed. CH_K2 (channel alluvium conductivity) ranks third ($t = 3.03$, $p \approx 0.003$), showing a quantifiable sensitivity of peak attenuation and baseflow to in-channel losses. GW_DELAY ($t = 2.02$, $p \approx 0.046$) and GWQMN ($t \approx -2.01$, $p \approx 0.048$) are also statistically significant at the 5% level, indicating that the initiation and timing of groundwater contributions substantially influence recessions and low flows.

In contrast, ESCO, RCHRG_DP, REVAPMN, SURLAG, CH_N2, SOL_AWC, and SOL_BD demonstrate p-values exceeding 0.28, indicating minimal global sensitivity in this series of simulations and hence a reduced priority for initial calibration, while they continue to serve as valuable fine-tuning "polishers" once primary controls are established.

The ranking directed the calibration process towards (i) infiltration–runoff partitioning (SOL_K, CN2), (ii) in-channel exchange (CH_K2), and (iii) groundwater timing thresholds (GW_DELAY, GWQMN), with subsequent modifications for evaporation partitioning and minor routing adjustments.

Table 4.7: Global sensitivity of runoff parameters and their ranking for the Dzuza watershed

Rank	Qualifier	Parameter	Related process	t-Stat	p-Value
1	V	SOL_K	Soil (infiltration capacity)	8.7438	0
2	R	CN2	Runoff generation	5.7171	0
3	V	CH_K2	Channel exchange	3.0315	0.0032
4	V	GW_DELAY	Groundwater timing	2.0215	0.0463
5	V	GWQMN	Baseflow threshold	−2.0050	0.0481
6	V	ESCO	Soil evaporation partitioning	−1.0752	0.2853
7	V	RCHRG_DP	Deep percolation fraction	0.7889	0.4328
8	V	REVAPMN	Revap threshold	0.7851	0.4345
9	V	SURLAG	Surface runoff lag	0.7474	0.4568
10	V	CH_N2	Channel roughness	0.6414	0.5229
11	R	SOL_AWC	Soil water holding	−0.6009	0.5495
12	V	SOL_BD	Soil bulk density	0.3278	0.7438

Note- R multiplies the existing value with (1+ the given value), **A** adds the given value to the existing value, **V** replace the existing value with the given value

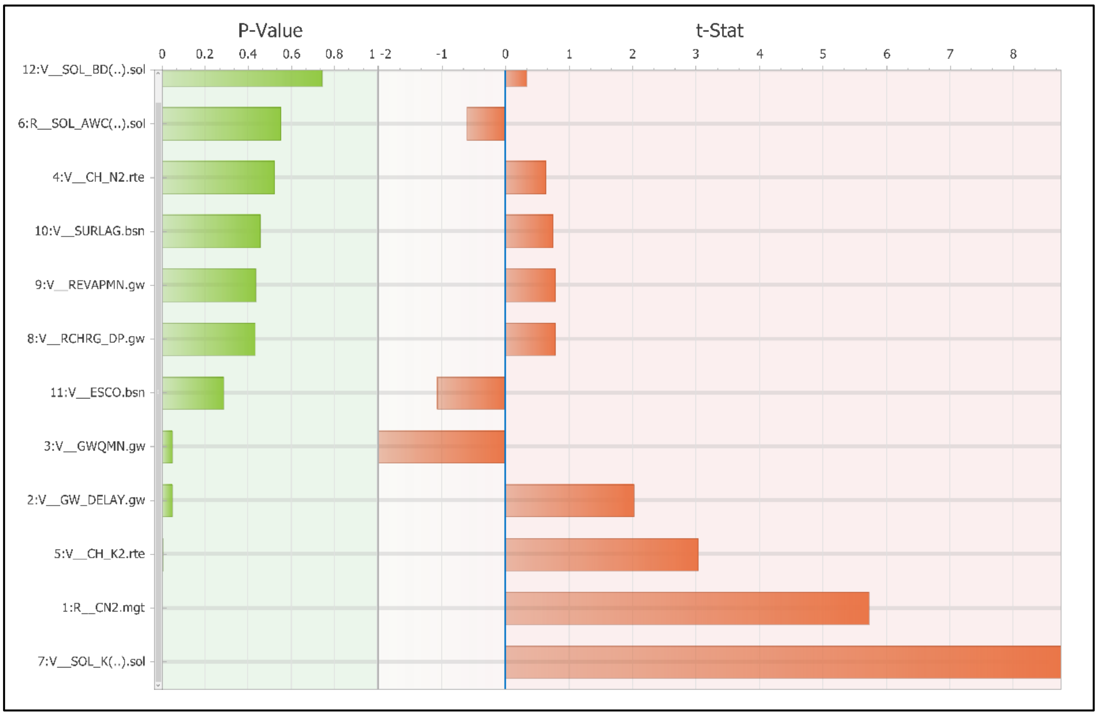

Figure 4.5: Sensitivity analysis of runoff parameters using SWAT CUP for Dzuza watershed

4.3.5 Global Sensitivity Analysis of Dhansiri River Basin

The global sensitivity of the Dhansiri Basin (FLOW_OUT_1) was assessed using SWAT-CUP (SUFI-2), employing the t-statistic and p-value to prioritize factors based on their impact on simulated discharge. The analysis reveals that groundwater thresholds and hillslope runoff generation predominantly influence the basin response. The threshold depth of water in the shallow aquifer necessary for return flow (GWQMN) proved to be the most significant parameter ($t = -9.11$, $p < 0.001$) as shown in **Figure 4.6**, exhibiting substantial influence on the initiation and duration of baseflow, and hence affecting recession dynamics and inter-event flows. The SCS curve number (CN2) ranks second ($t = 5.62$, $p < 0.001$), affirming its essential function in storm-runoff generation and peak intensities. From **Table 4.8,** we can see that the groundwater delay (GW_DELAY) significantly affects the timing of groundwater contributions and influences the recession limbs ($t = -4.04$, $p < 0.001$). Channel interchange is substantial: the hydraulic conductivity of channel alluvium (CH_K2) demonstrates considerable sensitivity ($t = -2.12$, $p = 0.038$), suggesting that in-channel leakage and attenuation significantly influence peak damping and low-flow support. The soil available water capacity (SOL_AWC) has marginal relevance ($t = -1.82$, $p = 0.073$), exerting a secondary influence on event volumes and peak rounding.

Table 4.8: Global sensitivity of runoff parameters and their ranking for the Dhansiri river basin

Rank	Qualifier	Parameter	Hydrologic role	t-Stat	p-Value
1	V	GWQMN	Baseflow threshold	−9.105	0
2	R	CN2	Runoff generation (curve number)	5.616	0
3	V	GW_DELAY	GW response time	−4.037	0.000116
4	V	CH_K2	Channel alluvium conductivity	−2.116	0.03781
5	R	SOL_AWC	Soil available water capacity	−1.816	0.072886
6	V	CH_N2	Channel roughness (Manning's n)	1.168	0.245846
7	V	ALPHA_BF	Baseflow recession constant	0.963	0.338182
8	V	RCHRG_DP	Deep-aquifer percolation fraction	0.749	0.455771
9	R	SOL_K	Soil saturated hydraulic conductivity	0.576	0.566286
10	V	REVAPMN	Revap threshold (shallow aquifer)	0.239	0.811588
11	V	SURLAG	Surface runoff lag time	−0.155	0.87692
12	V	OV_N	Overland roughness (Manning's n)	0.027	0.978887

Note- R multiplies the existing value with (1+ the given value), **A** adds the given value to the existing value, **V** replace the existing value with the given value

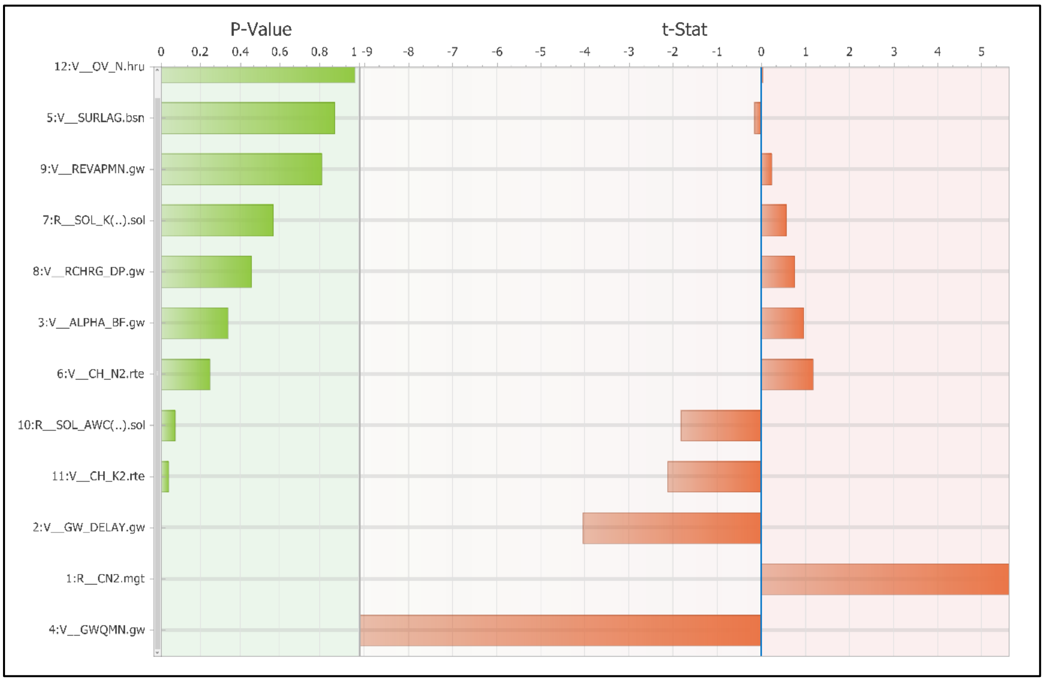

Figure 4.6: Sensitivity analysis of runoff parameters using SWAT CUP for Dhansiri river basin

4.3.6 Global Sensitivity Analysis of Khova Sub-Watershed

The global sensitivity analysis using SWAT-CUP/SUFI-2 for the Khova basin (FLOW_OUT_2) indicates that runoff generation and near-surface controls predominantly influence the discharge response. The SCS curve number (CN2) is the most significant parameter (t-stat = −3.07, p = 0.0028) from **Figure 4.7** and **Table 4.9**, demonstrating a strong, statistically significant impact on simulated flow; elevations in CN2 augment storm runoff and peak magnitudes. Soil saturation hydraulic conductivity (SOL_K) is ranked second (t-stat = −2.57, p = 0.0118), indicating that diminished infiltration redirects water to quickflow, hence intensifying peaks and abbreviating recessions. Channel Manning's n (CH_N2) is the subsequent critical control (t-stat = −1.84, p = 0.069; marginally significant), predominantly influencing peak attenuation and trip time. The deep-aquifer percolation percentage (RCHRG_DP) has a moderate, nearly significant impact (t-stat = −1.67, p = 0.098) by reallocating water from quickflow to groundwater, hence modifying late-event recessions. All remaining parameters—GW_DELAY (t-stat = −0.89, p = 0.376),

SOL_AWC (0.88, 0.379), OV_N (0.72, 0.475), GW_REVAP (0.57, 0.572), ALPHA_BNK (0.54, 0.592), SOL_BD (0.38, 0.706), GWQMN (0.08, 0.935), and CH_K2 (−0.04, 0.968) exhibit minimal statistical evidence of sensitivity within the examined ranges. Calibration should commence by establishing event volumes using CN2 and SOL_K, subsequently refining peak shape and routing with CH_N2, and if necessary, adjusting recessions through RCHRG_DP; less sensitive parameters may remain near baseline and be modified solely for the final optimization of evapotranspiration and groundwater feedbacks.

In hilly and mountainous watersheds, runoff generation is influenced not only by direct surface runoff but also by subsurface flow processes. A considerable portion of rainfall infiltrates into the soil and contributes to lateral flow and groundwater discharge, which ultimately affect streamflow at the watershed outlet. In such terrains, the movement and release of subsurface water are controlled by factors such as slope, soil properties, geological conditions, storage behaviour, and groundwater delay (Luo *et al.,* 2012). Therefore, groundwater-related parameters in SWAT significantly influence the simulation of total runoff by regulating recharge, baseflow recession, groundwater delay, and groundwater contribution to streamflow (Ranatunga *et al.,* 2017). Since the Dzuza watershed, Dhansiri river basin, and Khova sub-watershed are located in hilly regions with high elevations, groundwater processes constitute an important component of watershed hydrology, which explains why groundwater parameters were identified among the most sensitive parameters in the present study.

Table 4.9: Global sensitivity of runoff parameters and their ranking for the Khova sub-watershed

Rank	Qualifier	Parameter	Related process	t-Stat	p-Value
1	R	CN2	Runoff generation	−3.0739	0.0028
2	R	SOL_K	Soil (infiltration capacity)	−2.5715	0.0118
3	V	CH_N2	Channel roughness	−1.8401	0.0692
4	V	RCHRG_DP	Deep percolation fraction	−1.6702	0.0985

Table 4.9 (continued)

5	V	GW_DELAY	Groundwater timing (lag)	−0.8895	0.3762
6	R	SOL_AWC	Soil water holding	0.8842	0.379
7	V	OV_N	Overland roughness	0.7168	0.4754
8	V	GW_REVAP	GW soil revap coefficient	0.567	0.5722
9	V	ALPHA_BNK	Bank-storage alpha	0.5377	0.5921
10	R	SOL_BD	Soil bulk density	0.3786	0.7059
11	V	GWQMN	Baseflow threshold	0.0816	0.9351
12	V	CH_K2	Channel exchange (alluvium K)	−0.0409	0.9675

Note- **R** multiplies the existing value with (1+ the given value), **A** adds the given value to the existing value, **V** replace the existing value with the given value

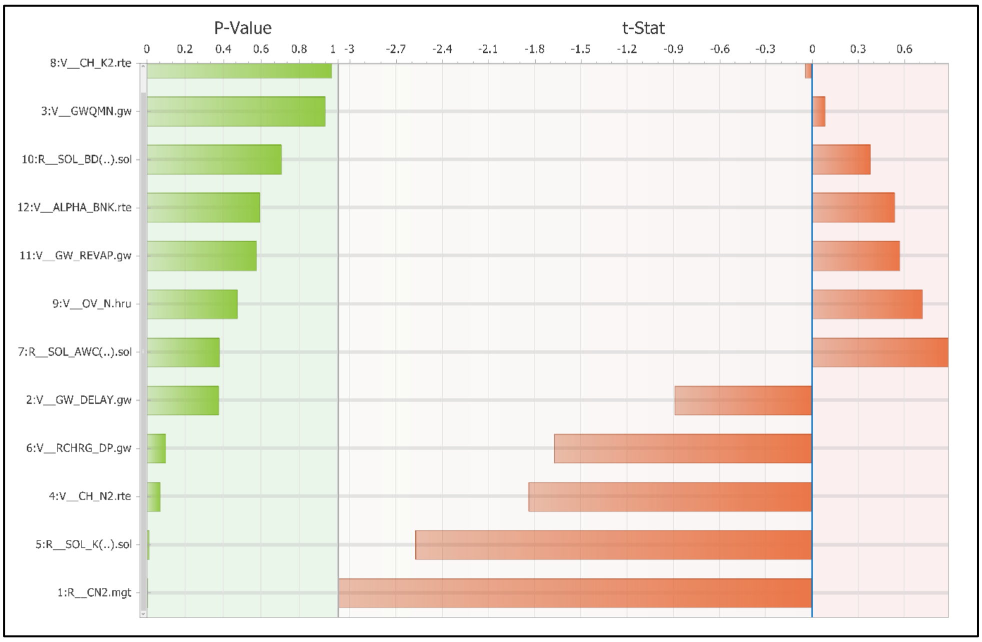

Figure 4.7: Sensitivity analysis of runoff parameters using SWAT CUP for Khova sub-watershed

4.4 Calibration and Validation of the SWAT Model

During the calibration and validation of the SWAT model, input parameters were consistently kept within a realistic range of uncertainty, as specified by SWAT-

CUP. Essential metrics related to the Dzuza watershed, Dhansiri river basin, and Khova sub-watershed were identified during this process. Sensitivity Analysis (SA) played a crucial role in evaluating how parameter variations affected model outputs, enabling the identification of the most influential parameters driving hydrological responses. These characteristics were used for model calibration using the SUFI-2 technique within SWAT-CUP. Calibration for runoff and sediment output was performed with monthly observed data from 2014 to 2018, and then validated against independent datasets from 2019 to 2021 for all three watersheds.

4.4.1 Calibration and Validation of Runoff Simulation for Dzuza Watershed

The dotty plot (**Figure 4.8**) showed that the objective function (R^2) for runoff simulation ranged from 0.70 to 0.89 for the most sensitive hydrological parameters, including CN2.mgt, GW_DELAY.gw, GWQMN.gw, RCHRG_DP.gw, REVAPMN.gw, CH_N2.rte, CH_K2.rte, SOL_AWC.sol, SOL_K.sol, SOL_BD.sol, SURLAG.bsn, ESCO.bsn, ALPHA_BF.gw, and EPCO.hru over 1000 simulation iterations. The best R^2 value of 0.89 and NSE of 0.87 were reached during calibration at iteration 530, indicating strong model performance for runoff simulation in the basin.

Calibration took place from 2014 to 2018, while validation of the model occurred from 2019 to 2021. The calibration ensured that parameter adjustments stayed within plausible hydrological limits (**Table 4.10**). Among the parameters, CN2.mgt (Curve Number) notably impacted surface runoff responses to land use practices, calibrated to –0.175 within the acceptable range of –0.18 to –0.08. Similarly, SOL_AWC.sol (Soil Available Water Content) was adjusted to 0.265, highlighting the soil's water retention capability, while GWQMN.gw (Threshold depth of water in the shallow aquifer for return flow) was set to 119.55, emphasizing groundwater contributions to baseflow.

The Curve Number is assigned not solely based on land use but on the combined effect of land use and soil hydrologic group at the Hydrologic Response Unit (HRU) level. Therefore, although the land-use map used in the present study shows only one generalized category as “forest,” this does not imply that a single Curve Number value was used for all forested areas. Different forest HRUs may have different CN values depending on the associated soil hydrologic group and local conditions. Thus, the CN values for forest land in the model were ascertained internally through the land use–soil combination used during HRU generation, rather than by assigning one fixed value to the entire forest class.

4.4.1.1 Model Performance for Calibration and Validation of Dzuza watershed

The iterative calibration method achieved a good match between observed and simulated runoff. During validation, the model's performance declined slightly, with an NSE of 0.51 and an R^2 of 0.79 (**Table 4.11**), indicating reduced predictive accuracy but still maintaining an acceptable level of agreement with observed flows in an independent dataset. The SWAT model for the Dzuza watershed showed better calibration results (NSE = 0.87; R^2 = 0.89), indicating a strong correlation between observed and simulated runoff. The PBIAS value (+12.8%) indicated a slight overestimation of streamflow during calibration. During validation, the model performed modestly (NSE = 0.51; R^2 = 0.79), with an increased bias (+33.3%), suggesting decreased predictive ability with independent data. However, the results still met acceptable hydrological modeling standards and confirmed its suitability for runoff simulation in the basin.

i. Nash–Sutcliffe Efficiency (NSE): The NSE values during calibration and validation were 0.87 and 0.51, respectively. As per Santhi *et al.,* (2001) and Moriasi *et al.,* (2007), NSE values greater than 0.50 are considered satisfactory, while values above 0.75 indicate very good model performance. Thus, the Dzuza SWAT model achieved very good performance during calibration and adequate performance during validation.
ii. Coefficient of Determination (R^2): The R^2 values obtained during calibration and validation were 0.89 and 0.79, respectively. Since R^2 values above 0.60 are considered acceptable (Kang *et al.,* 2006), the model exhibited a strong correlation between simulated and observed runoff during both phases, with particularly strong performance in the calibration period.
iii. Percent Bias (PBIAS): The PBIAS values recorded were +12.8% in calibration and +33.3% in validation. According to Van Liew *et al., (*2007), PBIAS within ±25% is considered satisfactory for streamflow simulation.

Hence, calibration bias was within acceptable limits, but the validation period indicated a higher overestimation of streamflow, which reduced model efficiency under independent datasets.

iv. Root Mean Square Error – Standard Deviation Ratio (RSR): The RSR values were 0.37 during calibration and 0.70 during validation. As per Moriasi *et al.,* (2007), RSR $\leq$ 0.50 reflects very good model performance, while values between 0.50–0.70 are satisfactory. Therefore, the Dzuza model demonstrated very good calibration performance and moderately satisfactory validation performance.

v. Kling–Gupta Efficiency (KGE) and Uncertainty Statistics: The KGE values were 0.81 in calibration and 0.61 in validation, supporting the reliability of the model to reproduce both variability and correlation in flows. Furthermore, the p-factor (0.45 for calibration, 0.36 for validation) and r-factor (0.32 and 0.63, respectively) suggested that while calibration adequately captured most observed variability, the prediction uncertainty increased during validation.

vi. Scatter plot of simulated runoff and observed runoff: **Figures 4.10** and **4.12** illustrate the scatter plots of simulated versus observed monthly surface runoff for the Dzuza watershed during the calibration period (2014–2018) and the validation period (2019–2021), respectively. The data indicate that the model attained a satisfactory fit for the majority of the simulation years. The monthly observed and simulated runoff values exhibit a distinct correlation, although specific peak flows were underestimated, especially during high-flow occurrences (e.g., observed 29.90 m^3/s against simulated 18.64 m^3/s).

During calibration, the scatter plot indicated that the model accurately replicated both low and medium flows, while marginally underestimating higher peaks. During validation, a comparable trend was noted, as the model typically aligned with the seasonal trends of runoff while underestimating multiple high-flow instances. Nonetheless, the coefficient of determination (R^2 = 0.89 during calibration; R^2 = 0.79 during validation) affirmed that the model exhibited a robust link between observed and simulated flows.

The green uncertainty band (95PPU) in both calibration (**Figure 4.9**) and validation (**Figure 4.11**) signifies the prediction interval. The observed streamflow values (blue line) predominantly resided within this uncertainty zone, indicating that the SUFI-2 method proficiently encapsulated the variability in runoff. This further substantiates that the chosen sensitive factors well represented watershed processes.

Parameter uncertainty in SUFI-2 encompasses various sources of error, such as rainfall variability, conceptual model assumptions, parameter ranges, and measurement imperfections (Abbaspour *et al.,* 2004). Consequently, although inconsistencies were noted at specific peaks, the comprehensive scatter plot analysis validated that the SWAT model calibrated for 2014–2018 exhibited commendable performance and remained excellent across the validation period (2019–2021) for runoff simulation in the Dzuza watershed.

Table 4.10: Fitted parameters during calibration of runoff for Dzuza watershed

Sl. No.	Parameter Name	Fitted Value	Min Value	Max Value
1	R__CN2.mgt	–0.175	–0.18	–0.08
2	V__GW_DELAY.gw	26.19	25	120
3	V__GWQMN.gw	119.55	50	150
4	V__RCHRG_DP.gw	0.062	0.03	0.12
5	V__REVAPMN.gw	146.04	100	180
6	V__CH_N2.rte	0.06	0.06	0.14
7	V__CH_K2.rte	37.36	25	50
8	R__SOL_AWC(..).sol	0.265	0.12	0.28
9	R__SOL_K(..).sol	2.006	1.5	5
10	V__SOL_BD(..).sol	1.377	1.3	1.6
11	V__SURLAG.bsn	6.298	6	10
12	V__ESCO.bsn	0.2	0.2	0.5
13	V__ALPHA_BF.gw	0.105	0.1	0.25
14	V__EPCO.hru	0.992	0.9	1

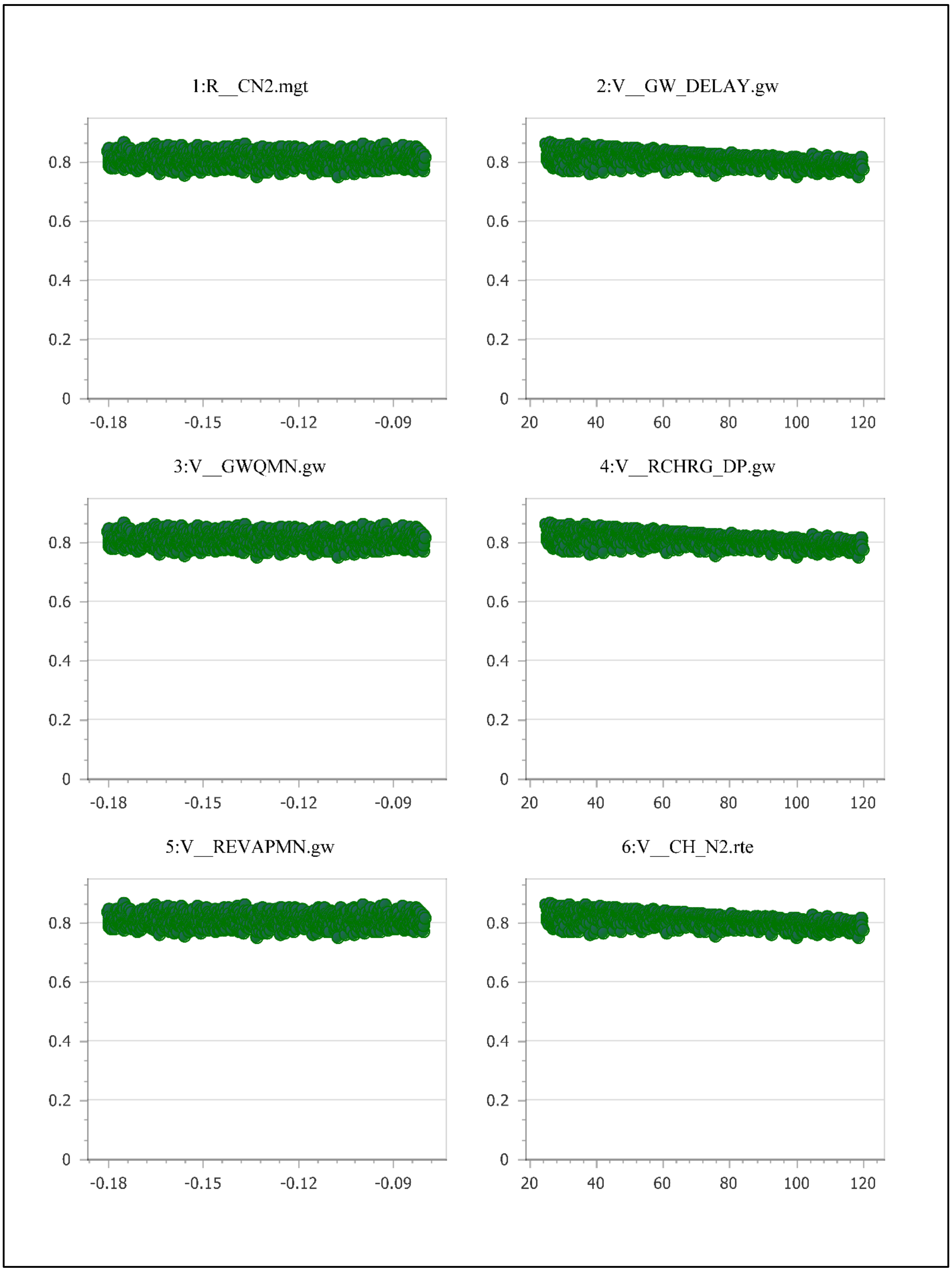

Figure 4.8: Dotty plots of runoff parameters calibration for Dzuza watershed

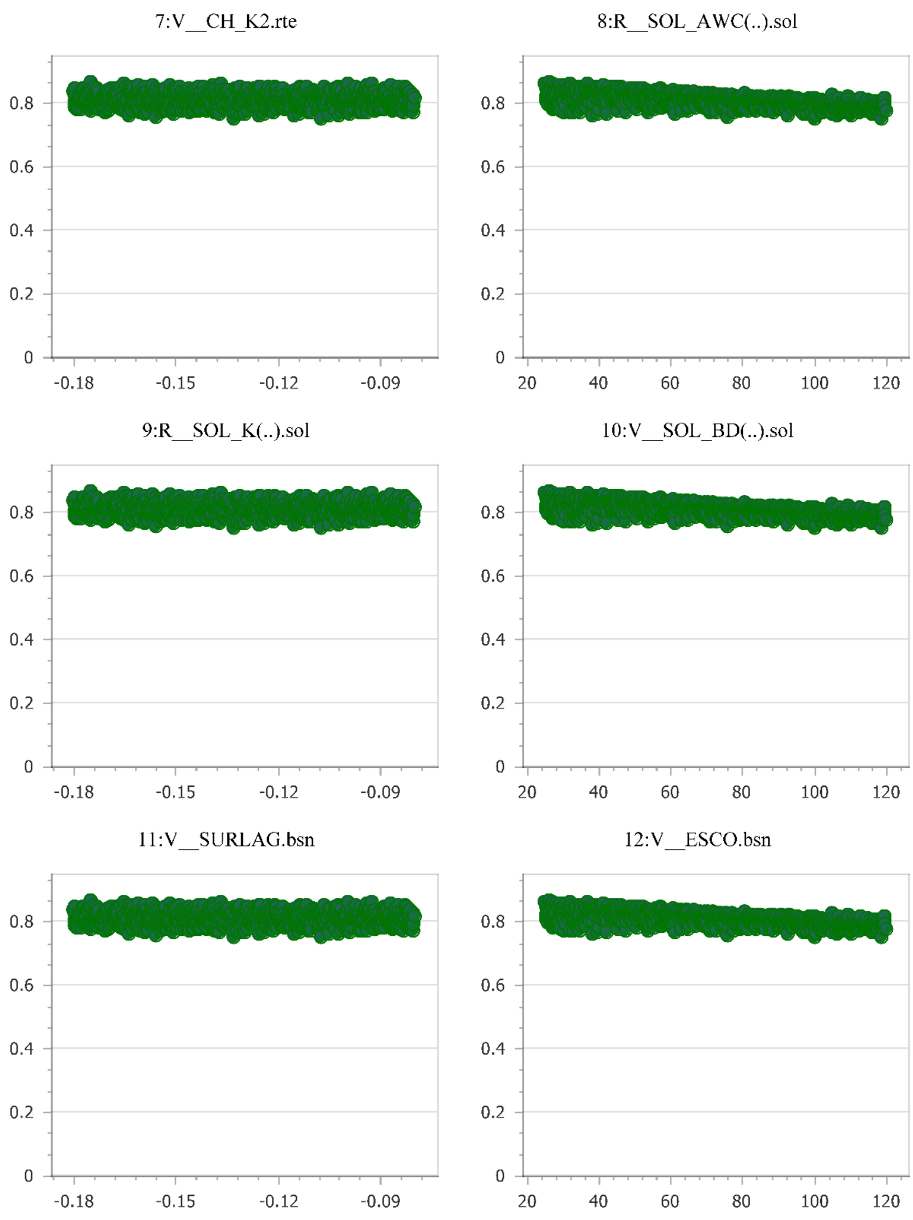

Figure 4.8: Dotty plots of runoff parameters calibration for Dzuza watershed

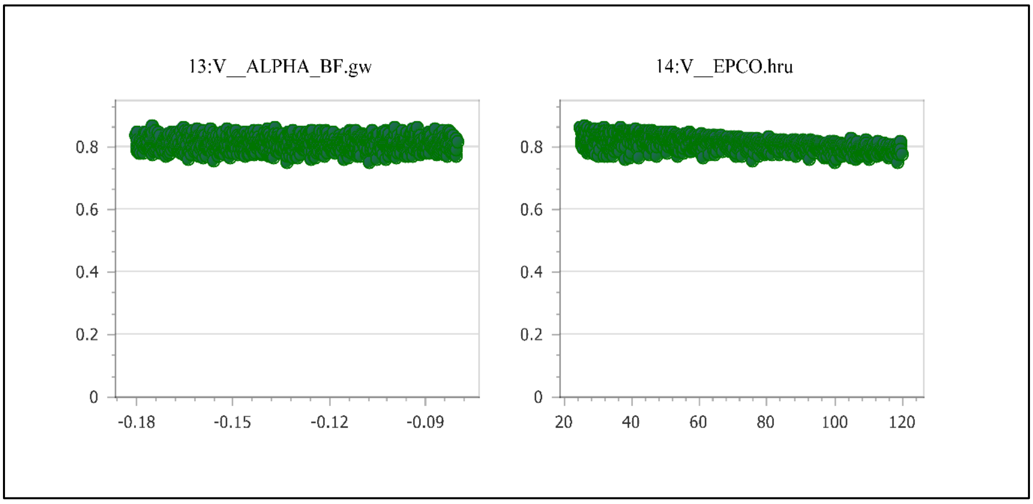

Figure 4.8: Dotty plots of runoff parameters calibration for Dzuza watershed

Table 4.11: Summary of statistical analysis for runoff during calibration and validation of the SWAT model (Dzuza watershed)

Sl. No.	Statistical Indices	Calibration (2014–2018)	Validation (2019–2021)
1	NSE	0.87	0.51
2	R^2	0.89	0.79
3	PBIAS (%)	12.8	33.3
4	RSR	0.37	0.7
5	KGE	0.81	0.61
6	P-factor	0.45	0.36
7	r-factor	0.32	0.63

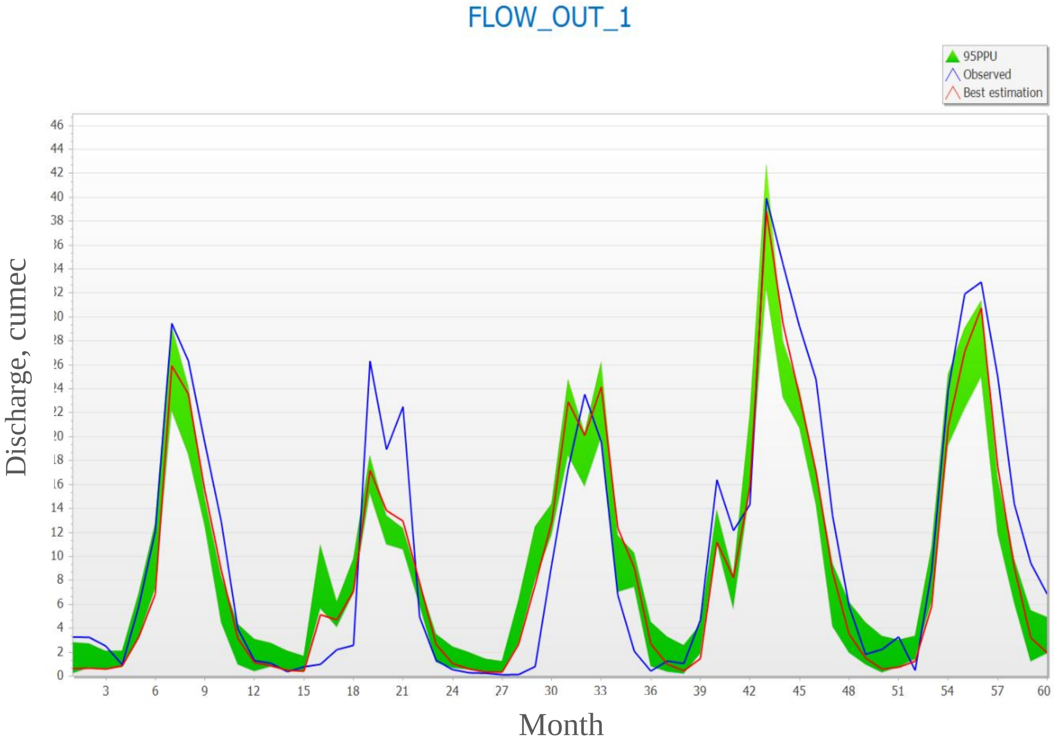

Figure 4.9: Dzuza observed and simulated monthly runoff for the calibration period (2014-2018)

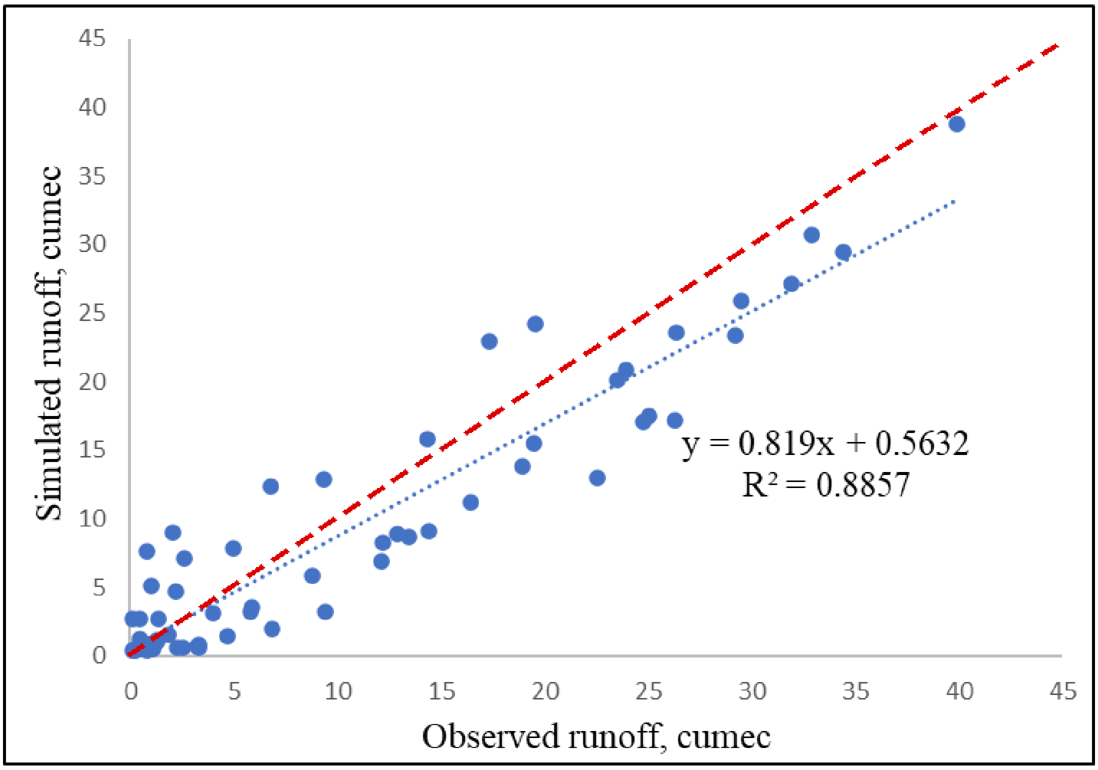

Figure 4.10: Scatter plot for the observed and simulated monthly surface runoff during the calibration period for Dzuza (2014-2018)

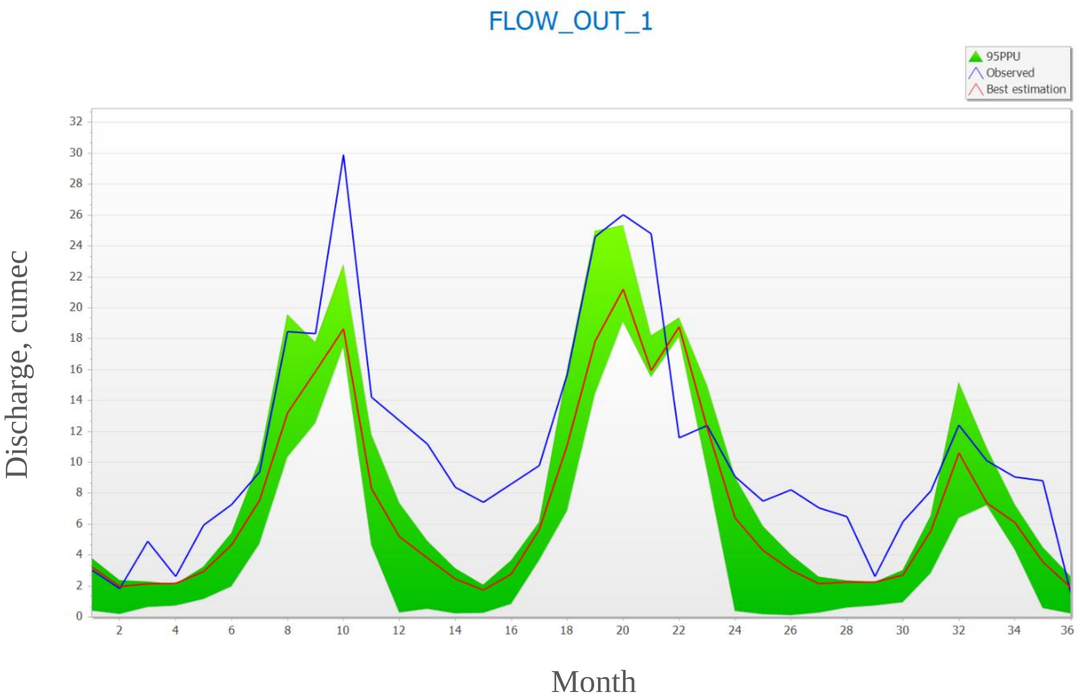

Figure 4.11: Dzuza observed and simulated monthly runoff for the validation period (2019-2021)

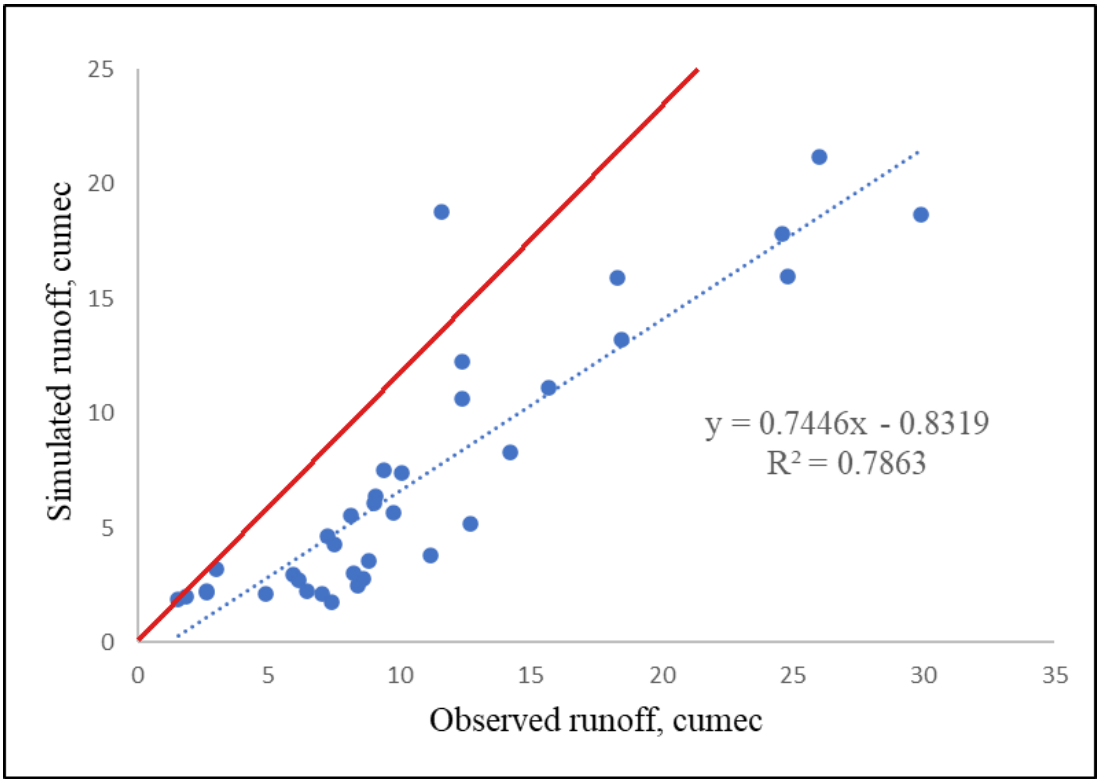

Figure 4.12: Scatter plot for the observed and simulated monthly surface runoff during the calibration period for Dzuza (2019-2021)

4.4.2 Calibration and Validation of Runoff Simulation for Dhansiri River Basin

The dotty plot (**Figure 4.13**) for the Dhansiri river basin indicated that the objective function (R^2) for runoff simulation ranged from 0.70 to 0.88 for the most sensitive hydrological parameters. These included CN2.mgt, GW_DELAY.gw, GWQMN.gw, RCHRG_DP.gw, REVAPMN.gw, CH_N2.rte, CH_K2.rte, SOL_AWC.sol, SOL_K.sol, SURLAG.bsn, and OV_N.hru. The best R^2 value of 0.88 and NSE of 0.82 were obtained during calibration, confirming strong model performance. Calibration was carried out for the period 2014–2018, while validation was performed for 2019–2021. Parameter adjustments were made within plausible hydrological limits (**Table 4.12**). The monthly observed and simulated runoff for the calibration and validation periods are shown in **Figures 4.14** and **4.16**, respectively, while scatter plots are given in **Figures 4.15** and **4.17.**

4.4.2.1 Model Performance for Calibration and Validation

The statistical indices for calibration and validation are summarized in **Table 4.13**

i. NSE values were 0.82 during calibration and 0.85 during validation. According to Moriasi *et al.,* (2007), NSE values above 0.75 are rated very good. Thus, the Dhansiri model showed very good agreement between observed and simulated runoff across both phases.
ii. Coefficient of Determination (R^2): R^2 values of 0.88 (calibration) and 0.86 (validation) confirmed a strong correlation. Since R^2 above 0.60 is considered acceptable (Kang *et al.,* 2006), the Dhansiri model showed high reliability in replicating flow dynamics.
iii. Percent Bias (PBIAS): PBIAS was +12.6% (calibration) and +2.7% (validation), both within the ±25% satisfactory threshold (Van Liew *et al.,* 2007). The calibration showed a mild overestimation, while validation bias was negligible.
iv. Root Mean Square Error – Standard Deviation Ratio (RSR): RSR values were 0.42 (calibration) and 0.38 (validation)**.** Since RSR ≤ 0.50 is considered very good, the Dhansiri model achieved very high accuracy**.**

v. Kling–Gupta Efficiency (KGE) and Uncertainty Statistics: KGE improved from 0.72 (calibration) to 0.90 (validation)**,** confirming excellent model reliability. The p-factor increased from 0.73 to 0.89, while the r-factor rose from 1.19 to 1.97, indicating improved uncertainty coverage during validation.

vi. Scatter Plot and Hydrographs: Scatter plots (**Figures 4.19** and **4.21**) show close clustering along the 1:1 line, confirming strong predictive accuracy. Hydrographs (**Figures 4.18** and **4.20**) illustrate that most observed flows fell within the 95PPU uncertainty band. While some peaks were underestimated, overall model performance was very good.

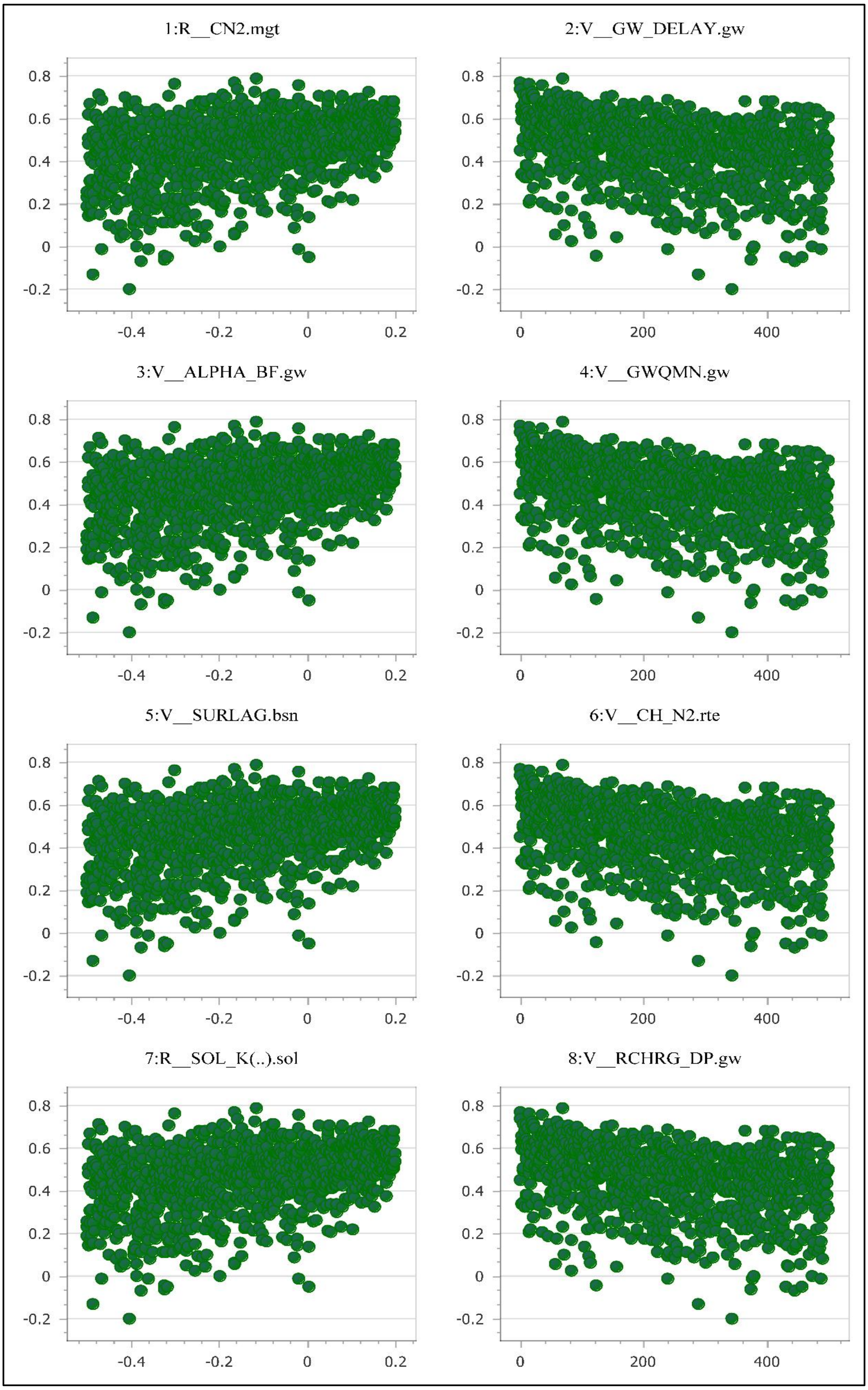

Figure 4.13: Dotty plots of runoff parameters calibration for Dhansiri river basin (1-12) and Khova sub-watershed (13-24)

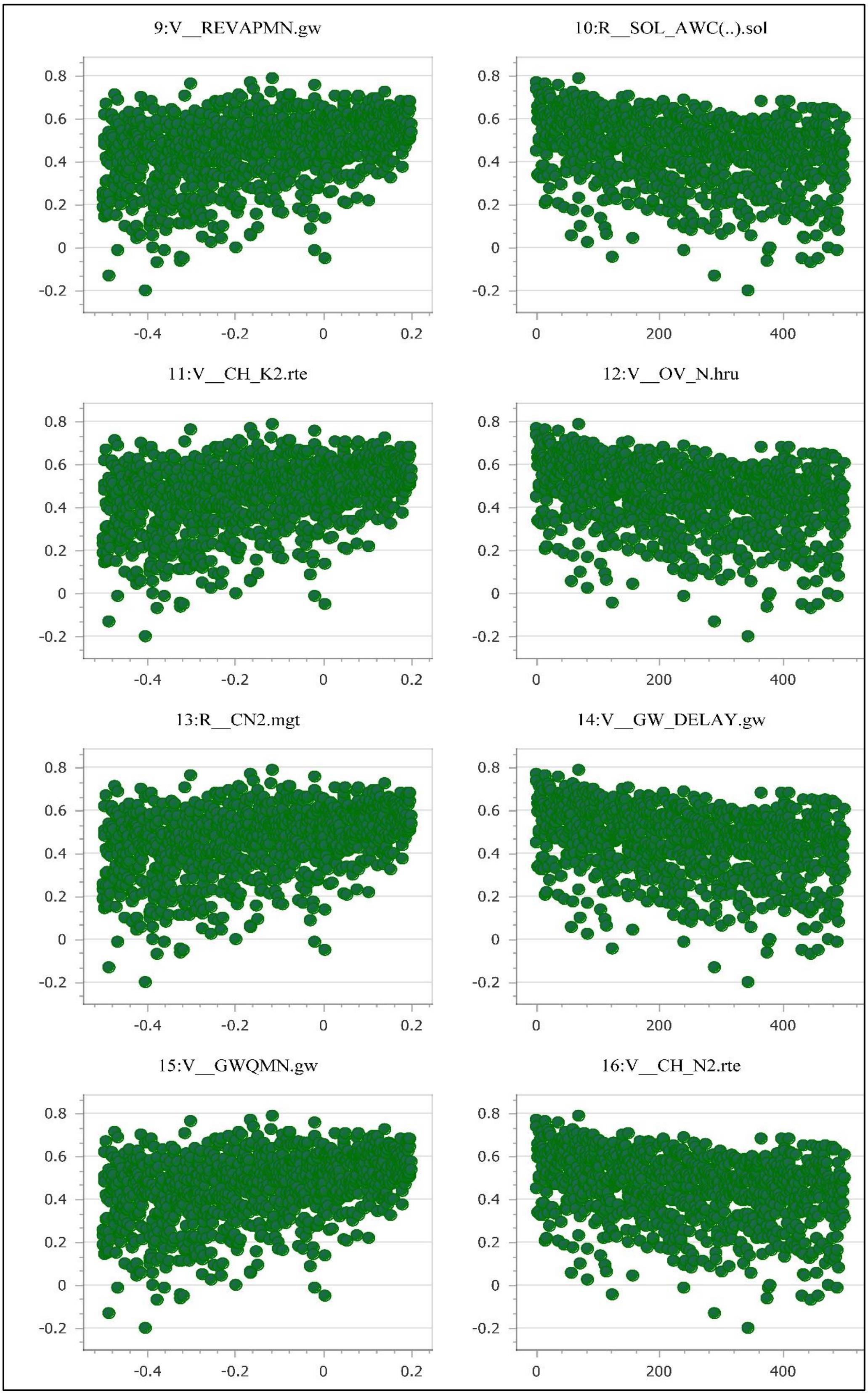

Figure 4.13: Dotty plots of runoff parameters calibration for Dhansiri river basin (1-12) and Khova sub-watershed (13-24)

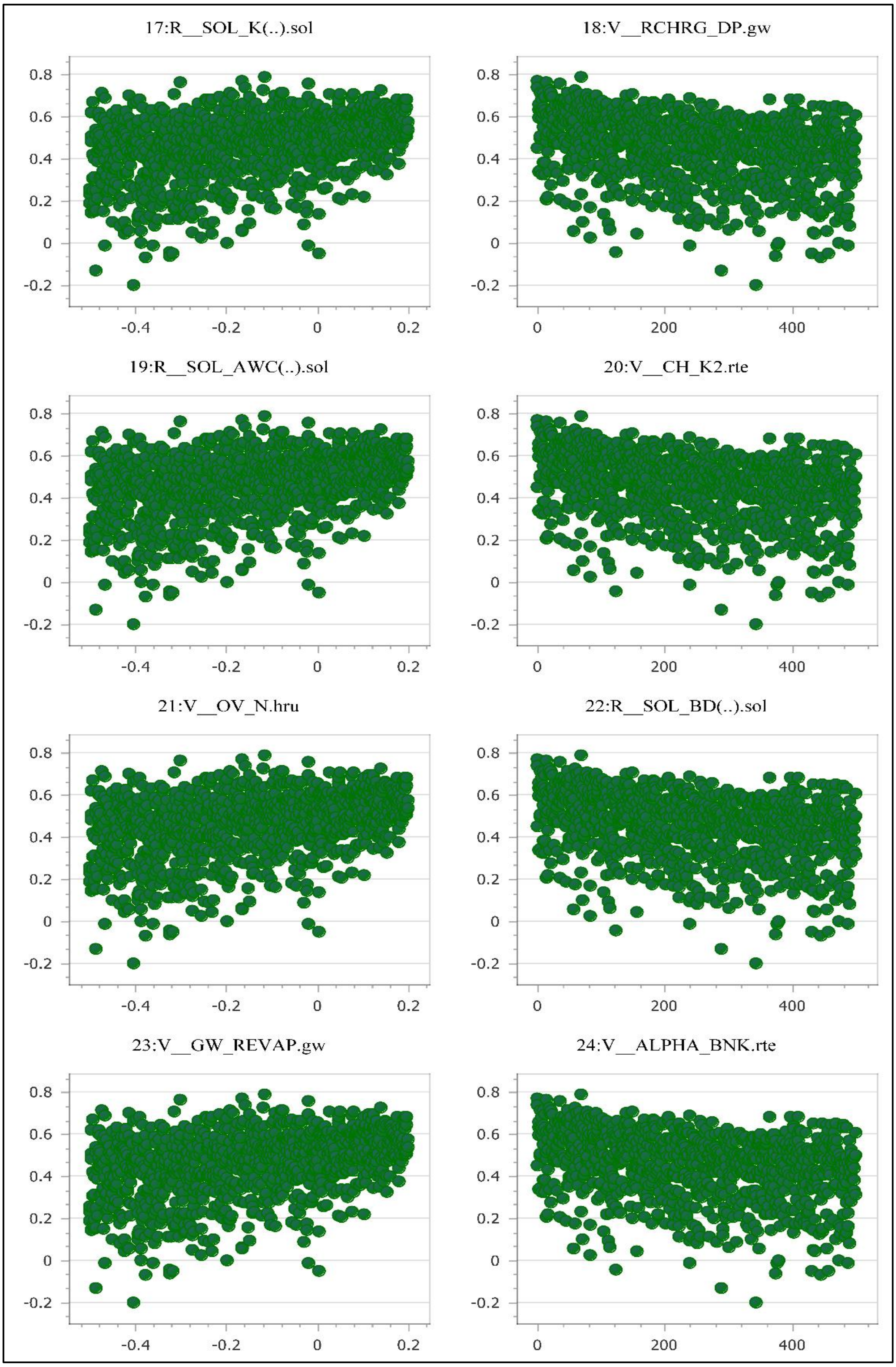

Figure 4.13: Dotty plots of runoff parameters calibration for Dhansiri river basin (1-12) and Khova sub-watershed (13-24)

Table 4.12: Fitted parameters during calibration of runoff for the Dhansiri river basin

Sl. No.	Parameter Name	Fitted Value	Min Value	Max Value
1	R__CN2.mgt	–0.12	–0.50	0.2
2	V__GW_DELAY.gw	68.25	0	500
3	V__ALPHA_BF.gw	0.19	0	1
4	V__GWQMN.gw	262.5	0	5000
5	V__SURLAG.bsn	19.64	1	24
6	V__CH_N2.rte	0.05	–0.07	0.3
7	R__SOL_K(..).sol	0.28	–0.30	0.6
8	V__RCHRG_DP.gw	0.18	0	1
9	V__REVAPMN.gw	259.75	0	500
10	R__SOL_AWC(..).sol	–0.487	–0.50	0.2
11	V__CH_K2.rte	5.3	–0.01	180
12	V__OV_N.hru	0.38	0.01	0.5

Table 4.13: Summary of statistical analysis for runoff during calibration and validation of the SWAT model (Dhansiri river basin)

Sl. No.	Statistical Indices	Calibration (2014–2018)	Validation (2019–2021)
1	NSE	0.82	0.85
2	R^2	0.88	0.86
3	PBIAS (%)	12.6	2.7

Table 4.13 (continued)

4	RSR	0.42	0.38
5	KGE	0.72	0.9
6	P-factor	0.73	0.89
7	r-factor	1.19	1.97

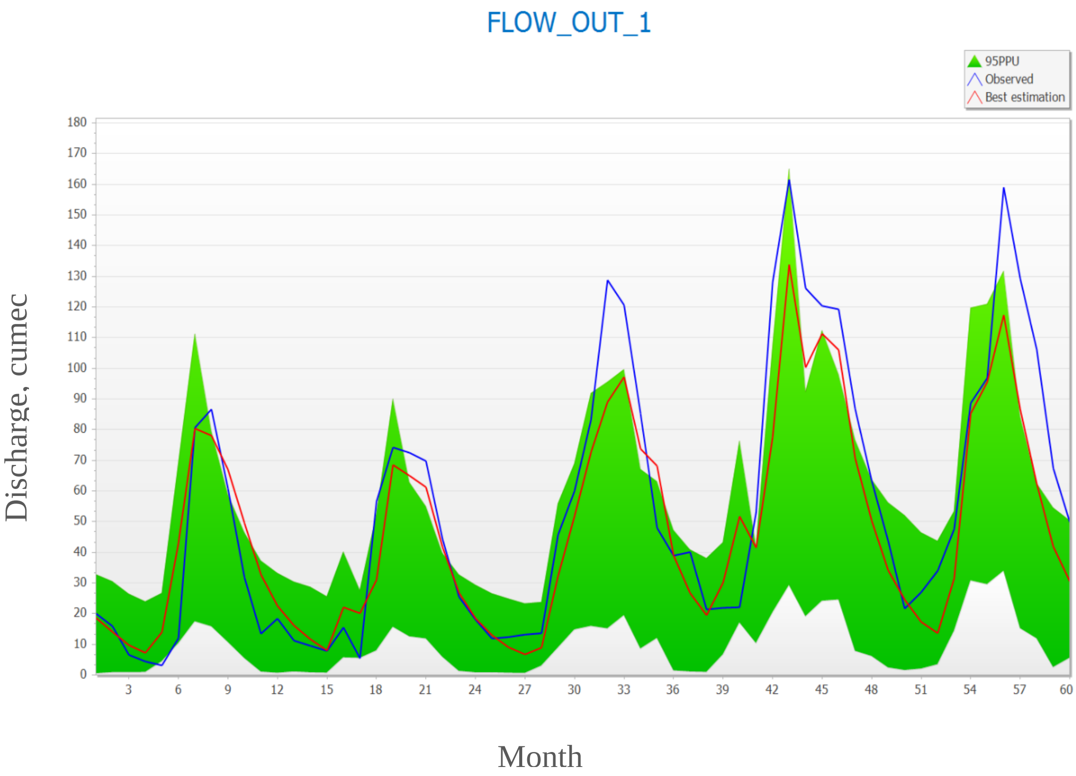

Figure 4.14: Dhansiri observed and simulated monthly runoff for the calibration period (2014-2018)

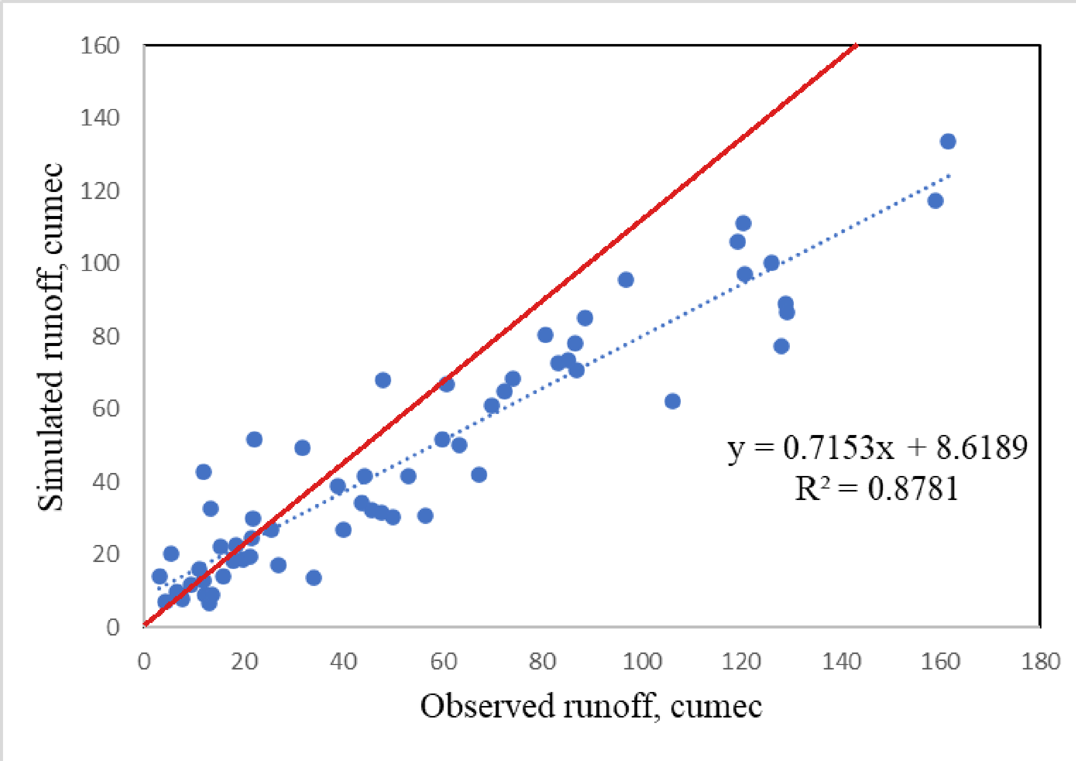

Figure 4.15: Scatter plot for the observed and simulated monthly surface runoff during the calibration period for Dhansiri (2014-2018)

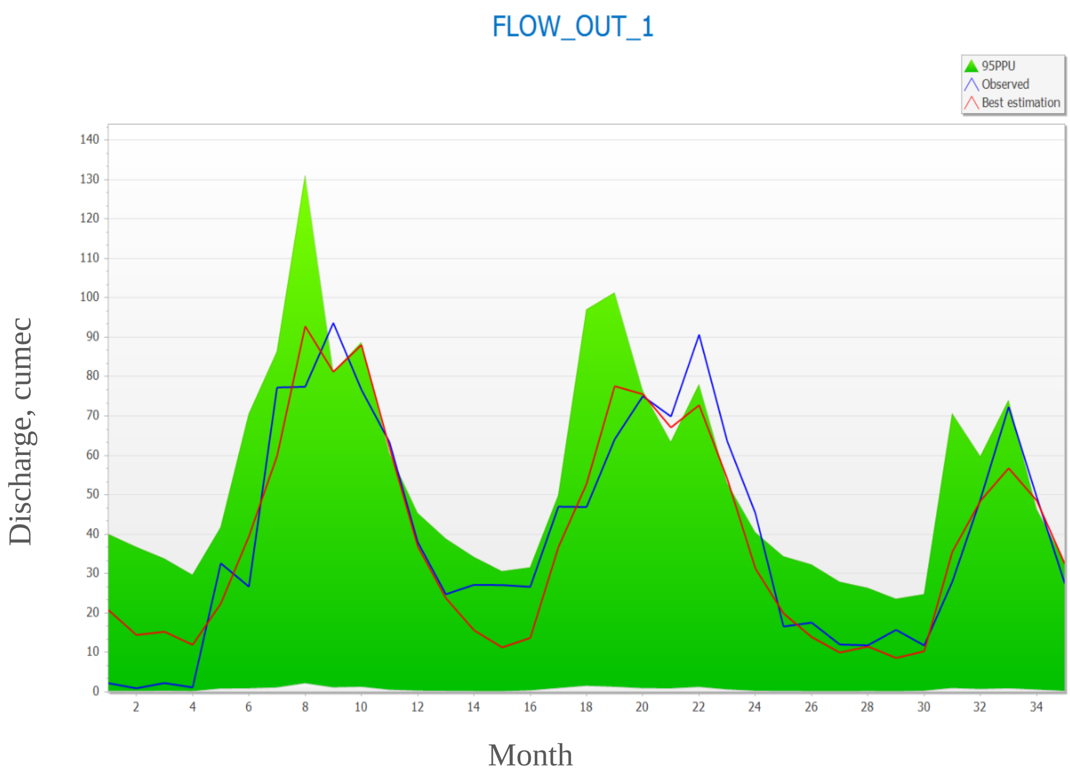

Figure 4.16: Dhansiri observed and simulated monthly runoff for the calibration period (2019-2021)

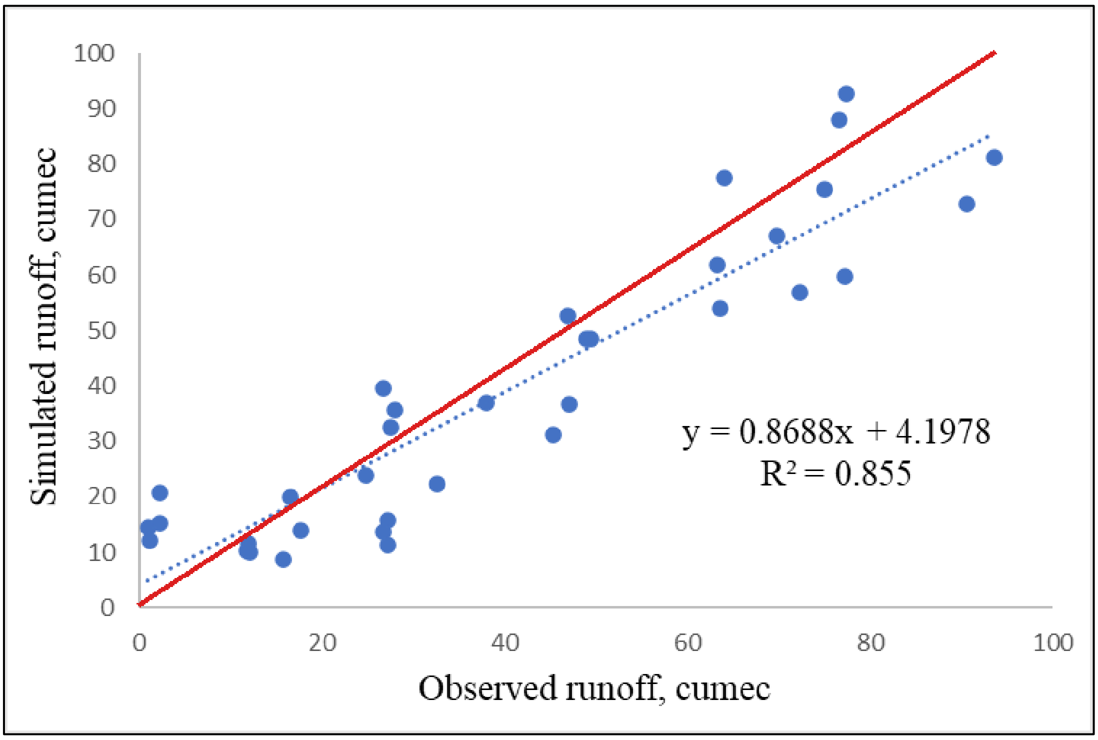

Figure 4.17: Scatter plot for the observed and simulated monthly surface runoff during the calibration period for Dhansiri (2019-2021)

4.4.3 Calibration and Validation of Runoff Simulation for Khova Sub-Watershed (FLOW_OUT2)

The dotty plot (**Figure 4.19**) for the Khova sub-watershed showed that the objective function (R^2) for runoff simulation ranged from 0.70 to 0.78 for the most sensitive parameters, including CN2.mgt, GW_DELAY.gw, GWQMN.gw, CH_N2.rte, SOL_K.sol, RCHRG_DP.gw, SOL_AWC.sol, CH_K2.rte, OV_N.hru, SOL_BD.sol, GW_REVAP.gw, and ALPHA_BNK.rte. The best calibration run achieved an R^2 of 0.78 and NSE of 0.76, suggesting satisfactory performance. Calibration was conducted for 2014–2018, while validation was undertaken for 2019–2021. The parameter ranges and fitted values are shown in **Table 4.14**. Monthly observed and simulated flows for calibration and validation are shown in **Figures 4.18** and **4.20**, respectively, while scatter plots are given in **Figures 4.19** and **4.21.**

4.4.3.1 Model Performance for Calibration and Validation

The statistical indices for FLOW_OUT_2 (Khova) is summarized in **Table 4.15.**

i. Nash–Sutcliffe Efficiency (NSE): NSE values were 0.76 in calibration and 0.70 in validation, reflecting very good calibration performance and satisfactory validation performance (Moriasi *et al.,* 2007).

ii. Coefficient of Determination (R^2): R^2 was 0.78 (calibration) and 0.70 (validation), indicating acceptable correlation between observed and simulated flows.

iii. Percent Bias (PBIAS): PBIAS was –18.2% in calibration, showing underestimation of flows, but improved to +3.0% in validation, which is well within satisfactory limits. This demonstrates that model performance improved with independent data.

iv. Root Mean Square Error – Standard Deviation Ratio (RSR): RSR was 0.49 during calibration (very good) and 0.55 during validation (satisfactory).

v. Kling–Gupta Efficiency (KGE) and Uncertainty Statistics: KGE remained stable at 0.78 in both calibration and validation, reflecting consistent model reliability. The p-factor slightly reduced from 0.83 to 0.80, while the r-factor declined from 1.23 to 1.15, showing stable but slightly reduced uncertainty coverage during validation.

vi. Scatter Plot and Hydrographs: Scatter plots (**Figures 4.19** and **4.21**) indicated moderate clustering near the 1:1 line, while hydrographs (**Figures 4.18** and **4.20**) revealed that most observed flows were captured within the 95PPU uncertainty band. Although several high-flow events were underestimated, the model adequately represented seasonal runoff variability. Overall, Khova FLOW_OUT_2 exhibited very good calibration results and satisfactory validation performance, supporting its application for sub-basin scale runoff prediction.

Table 4.14: Fitted parameters during calibration of runoff for Khova sub-watershed

Sl. No.	Parameter Name	Fitted Value	Min Value	Max Value
1	R__CN2.mgt	–0.067	–0.20	0.2
2	V__GW_DELAY.gw	8.75	0	500
3	V__GWQMN.gw	2512.5	0	5000
4	V__CH_N2.rte	–0.156	–0.25	0.35
5	R__SOL_K(..).sol	0.663	–1.09	2.1
6	V__RCHRG_DP.gw	0.257	0	1
7	R__SOL_AWC(..).sol	–0.298	–0.30	0.9
8	V__CH_K2.rte	81.315	–0.01	153
9	V__OV_N.hru	20.718	0.01	30
10	R__SOL_BD(..).sol	0.197	–0.60	1.4
11	V__GW_REVAP.gw	0.066	0.02	0.2
12	V__ALPHA_BNK.rte	0.9	0	1

Table 4.15: Summary of statistical analysis for runoff during calibration and validation of the SWAT model (Khova sub-watershed)

Sl. No.	Statistical Indices	Calibration (2014–2018)	Validation (2019–2021)
1	NSE	0.76	0.7
2	R^2	0.78	0.7
3	PBIAS (%)	–18.2	3
4	RSR	0.49	0.55
5	KGE	0.78	0.78
6	P-factor	0.83	0.8
7	r-factor	1.23	1.15

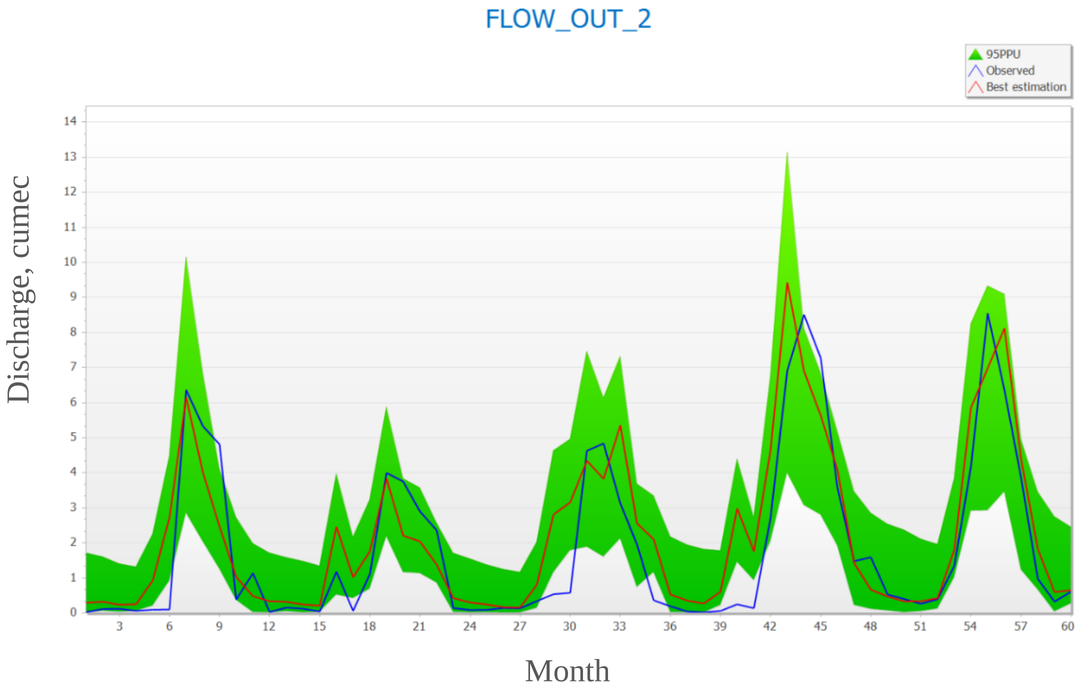

Figure 4.18: Khova observed and simulated monthly runoff for the calibration period (2014-2018)

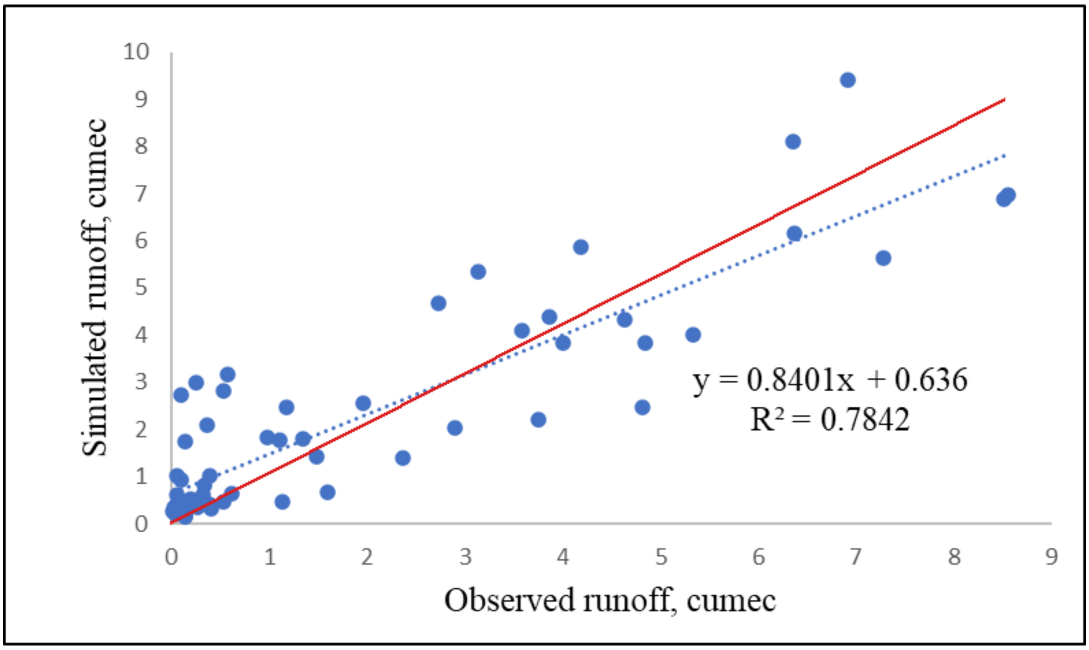

Figure 4.19: Scatter plot for the observed and simulated monthly surface runoff during the calibration period for Khova (2014-2018)

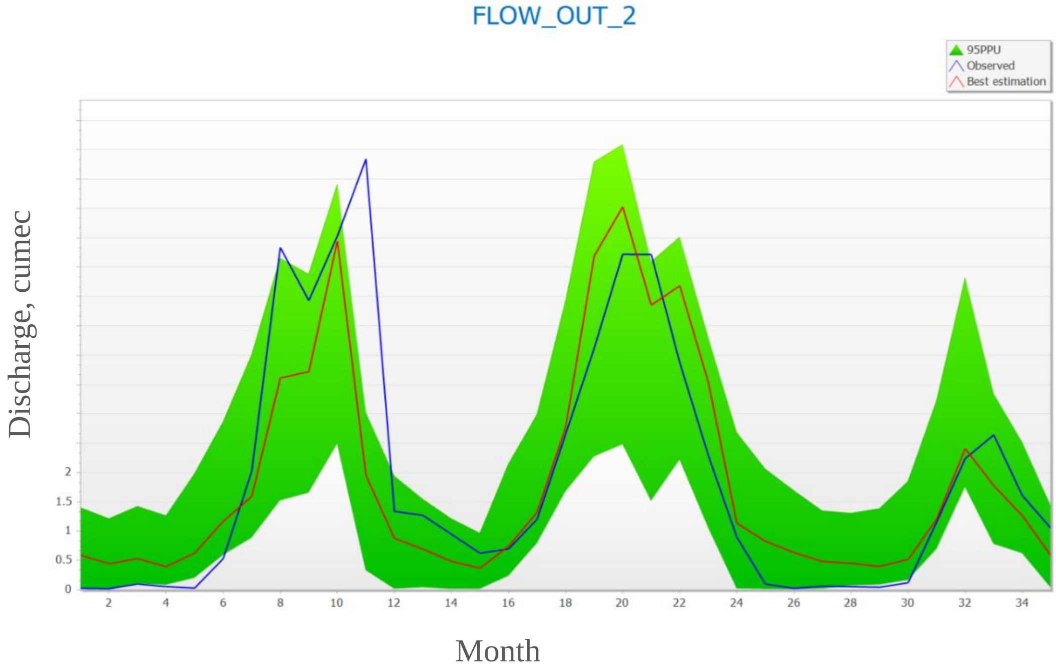

Figure 4.20: Khova observed and simulated monthly runoff for the validation period (2019-2021)

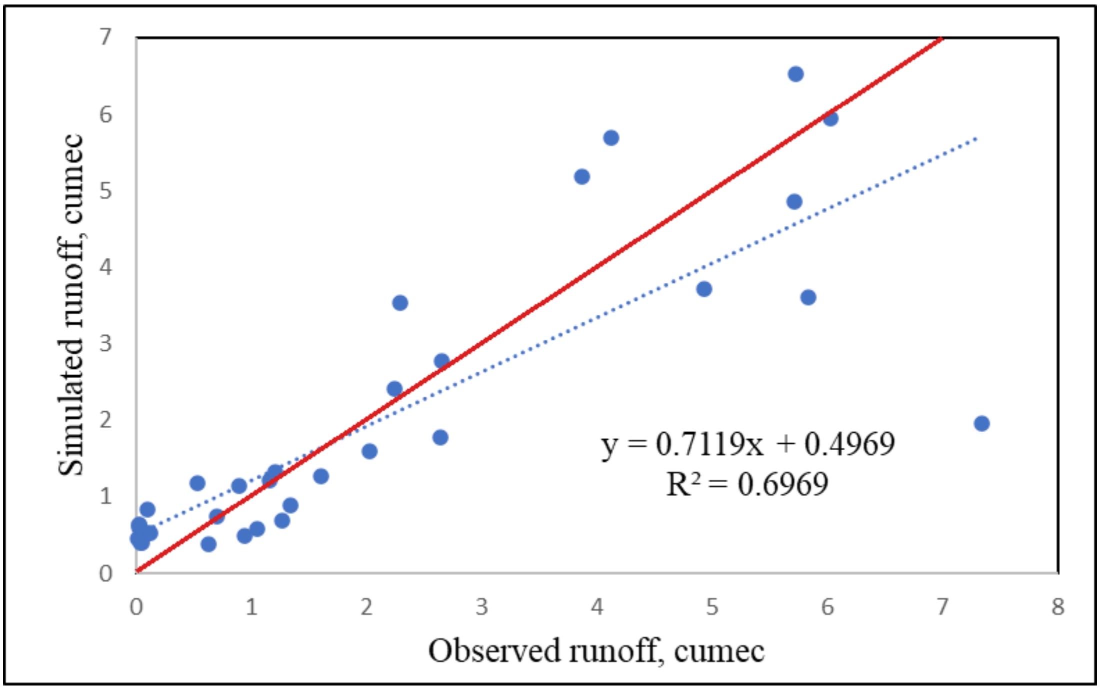

Figure 4.21: Scatter plot for the observed and simulated monthly surface runoff during the validation period for Khova (2019-2021)

The calibration and validation statistics obtained for the Dzuza, Dhansiri, and Khova watersheds indicate that the SWAT model performed satisfactorily to very well in simulating monthly streamflow. The NSE and R^2 values for most simulations were above commonly accepted thresholds, demonstrating that the model was able to capture both seasonal runoff variability and the magnitude of flows. Similar performance levels have been reported in many watershed studies where SWAT was successfully applied in data-scarce and mountainous regions. For example, Moriasi *et al.*, 2007 suggested that NSE values greater than 0.50 indicate satisfactory model performance, while values above 0.75 indicate very good performance. The results of the present study, therefore, confirm that SWAT is suitable for representing hydrological processes in the hilly watersheds of Nagaland.

The relatively stronger performance of the Dhansiri model compared with Dzuza and Khova may be attributed to its larger basin size and better representation of hydrological response at the monthly scale. Larger watersheds often smooth localized rainfall errors and produce more stable runoff responses, leading to improved calibration statistics. In contrast, smaller watersheds such as Khova are generally more sensitive to short-term rainfall variability, parameter uncertainty, and local catchment characteristics.

Groundwater-related parameters were identified among the most sensitive parameters in all three watersheds. This finding is hydrologically reasonable because hilly terrains often generate streamflow not only through surface runoff but also through lateral subsurface flow and delayed groundwater return flow. Thus, the sensitivity analysis confirms that subsurface pathways play a major role in sustaining streamflow in the study area.

4.4.4 Hydrology/ Water Balance Components of Dzuza Watershed

Figure 4.22 illustrates the water balance components of the Dzuza watershed, and **Table 4.16** summarizes the average monthly basin values derived from the SWAT model. **Figure 4.22** indicates that the average annual precipitation of the Dzuza watershed is 1420.9 mm. Of this total, 293.28 mm was attributed to surface runoff, and 567.16 mm was lost through evapotranspiration (ET). The lateral flow accounted for 564.96 mm, while the total water yield was assessed at 859.68 mm. Minor elements comprised a sediment yield of 3.39 t/ha and an annual potential evapotranspiration (PET) of 1142.55 mm. **Table 4.16** indicates that the peak monthly precipitation occurred in July (290.92 mm), which corresponded with the largest surface runoff (77.05 mm), lateral flow (122.43 mm), and water yield (199.31 mm). This was succeeded by August, which had 243.14 mm of rainfall, 63.34 mm of surface runoff, and 160.40 mm of water yield. January recorded the minimal rainfall at 11.37 mm, accompanied by reduced surface runoff at 0.40 mm, lateral flow at 4.66 mm, and water yield at 5.08 mm.

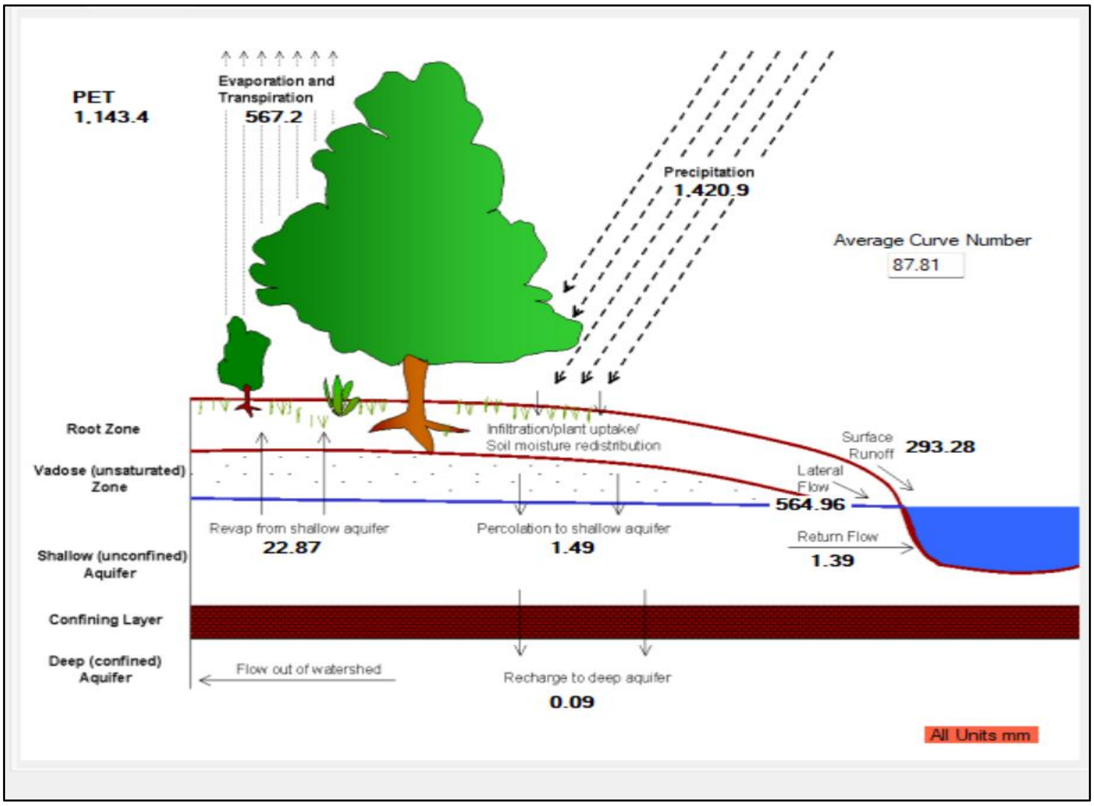

Figure 4.22: Hydrology/water balance components of Dzuza watershed

Table 4.16: Average monthly basin values obtained from SWAT model (Dzuza watershed)

Month	Rain (mm)	SURF Q (mm)	LAT Q (mm)	Water Yield (mm)	ET (mm)	Sediment Yield (t/ha)	PET (mm)
1	11.37	0.4	4.66	5.08	0.93	0	88.17
2	11.62	0.06	4.91	4.97	2.02	0	100.39
3	45.35	3.2	16.87	20.06	25.58	0.04	123.71
4	110.81	10.31	43.42	53.75	52.27	0.13	130.09
5	152.25	19.53	59.97	79.24	70.38	0.27	103.68
6	208.29	37.97	88.05	126.28	59.38	0.44	74.36
7	290.92	77.05	122.43	199.31	66.52	0.9	78.83
8	243.14	63.34	96.44	160.4	72.98	0.73	89.92
9	189.72	40.78	75.37	116.7	74.2	0.42	92.38
10	116.16	31.19	39.92	71.44	75.12	0.36	94.57
11	27.4	7.9	8.03	16.04	48.24	0.08	86.36
12	13.72	1.54	4.83	6.41	19.54	0.02	80.09
Total	**1420.85**	**293.27**	**564.9**	**859.68**	**567.16**	**3.39**	**1142.55**

(SURF - surface runoff; LAT - lateral flow; ET - evapotranspiration; PET - potential evapotranspiration)

4.4.4.1 Water Balance Ratio of Dzuza Watershed

The water balance ratios for the Dzuza watershed were calculated utilizing the mean annual values of precipitation, streamflow, baseflow, surface runoff, percolation, recharge, and evapotranspiration derived from the SWAT model (**Figure 4.22**). The findings are represented in **Table 4.17.** The ratio analysis indicated that around 60% of total precipitation contributed to streamflow, whereas 40% was lost by evapotranspiration. No contributions were documented for percolation or deep recharging. Approximately 66% of the total flow originated from baseflow, whereas 34% was produced by surface runoff, underscoring the preeminent influence of subterranean contributions on the watershed's hydrological balance.

Table 4.17: Water balance ratio for Dzuza Watershed

Sl. No.	Ratio	Value
1	Streamflow / Precipitation	0.6
2	Percolation / Precipitation	0
3	Deep Recharge / Precipitation	0
4	ET / Precipitation	0.4
5	Baseflow / Total Flow	0.66
6	Surface Runoff / Total Flow	0.34

4.4.5 Hydrology / Water Balance Components of Dhansiri River Basin

The water balance components of the Dhansiri river basin are represented in **Figure 4.23**, and the average monthly basin values that the SWAT model generated are shown in **Table 4.18**. According to **Figure 4.23**, the mean annual precipitation of the Dhansiri basin was 1654.6 mm. Of this total, 337.49 mm was attributed to surface runoff, whereas 528.84 mm was lost via evapotranspiration (ET). The lateral flow measured 89.26 mm, while the total water yield was 865.37 mm. Supplementary elements comprised a sediment yield of 3.20 t/ha and an annual potential evapotranspiration (PET) of 1070.16 mm. **Table 4.18** indicates that the peak monthly precipitation occurred in July (287.25 mm), coinciding with the largest surface runoff (32.43 mm), lateral flow (18.36 mm), and water yield (127.87 mm). Subsequently, August recorded 230.03 mm of precipitation, 20.29 mm of surface runoff, and 136.07 mm of water yield. Conversely, January experienced the lowest precipitation (11.30 mm), resulting in less surface runoff and reduced water yield (39.41 mm).

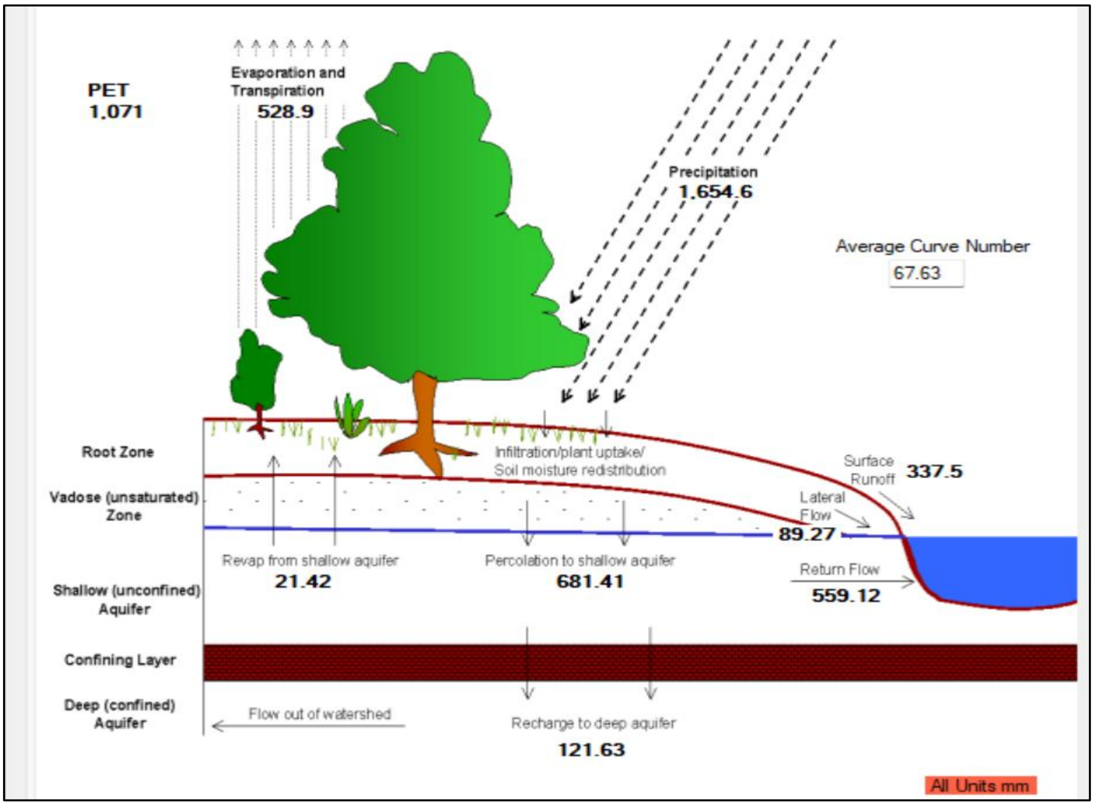

Figure 4.23: Hydrology/water balance components of Dhansiri river basin

Table 4.18: Average monthly basin values obtained from SWAT model (Dhansiri river basin)

Month	Rain (mm)	SURF Q (mm)	LAT Q (mm)	Water Yield (mm)	ET (mm)	Sediment Yield (t/ha)	PET (mm)
1	11.3	0	0.55	39.41	1.04	0	71.95
2	11.02	0.01	0.32	25.07	2.53	0	95.16
3	49.74	4.5	1.5	26.04	23.62	0.02	120.05
4	105.05	5.73	5.25	32.42	50.41	0.03	122.59
5	154.64	13.27	7.49	49.95	68.72	0.09	100.78
6	219.96	24.64	12.49	80.71	56.63	0.16	73.03
7	287.25	32.43	18.36	127.87	59.26	0.19	72.49
8	230.03	20.29	16.09	136.07	71.83	0.1	90.65
9	187.85	13.1	12.74	126.04	71.88	0.08	87.56

Table 4.18 (continued)

10	117.51	9.24	8.71	113.91	69.99	0.05	87.23
11	26.14	2.72	3.18	80.29	40.17	0.01	80.85
12	254	211.56	2.58	27.59	12.76	2.47	67.82
Total	**1654.49**	**337.49**	**89.26**	**865.37**	**528.84**	**3.2**	**1070.16**

(SURF - surface runoff; LAT - lateral flow; ET - evapotranspiration; PET - potential evapotranspiration)

4.4.5.1 Water Balance Ratio of Dhansiri River Basin

The water balance ratios of the Dhansiri basin were determined using the mean annual values of precipitation, streamflow, baseflow, surface runoff, percolation, recharge, and evapotranspiration obtained from the SWAT model (**Figure 4.23**). The findings are represented in **Table 4.19**. The ratio analysis indicated that 60% of the total precipitation contributed to streamflow, whilst 32% was lost to evapotranspiration. Furthermore, 41% of precipitation facilitated percolation, whereas 7% contributed to deep recharging. Of the entire flow, 66% was derived from baseflow, while 34% resulted from surface runoff, highlighting the equitable contribution of both groundwater and surface runoff processes in the Dhansiri watershed.

Table 4.19: **Water balance ratio for Dhansiri river basin**

Sl. No.	Ratio	Value
1	Streamflow / Precipitation	0.6
2	Percolation / Precipitation	0.41
3	Deep Recharge / Precipitation	0.07
4	ET / Precipitation	0.32
5	Baseflow / Total Flow	0.66
6	Surface Runoff / Total Flow	0.34

4.4.6 *Hydrology / Water Balance Components of Khova Sub-Watershed*

The water balance dynamics of the Khova sub-watershed are illustrated in **Figure 4.24**, while the detailed average monthly basin values are presented in **Table 4.20.** Over the simulation period, the watershed received an annual precipitation of 1654.49 mm. Of this, nearly one-fifth (335.01 mm) was translated into surface runoff, while a substantial proportion (528.06 mm) was lost to evapotranspiration (ET). The lateral flow contributed 88.68 mm, and the total water yield was calculated at an impressive 1099.46 mm, highlighting the watershed's strong runoff generation potential. The basin also experienced a modest sediment yield of 3.18 t/ha, alongside an annual potential evapotranspiration (PET) of 1070.16 mm.

The seasonal behavior of the Khova sub-watershed reveals the intimate link between monsoon rainfall and hydrological responses. The peak rainfall in July (287.25 mm) produced the largest water yield (129.32 mm), alongside 31.80 mm surface runoff and 18.21 mm lateral flow, reflecting the high responsiveness of the basin to intense precipitation. August followed with a water yield of 136.24 mm from 230.03 mm of rainfall. In stark contrast, the dry months of January (11.30 mm rainfall) and February (11.02 mm rainfall) contributed negligible water yields of 37.85 mm and 24.10 mm, respectively, with almost no surface runoff. This seasonal rhythm underscores the dominance of the monsoon in regulating water availability in the basin.

4.4.6.1 Water Balance Ratio of Khova Sub-Watershed

The estimated water balance ratios (**Table 4.21**) demonstrate the internal dynamics of the Khova sub-watershed. Of the total precipitation, approximately 59% was transformed into streamflow, while 32% was utilized via evapotranspiration, indicating a balanced distribution between runoff and atmospheric losses. The basin had significant subsurface activity, with 41% of rainfall infiltrating the soil profile and 8% replenishing the deeper aquifers. An examination of the flow contributions reveals that the Khova sub-watershed is predominantly sustained by subsurface mechanisms rather than surface reactions. Approximately two-thirds (66%) of the total flow was derived from baseflow, whereas one-third (34%) resulted from surface runoff. This underscores the essential function of groundwater channels and lateral subsurface flow in sustaining streamflow, even amid periods of minimal precipitation. The Khova sub-watershed exhibits a dual nature: it is extremely reactive to monsoon rainfall peaks, resulting in rapid surface runoff, while also relying on subterranean inputs to maintain flow throughout the seasons. The equilibrium between high runoff occurrences and groundwater-sustained baseflow delineates the hydrological resilience of the watershed.

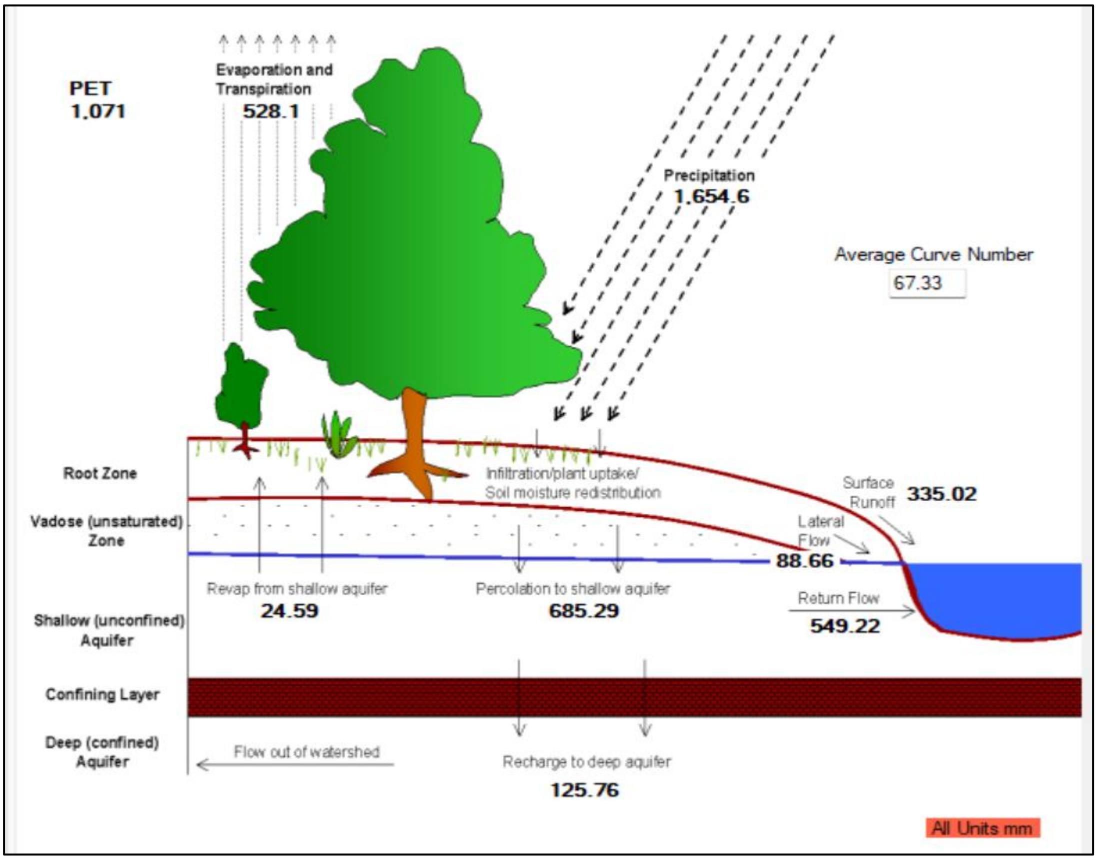

Figure 4.24: Hydrology/water balance components of Khova sub-watershed

Table 4.20: Average monthly basin values obtained from SWAT model (Khova sub-watershed)

Month	Rain (mm)	SURF Q (mm)	LAT Q (mm)	Water Yield (mm)	ET (mm)	Sediment Yield (t/ha)	PET (mm)
1	11.3	0	0.55	37.85	1.05	0	71.95
2	11.02	0.01	0.31	24.1	2.54	0	95.16

Table 4.20 (continued)

3	49.74	4.46	1.49	25.25	23.63	0.02	120.05
4	105.05	5.59	5.2	32.01	50.27	0.03	122.59
5	154.64	13.03	7.43	49.61	68.65	0.09	100.78
6	219.96	24.27	12.38	81.38	56.61	0.15	73.03
7	287.25	31.8	18.21	129.32	59.28	0.19	72.49
8	230.03	19.81	15.98	136.24	71.85	0.1	90.65
9	187.85	12.82	12.66	125.11	71.86	0.07	87.56
10	117.51	9.04	8.68	112.14	69.72	0.05	87.23
11	26.14	2.68	3.2	77.97	39.93	0.01	80.85
12	254	211.5	2.59	268.48	12.67	2.47	67.82
Total	**1654.49**	**335.01**	**88.68**	**1099.46**	**528.06**	**3.18**	**1070.16**

(SURF - surface runoff; LAT - lateral flow; ET - evapotranspiration; PET - potential evapotranspiration)

Table 4.21: Water balance ratio for Khova sub-watershed

Sl. No.	Ratio	Value
1	Streamflow / Precipitation	0.59
2	Percolation / Precipitation	0.41
3	Deep Recharge / Precipitation	0.08
4	ET / Precipitation	0.32
5	Baseflow / Total Flow	0.66
6	Surface Runoff / Total Flow	0.34

4.5 Prioritization of the Watershed

The results of watershed prioritization were obtained by the Sub-Watershed Prioritization Tool (SWPT), which incorporates morphometric, topographic, and hydrological characteristics within an automated GIS framework. SWPT produced values for twelve essential indices, including stream frequency (Fs), bifurcation ratio (Rb), form factor (Rf), elongation ratio (Re), circularity ratio (Rc), drainage density (Dd), texture ratio (Rt), compactness coefficient (Cc), constant of channel maintenance (C), topographic wetness index (TWI), stream power index (SPI), and sediment transport index (STI). Relative weights were assigned to each parameter by weighted sum analysis, and compound parameter (Cp) values were calculated for all sub-watersheds. The results were subsequently ranked, with lower Cp values signifying greater sensitivity to erosion and hydrological stress, therefore indicating a higher need for soil and water conservation initiatives. According to these rankings, the sub-watersheds were classified into high, medium, and low priority zones. High-priority sub-watersheds generally demonstrated elevated drainage density, bifurcation ratio, and sediment transport indices, indicating increased runoff potential and erosion hazards. In contrast, low-priority sub-watersheds exhibited more stable morphometric attributes with diminished hydrological susceptibility. This methodical technique facilitated objective and reproducible prioritizing, ensuring that conservation efforts are first focused on the most at-risk locations. The integration of SWPT in the findings offers a thorough comprehension of sub-watershed conditions, connecting quantitative morphometric analysis with actionable management recommendations.

To perform effective watershed analysis and prioritization, the three study areas—Dzuza, Dhansiri, and Khova—were subdivided into sub-watersheds utilizing SRTM-DEM and GIS-based hydrological methods.

I. The Dzuza Sub-Basin (**Figure 4.25 (a)**) was divided into nine sub-basins to account for drainage variations over its lengthy catchment area.
II. The Dhansiri Sub-Basin (**Figure 4.25 (b)**), being relatively larger and more heterogeneous, was segmented into 19 sub-basins to reflect the changes in morphometric and hydrological attributes.

III. The Khova Sub-Basin (**Figure 4.25 (c)**) was divided into six sub-basins, ensuring precise representation of its drainage network, slope configurations, and runoff dynamics.

This segmentation is essential due to the significant variability of watershed processes, even within a singular basin. Analyzing at the sub-basin level enables a more complete and accurate evaluation of morphometric characteristics, SWPT-based prioritizing, soil erosion susceptibility, and hydrological behavior. This delineation establishes the basis for later morphometric study, sub-watershed prioritization, and conservation planning.

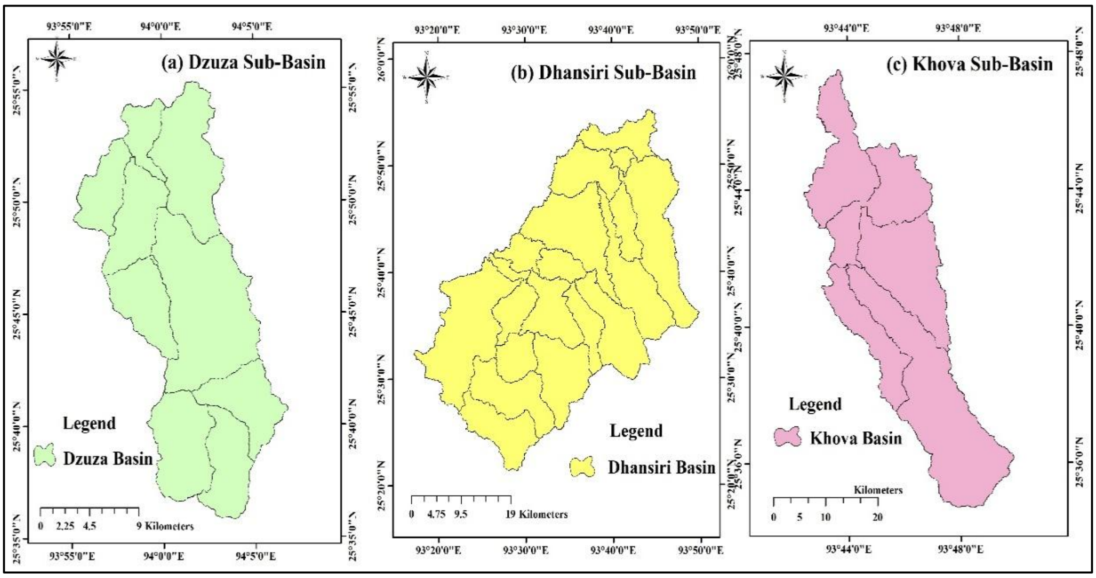

Figure 4.25: Delineation of the study area into sub-basins: (a) Dzuza watershed (9 sub-basins), (b) Dhansiri river basin (19 sub-basins), and (c) Khova sub-watershed (6 sub-basins).

4.5.1 Geomorphometric Characteristics of Dzuza Watershed

Table 4.22 presents the morphometric and topo-hydrological parameters of the Dzuza watershed, which is divided into 9 sub-watersheds (**Figure 4.26**). The stream frequency (Fs) ranges from 8.27×10^{-7} in sub-watershed D6 to 8.17×10^{-6} in sub-watershed D1. These values, however minimal, reflect the extent of drainage dissection and are pertinent when normalized across the basin for comparative ranking. The bifurcation ratio (Rb) varies from 1.71 in D2 to 2.36 in D4, indicating that D4 has a more complex branching pattern, whilst D2 demonstrates a more straightforward drainage configuration. The form factor (Rf) is maximal in D7 (0.571) and minimal in D1 (0.285), suggesting that D1 exhibits greater elongation relative to the almost circular configuration of D7. The elongation ratio (Re) exhibits a comparable pattern, with D7 (0.853) at the higher end and D1 (0.602) at the lower, underscoring divergent hydrological responses within the basin. The circularity ratio (Rc) ranges from 0.235 in D1 to 0.380 in D8, further substantiating variations in sub-basin morphology and flood susceptibility. Drainage density (D) ranges from 0.000969 km/km² in D6 to 0.00304 km/km² in D1, indicating a predominance of surface runoff in the latter. The channel maintenance constant (C) values demonstrate that D6 (1032.40) necessitates the highest maintenance, while D1 (328.93) requires the least. The Topographic Wetness Index (TWI) readings exhibit reasonable uniformity, with D6 (9.64) being marginally elevated, and D9 (9.06) has the lowest value. The Stream Power Index (SPI) is maximal in D9 at 7.61 and minimal in D2 at 6.82. The Sediment Transport Index (STI) is higher in D6 (20.57) than in D1 (16.30).

4.5.1.1 Automated Prioritization of Sub-Watersheds

The correlation matrix obtained from Weighted Sum Analysis (WSA) is shown in **Table 4.23** and the correlation heat map in **Figure 4.27**. Strong positive correlations were identified between stream frequency (Fs) and drainage density (D) (r = 0.94), as well as between Fs and drainage texture (R_t) (r = 0.97), suggesting that dense drainage networks with elevated stream frequencies enhance erosive potential. In contrast, F_s and the channel maintenance constant (C) exhibited a negative correlation (r = –0.75), indicating that highly dissected basins are prone to unstable channels. The elongation ratio (R_e) and form factor (R_f) exhibited a strong correlation (r = 0.99), as anticipated, indicating shape-driven hydrological responses. The circularity ratio (R_c) exhibited a strong negative connection with the compactness coefficient (C_c) (r = –0.99), confirming that compact basins are generally less circular. Subsequent to the Weighted Sum prioritizing, compound parameter values (CPVs) were produced (**Table 4.24**). The findings indicate that sub-watershed Sw1 (CPV = 62.48) is ranked highest (**Figure 4.28**), followed by Sw2 (90.56) and Sw7 (98.04), identifying them as the most susceptible to erosion and hydrologically sensitive regions. Sub-watershed Sw6 (185.22) has the highest CPV, categorizing it as the lowest priority.

Table 4.22: Morphometric and topo-hydrological parameters of the Dzuza sub-watersheds

Sub-watershed code	Parameters											
	F_s	R_b	R_f	R_e	R_c	D	R_t	C_c	C	TWI	SPI	STI
Sw 1	8.17E-06	1.72	0.285	0.602	0.235	0.00304	0.00435	2.06	328.93	9.27	7.08	16.3
Sw 2	2.17E-06	1.71	0.437	0.746	0.301	0.00205	0.00163	1.82	488.19	9.41	6.82	18.65
Sw 3	1.33E-06	1.94	0.564	0.847	0.272	0.0014	0.00143	1.92	713.75	9.29	7.25	19.72
Sw 4	2.50E-06	2.36	0.326	0.645	0.268	0.00177	0.00206	1.93	565.74	9.5	7.23	19.42
Sw 5	2.47E-06	2.03	0.4	0.714	0.34	0.00173	0.00224	1.71	576.73	9.53	7.2	19.35
Sw 6	8.28E-07	1.9	0.571	0.853	0.306	0.00097	0.00126	1.81	1032.4	9.64	7.11	20.57
Sw 7	3.06E-06	2.14	0.571	0.853	0.271	0.00189	0.00249	1.92	530.44	9.54	7.12	18.69
Sw8	2.04E-06	1.96	0.56	0.844	0.38	0.00153	0.00226	1.62	654.69	9.21	7.6	19.28
Sw 9	2.12E-06	2.04	0.328	0.646	0.311	0.00149	0.00185	1.79	672.63	9.06	7.61	18.67

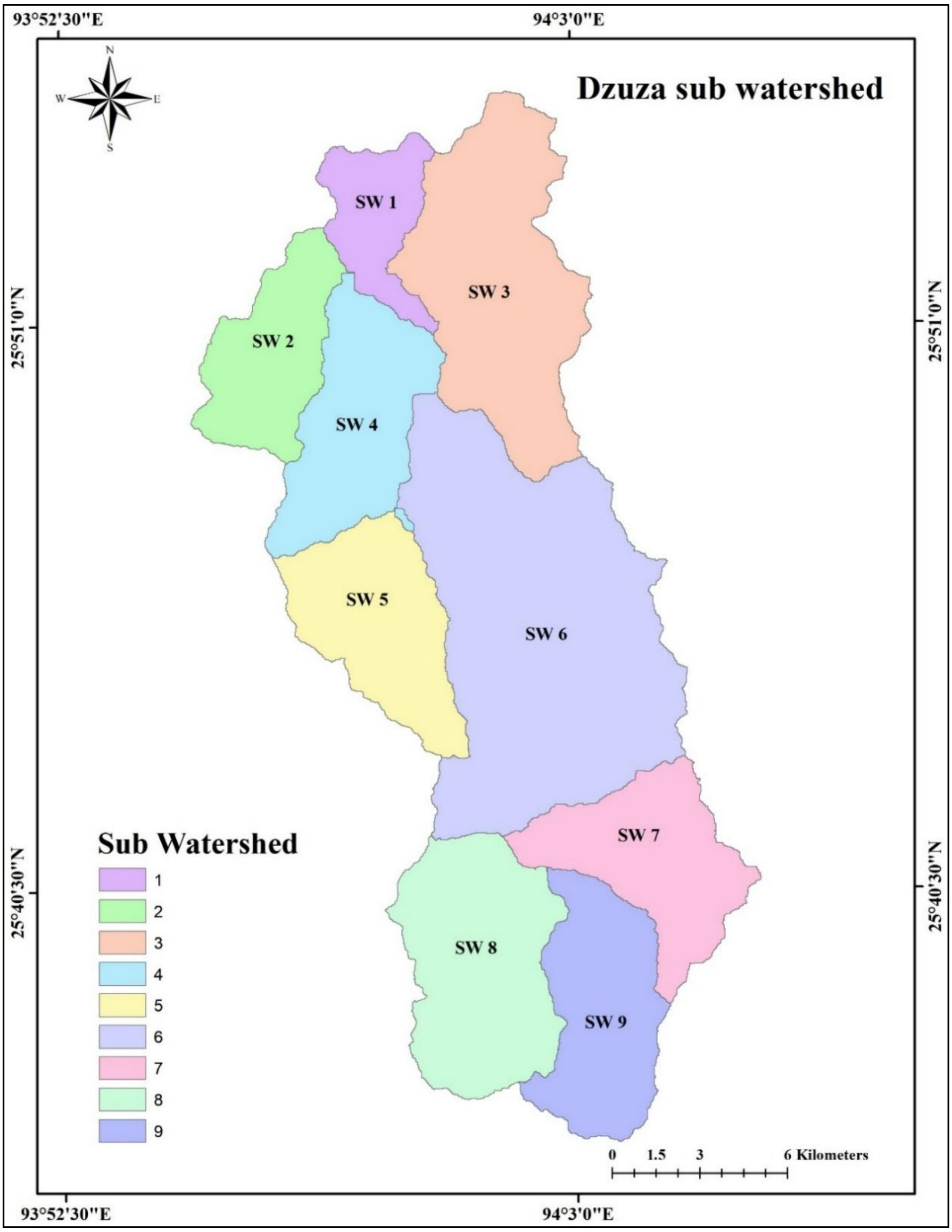

Figure 4.26: Sub watersheds of Dzuza watershed

4.5.1.2 *Sub-Watershed Priority Ranking*

The nine sub-watersheds of the Dzuza watershed were classified into three categories based on CPV values (**Table 4.25; Figure 4.29**):

High priority: SW1, SW2, SW7
Moderate priority: SW4, SW5, SW8
Low priority: SW9, SW3, SW6

High-priority watersheds, encompassing the most susceptible regions, necessitate immediate conservation measures like the construction of check dams, the establishment of vegetative barriers, and afforestation efforts. Medium-priority basins necessitate semi-intensive management, encompassing agroforestry and rainwater collection. Although low-priority watersheds are reasonably stable, they nonetheless require monitoring to preserve their hydrological equilibrium.

***T*able 4.23: Correlation of morphometric properties of the Dzuza sub-watersheds**

	F_s	R_b	R_f	R_e	R_c	D	R_t	C_c	C	TWI	SPI	STI
F_s	1	-0.33	-0.59	-0.61	-0.54	0.94	0.97	0.62	-0.75	-0.22	-0.22	-0.94
R_b	-0.33	1	-0.04	-0.04	0.03	-0.35	-0.22	-0.06	0.13	0.22	0.38	0.39
R_f	-0.59	-0.04	1	1	0.34	-0.6	-0.51	-0.36	0.57	0.31	0.01	0.61
R_e	-0.61	-0.04	1	1	0.36	-0.61	-0.53	-0.38	0.57	0.32	0	0.63
R_c	-0.54	0.03	0.34	0.36	1	-0.52	-0.4	-0.99	0.37	-0.13	0.51	0.48
D	0.94	-0.35	-0.6	-0.61	-0.52	1	0.89	0.59	-0.91	-0.19	-0.38	-0.95
R_t	0.97	-0.22	-0.51	-0.53	-0.4	0.89	1	0.49	-0.74	-0.22	-0.08	-0.9
C_c	0.62	-0.06	-0.36	-0.38	-0.99	0.59	0.49	1	-0.42	0.08	-0.49	-0.54
C	-0.75	0.13	0.57	0.57	0.37	-0.91	-0.74	-0.42	1	0.27	0.25	0.85
TWI	-0.22	0.22	0.31	0.32	-0.13	-0.19	-0.22	0.08	0.27	1	-0.63	0.42
SPI	-0.22	0.38	0.01	0	0.51	-0.38	-0.08	-0.49	0.25	-0.63	1	0.17
STI	-0.94	0.39	0.61	0.63	0.48	-0.95	-0.9	-0.54	0.85	0.42	0.17	1

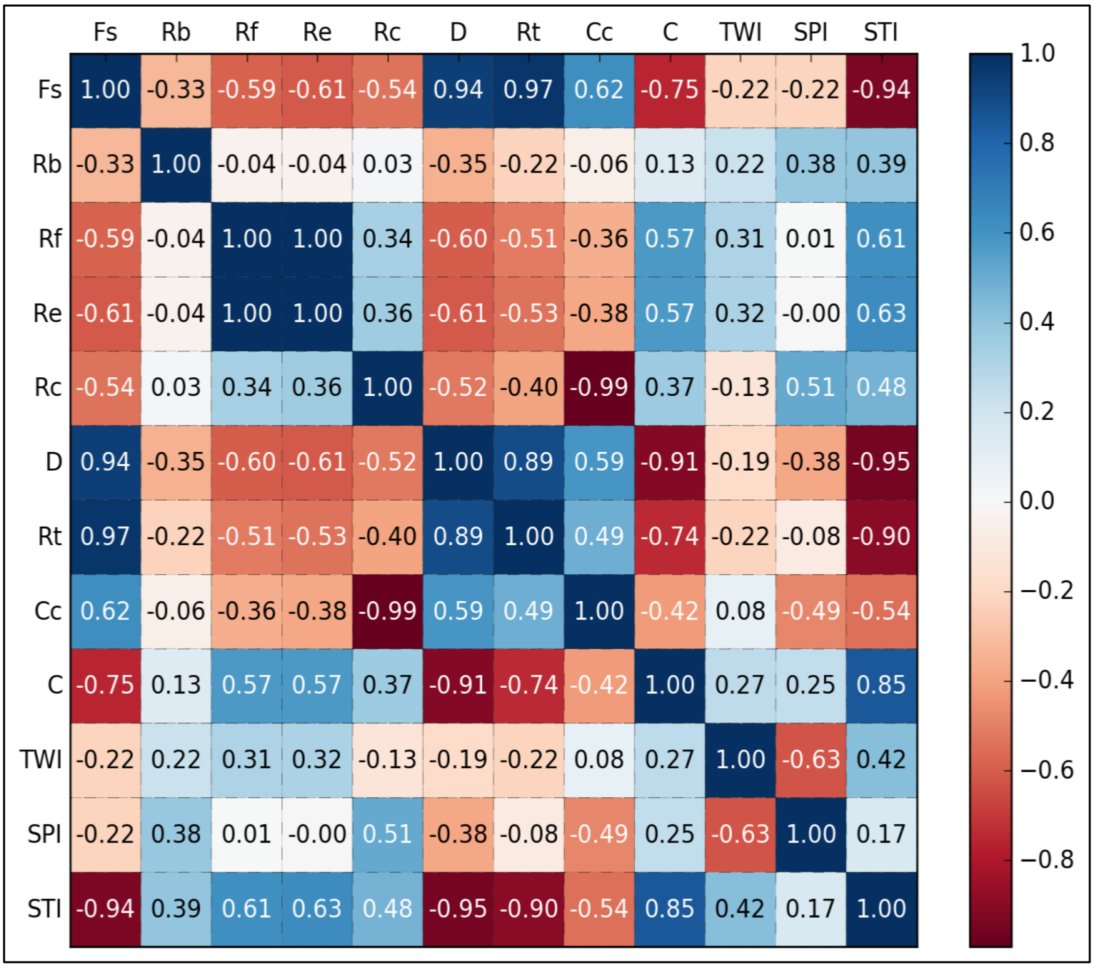

Figure 4.27: Correlation heatmap of geomorphometric and topo-hydrological parameters of the Dzuza sub-watersheds

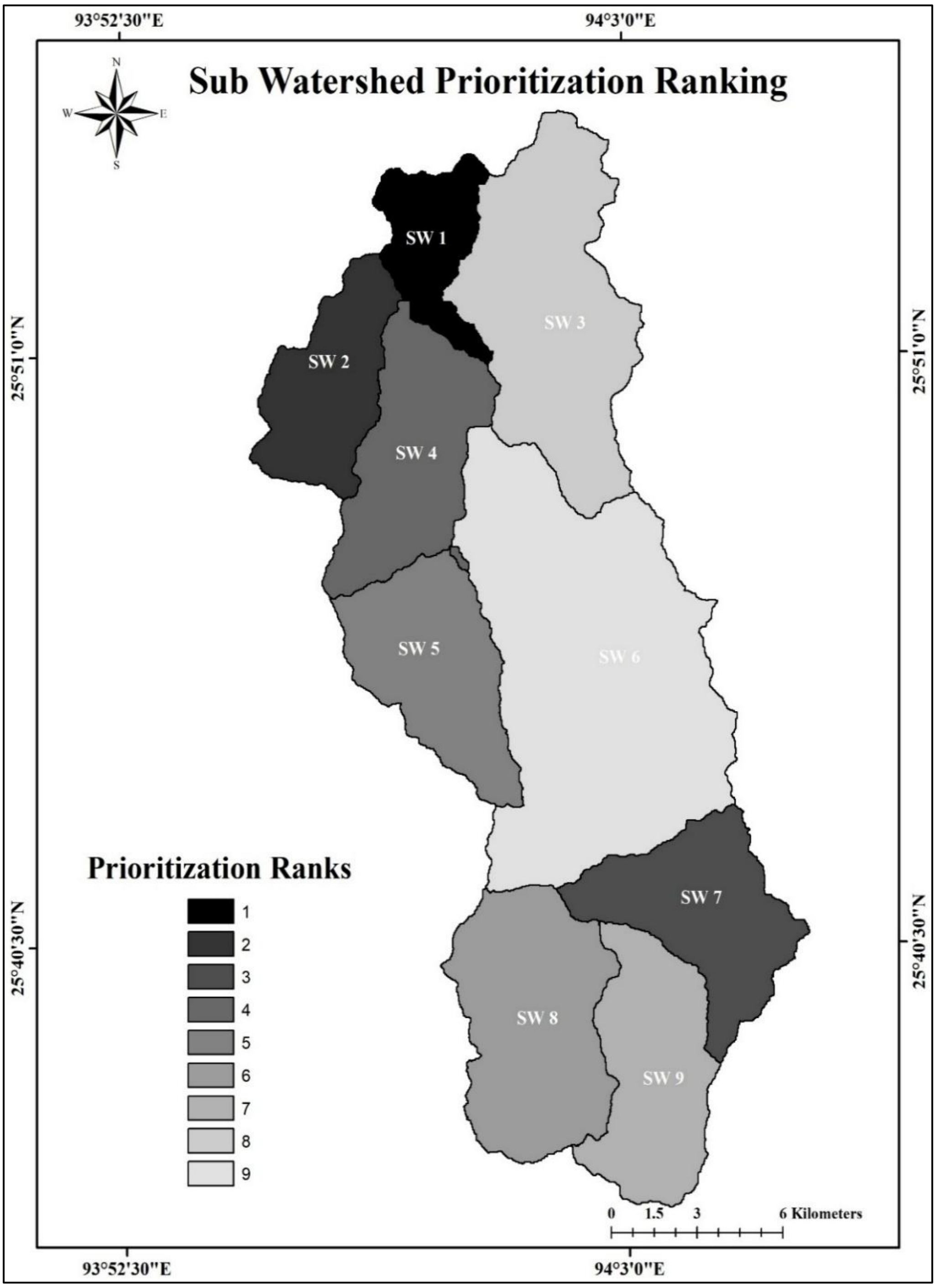

Figure 4.28: Dzuza Subwatershed prioritization ranking

Table 4.24: Prioritization and final ranking of Dzuza sub-watersheds.

Name	Prioritization	Rank
Sw 1	62.4799	1
Sw 2	90.5594	2
Sw 7	98.0446	3
Sw 4	104.2059	4
Sw 5	106.1001	5
Sw 8	119.6198	6
Sw9	122.4749	7
Sw 3	129.875	8
Sw 6	185.2219	9

Table 4.25: Categorization of Dzuza sub-watersheds priority ranking

Priority type	Sub-watersheds	Percent of basin area
High Priority	Sw1, Sw2, Sw7	16.86
Medium Priority	Sw4, Sw5, Sw8	30.27
Low Priority	Sw9, Sw3, Sw6	52.87

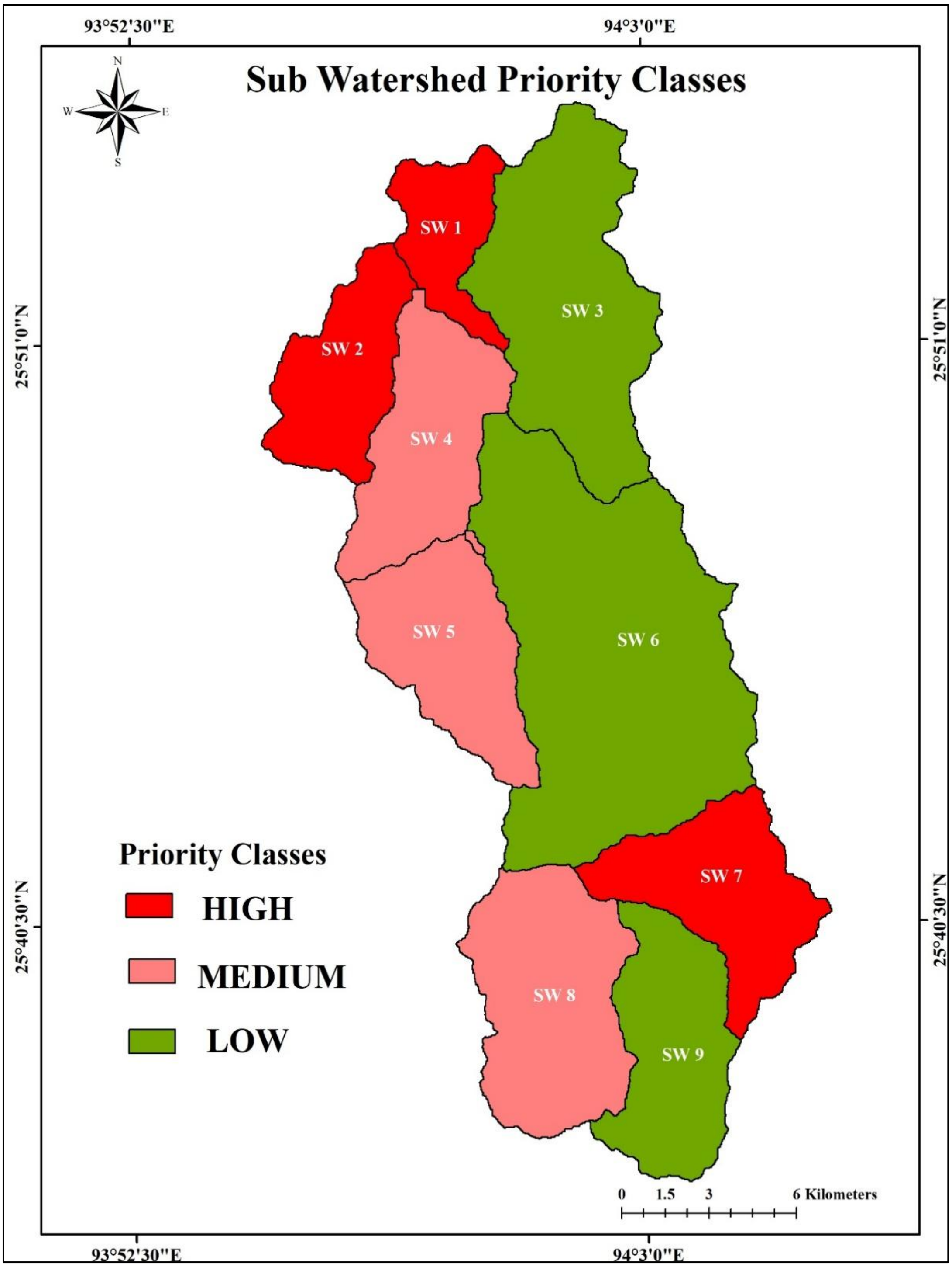

Figure 4.29: Dzuza sub watershed priority classes

4.5.2 Geomorphometric Characteristics of Dhansiri River Basin

Table 4.26 presents the outcomes of geomorphometric parameters derived from an automated GIS-based method for sub-watershed prioritization. The study region comprises 19 sub-watersheds, as illustrated in **Figure 4.30**, with stream frequency (F_s) varying from 0.00000033 in sub-watershed 17 to 0.00001103 in sub-watershed 2. Although values like 0.00000033 and 0.00001103 may seem proximate to zero, their importance is ascertained by normalization and comparative analysis within the study area. The variations in these numbers indicate different erosion potentials and hydrological behaviors, highlighting the necessity of presenting data in a comparative context. The bifurcation ratio (R_b) indicates that sub-watershed 13 has the highest value at 2.26, whereas sub-watershed 3 has the lowest at 1.68. Regarding form factor (R_f), the SWPT indicated that sub-watershed 4 exhibited the highest value of 1.12, while sub-watershed 8 had the lowest value of 0.15. The prioritization of the elongation ratio (R_e) findings is identical to that of the R_f index. Sub-watershed 4 had the highest R_e value, followed by sub-watersheds 7, 15, 2, 10, 1, 16, 3, 18, 5, 14, 19, 11, 17, 13, 9, 6, 12, and 8. Sub-watershed 15 exhibited the highest circularity ratio (R_c) value of 0.35, while sub-watershed 8 recorded the lowest value of 0.12. Based on drainage density (D) data, sub-watershed 2 ranks first, while sub-watershed 17 ranks bottom. The values of the channel maintenance constant (C) indicate that sub-watershed 17 (1327.73) ranks top, while sub-watershed 2 (258.11) ranks last. According to the prioritization results, sub-watersheds 12, 16, and 19 exhibit the highest values for the Topographic Wetness Index (TWI), Stream Power Index (SPI), and Sediment Transport Index (STI), indicating higher susceptibility to erosion and runoff. Conversely, sub-watersheds 16 and 2 show the lowest values for TWI and SPI, with sub-watershed 2 also scoring the lowest for STI, suggesting lower vulnerability in these regions.

Table 4.26: Morphometric and topo-hydrological parameters of the Dhansiri sub-watersheds

Sub-watershed code	Parameters											
	F_s	R_b	R_f	R_e	R_c	D	R_t	C_c	C	TWI	SPI	STI
Sw1	0.00000155	2.24	0.43	0.74	0.12	0.001	0.001	2.27	663.14	11.12	4.98	14.28
Sw2	0.00001103	2.08	0.54	0.83	0.20	0.004	0.005	2.21	258.11	11.26	4.85	13.02
Sw3	0.00000209	1.68	0.36	0.68	0.15	0.002	0.002	2.54	493.57	10.64	5.48	16.30
Sw4	0.00000171	1.88	1.12	1.19	0.19	0.002	0.002	2.24	587.40	10.99	5.07	14.55
Sw5	0.00000041	1.86	0.35	0.67	0.15	0.0009	0.0006	2.55	1102.15	10.95	5.14	15.58
Sw6	0.00000040	1.92	0.20	0.50	0.16	0.0009	0.0006	2.47	1074.24	10.47	5.85	17.99
Sw7	0.00000379	1.75	0.65	0.91	0.16	0.002	0.030	2.53	437.41	10.76	5.20	13.89
Sw8	0.00000053	1.79	0.15	0.44	0.12	0.001	0.0006	2.86	916.05	10.35	5.96	18.74
Sw9	0.00000447	2.07	0.20	0.51	0.14	0.002	0.002	2.65	393.82	10.64	5.21	14.20
Sw10	0.00000206	2.03	0.51	0.81	0.24	0.002	0.002	2.05	583.30	10.53	5.48	14.51
Sw11	0.00000132	1.83	0.34	0.65	0.22	0.002	0.001	2.12	613.58	10,43	5.66	15.88
Sw12	0.00000136	1.85	0.18	0.48	0.17	0.001	0.001	2.39	633.89	9,92	6.38	18.11
Sw13	0.00000066	2.26	0.27	0.59	0.22	0.001	0.0009	2.15	980.52	9.90	6.44	19.22
Sw14	0.00000073	1.80	0.35	0.67	0.18	0.001	0.0008	2.37	883.16	10.09	6.14	17.68
Sw15	0.00000157	2.08	0.56	0.84	0.35	0.001	0.002	1.69	637.04	9.93	6.22	17.24

Table 4.26 (continued)

Sw16	0.00000059	1.85	0.40	0.72	0.28	0.0009	0.0009	1.89	1025.96	9.67	6.81	18.81
Sw17	0.00000033	2.02	0.33	0.65	0.15	0.0007	0.0005	2.53	1327.73	10.02	6.14	17.65
Sw18	0.00000063	1.89	0.35	0.67	0.19	0.001	0.0008	2.28	967.37	9.80	6.46	18.26
Sw19	0.00000068	1.77	0.34	0.66	0.21	0.001	0.0009	2.15	933.85	9.78	6.59	18.24

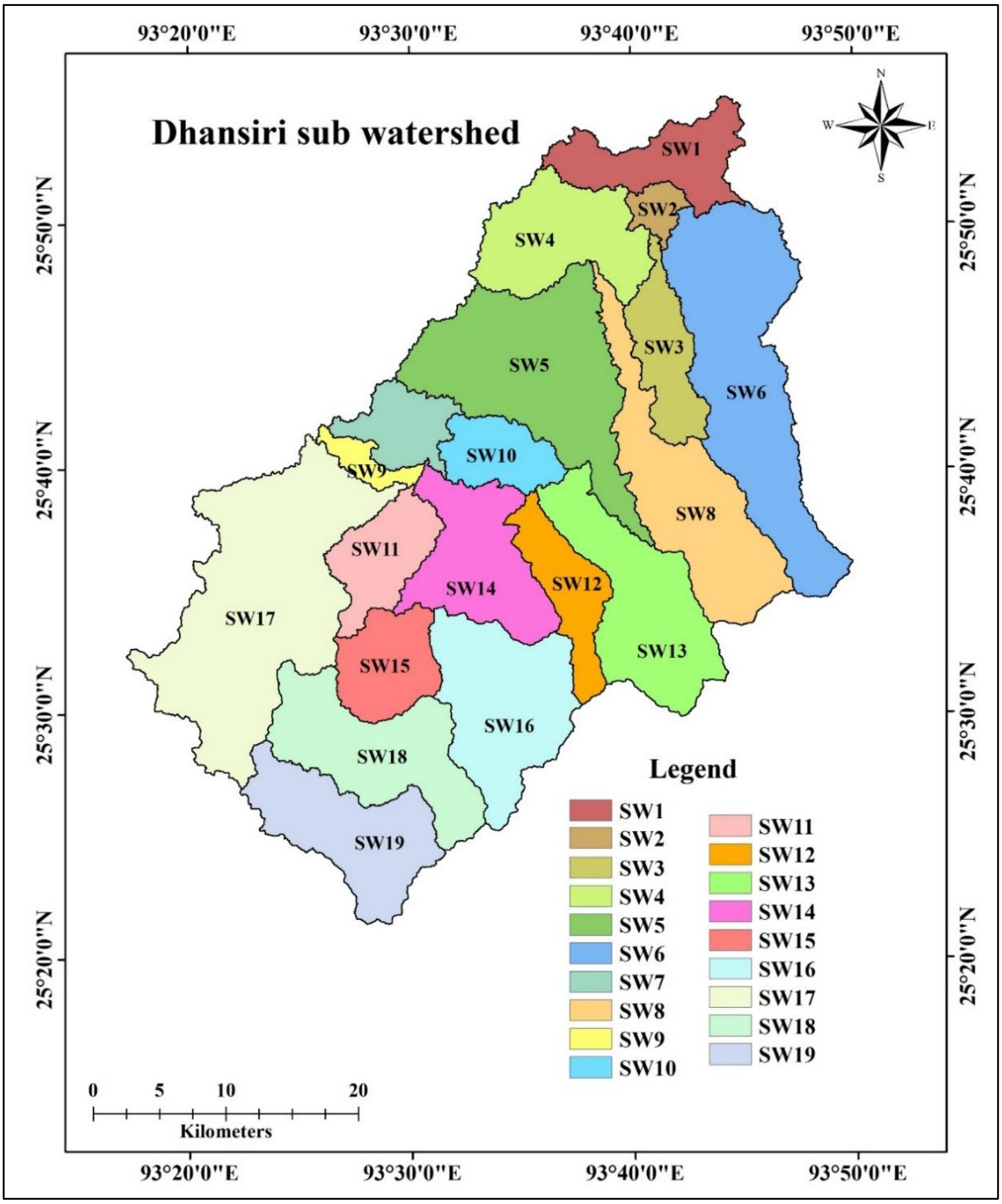

Figure 4.30: Sub watersheds of Dhansiri river basin

4.5.2.1 Automated Prioritization of Sub-Watersheds

Table 4.27 presents the correlation matrix derived from the Weighted Sum Analysis (WSA) of morphometric parameters for the sub-watersheds, and **Figure 4.31** shows the correlation heat map. F_s has a positive association with drainage density (D) (r = 0.96): A high stream frequency signifies a more developed or mature watershed characterized by well-connected streams (Dikpal *et al.*, 2017). There exists a negative association with the Constant of Channel Maintenance (C) (r = -0.73): Watersheds with elevated Stream Frequency generally demonstrate reduced C, indicating that an increased quantity of smaller, less stable streams may compromise overall channel stability. The compactness coefficient exhibits a substantial negative association with the circularity ratio (R_c) (r = -0.97), indicating that compact watersheds typically exhibit decreased circularity, perhaps attributable to their morphology and the development of the drainage network. C exhibits a negative connection with D (r = -0.89) and F_s (r = -0.73). The Bifurcation Ratio (R_b) indicates a poor correlation with most parameters, suggesting that the watershed's branching pattern may not directly influence its other morphometric characteristics (Strahler 1964), such as drainage density or stream frequency. D demonstrates a robust positive connection with F_s (r = 0.96): A dense drainage network is generally linked to a high stream frequency and exhibits a negative association with C (r = -0.89); watersheds with an increased number of streams (higher D) tend to possess fewer stable channels (C), suggesting a more erosive or dynamic hydrological environment (Jothimani *et al.*, 2021). The Elongation Ratio (R_e) exhibits a strong positive association with the Form Factor (R_f) (r = 0.99). Watersheds characterized by a higher elongation ratio typically possess a greater form factor, indicating that more elongated watersheds are generally less circular and exhibit distinct hydrological responses (Horton 1945). The circularity ratio (R_c) has a robust negative connection with C_c (r = -0.97). The Form Factor (R_f) exhibits a strong positive connection with Re (r = 0.99). The Drainage Texture Ratio (R_t) exhibits a negative connection with D (r = -0.78). The Topographic Wetness Index has a negative correlation with SPI, r = -0.98, and a positive correlation with D, r = 0.6. The Stream Power Index shows a strong positive correlation with TWI, r = 0.92, and a moderate negative correlation with D, r = -0.56. There was an evident positive correlation between the Streams (r = 0.73) and SPI values (r = 0.92), whereas STI shows a negative relationship with C (r = -0.76). After the final ranking, it provides a ranking for all sub-watersheds as determined by CPV after the application of WSA methods. The CPV integrates numerous morphometric characteristics, offering a thorough evaluation of each sub-watershed's vulnerability to diverse hydrological and environmental issues, including erosion, drainage patterns, and water retention capacity. The sub-watershed with the lowest CPV signifies the utmost requirement for intervention. The negative values denote the degree of concern, with lower (more negative) values indicating heightened urgency for management. Sub-watershed Sw17 exhibits the lowest CPV of -199.71, designating it as the highest priority (Rank 1) for management interventions (**Figure 4.32**). After Sw17, Sw5 and Sw6 are positioned 2nd and 3rd, with CPVs of -165.56 and -162.03, respectively. These sub-watersheds demonstrate elevated risk circumstances and hence necessitate targeted attention and conservation initiatives. Sw16 and Sw13, with CPVs of -155.06 and -148.33, are positioned 4th and 5th, signifying they are notable issues, albeit less severe than the top three sub-watersheds. Additional sub-watersheds, including Sw18 (Rank 6), Sw19 (Rank 7), and Sw8 (Rank 8), also display negative CPV values, indicating they are of significant concern and require management, albeit to a lower extent than the highest-ranked sub-watersheds. Conversely, Sw2 is positioned 19th with the highest CPV of -39.32. **Table 4.28** shows the Prioritization and final ranking of sub-watersheds. Although it necessitates care, it is deemed a lower priority than the others owing to its comparatively superior morphometric properties. The CPV-based ranking method facilitates the identification of sub-watersheds susceptible to problems such as erosion, inadequate drainage, or waterlogging, hence optimizing the allocation of resources and management initiatives. The sub-watersheds with lower CPV values necessitate the most urgent and rigorous actions, whilst those with elevated CPV values are comparatively less concerning but demand continuous oversight and management. This will serve as a guide for focused conservation efforts, land use planning, and watershed management to address the most vulnerable sub-watersheds (Mishra & Nagarjan 2010).

4.5.2.2 Sub-Watershed Priority Ranking

Figure 4.33 and **Table 4.29** illustrate the prioritization ranking of sub-watersheds based on their susceptibility to soil erosion and hydrological impacts. High-priority regions, encompassing 48.13% of the watershed, necessitate prompt action owing to the threat of severe soil erosion, deterioration of water quality, and considerable hydrological impacts. Proposed strategies encompass soil conservation methods, afforestation, the establishment of check dams, and regulated land-use practices. Medium-priority areas, comprising 37.38%, encounter moderate threats and may necessitate partial conservation interventions, including integrated land-use planning, agroforestry, and semi-intensive conservation strategies. Ultimately, low-priority areas, constituting 14.50%, demonstrate negligible risk and may necessitate merely regular monitoring and sustainable land management to preserve their existing state.

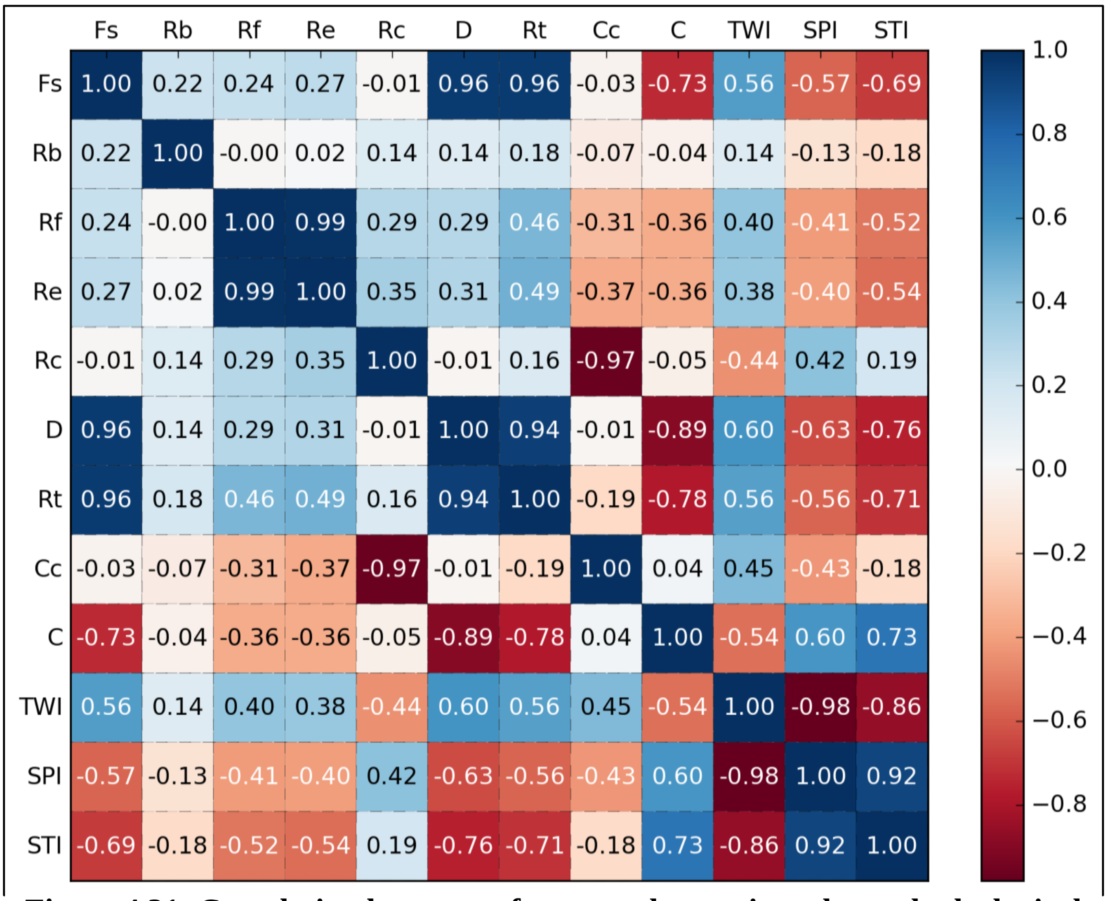

Figure 4.31: Correlation heatmap of geomorphometric and topo-hydrological parameters of the Dhansiri sub-watersheds

Table 4.27: Correlation of morphometric properties of the Dhansiri sub-watersheds

	F_s	R_b	R_f	R_e	R_c	D	R_t	C_c	C	TWI	SPI	STI
F_s	1.0	0.22	0.24	0.27	-0.01	0.96	0.96	-0.03	-0.73	0.56	-0.57	-0.69
R_b	0.22	1.0	-0.0	0.02	0.14	0.14	0.18	-0.07	-0.04	0.14	-0.13	-0.18
R_f	0.24	-0.0	1.0	0.99	0.29	0.29	0.46	-0.31	-0.36	0.4	-0.41	-0.52
R_e	0.27	0.02	0.99	1.0	0.35	0.31	0.49	-0.37	-0.36	0.38	-0.4	-0.54
R_c	-0.01	0.14	0.29	0.35	1.0	-0.01	0.16	-0.97	-0.05	-0.44	0.42	0.19
D	0.96	0.14	0.29	0.31	-0.01	1.0	0.94	-0.01	-0.89	0.6	-0.63	-0.76
R_t	0.96	0.18	0.46	0.49	0.16	0.94	1.0	-0.19	-0.78	0.56	-0.56	-0.71
C_c	-0.03	-0.07	-0.31	-0.37	-0.97	-0.01	-0.19	1.0	0.04	0.45	-0.43	-0.18
C	-0.73	-0.04	-0.36	-0.36	-0.05	-0.89	-0.78	0.04	1.0	-0.54	0.6	0.73
TWI	0.56	0.14	0.4	0.38	-0.44	0.6	0.56	0.45	-0.54	1.0	-0.98	-0.86
SPI	-0.57	-0.13	-0.41	-0.4	0.42	-0.63	-0.56	-0.43	0.6	-0.98	1.0	0.92
STI	-0.69	-0.18	-0.52	-0.54	0.19	-0.76	-0.71	-0.18	0.73	-0.86	0.92	1.0

Table 4.28: Prioritization and final ranking of Dhansiri sub-watersheds.

Name	Prioritization	Priority ranking
Sw17	-199.712897129	1
Sw5	-165.561667372	2
Sw6	-162.031196143	3
Sw16	-155.060006551	4
Sw13	-148.334365268	5
Sw18	-146.268016568	6
Sw19	-141.292318393	7
Sw8	-138.751384343	8
Sw14	-133.575552215	9
Sw1	-99.9357801996	10
Sw12	-96.6950919981	11
Sw15	-96.6940847301	12
Sw11	-93.0213316578	13
Sw4	-88.4625542727	14
Sw10	-88.1329227508	15
Sw3	-75.2565081518	16
Sw7	-66.3077964639	17
Sw9	-60.0490270754	18
Sw2	-39.321589632	19

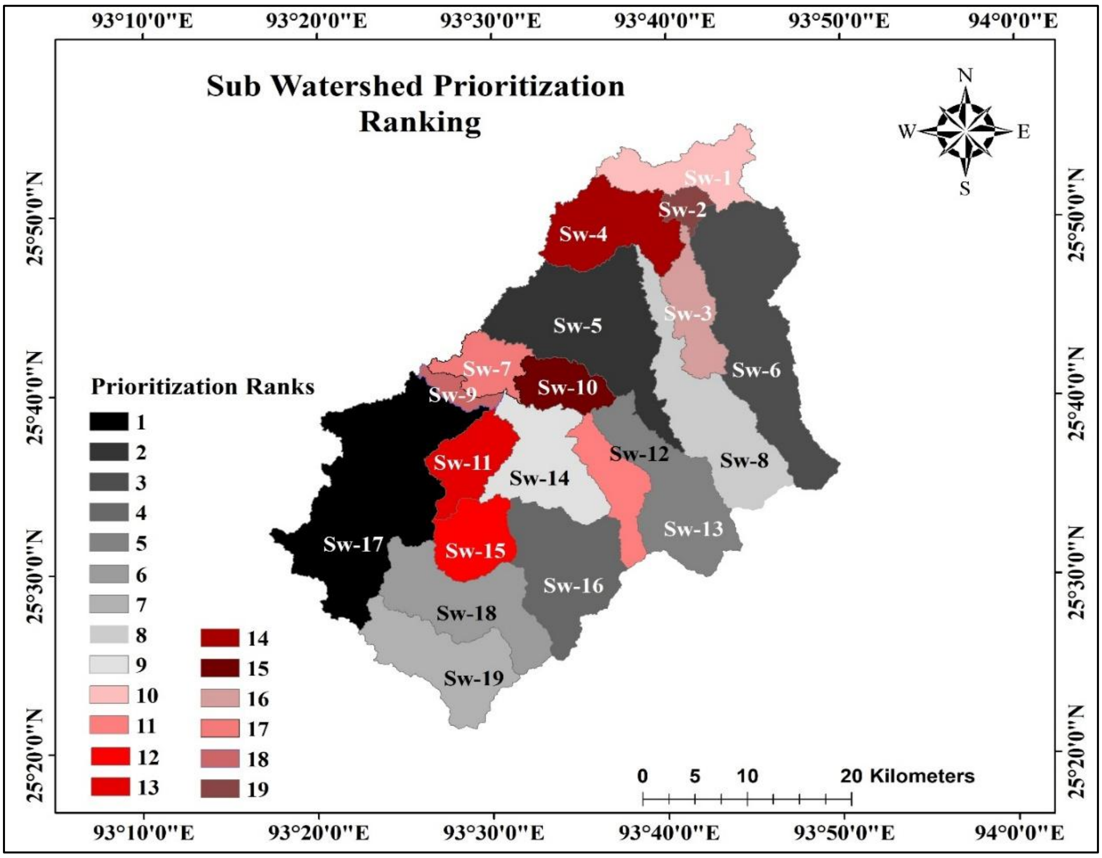

Figure 4.32: Dhansiri sub watershed prioritization ranking

Table 4.29: Categorization of Dhansiri sub-watersheds priority ranking

Priority type	Sub watersheds	Percent of basin area
High	Sw17, Sw5, Sw6, Sw16, Sw13	48.13
Medium	Sw18, Sw19, Sw8, Sw14, Sw1, Sw12, Sw15, Sw11	37.38
low	Sw4, Sw10, Sw3, Sw7, Sw9, Sw2	14.50

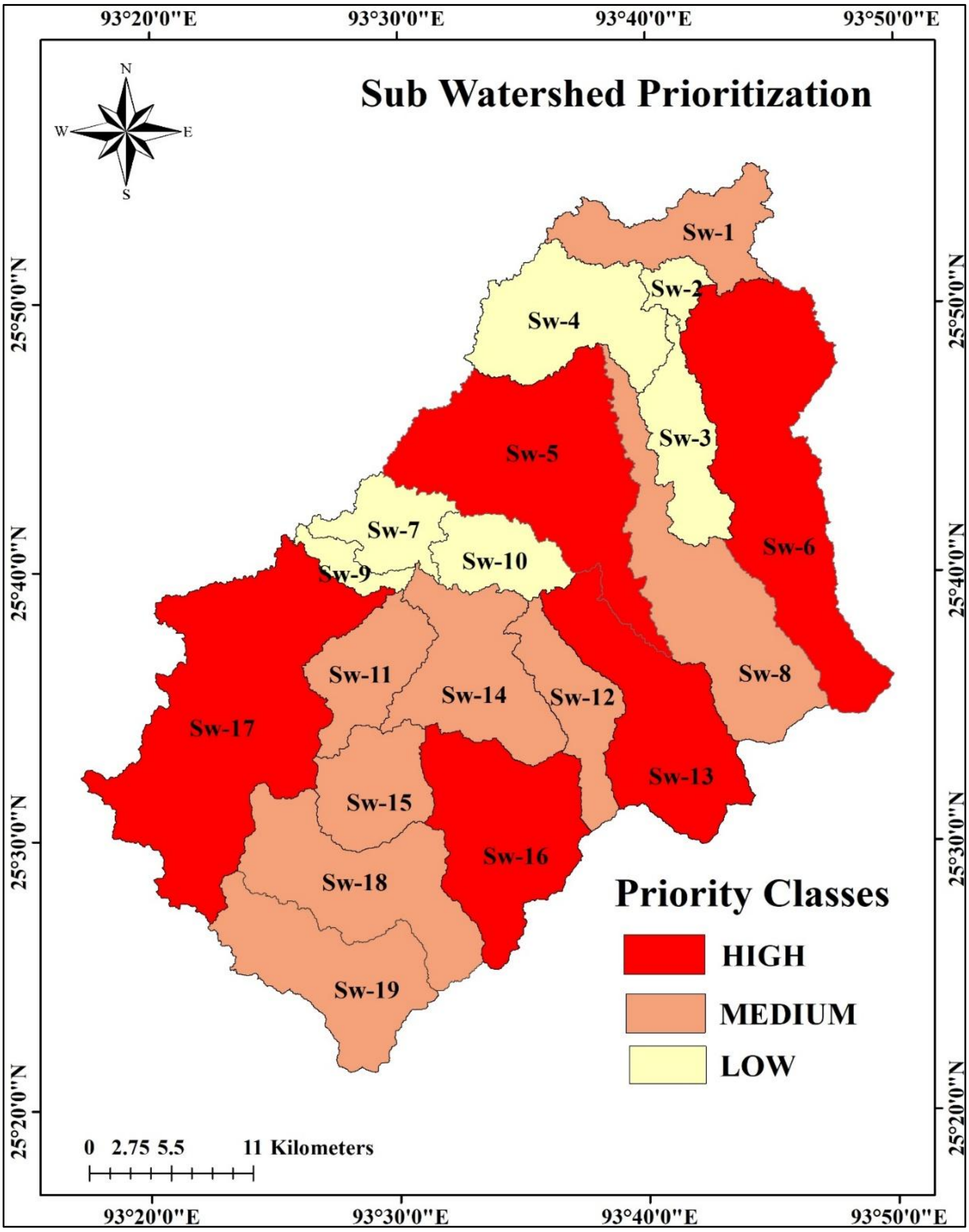

Figure 4.33: Dhansiri sub watershed priority class

4.5.3 Geomorphometric Characteristics of Khova Sub-Watershed

The morphometric and topohydrological characteristics of the Khova sub-watershed, which has been further divided into six sub-watersheds, are shown in **Table 4.30** and **Figure 4.34.** The stream frequency (F_s) ranges from 1.70×10^{-6} in Sw6 to 1.31×10^{-5} in Sw4, reflecting variations in drainage texture throughout the basin. Sub-watershed 4, with the highest Fs, indicates a more fragmented drainage network, whereas Sw6 demonstrates the least fragmentation. The bifurcation ratio (R_b) varies from 1.58 in Sw3 to 2.26 in Sw1, indicating that Sw1 demonstrates more irregular branching patterns, whilst Sw3 is somewhat more stable. The form factor (R_f) is highest in Sw2 (0.709), indicating a more circular watershed geometry, and minimal in Sw6 (0.180), implying an elongated shape and a delayed runoff response. The elongation ratio (R_e) varies from 0.478 in Sw6 to 0.950 in Sw2, further demonstrating differing forms and hydrological characteristics. The circularity ratio (R_c) is maximal in Sw4 (0.317) and minimal in Sw5 (0.156), indicating that Sw5 is elongated and has a less circular morphology. Drainage density (D) values vary from 0.00142 km/km² in Sw6 to 0.00554 km/km² in Sw4, indicating that Sw4 is significantly dissected with a strong runoff potential. The channel maintenance constant (C) is minimal in Sw4 (180.58) and maximal in Sw6 (706.21), corroborating Sw4's significant erosion vulnerability and Sw6's comparatively stable characteristics. The Topographic Wetness Index (TWI) exhibits minor variance among sub-watersheds, with values ranging from 9.39 in Sw2 to 10.09 in Sw5, whilst the Stream Power Index (SPI) spans from 5.99 in Sw5 to 6.80 in Sw6. The Sediment Transport Index (STI) is minimal in Sw5 (14.81) and maximal in Sw6 (18.70), indicating sediment transport potential.

4.5.3.1 Automated Sub-Watershed Prioritization

The correlation study (**Table 4.31, Figure 4.35**) demonstrates strong positive correlations between stream frequency (F_s) and drainage density (D) ($r = 0.96$), as well as between Fs and drainage texture (R_t) ($r = 0.97$), thus affirming that denser drainage networks correlate with increased stream frequency. A robust positive connection is present between form factor (R_f) and elongation ratio (R_e) ($r = 0.99$), indicating geometric interdependence. The compactness coefficient (C_c) has a robust negative association with the circularity ratio (R_c) ($r = –0.99$), suggesting that more compact sub-watersheds are generally less circular. The channel maintenance constant (C) has a negative correlation with Fs (r = –0.86) and D (r = –0.88), indicating that dissected sub-watersheds necessitate reduced channel maintenance while being more susceptible to erosion. SPI and STI exhibit a good correlation (r = 0.92), indicating their joint influence on erosion susceptibility.

4.5.3.2 Prioritization of Sub-Watersheds

Utilizing Weighted Sum Analysis (WSA), compound prioritization values (CPVs) were calculated for the Khova watershed (**Table 4.32**). The findings indicate that Sw6 (CPV = –95.89) is ranked first (**Figure 4.36**), followed by Sw3 (–58.34) and Sw2 (–51.15), identifying them as the most susceptible sub-watersheds for prompt management actions. In contrast, Sw4 (–23.51) has the highest CPV, placing it last and categorizing it as low-priority.

The sub-watersheds were classified into three categories (**Table 4.33; Figure 4.37**):

High Priority: Sw6, Sw3, Sw2

Medium Priority: Sw1, Sw5

Low Priority: Sw4

High-priority sub-watersheds necessitate immediate conservation actions, such as the construction of check dams, afforestation, and the establishment of vegetative barriers. Medium-priority sub-watersheds necessitate moderate interventions, like agroforestry and rainwater collection, whilst low-priority areas should be monitored to maintain their relative stability.

Table 4.30: Morphometric and topo-hydrological parameters of the Khova sub-watersheds

Sub-watershed code	Parameters											
	F_s	R_b	R_f	R_e	R_c	D	R_t	C_c	C	TWI	SPI	STI
Sw1	5.93E-06	2.26	0.266	0.582	0.21	0.00284	0.00326	2.18	352.63	10.07	6.02	16.12
Sw2	5.79E-06	1.9	0.709	0.95	0.3	0.00262	0.00313	1.82	382.36	9.39	6.69	18.57
Sw3	1.85E-06	1.58	0.287	0.604	0.258	0.00231	0.00126	1.97	432.88	9.8	6.24	17.63
Sw4	1.31E-05	2.15	0.38	0.696	0.317	0.00554	0.00481	1.78	180.58	10.05	6.44	17.54
Sw5	8.42E-06	2.25	0.327	0.646	0.156	0.00334	0.00329	2.53	298.97	10.09	5.99	14.81
Sw6	1.70E-06	2.18	0.18	0.478	0.182	0.00142	0.00132	2.34	706.21	9.67	6.8	18.7

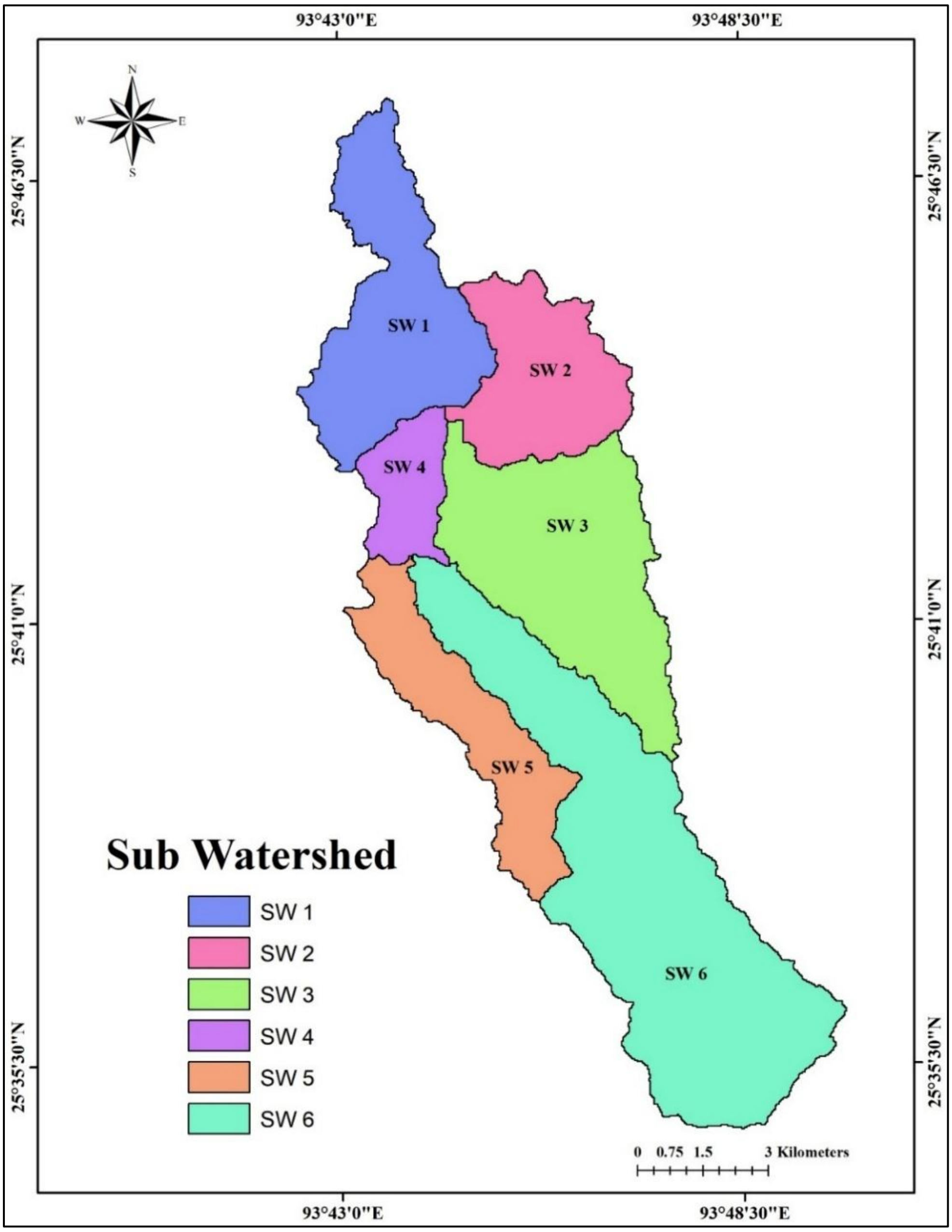

Figure 4.34: Sub watersheds of Khova

Table 4.31: Correlation of morphometric properties of the Khova sub-watersheds

	F_s	R_b	R_f	R_e	R_c	D	R_t	C_c	C	TWI	SPI	STI
F_s	1	0.45	0.27	0.34	0.36	0.96	0.97	-0.26	-0.86	0.51	-0.24	-0.37
R_b	0.45	1	-0.27	-0.27	-0.47	0.25	0.48	0.52	-0.11	0.5	-0.18	-0.45
R_f	0.27	-0.27	1	0.99	0.62	0.2	0.38	-0.57	-0.37	-0.57	0.29	0.26
R_e	0.34	-0.27	0.99	1	0.64	0.28	0.45	-0.58	-0.46	-0.49	0.21	0.19
R_c	0.36	-0.47	0.62	0.64	1	0.5	0.41	-0.99	-0.44	-0.32	0.36	0.54
D	0.96	0.25	0.2	0.28	0.5	1	0.9	-0.42	-0.88	0.54	-0.26	-0.29
R_t	0.97	0.48	0.38	0.45	0.41	0.9	1	-0.32	-0.86	0.43	-0.23	-0.34
C_c	-0.26	0.52	-0.57	-0.58	-0.99	-0.42	-0.32	1	0.37	0.35	-0.36	-0.58
C	-0.86	-0.11	-0.37	-0.46	-0.44	-0.88	-0.86	0.37	1	-0.52	0.54	0.51
TWI	0.51	0.5	-0.57	-0.49	-0.32	0.54	0.43	0.35	-0.52	1	-0.78	-0.79
SPI	-0.24	-0.18	0.29	0.21	0.36	-0.26	-0.23	-0.36	0.54	-0.78	1	0.92
STI	-0.37	-0.45	0.26	0.19	0.54	-0.29	-0.34	-0.58	0.51	-0.79	0.92	1

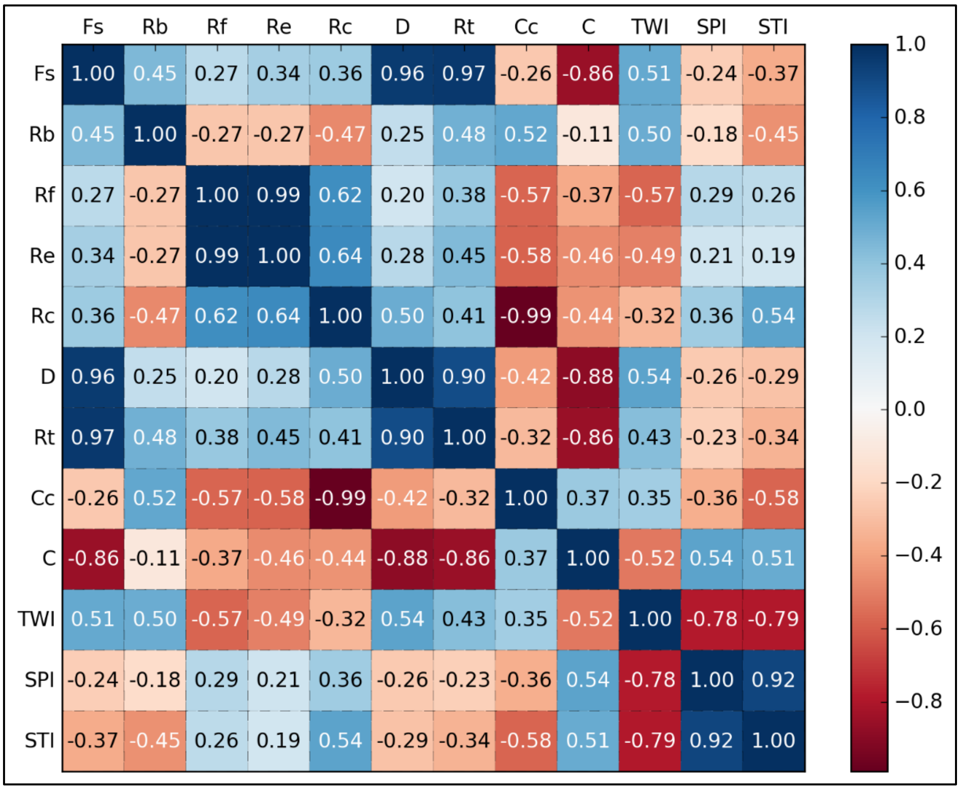

Figure 4.35: Correlation heatmap of geomorphometric and topo-hydrological parameters of the Khova sub-watersheds

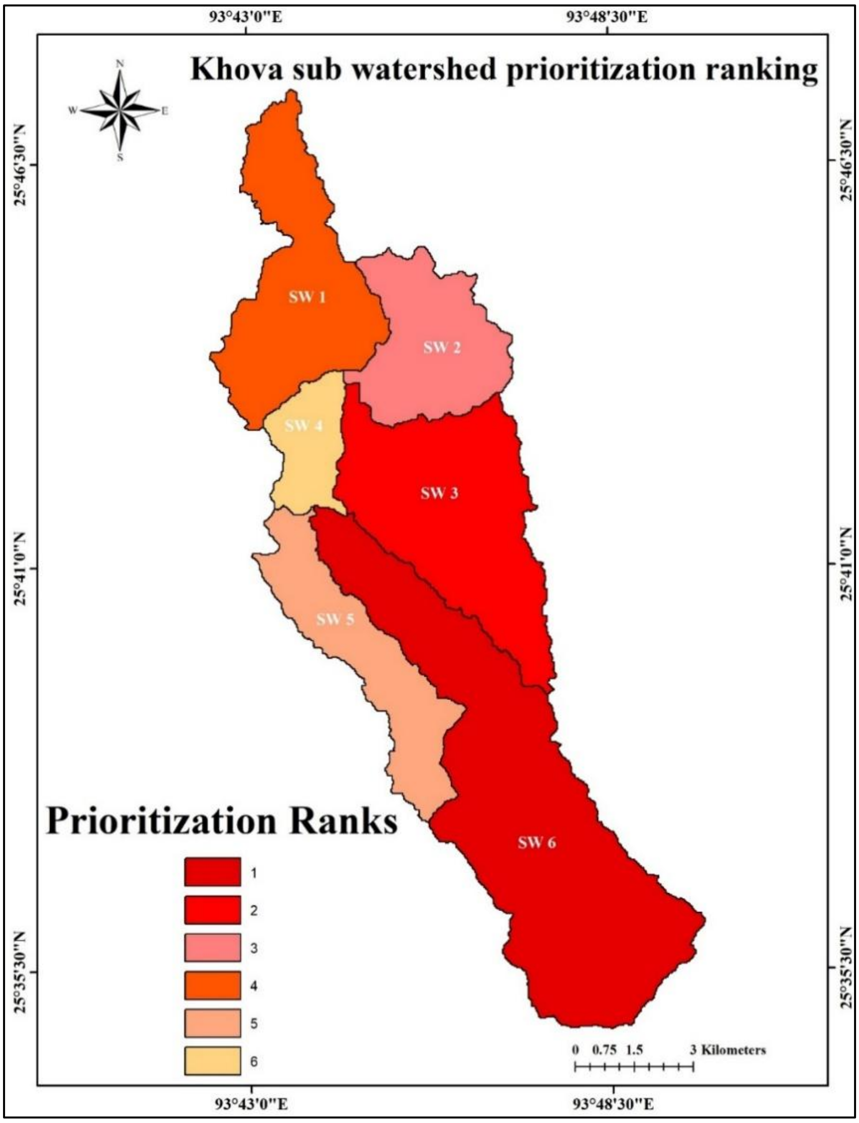

Figure 4.36: Khova sub watershed prioritization ranking

Table 4.32: Prioritization and final ranking of Khova sub-watersheds.

Name	Prioritization	Rank
Sw6	-95.8898	1
Sw3	-58.3427	2
Sw2	-51.1455	3
Sw1	-47.3569	4
Sw5	-40.0637	5
Sw4	-23.508	6

Table 4.33: Categorization of Khova sub-watersheds priority ranking

Priority type	Sub-watersheds	Percent of basin area
High Priority	Sw6, Sw3, Sw2	64.3
Medium Priority	Sw1,	18
Low Priority	Sw5, Sw4	17.7

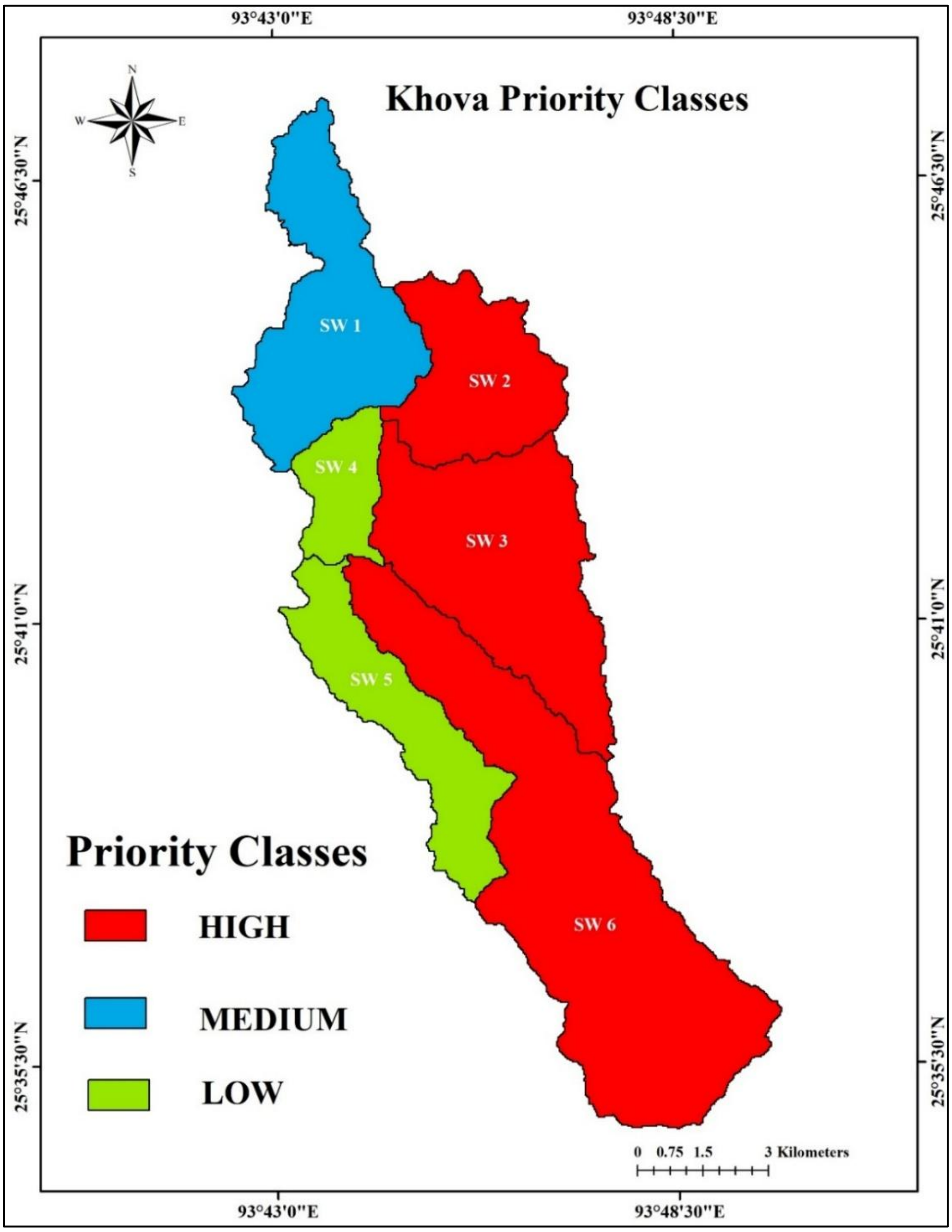

Figure 4.37: Khova sub watershed priority class

4.6 Climate Change Study

To extend the application of the calibrated SWAT model beyond present-day hydrological simulation, future climate projections were incorporated to assess potential changes in watershed hydrology. Climate data derived from selected global climate models under the SSP2-4.5 scenario were used as inputs to simulate future hydrological behaviour in the Dhansiri River basin. This approach allows the evaluation of how projected changes in precipitation and temperature may influence runoff generation processes and overall watershed response.

4.6.1 Justification for Scenario Selection

This study uses SSP2-4.5 from the Shared Socioeconomic Pathways (SSPs) under CMIP6 to assess future rainfall and runoff patterns in the study area. SSP2-4.5 represents a "middle-of-the-road" scenario, indicating moderate socioeconomic growth and the stabilization of radiative forcing at around 4.5 W/m² by 2100. This scenario is often seen as a baseline projection, falling between low-emission (SSP1-2.6) and high-emission (SSP5-8.5) pathways. Utilizing SSP2-4.5 helps the study focus on a practical, policy-relevant scenario that balances mitigation and adaptation assumptions, while also simplifying the analysis and reducing computational demands. The expected precipitation under this scenario was used as input for the SWAT model to predict future runoff patterns, linking climate changes with hydrological responses in the watershed. While excluding other SSPs limits exploration of extreme uncertainty, SSP2-4.5 provides a useful framework for examining the impact of climate change on rainfall variability and runoff generation in the region.

4.6.2 Selection of GCM Model

Five CMIP6 Global Climate Models (ACCESS-CM2, BCC-CSM2-MR, CanESM5, MPI-ESM1-2-HR, and MRI-ESM2-0) were assessed for the Dhansiri river basin. Historical daily precipitation from each GCM was compared with IMD gridded rainfall for the baseline period 2014–2021 using three standard indicators: the coefficient of determination (R^2), Nash–Sutcliffe Efficiency (NSE), and Kling–Gupta Efficiency (KGE). The model-wise indicator values and the resulting ranks are summarised in **Table 4.34**.

Because R^2, NSE, and KGE operate on different scales, all indicator values were first normalised (Equation 3.38). We then applied the entropy weight method to obtain objective indicator weights. As shown in **Table 4.34**, the derived weights assign the highest importance to NSE (0.385), with KGE (0.309) and R^2 (0.307) contributing comparably.

After normalisation and weighting, the aggregate weighted-sum scores (**Table 4.35**) rank the models as follows: CanESM5 (−0.213; Rank 1) ≥ MRI-ESM2-0 (−0.420; Rank 2) > ACCESS-CM2 (−0.620; Rank 3) > MPI-ESM1-2-HR (−0.625; Rank 4) > BCC-CSM2-MR (−0.650; Rank 5). *Note:* because some raw performance values (e.g., NSE) are negative, the weighted sums can be negative; the relative magnitude of the weighted sum—not its sign—determines the ranking.

Consistent with these results, CanESM5 and MRI-ESM2-0 were selected as the two best-performing GCMs for subsequent bias correction and SWAT-based hydrologic simulations. This ensures that future scenario analysis is grounded in models that exhibit the strongest statistical fidelity to IMD observations for the Dhansiri river basin (and are consistent across its sub-basins).

Table 4.34: Entropy weight of various performance indicators

Sl. No.	Performance index	Entropy weight
1	R^2	0.307
2	NSE	0.385
3	KGE	0.309

Table 4.35: Performance indicator and rank of various GCMs

Model	R^2	NSE	KGE	Weighted sum	Rank subbasin
ACCESS-CM2	0.051	-1.606	-0.056	-0.62	3
BCC-CSM2-MR	0.033	-1.684	-0.038	-0.65	5
CanESM5	0.039	-0.685	0.124	-0.213	1
MPI-ESM1-2-HR	0.02	-1.61	-0.037	-0.625	4
MRI-ESM2-0	0.047	-1.183	0.069	-0.42	2

Among the five CMIP6 models evaluated, CanESM5 and MRI-ESM2-0 ranked highest based on R^2, NSE, KGE, and entropy-weighted performance analysis. This indicates that these models reproduced the historical rainfall pattern of the Dhansiri river basin better than the other tested GCMs. The use of multiple statistical indicators improves confidence in model selection because each metric evaluates different aspects of performance, such as correlation, bias, and variability.

The need for bias correction was clearly evident, as raw GCM rainfall generally overestimated observed rainfall. After correction, the mean rainfall values became much closer to IMD observations, demonstrating the importance of bias adjustment before hydrological impact studies. Similar conclusions have been reported in previous climate impact assessments, where uncorrected GCM outputs often contain systematic bias at the watershed scale. Therefore, the use of corrected CanESM5 and MRI-ESM2-0 data strengthens the reliability of future runoff projections in the present study.

4.6.3 CanESM5 and MRI-ESM2-0 Scenario Rainfall under SSP 2-4.5

Using the bias-corrected SSP2-4.5 projections, annual rainfall for the Dhansiri watershed was derived for the period 2030–2040 for the two selected GCMs (CanESM5 and MRI-ESM2-0). **Figure 4.38** shows the interannual variability for both models. Over this decade, MRI-ESM2-0 exhibits higher variability than CanESM5, with pronounced peaks in 2030 and 2034, whereas CanESM5 peaks in 2039. A relative dip appears around 2035–2036 in both series, indicating a coherent signal across models.

Decadal summary (2030–2040):

- CanESM5: mean ≈ 4.85, SD ≈ 0.57; min ≈ 4.33 (2035), max ≈ 6.38 (2039).
- MRI-ESM2-0: mean ≈ 5.08 (mm), SD ≈ 1.04; min ≈ 3.36 (2035), max ≈ 6.60 (2030).

Both CanESM5 and MRI-ESM2-0 indicate substantial interannual variability under SSP2-4.5, with MRI-ESM2-0 showing a larger spread (SD ≈ 1.04) than CanESM5 (SD ≈ 0.57). The timing of local minima (2035–2036) is consistent across models, while the amplitude of wet years is higher in MRI-ESM2-0 (2030, 2034). These differences underscore the merit of carrying both models forward into hydrological scenario analysis.

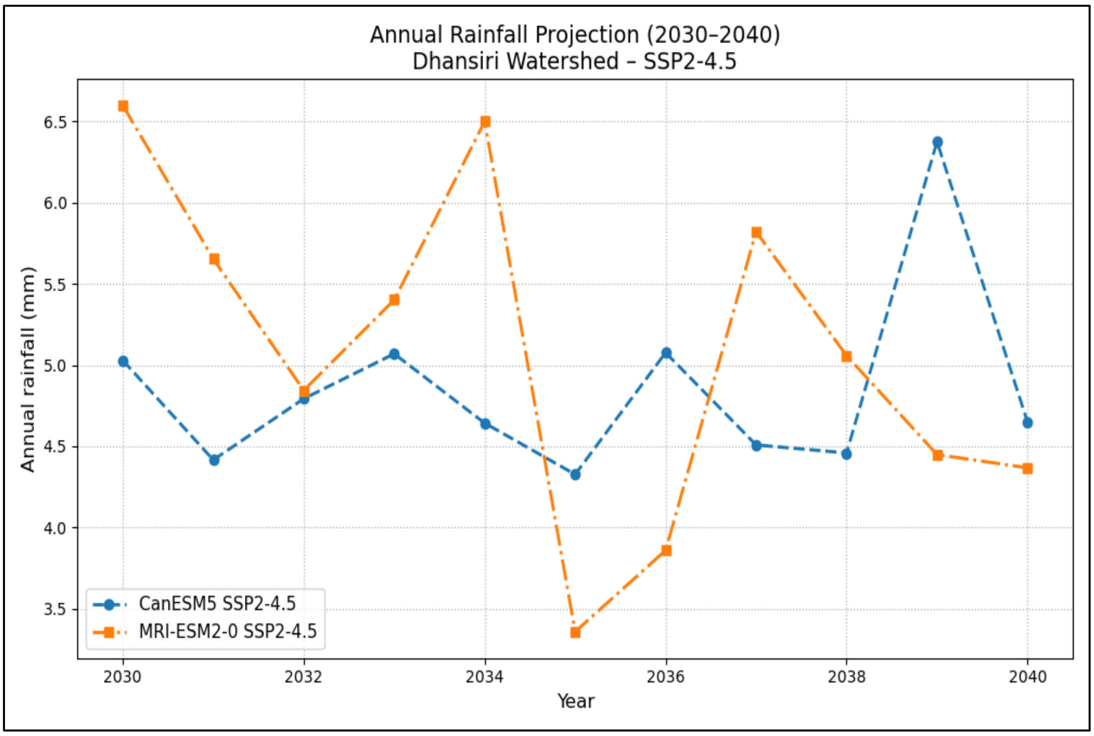

Figure 4.38: CanESM5 and MRI-ESM2-0 scenarios for rainfall

4.6.4 Validation against IMD (2014–2021)

Before employing the bias-corrected SSP2-4.5 series for projection, the historical overlap between IMD observations and the two selected GCMs was evaluated for 2014–2021. **Figures 4.39** and **4.40** present the comparison of IMD annual rainfall with the raw and bias-corrected series of CanESM5 and MRI-ESM2-0, respectively. The raw GCM outputs clearly overestimate rainfall relative to IMD, with CanESM5 recording a mean of ~5.3 compared to 3.8 for IMD, and MRI-ESM2-0 showing an even larger deviation (~5.8 vs 3.8). After applying linear scaling, the corrected GCM series aligned much more closely with IMD, reducing systematic bias while preserving interannual variability. **Table 4.36** summarises the bias factors and performance statistics (R^2, NSE, and KGE) for the raw and corrected series. For CanESM5, the mean rainfall decreased from 5.33 to ~3.98, closely matching the IMD mean (3.81), while MRI-ESM2-0 reduced from 5.84 to ~3.99. Although R^2 values remain low and NSE remains negative due to the short overlap period, KGE values show improvement, particularly for MRI-ESM2-0 (0.25 → 0.34), indicating a more realistic representation of observed variability after correction.

This validation step confirms that bias correction was essential and effective. By scaling the GCM series to the IMD climatology, systematic deviations were removed, and the corrected series provides a consistent foundation for future projections. Consequently, the scenario analysis presented earlier builds upon validated, bias-adjusted model outputs, ensuring a more credible assessment of climate impacts on the Dhansiri river basin.

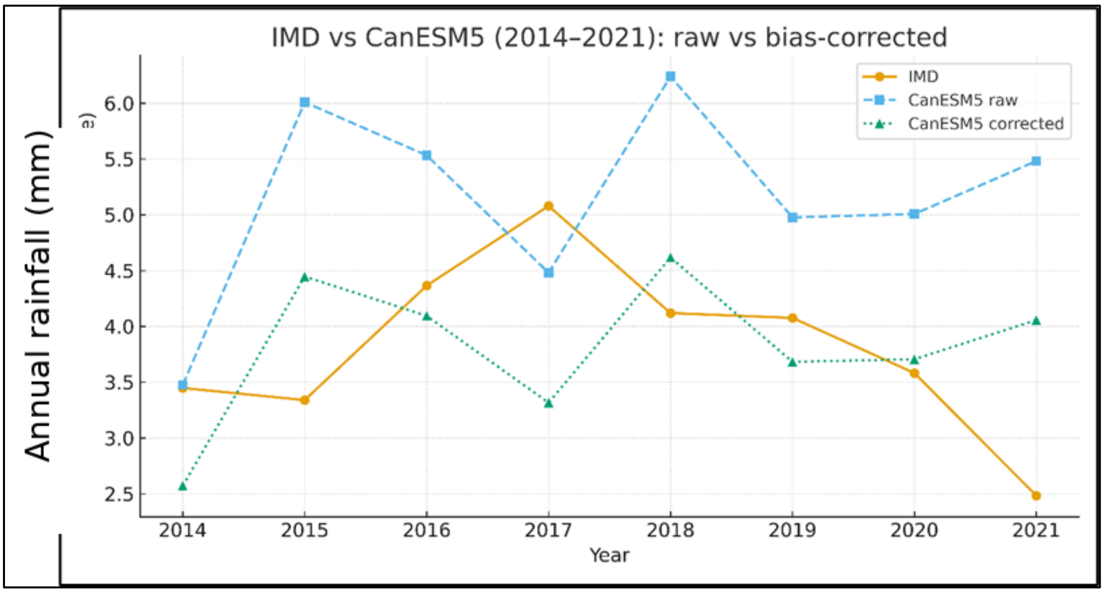

Figure 4.39: IMD vs CanESM5 (raw & corrected) validation.

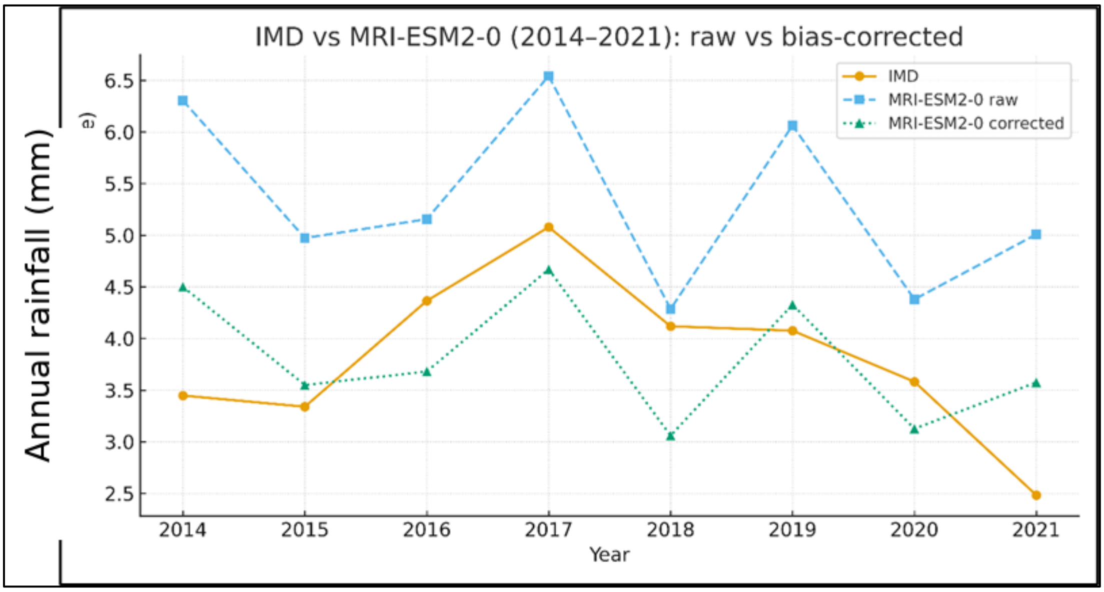

Figure 4.40: IMD vs MRI-ESM2-0 (raw & corrected) validation.

4.6.5 Future Streamflow Changes under SSP2-4.5 (CanESM5 vs MRI-ESM2-0).

Bias-corrected precipitation from two CMIP6 GCMs (CanESM5 and MRI-ESM2-0) was routed through the SWAT model for the future period 2032–2040. The projected monthly streamflow climatology (**Figure 4.41**) indicates that both scenarios maintain a monsoon-dominated hydrological regime in the Dhansiri river basin. However, MRI-ESM2-0 produced earlier and higher streamflow peaks during the JJAS season, with maximum discharge occurring in July–August, suggesting greater flood potential. In contrast, CanESM5 generated relatively lower monsoon peaks but higher flows during the post-monsoon and winter months, indicating stronger subsurface water contributions and delayed flow release.

The annual mean streamflow series for 2032–2040 (**Figure 4.42**) further demonstrates inter-model variability in projected runoff. MRI-ESM2-0 generally showed higher annual discharge during the early part of the decade (2034–2035), whereas CanESM5 exhibited comparatively higher flows in later years, particularly in 2039–2040. These differences highlight uncertainty among climate models and justify presenting the two projections separately rather than combining them into a single estimate. Nevertheless, both scenarios indicate substantially higher future flows compared with the historical baseline, implying increased hydrological sensitivity under climate change conditions.

To better understand the causes of these streamflow differences, SWAT water-balance diagnostics were analysed. Under the CanESM5 scenario (**Figure 4.43**), the projected mean annual precipitation was 1,793 mm, of which 497 mm was lost through evapotranspiration, 68.5 mm became surface runoff, 130.8 mm contributed as lateral flow, and 902.8 mm appeared as return flow (baseflow). Percolation to the shallow aquifer reached 1,099 mm, while 196 mm recharged the deep aquifer. The average curve number was 59.8, indicating relatively high infiltration capacity and lower runoff generation. These results suggest that a large portion of rainfall infiltrates into the soil and subsequently sustains streamflow through groundwater pathways.

Under the MRI-ESM2-0 scenario (**Figure 4.44**), annual precipitation increased to 1,869 mm, while PET and ET also increased to 1,136 mm and 557 mm, respectively. Surface runoff rose sharply to 284.3 mm, which was nearly four times higher than that of CanESM5, whereas lateral flow declined slightly to 115.1 mm. Return flow decreased to 748.8 mm, percolation reduced to 912 mm, and deep recharge declined to 162.7 mm. The higher average curve number (67.6) indicates greater runoff potential and reduced infiltration under this scenario. As a result, more rainfall was converted into quickflow, producing the larger monsoon peaks observed earlier in **Figure 4.41**.

The contrasting diagnostics reveal substantial differences in the partitioning of future water balance components. MRI-ESM2-0 represents a runoff-dominated future with flashier hydrographs, higher flood risk, and reduced groundwater recharge, whereas CanESM5 represents an infiltration-dominated future where greater percolation and baseflow help sustain dry-season flows. Although both scenarios produced a similar Streamflow/Precipitation ratio (~0.61), the hydrological pathways differed markedly (**Figures 4.43 and 4.44**). Therefore, climate change is expected to alter not only the quantity of streamflow but also the internal runoff-generation mechanisms of the hilly Dhansiri river basin.

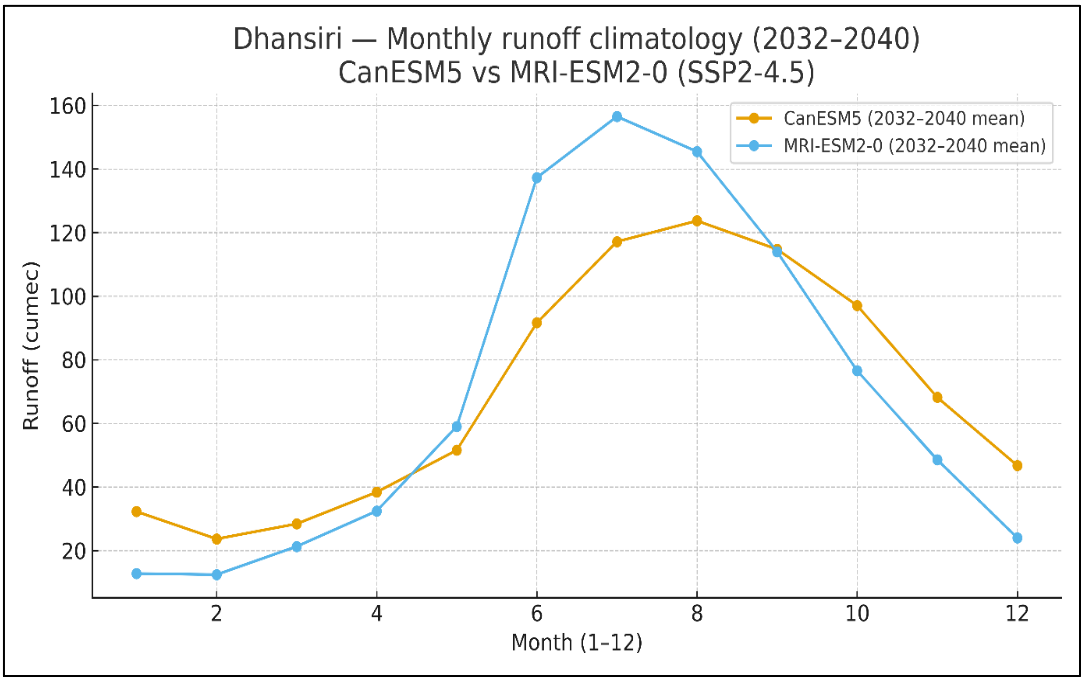

Figure 4.41: Monthly streamflow climatology (cumec), 2032–2040 under SSP2-4.5 for CanESM5 and MRI-ESM2-0. MRI-ESM2-0 peaks in July–August and exceeds CanESM5 during JJAS; CanESM5 is higher in the post-monsoon/winter months.

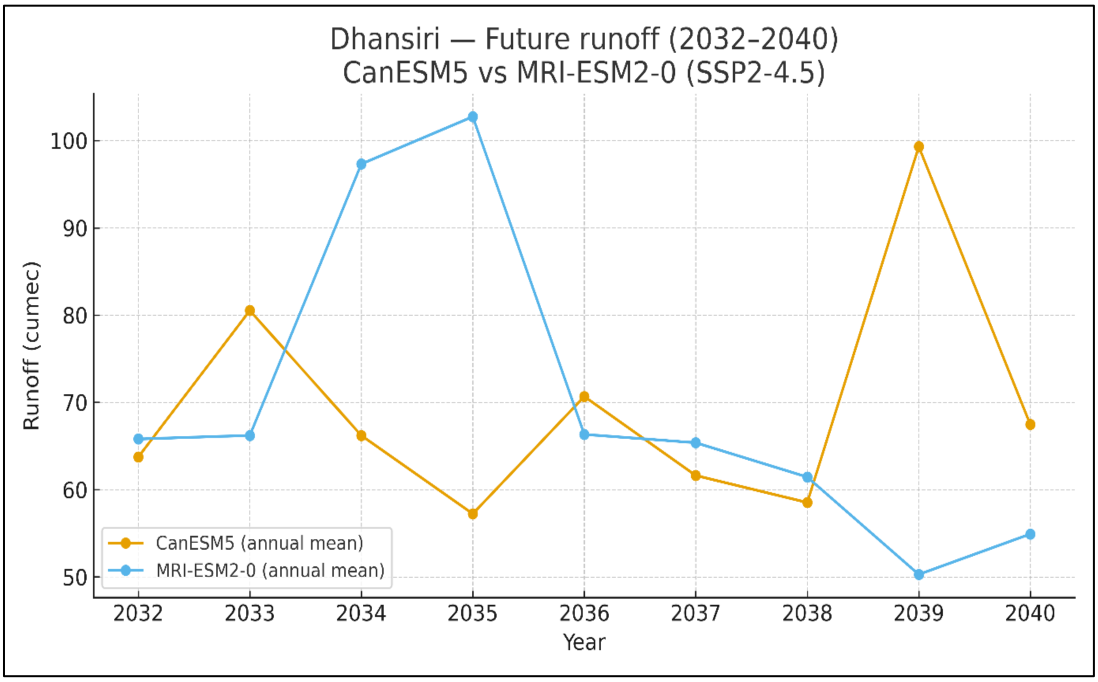

Figure 4.42: Annual mean streamflow (cumec), 2032–2040 for the two GCMs. Differences illustrate inter-model uncertainty; both indicate much larger flows than the historical baseline.

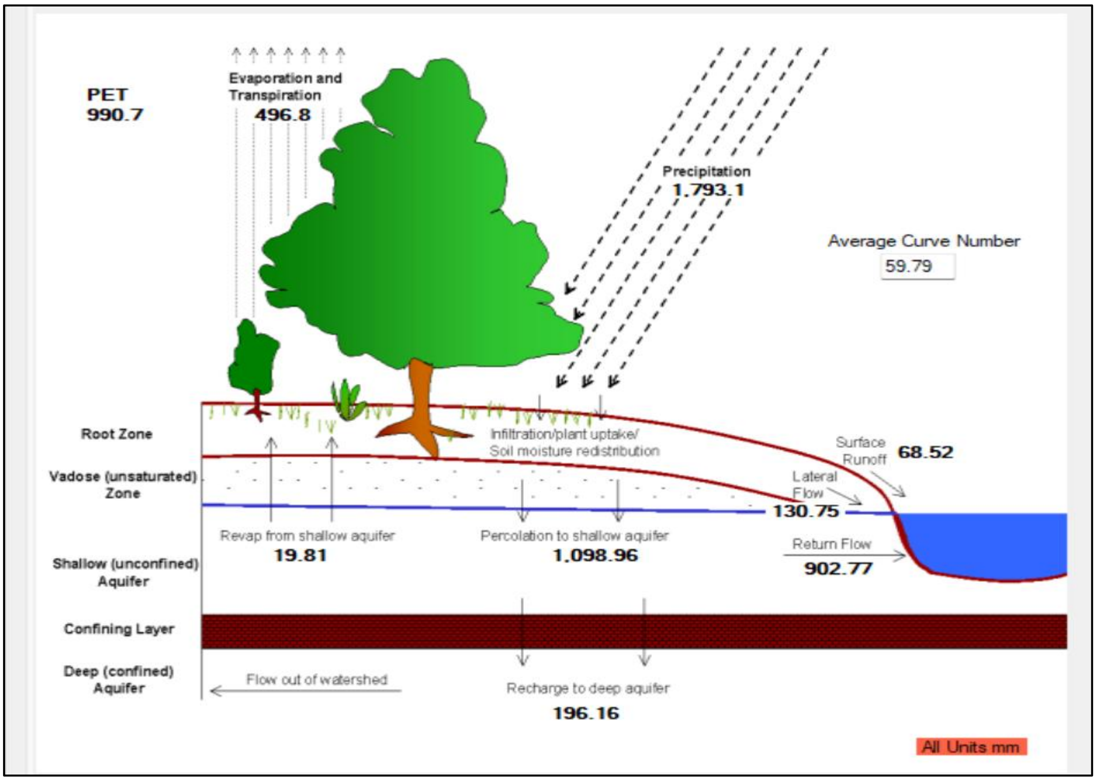

Figure 4.43: CanESM5: SWAT water-balance summary (2032–2040 mean).

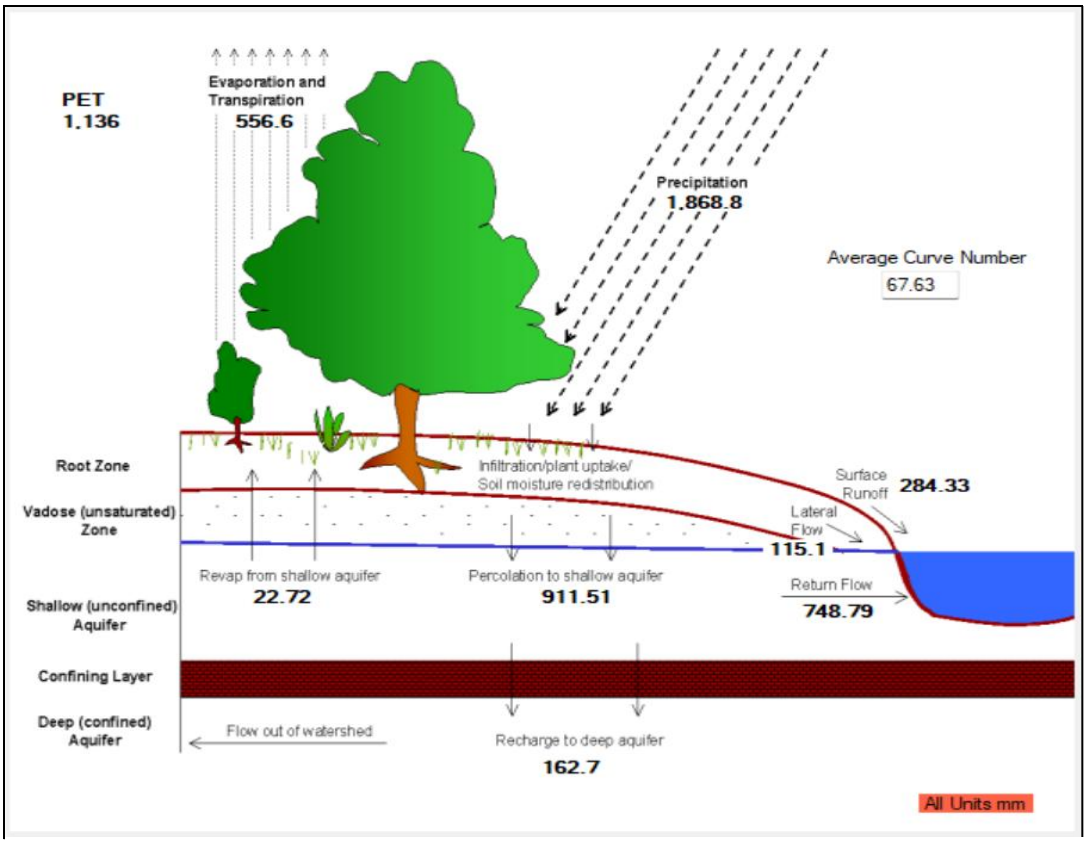

Figure 4.44: MRI-ESM2-0: SWAT water-balance summary (2032–2040 mean)

Table 4.36: Bias correction factors and performance statistics (2014–2021) for CanESM5 and MRI-ESM2-0 compared with IMD annual rainfall

Model	Bias factor (k)	Mean IMD	Mean GCM (raw)	Mean GCM (corrected)	R^2 (raw)	NSE (raw)	KGE (raw)	R^2 (corrected)	NSE (corrected)	KGE (corrected)
CanESM5	0.74	3.81	5.15	3.81	0.013	-4.923	-0.176	0.013	-0.898	-0.125
MRI-ESM2-0	0.71	3.81	5.34	3.81	0.142	-4.786	0.251	0.142	-0.029	0.342

The two selected CMIP6 climate models, CanESM5 and MRI-ESM2-0, represent contrasting but complementary simulations of monsoon dynamics over Northeast India. Rainfall in this region is strongly influenced by the Indian summer monsoon and complex orographic interactions along the eastern Himalayas and the Indo–Myanmar ranges, which global climate models often struggle to reproduce accurately. Previous evaluations of CMIP6 models have reported considerable variability in the simulation of monsoon rainfall intensity and seasonal distribution across South Asia (Krishnan *et al.,* 2020; Almazroui *et al.,* 2021). In the present study, MRI-ESM2-0 tends to simulate higher-intensity rainfall events during the peak monsoon months (July–August), which in turn produce greater surface runoff and sharper streamflow peaks in the SWAT simulations. This pattern suggests a stronger representation of convective rainfall extremes, resulting in a more rapid hydrological response during the monsoon period. Similar tendencies of certain CMIP6 models to intensify extreme precipitation over the Indian monsoon region have also been reported in previous studies (Mishra *et al.*, 2020; Gusain *et al.*, 2021). In contrast, CanESM5 produces more evenly distributed seasonal precipitation, leading to comparatively lower surface runoff but higher infiltration, groundwater recharge, and sustained baseflow during the post-monsoon and winter periods.

The future simulations under SSP2-4.5 suggest that climate change may significantly alter the hydrological behaviour of the Dhansiri river basin. Although both models produced similar streamflow-to-precipitation ratios, the pathways of runoff generation differed markedly. Notably, MRI-ESM2-0 predicted approximately 284 mm of surface runoff, nearly four times higher than the ~69 mm simulated under CanESM5, indicating a substantially stronger runoff response. Such a large difference highlights the sensitivity of the basin to rainfall intensity and suggests that more intense monsoon events may trigger rapid rainfall–runoff conversion.

These differences are particularly important in hilly watersheds, where steep slopes and intense rainfall can quickly translate precipitation into surface runoff, increasing the likelihood of flash floods, channel erosion, and sediment transport. Conversely, greater infiltration and groundwater recharge may enhance subsurface storage and sustain baseflow during the post-monsoon and winter seasons.

The projected increase in evapotranspiration under future climate scenarios also indicates stronger atmospheric water demand. Higher evapotranspiration may reduce effective soil moisture and influence vegetation and agricultural water availability during dry periods.

CHAPTER 5
SUMMARY AND CONCLUSIONS

5.1 Summary

The present research was undertaken to evaluate the morphometric, hydrological, and management characteristics of three hilly watersheds of Nagaland, Dzuza, Dhansiri, and Khova, using an integrated Geographic Information System (GIS) and the Soil and Water Assessment Tool (SWAT). The analysis also incorporated sensitivity assessment of model parameters, watershed prioritization, and climate projections (2032–2040) using bias-corrected CMIP6 GCMs. The results provide a comprehensive insight into watershed behavior and its implications for effective planning and management.

5.1.1 Morphometric analysis

1. Morphometric evaluation revealed dendritic drainage patterns in all watersheds, reflecting homogeneous lithology and minimal structural disturbance (Soni, 2017; Kichu *et al.,* 2022).

2. Relief ratio and ruggedness number were higher in Dzuza and Khova, indicating steeper slopes, rapid runoff, and higher erosion susceptibility, while Dhansiri displayed moderate relief and relatively stable hydrological conditions.

3. Basin form parameters, such as elongation ratio and circularity ratio, classified the watersheds as elongated, which reduces flood peaks but increases erosion over longer flow paths.

4. Drainage density values varied from coarse to moderate, suggesting differences in infiltration potential and runoff response.

5.1.2 Rainfall runoff modelling using SWAT

1. SWAT simulations (2012–2021) provided satisfactory calibration and validation, with Nash–Sutcliffe Efficiency (NSE) values ranging from 0.70 to 0.87

and R^2 values above 0.75 in most cases, confirming the reliability of the model in hilly catchments (Arnold *et al.,* 2012; Malik *et al.,* 2022).

2. Water balance analysis indicated that 59–60% of precipitation contributed to streamflow, with baseflow accounting for nearly two-thirds of discharge, underscoring the dominance of subsurface contributions in sustaining dry-season flows.

3. Among the three, Dhansiri performed best statistically, Dzuza showed strong calibration but weaker validation, and Khova achieved satisfactory fits despite its smaller size and rugged topography.

5.1.3 Sensitivity analysis of calibration parameters

1. Global sensitivity analysis using SWAT-CUP (SUFI-2) identified curve number (CN2), soil hydraulic conductivity (SOL_K), and groundwater parameters (GWQMN, GW_DELAY) as the most influential factors governing runoff generation and baseflow.

2. Dzuza was primarily influenced by infiltration and channel conductivity, Dhansiri by shallow aquifer exchange processes, and Khova by channel storage and roughness.

3. These findings are consistent with previous SWAT-based sensitivity studies in Himalayan and tropical watersheds (Abbaspour *et al.,* 2004; Kushwaha and Jain, 2013; Hosseini and Khaleghi, 2020).

5.1.4 Watershed prioritization

1. Sub-watershed prioritization using morphometric and hydrological indices revealed significant variability in erosion susceptibility.

2. In Dzuza, sub-watersheds SW1 and SW2 were ranked as high-priority zones, demanding immediate soil conservation. In Dhansiri, SW2 and SW4 were most critical, while in Khova, select sub-basins also exhibited elevated erosion risk.

3. The classification into high, medium, and low priority classes provides a practical framework for allocating resources and designing location-specific management measures.

5.1.5 Climate projections (2030-2040)

1. Climate change assessment using bias-corrected CMIP6 GCMs (CanESM**5** and MRI-ESM2-0) routed through SWAT highlighted divergent yet plausible hydrological futures for the watershed.

2. MRI-ESM2-0 projected earlier and sharper JJAS peaks, indicating higher flood potential and flash runoff risk. The model estimated about 284 mm of surface runoff, nearly four times the ~69 mm projected by CanESM5 for the same period. This substantial difference in simulated runoff magnitude highlights the potential for rapid hydrological responses within the watershed and strongly supports the flash flood risk warning in the study's recommendations.

3. CanESM5 projected lower monsoon peaks but enhanced post-monsoon and winter flows, suggesting comparatively higher subsurface recharge potential and a more gradual hydrological response.

4. The spread between GCM outputs reflects inherent climate model uncertainty but emphasizes the need for adaptive watershed management strategies that consider both flood mitigation and groundwater sustainability (Jha *et al.*, 2006; Gosain *et al.*, 2006).

5.2 Conclusions

From this integrated analysis, several key conclusions can be drawn:

1. Morphometric analysis confirmed that basin form and relief strongly influence runoff generation and erosion risk in Nagaland's hilly watersheds.

2. SWAT modeling successfully simulated rainfall–runoff dynamics, with baseflow emerging as a dominant contributor to streamflow, critical for sustaining water availability during lean periods.

3. Sensitivity analysis identified CN2, SOL_K, and groundwater parameters as the most critical for model calibration, enhancing confidence in future scenario simulations.

4. Watershed prioritization provided actionable rankings of sub-watersheds, enabling efficient targeting of soil and water conservation measures.

5. Climate projections revealed uncertainty but also important contrasts: while some futures imply increased flood potential, others indicate enhanced groundwater recharge, underlining the importance of adaptive and flexible watershed management strategies.

Overall, this research demonstrates that integrating GIS, SWAT, and climate models offers a powerful decision-support framework for planning and management of hilly watersheds in Nagaland.

5.3 Recommendations and Future Work

Based on the findings, the following recommendations are proposed:

1. Targeted soil and water conservation: High-priority sub-watersheds should be targeted with check dams, contour bunding, afforestation, and vegetative barriers to reduce erosion and enhance infiltration.

2. Flood and drought management: Given the projected variability in monsoon flows, adaptive strategies such as rainwater harvesting, small reservoirs, and floodplain zoning should be adopted.

3. Groundwater recharge enhancement: Sub-basins with higher post-monsoon baseflow potential should be managed to increase groundwater storage through recharge pits and infiltration trenches.

4. Integration of climate projections in policy: Planning agencies should incorporate multi-model climate projections in watershed development programs to account for future hydrological uncertainty.

5. Community participation: Since land use practices such as shifting cultivation directly influence erosion, involving local communities in conservation planning is crucial.

6. Continuous monitoring: Expansion of hydrological and climatic monitoring networks in Nagaland is recommended to refine model calibration and improve the reliability of long-term projections.

Future research directions

- Incorporating high-resolution climate models and land use change scenarios to refine hydrological projections.
- Extending the modeling framework to sediment yield and water quality for comprehensive watershed assessments.
- Applying machine learning techniques for sub-watershed prioritization and climate scenario downscaling.
- Evaluating the socio-economic impacts of watershed interventions to design holistic and people-centered management strategies.

REFERENCES

Abbaspour, K. C. (2015). SWAT calibration and uncertainty programs. *A user manual*, *103*, 17–66.

Abbaspour, K. C., Johnson, C. A., & Van Genuchten, M. T. (2004). Estimating uncertain flow and transport parameters using a sequential uncertainty fitting procedure. *Vadose zone journal*, *3*(4), 1340–1352.

Abbaspour, K. C., Rouholahnejad, E., Saeid, A. V., Srinivasan, R., Yang, H., & Kløve, B. (2015). A continental-scale hydrology and water quality model for Europe: Calibration and uncertainty of a high-resolution large-scale SWAT model. *Journal of hydrology*, *524*, 733–752.

Abbaspour, K. C., Yang, J., Maximov, I., Siber, R., Bogner, K., Mieleitner, J., ... & Srinivasan, R. (2007). Modelling hydrology and water quality in the pre-alpine/alpine Thur watershed using SWAT. *Journal of hydrology*, *333*(2-4), 413–430.

Abdulkareem, J. H., Pradhan, B., Sulaiman, W. N. A. & Jamil, N. R. (2018) Quantification of runoff as influenced by morphometric characteristics in a rural complex catchment, Earth Syst. Environ., 2 (1), 145–162.

Adham, M. I., Jahan, C. S., Mazumder, Q. H., Hossain, M. M. A., & Haque, A. M. (2010). Study on groundwater recharge potentiality of Barind Tract, Rajshahi District, Bangladesh using GIS and remote sensing technique. *Journal of the Geological Society of India*, *75*(2), 432–438.

Agarwal, R., Garg, P. K., & Garg, R. D. (2013). Remote sensing and GIS based approach for identification of artificial recharge sites. *Water resources management*, *27*(7), 2671–2689.

Agrawal, N., Verma, M. K., & Tripathi, M. P. (2009). Effective Management of Critical Sub-watersheds Using SWAT Model, Remote Sensing and GIS. *Agricultural Engineering Today, 33*(4), 15–20.

Agrawal, N., Verma, M. K., & Tripathi, M. P. (2011). Hydrological modelling of chhokranala watershed using weather generator with SWAT model. *Indian Journal of Soil Conservation*, *39*(2), 89–94.

Aher, P. D., Adinarayana, J. & Gorantiwar, S. D. (2014) Quantification of morphometric characterization and prioritization for management planning in semi-arid tropics of India: a remote sensing and GIS approach, J. Hydrol., 511, 850–860.

Aherwar, P., & Aherwar, H. (2018). Rainfall runoff simulation by using SCS-CN model in Shipra river basin of Madhya Pradesh, India, India. *Journal of Pharmacognosy and Phytochemistry*, *7*(12), 385–390.

Aherwar, P., & Aherwar, H. (2019). Comparison of rainfall runoff simulation by SCS-CN and NAM model in Shipra river basin of Madhya Pradesh, India. *Journal of Pharmacognosy and Phytochemistry*, *8*(4), 3419–3427.

Ahirwar, R., Malik, M. S., & Shukla, J. P. (2019). Prioritization of sub-watersheds for soil and water conservation in parts of Narmada River through morphometric analysis using remote sensing and GIS. *Journal of the Geological Society of India*, *94*(5), 515–524.

Almazroui, M., Saeed, S., Saeed, F., Islam, M. N., Ismail, M., Klutse, N. A. B., & Siddiqui, M. H. (2021). Assessment of CMIP6 climate models in simulating the Indian summer monsoon. *Atmospheric Research*, 248, 105200.

Aloui, S., Mazzoni, A., Elomri, A., Aouissi, J., Boufekane, A., & Zghibi, A. (2023). A review of Soil and Water Assessment Tool (SWAT) studies of Mediterranean catchments: Applications, feasibility, and future directions. *Journal of Environmental Management*, *326*, 116799.

Amatya, D. M., Williams, T. M., Edwards, A. E., Levine, N. S., & Hitchcock, D. R. (2008). Application of SWAT hydrologic model for TMDL development on Chapel Branch Creek watershed, SC.

American Society of Civil Engineers (1993). Task Committee on Definition of Criteria for Evaluation of Watershed Models of the Watershed Management Committee, Irrigation and Drainage Division. (1993). Criteria for evaluation of watershed models. *Journal of Irrigation and Drainage Engineering*, *119*(3), 429–442.

Arefin, R., Mohir, M. M. I., & Alam, J. (2020). Watershed prioritization for soil and water conservation aspect using GIS and remote sensing: PCA-based approach at northern elevated tract Bangladesh. *Applied Water Science*, *10*, 1–19.

Arnold, J. G., & Fohrer, N. (2005). SWAT2000: current capabilities and research opportunities in applied watershed modelling. *Hydrological Processes: An International Journal*, *19*(3), 563–572.

Arnold, J. G., Allen, P. M., & Bernhardt, G. (1993). A comprehensive surface-groundwater flow model. *Journal of hydrology*, *142*(1-4), 47–69.

Arnold, J. G., Moriasi, D. N., Gassman, P. W., Abbaspour, K. C., White, M. J., Srinivasan, R., ... & Jha, M. K. (2012). SWAT: Model use, calibration, and validation. *Transactions of the ASABE*, *55*(4), 1491–1508.

Arnold, J. G., Srinivasan, R., Muttiah, R. S., & Williams, J. R. (1998). Large area hydrologic modeling and assessment part I: model development 1. *JAWRA Journal of the American Water Resources Association*, *34*(1), 73–89.

Asres, M. T., & Awulachew, S. B. (2010). SWAT based runoff and sediment yield modelling: a case study of the Gumera watershed in the Blue Nile basin. *Ecohydrology & Hydrobiology*, *10*(2-4), 191–199.

Baker, T. J., & Miller, S. N. (2013). Using the Soil and Water Assessment Tool (SWAT) to assess land use impact on water resources in an East African watershed. *Journal of hydrology*, *486*, 100–111.

Bali, R., Agarwal, K. K., Nawaz Ali, S., Rastogi, S. K., & Krishna, K. (2012). Drainage morphometry of Himalayan Glacio-fluvial basin, India: hydrologic and neotectonic implications. *Environmental Earth Sciences*, *66*(4), 1163–1174.

Bates, B. C., & Campbell, E. P. (2001). A Markov chain Monte Carlo scheme for parameter estimation and inference in conceptual rainfall-runoff modeling. *Water resources research*, *37*(4), 937–947.

Bennour, A., Jia, L., Menenti, M., Zheng, C., Zeng, Y., Asenso Barnieh, B., & Jiang, M. (2022). Calibration and validation of SWAT model by using hydrological remote sensing observables in the Lake Chad Basin. *Remote Sensing*, *14*(6), 1511.

Beran, M., & Rodier, J. A. (1985). Hydrological aspects of drought. Studies and reports in hydrology 39. *UNESCOWMO, Paris, France*.

Betrie, G. D., Mohamed, Y. A., van Griensven, A., & Srinivasan, R. (2011). Sediment management modelling in the Blue Nile Basin using SWAT model. *Hydrology and Earth System Sciences*, *15*(3), 807–818.

Beven, K. J. (2012). *Rainfall-runoff modelling: the primer*. John Wiley & Sons.

Beven, K. J., & Kirkby, M. J. (1979). A physically based, variable contributing area model of basin hydrology/Un modèle à base physique de zone d'appel variable de l'hydrologie du bassin versant. *Hydrological sciences journal*, *24*(1), 43–69.

Beven, K., & Binley, A. (1992). The future of distributed models: model calibration and uncertainty prediction. *Hydrological processes*, *6*(3), 279–298.

Bhunia, G. S., Shit, P. K., & Maiti, R. (2018). Comparison of GIS-based interpolation methods for spatial distribution of soil organic carbon (SOC). *Journal of the Saudi Society of Agricultural Sciences*, *17*(2), 114–126.

Bicknell, B. R., Imhoff, J. C., Kittle, J. L., Donigan, A. S., & Johanson, R. C. (1993). *Hydrologic Simulation Program–Fortran (HSPF): User’s manual for release 10.0*. EPA 600/3-84-066, Environmental Research Laboratory, Athens, GA.

Borah, D. K., & Bera, M. (2004). Watershed-scale hydrologic and nonpoint-source pollution models: Review of applications. *Transactions of the ASAE*, *47*(3), 789–803.

Borah, D. K., Yagow, G., Saleh, A., Barnes, P. L., Rosenthal, W., Krug, E. C., & Hauck, L. M. (2006). Sediment and nutrient modeling for TMDL development and implementation. *Transactions of the ASABE*, *49*(4), 967–986.

Bracmort, K. S., Arabi, M., Frankenberger, J. R., Engel, B. A., & Arnold, J. G. (2006). Modeling long-term water quality impact of structural BMPs. *Transactions of the ASABE*, *49*(2), 367–374.

Burnash, R. J. (1973). *A generalized streamflow simulation system: Conceptual modeling for digital computers*. US Department of Commerce, National Weather Service, and State of California, Department of Water Resources.

Chandrashekar, H., Lokesh, K. V., Sameena, M., & Ranganna, G. (2015). GIS–based morphometric analysis of two reservoir catchments of Arkavati River, Ramanagaram District, Karnataka. *Aquatic Procedia*, *4*, 1345–1353.

Chau, K. W. (2017). Use of meta-heuristic techniques in rainfall-runoff modelling. *Water*, *9*(3), 186.

Chavare, S., & Shinde, S. D. (2013). Morphometric analysis of Urmodi basin, Maharashtra using geo-spatial techniques. *International journal of geomatics and geosciences*, *4*(1), 224–231.

Chen, J., & Adams, B. J. (2006). Integration of artificial neural networks with conceptual models in rainfall-runoff modeling. *Journal of Hydrology*, *318*(1-4), 232–249.

Chiang, L., Chaubey, I., Gitau, M. W., & Arnold, J. G. (2010). Differentiating impacts of land use changes from pasture management in a CEAP watershed using the SWAT model. *Transactions of the ASABE*, *53*(5), 1569–1584.

Chouhan, D., Tiwari, H. L., & Galkate, R. V. (2016). Rainfall runoff simulation of Shipra river basin using AWBM RRL toolkit. *International Journal of Civil Engineering and Technical Research (IJETR)*, *5*(3), 73–76.

Chow, V. T., Maidment, D. R., & Mays, L. W. (1988). *Applied hydrology*.

Crawford, N. H., & Linsley, R. K. (1962). *The synthesis of continuous streamflow hydrographs on a digital computer* (Vol. 12). Stanford, CA: Department of Civil Engineering, Stanford University.

Crawford, N. H., & Linsley, R. K. (1966). Digital Simulation in Hydrology: Stanford Watershed Model 4.

Cunderlik, J. (2003). *Hydrologic model selection for the CFCAS project: assessment of water resources risk and vulnerability to changing climatic conditions*. Department of Civil and Environmental Engineering, The University of Western Ontario.

Da Silva, R. M., Santos, C. A. G., de Lima Silva, V. C., & e Silva, L. P. (2013). Erosivity, surface runoff, and soil erosion estimation using GIS-coupled runoff–erosion model in the Mamuaba catchment, Brazil. *Environmental monitoring and assessment*, *185*, 8977–8990.

Daniel, E. B., Camp, J. V., LeBoeuf, E. J., Penrod, J. R., Dobbins, J. P., & Abkowitz, M. D. (2011). Watershed modeling and its applications: A state-of-the-art review. *The Open Hydrology Journal*, *5*(1).

Das, S., Patel, P. P., & Sengupta, S. (2016). Evaluation of different digital elevation models for analyzing drainage morphometric parameters in a mountainous terrain: a case study of the Supin–Upper Tons Basin, Indian Himalayas. *SpringerPlus*, *5*, 1–38.

Das, T. & Das, S. (2024a) Event-based flood estimation in un-gauged sub-basins: a comparative assessment of SCS-UH, CWC-UH and Nash- GIUH based rainfall-runoff models in Shilabati River, Eastern India, Nat. Hazards, 120 (15), 14153–14178.

Das, T. & Das, S. (2024b) A hydro-geomorphologic assessment of flood generation potentiality in ungauged sub-basins and their prioritization based on traditional, statistical, MCDM and Nash-GIUH models of a tropical plateau-fringe River, J. Hydrol., 640, 131689.

Dawdy, D. R., & O'Donnell, T. (1965). Mathematical models of catchment behavior. *Journal of the Hydraulics Division*, *91*(4), 123–137.

Department of Agriculture, Nagaland (n.d.) *Jhum-Fallow Management.* Government of Nagaland.

Dey, S., Yadav, V., Pan, S., Chattaraj, S. & Bera, S. (2025) Assessment of soil erosion dynamics and flood zonation using integrated RS and GIS-based RUSLE model for prioritization of sub-watersheds morphometry: A case study of Shilabati River Basin, West Bengal, India. In: Pal, S. C., Chatterjee, U. (eds) Surface, Sub-Surface Hydrology and Management. Cham, Switzerland: Springer Geography, pp. 415–443.

Dikpal, R. L., Renuka Prasad, T. J., & Satish, K. (2017). Evaluation of morphometric parameters derived from Cartosat-1 DEM using remote sensing and GIS techniques for Budigere Amanikere watershed, Dakshina Pinakini Basin, Karnataka, India. *Applied Water Science*, *7*, 4399–4414.

Du, J., Rui, H., Zuo, T., Li, Q., Zheng, D., Chen, A., ... & Xu, C. Y. (2013). Hydrological simulation by SWAT model with fixed and varied parameterization approaches under land use change. *Water resources management*, *27*, 2823–2838.

Duan, Q., Sorooshian, S., & Gupta, V. (1992). Effective and efficient global optimization for conceptual rainfall-runoff models. *Water resources research*, *28*(4), 1015–1031.

Easton, Z. M., Fuka, D. R., White, E. D., Collick, A. S., Biruk Ashagre, B., McCartney, M., ... & Steenhuis, T. S. (2010). A multi basin SWAT model analysis of runoff and sedimentation in the Blue Nile, Ethiopia. *Hydrology and earth system sciences, 14*(10), 1827–1841.

El Harraki, W., Ouazar, D., Bouziane, A., El Harraki, I., & Hasnaoui, D. (2021). Streamflow prediction upstream of a dam using SWAT and assessment of the impact of land use spatial resolution on model performance. *Environmental Processes*, *8*, 1165–1186.

Eyring, V., Bony, S., Meehl, G. A., Senior, C. A., Stevens, B., Stouffer, R. J., & Taylor, K. E. (2016). Overview of the Coupled Model Intercomparison Project Phase 6 (CMIP6) experimental design and organization. *Geoscientific Model Development*, *9*(5), 1937–1958.

Fallah, M., Kavian, A., & Omidvar, E. (2016). Watershed prioritization in order to implement soil and water conservation practices. *Environmental Earth Sciences*, *75*, 1–17.

Faniran A (1968). The index of drainage intensity—a provisional new drainage factor. *Aust J Sci,* 31, 328–330.

Farhan, Y., Anbar, A., Al-Shaikh, N., Almohammad, H., Alshawamreh, S., & Barghouthi, M. (2018). Prioritization of sub-watersheds in a large semi-arid drainage basin (Southern Jordan) using morphometric analysis, GIS, and multivariate statistics. *Agricultural Sciences*, *9*(04), 437.

Forkuor, G., & Maathuis, B. (2012). Comparison of SRTM and ASTER derived digital elevation models over two regions in Ghana-Implications for hydrological and environmental modelling. *London, UK: INTECH Open Access Publisher*, 219–240.

Fukunaga, D. C., Cecílio, R. A., Zanetti, S. S., Oliveira, L. T., & Caiado, M. A. C. (2015). Application of the SWAT hydrologic model to a tropical watershed at Brazil. *Catena*, *125*, 206–213.

Gajbhiye, S. (2015). Estimation of surface runoff using remote sensing and geographical information system. *International Journal of u-and e-Service, Science and Technology*, *8*(4), 113–122.

Gassman, P. W., Reyes, M. R., Green, C. H., & Arnold, J. G. (2007). The soil and water assessment tool: historical development, applications, and future research directions. *Transactions of the ASABE, 50*(4), 1211–1250.

Gholami, A., Roshan, M. H., Shahedi, K., Vafakhah, M., & Solaymani, K. (2016). Hydrological stream flow modeling in the Talar catchment (central section of the Alborz Mountains, north of Iran): Parameterization and uncertainty analysis using SWAT-CUP. *Journal of Water and Land Development*, *30*(1), 57.

Githui, F., Mutua, F., & Bauwens, W. (2009). Estimating the impacts of land-cover change on runoff using the soil and water assessment tool (SWAT): case study of Nzoia catchment, Kenya/Estimation des impacts du changement d'occupation du sol sur l'écoulement à l'aide de SWAT: étude du cas du bassin de Nzoia, Kenya. *Hydrological sciences journal*, *54*(5), 899–908.

Gosain, A. K., Mani, A., & Dwivedi, C. (2009). Hydrological modelling-literature review. *Advances in fluid mechanics*, *339*, 63–70.

Gosain, A. K., Rao, S., & Basuray, D. (2006). Climate change impact assessment on hydrology of Indian river basins. *Current science*, 346–353.

Green, C. H., & van Griensven, A. (2008). Autocalibration in hydrologic modeling: Using SWAT2005 in small-scale watersheds. *Environmental Modelling & Software*, *23*(4), 422–434.

Green, W. H., & Ampt, G. A. (1911). Studies on Soil Phyics. *The Journal of Agricultural Science*, *4*(1), 1–24.

Grimaldi, S., Petroselli, A., & Nardi, F. (2012). A parsimonious geomorphological unit hydrograph for rainfall–runoff modelling in small ungauged basins. *Hydrological Sciences Journal*, *57*(1), 73–83.

Grohmann, C. H. (2004) Morphometric analysis in geographic information systems: applications of free software GRASS and R, ComputGeosci, 30 (9–10), 1055–1067.

Gupta, H. V., Beven, K. J., & Wagener, T. (2006). Model calibration and uncertainty estimation. *Encyclopedia of hydrological sciences*.

Gupta, H. V., Kling, H., Yilmaz, K. K., & Martinez, G. F. (2009). Decomposition of the mean squared error and NSE performance criteria: Implications for improving hydrological modelling. *Journal of hydrology*, *377*(1-2), 80–91.

Gupta, H. V., Sorooshian, S., & Yapo, P. O. (1999). Status of automatic calibration for hydrologic models: Comparison with multilevel expert calibration. *Journal of hydrologic engineering*, *4*(2), 135–143.

Gupta, L., & Dixit, J. (2022). Estimation of rainfall-induced surface runoff for the Assam region, India, using the GIS-based NRCS-CN method. *Journal of Maps*, *18*(2), 428–440.

Gusain, A., Ghosh, S., & Karmakar, S. (2021). Added value of CMIP6 climate models in simulating Indian summer monsoon rainfall. *Climate Dynamics*, 57, 1787–1808.

Ha, L. T., Bastiaanssen, W. G., van Griensven, A., van Dijk, A. I., & Senay, G. B. (2017). SWAT-CUP for calibration of spatially distributed hydrological processes and ecosystem services in a Vietnamese river basin using remote sensing. *Hydrology and Earth System Sciences Discussions*, *2017*, 1–35.

Halder, S., RoyChowdhury, A., Kar, S., Ray, D., & Bhandari, G. (2024). Critical Watershed Prioritization through Multi-Criteria Decision-Making Techniques and Geographical Information System Integration for Watershed Management. *Sustainability*, *16*(8), 3467.

Hamby, D. M. (1994). A review of techniques for parameter sensitivity analysis of environmental models. *Environmental monitoring and assessment*, *32*(2), 135-154.

Hashmi, A. K. (2005). *Rainfall-Runoff modeling from Kaha Hill Torrent Watershed DG Khan District* (Doctoral dissertation, M. Sc. Thesis of Centre of

Excellence in Water Resources Engineering. Lahore: University of Engineering and Technology).

Horton, R. E. (1932). Drainage basin characteristics. In Transactions American Geophysical Union Publications, 13, pp. 350–361.

Horton, R. E. (1945). Erosional development of streams and their drainage basins: Hydrophysical approach to quantitative morphology. *Geological Society of America Bulletin, 56,* pp. 275–370.

Hosseini, S. H., & Khaleghi, M. R. (2020). Application of SWAT model and SWAT-CUP software in simulation and analysis of sediment uncertainty in arid and semi-arid watersheds (case study: The Zoshk–Abardeh watershed). *Modeling Earth Systems and Environment*, *6*(4), 2003–2013.

Hsu, K. L., Gupta, H. V., & Sorooshian, S. (1995). Artificial neural network modeling of the rainfall-runoff process. *Water resources research*, *31*(10), 2517–2530.

Ivanova, E. I., Nedkov, R. D., Ivanova, I. B., & Radeva, K. L. (2012). Morpho-Hydrographic Analyze of Black Sea Catchment Area in Bulgaria. *Procedia Environmental Sciences*, *14*, 143–153.

Jain, S. K., Tyagi, J., & Singh, V. (2010). Simulation of runoff and sediment yield for a Himalayan watershed using SWAT model. *Journal of Water Resource and Protection*, *2*(3), 267–281.

Janjić, J., & Tadić, L. (2023). Fields of application of SWAT hydrological model—a review. *Earth*, *4*(2), 331–344.

Jeong, J., Kannan, N., Arnold, J., Glick, R., Gosselink, L., & Srinivasan, R. (2010). Development and integration of sub-hourly rainfall–runoff modeling capability within a watershed model. *Water resources management*, *24*(15), 4505–4527.

Jha, M., Arnold, J. G., Gassman, P. W., Giorgi, F., & Gu, R. R. (2006). Climate change sensitivity assessment on upper Mississippi river basin streamflow using

SWAT. 1. *JAWRA Journal of the American Water Resources Association*, *42*(4), 997–1015.

Jothimani, M., Lawrence, F. F., & Dawit, Z. (2021). Morphometric analysis and prioritization of sub-watersheds for soil erosion using geomatics technologies in Megech river catchment, Lake Tana Basin, North Western Ethiopia. Ethiopian Journal of Science and Sustainable Development, 8(1), 52–64.

Kadam, A. K., Jaweed, T. H., Kale, S. S., Umrikar, B. N., & Sankhua, R. N. (2019). Identification of erosion-prone areas using modified morphometric prioritization method and sediment production rate: a remote sensing and GIS approach. *Geomatics, Natural Hazards and Risk*, *10*(1), 986–1006.

Kang, M. S., Park, S. W., Lee, J. J., & Yoo, K. H. (2006). Applying SWAT for TMDL programs to a small watershed containing rice paddy fields. *Agricultural water management*, *79*(1), 72–92.

Kannan, N., White, S. M., Worrall, F., & Whelan, M. J. (2007). Hydrological modelling of a small catchment using SWAT-2000–Ensuring correct flow partitioning for contaminant modelling. *Journal of Hydrology*, *334*(1-2), 64–72.

Karki, R., Qi, J., Gonzalez-Benecke, C. A., Zhang, X., Martin, T. A., & Arnold, J. G. (2023). SWAT-3PG: Improving forest growth simulation with a process-based forest model in SWAT. *Environmental Modelling & Software*, *164*, 105705.

Kaya, C. M., Tayfur, G. & Gungor, O. (2019) Predicting flood plain inundation for natural channels having no upstream gauged stations, *J. Water Clim. Change*, 10 (2), 360–372.

Khaleghi, M. R., & Hosseini, S. H. (2024). Using SWAT and SWAT-CUP for hydrological simulation and uncertainty analysis of the arid and semiarid watersheds (Case study: Zoshk Watershed, Shandiz, Iran). *Applied Water Science*, *14*(12), 266.

Khan, M. Y. A., & ElKashouty, M. (2023). Watershed prioritization and hydro-morphometric analysis for the potential development of Tabuk Basin, Saudi Arabia using multivariate statistical analysis and coupled RS-GIS approach. *Ecological Indicators*, *154*, 110766.

Khare, D., Singh, R., & Shukla, R. (2014). Hydrological modelling of barinallah watershed using arc-swat model. *International Journal of Geology, Earth and Environment Sciences*, *4*(1), 224–235.

Khatun, S., Sahana, M., Jain, S. K., & Jain, N. (2018). Simulation of surface runoff using semi distributed hydrological model for a part of Satluj Basin: parameterization and global sensitivity analysis using SWAT CUP. *Modeling Earth Systems and Environment*, *4*, 1111–1124.

Khoi, D. N., & Suetsugi, T. (2014). Impact of climate and land-use changes on hydrological processes and sediment yield—a case study of the Be River catchment, Vietnam. *Hydrological Sciences Journal*, *59*(5), 1095–1108.

Kichu, R., Dutta, M., Nayak, R. C., & Hangshing, L. (2022). Quantitative morphometric analysis of dzumah watershed of upper dhansiri, Nagaland, India. *Indian Journal of Ecology*, *49*(3), 837–842.

Kithan, L. N. (2014). Indigenous system of Paddy cultivation in Terrace and Jhum fields among the Nagas of Nagaland. *International Journal of Scientific and Research Publications*, *4*(3), 1–4.

Koch, S., Bauwe, A., & Lennartz, B. (2013). Application of the SWAT model for a tile-drained lowland catchment in North-Eastern Germany on subbasin scale. *Water Resources Management*, *27*, 791–805.

Kouli, M., Vallianatos, F., Soupios, P. & Alexakis, D. (2007) GIS-based morphometric analysis of two major watersheds, western Crete, Greece, J. Environ. Hydrol., 15 (1), 1–17.

Krishnan, R., Shrestha, A. B., Ren, G., Rajbhandari, R., Saeed, S., Sanjay, J., Syed, M. A., Vellore, R., Xu, Y., You, Q., & others (2020). *Assessment of climate change over the Indian region.* Springer Nature.

Kudnar, N. S., & Rajasekhar, M. (2020). A study of the morphometric analysis and cycle of erosion in Waingangā Basin, India. *Modeling Earth Systems and Environment*, *6*(1), 311–327

Kumar, D., Dhaloiya, A., Nain, A. S., Sharma, M. P., & Singh, A. (2021). Prioritization of watershed using remote sensing and geographic information system. *Sustainability*, *13*(16), 9456.

Kumar, M., Denis, D. M., Kundu, A., Joshi, N., & Suryavanshi, S. (2022). Understanding land use/land cover and climate change impacts on hydrological components of Usri watershed, India. *Applied Water Science*, *12*(3), 39.

Kumar, M., Mahato, L. L., Suryavanshi, S., Singh, S. K., Kundu, A., Dutta, D., & Lal, D. (2024). Future prediction of water balance using the SWAT and CA-Markov model using INMCM5 climate projections: a case study of the Silwani watershed (Jharkhand), India. *Environmental Science and Pollution Research*, *31*(41), 54311–54324.

Kumar, S., Raghuwanshi, N. S., & Mishra, A. (2015). Identification and management of critical erosion watersheds for improving reservoir life using hydrological modeling. *Sustainable Water Resources Management*, *1*, 57–70.

Kushwaha, A., & Jain, M. K. (2013). Hydrological simulation in a forest dominated watershed in Himalayan region using SWAT model. *Water Resources Management*, *27*, 3005–3023.

Kusre, B. C. (2016). Morphometric analysis of Diyung watershed in northeast India using GIS technique for flood management. *Journal of the Geological Society of India*, *87*(3), 361–369.

Leavesley, G. H. (1984). *Precipitation-runoff modeling system: User's manual* (Vol. 83, No. 4238). US Department of the Interior.

Lee, J. M., Park, Y. S., Kum, D., Jung, Y., Kim, B., Hwang, S. J., ... & Lim, K. J. (2014). Assessing the effect of watershed slopes on recharge/baseflow and soil erosion. *Paddy and water environment*, *12*, 169–183.

Legates, D. R., & McCabe Jr, G. J. (1999). Evaluating the use of "goodness-of-fit" measures in hydrologic and hydroclimatic model validation. *Water resources research*, *35*(1), 233–241.

Lewarne, M. (2009). *Setting up ArcSWAT hydrological model for the Verlorenvlei catchment* (Doctoral dissertation, Stellenbosch: University of Stellenbosch).

Li, D., Chen, J., & Qiu, M. (2021). The evaluation and analysis of the entropy weight method and the fractional grey model study on the development level of modern agriculture in Huizhou. *Mathematical Problems in Engineering*, *2021*(1), 5543368.

Lidén, R., & Harlin, J. (2000). Analysis of conceptual rainfall–runoff modelling performance in different climates. *Journal of hydrology*, *238*(3-4), 231–247.

Lirong, S., & Jianyun, Z. (2012). Hydrological response to climate change in Beijiang River Basin based on the SWAT model. *Procedia Engineering*, *28*, 241–245.

Liu, J., Chen, X., Wu, J., Zhang, X., Feng, D., & Xu, C. Y. (2012). Grid parameterization of a conceptual distributed hydrological model through integration of a sub-grid topographic index: necessity and practicability. *Hydrological sciences journal*, *57*(2), 282–297.

Lubini, A., & Adamowski, J. (2013). Assessing the potential impacts of four climate change scenarios on the discharge of the Simiyu River, Tanzania using the SWAT model.

Luo, Y., Arnold, J., Allen, P., & Chen, X. (2012). Baseflow simulation using SWAT model in an inland river basin in Tianshan Mountains, Northwest China. *Hydrology and Earth System Sciences*, *16*(4), 1259–1267.

Luo, Y., Su, B., Yuan, J., Li, H., & Zhang, Q. (2011). GIS techniques for watershed delineation of SWAT model in plain polders. *Procedia Environmental Sciences*, *10*, 2050–2057.

Maddamsetty, R. & Pawar, U. (2023) Evaluation of the geomorphological scenario of Shimsha River basin, Karnataka, India, Water Sci. Technol., 87 (8), 1907–1924.

Malik, M. A., Dar, A. Q., & Jain, M. K. (2022). Modelling streamflow using the SWAT model and multi-site calibration utilizing SUFI-2 of SWAT-CUP model for high altitude catchments, NW Himalaya's. *Modeling Earth Systems and Environment*, *8*(1), 1203–1213.

Manaswi, C. M., & Thawait, A. K. (2014). Application of soil and water assessment tool for runoff modeling of Karam River basin in Madhya Pradesh. *International Journal of Scientific Engineering and Technology*, *3*(5), 529–532.

Mangan, P., Haq, M. A., & Baral, P. (2019). Morphometric analysis of watershed using remote sensing and GIS—a case study of Nanganji River Basin in Tamil Nadu, India. *Arabian Journal of Geosciences*, *12*, 1–14.

Melton, M. A. (1957). An analysis of the relations among elements of climate, surface properties, and geomorphology (Vol. 11). New York: Department of Geology, Columbia University.

Mengistu, D. T., & Sorteberg, A. (2012). Sensitivity of SWAT simulated streamflow to climatic changes within the Eastern Nile River basin. *Hydrology and Earth System Sciences*, *16*(2), 391–407.

Merritt, W. S., Letcher, R. A., & Jakeman, A. J. (2003). A review of erosion and sediment transport models. *Environmental modelling & software*, *18*(8-9), 761–799.

Migliaccio, K. W., & Srivastava, P. (2007). Hydrologic components of watershed-scale models. *Transactions of the ASABE*, *50*(5), 1695–1703.

Miller, V. C. (1953). A quantitative geomorphic study of drainage basin characteristics in the Clinch Mountain area, Virginia and Tennessee (Vol. 3). New York: Columbia University.

Mishra, S. K., & Singh, V. P. (2013). *Soil conservation service curve number (SCS-CN) methodology* (Vol. 42). Springer Science & Business Media.

Mishra, S. S., & Nagarajan, R. (2010). Morphometric analysis and prioritization of sub-watersheds using GIS and remote sensing techniques: a case study of Odisha, India. *International Journal of Geomatics and Geosciences*, *1*(3), 501.

Mishra, V., Bhatia, U., & Tiwari, A. D. (2020). Bias-corrected climate projections for South Asia from coupled model intercomparison project-6. *Scientific data*, *7*(1), 338.

Mishra, V., Bhatia, U., Tiwari, A., & Das, S. (2020). Changes in Indian summer monsoon rainfall and extremes under climate change. *Climate Dynamics*, 54, 3051–3070.

Moore, I. D., Grayson, R. B., & Ladson, A. R. (1991). Digital terrain modelling: a review of hydrological, geomorphological, and biological applications. *Hydrological processes*, *5*(1), 3–30.

Moore, I.D., & Wilson, J.P. (1992). *Length-slope factors for the Revised Universal Soil Loss Equation: Simplified method of estimation*. Journal of Soil and Water Conservation, 47(5), 423–428.

Moriasi, D. N., Arnold, J. G., Van Liew, M. W., Bingner, R. L., Harmel, R. D., & Veith, T. L. (2007). Model evaluation guidelines for systematic quantification of accuracy in watershed simulations. *Transactions of the ASABE*, *50*(3), 885–900.

Mulvaney, T. J. (1851). “On the use of self-registering rain and flood gauges in making observations of the relations of rainfall and flood discharges in a given catchment.” Proc. Inst. Civ. Engrs., Dublin, Ireland, 4, 18–31.

Nag, S. K. (1998). Morphometric analysis using remote sensing techniques in the Chaka sub-basin, Purulia district, West Bengal. *Journal of the Indian society of remote sensing*, *26*(1), 69–76.

Najmaddin, P. M., Whelan, M. J., & Balzter, H. (2017). Application of satellite-based precipitation estimates to rainfall-runoff modelling in a data-scarce semi-arid catchment. *Climate*, *5*(2), 32.

Narasimhan, B., Srinivasan, R., Arnold, J. G., & Di Luzio, M. (2005). Estimation of long-term soil moisture using a distributed parameter hydrologic model and verification using remotely sensed data. *Transactions of the ASAE*, *48*(3), 1101–1113.

Narendra, K., Nageswara Rao, K., & Swarna Latha, P. (2013). Integrating remote sensing and GIS for identification of groundwater prospective zones in the Narava basin, Visakhapatnam region, Andhra Pradesh. *Journal of the Geological Society of India*, *81*(2), 248–260.

Narsimlu, B., Gosain, A. K., Chahar, B. R., Singh, S. K., & Srivastava, P. K. (2015). SWAT model calibration and uncertainty analysis for streamflow prediction in the Kunwari River Basin, India, using sequential uncertainty fitting. *Environmental Processes*, *2*, 79–95.

Nash, J. E., & Sutcliffe, J. V. (1970). River flow forecasting through conceptual models part I—A discussion of principles. *Journal of hydrology*, *10*(3), 282–290.

Nautiyal, M. D. (1994). Morphometric analysis of a drainage basin using aerial photographs: a case study of Khairkuli Basin, District Dehradun, UP. *Journal of the Indian Society of Remote Sensing*, *22*(4), 251–261.

Neitsch, S. L., Arnold, J. G., Kiniry, J. R., & Williams, J. R. (2011). *Soil and water assessment tool theoretical documentation version 2009*. Texas Water Resources Institute.

Nourani, V., Kisi, Ö., & Komasi, M. (2011). Two hybrid artificial intelligence approaches for modeling rainfall–runoff process. *Journal of Hydrology*, *402*(1-2), 41–59.

NSDMA (n.d.) *Geography of Nagaland*. Nagaland State Disaster Management Authority.

Obi, R. G., Maji, A. K., & Gajbhiye, K. S. (2002). GIS for morphometric analysis of drainage basins. *GIS india*, *4*(11), 9–14.

Oeurng, C., Sauvage, S., & Sánchez-Pérez, J. M. (2011). Assessment of hydrology, sediment and particulate organic carbon yield in a large agricultural catchment using the SWAT model. *Journal of Hydrology*, *401*(3-4), 145–153.

O'Neill, B. C., Tebaldi, C., Van Vuuren, D. P., Eyring, V., Friedlingstein, P., Hurtt, G., ... & Sanderson, B. M. (2016). The scenario model intercomparison project (ScenarioMIP) for CMIP6. *Geoscientific Model Development*, *9*(9), 3461–3482.

Pachac-Huerta, Y., Lavado-Casimiro, W., Zapana, M., & Peña, R. (2024). Understanding Spatio-Temporal Hydrological Dynamics Using SWAT: A Case Study in the Pativilca Basin. *Hydrology*, *11*(10), 165.

Pan, S., Dey, S., Yadav, V., & Biswas, R. (2025). Prioritizing sub-watersheds for soil and water resource conservation using multi-analytical approaches: a study of Shilabati River Basin, WB, India. *Journal of Water and Climate Change*, *16*(4), 1477–1504.

Pareta, K., & Pareta, U. (2012). Quantitative geomorphological analysis of a watershed of Ravi River Basin, HP India. *International journal of remote sensing and GIS*, *1*(1), 41–56.

Park, J. Y., Park, M. J., Ahn, S. R., Park, G. A., Yi, J. E., Kim, G. S., ... & Kim, S. J. (2011). Assessment of future climate change impacts on water quantity and quality for a mountainous dam watershed using SWAT. *Transactions of the ASABE*, *54*(5), 1725–1737.

Patel, D. P., & Nandhakumar, N. (2016). Runoff potential estimation of Anjana Khadi Watershed using SWAT model in the part of lower Tapi Basin, West India. *Sustainable Water Resources Management, 2*(1), 103–118.

Pervez, M. S., & Henebry, G. M. (2015). Assessing the impacts of climate and land use and land cover change on the freshwater availability in the Brahmaputra River basin. *Journal of Hydrology: Regional Studies*, *3*, 285–311.

Prakash, K., Rawat, D., Singh, S., Chaubey, K., Kanhaiya, S., & Mohanty, T. (2019). Morphometric analysis using SRTM and GIS in synergy with depiction: a case study of the Karmanasa River basin, North central India. *Applied Water Science*, *9*, 1–10.

Praskievicz, S., & Chang, H. (2009). A review of hydrological modelling of basin-scale climate change and urban development impacts. *Progress in Physical Geography*, *33*(5), 650–671.

Principe, J. A., & Blanco, A. C. (2012). Integrated use of remote sensing, GIS and swat model to explore climate change effects on river discharge in the Cagayan River Basin and land cover-based adaptation measures. In *33rd Asian Conference on Remote Sensing* (pp. 1509–1518).

Qiu LinJing, Q. L., Zheng FenLi, Z. F., & Yin, R. S. (2012). SWAT-based runoff and sediment simulation in a small watershed, the loessial hilly-gullied region of China: capabilities and challenges. (2012), 226–234.

Rahmati, O., Samadi, M., Shahabi, H., Azareh, A., Rafiei-Sardooi, E., Alilou, H. & Shirzadi, A. (2019) SWPT: an automated GIS-based tool for prioritization of sub-watersheds based on morphometric and topo-hydrological factors, *Geosci. Front.*, 10 (6), 2167–2175.

Rai, P. K., Mohan, K., Mishra, S., Ahmad, A., & Mishra, V. N. (2017). A GIS-based approach in drainage morphometric analysis of Kanhar River Basin, India. *Applied Water Science*, *7*, 217–232.

Raj, S., Rawat, K. S., & Tripathi, V. K. (2024). Applications of Advanced Technology for Prioritization of Watershed. *Environment and Ecology, 42*(2B), 836–845.

Ranatunga, T., Tong, S. T., & Yang, Y. J. (2017). An approach to measure parameter sensitivity in watershed hydrological modelling. *Hydrological Sciences Journal*, *62*(1), 76–92.

Ratnam, K.N., Srivastava, Y. K., Venkateswara Rao, V., Amminedu, E. K. S. R., & Murthy, K. S. R. (2005). Check dam positioning by prioritization of micro-watersheds using SYI model and morphometric analysis—remote sensing and GIS perspective. *Journal of the Indian society of remote sensing*, *33*(1), 25–38.

Refsgaard, J. C. (1997). Parameterisation, calibration and validation of distributed hydrological models. *Journal of hydrology*, *198*(1-4), 69–97.

Reungsang, P., Kanwar, R. S., & Srisuk, K. (2010). Application of SWAT model in simulating stream flow for the Chi River Subbasin II in Northeast Thailand. *Trends Research in Science and Technology*, *2*(1), 23–28.

Riahi, K., Van Vuuren, D. P., Kriegler, E., Edmonds, J., O'neill, B. C., Fujimori, S., ... & Tavoni, M. (2017). The Shared Socioeconomic Pathways and their energy, land use, and greenhouse gas emissions implications: An overview. *Global environmental change*, *42*, 153–168.

Romanowicz, A. A., Vanclooster, M., Rounsevell, M., & La Junesse, I. (2005). Sensitivity of the SWAT model to the soil and land use data parametrisation: a case study in the Thyle catchment, Belgium. *Ecological modelling*, *187*(1), 27–39.

Rossi, C. G., Dybala, T. J., Moriasi, D. N., Arnold, J. G., Amonett, C. A. R. L., & Marek, T. O. D. D. (2008). Hydrologic calibration and validation of the Soil and Water Assessment Tool for the Leon River watershed. *Journal of soil and water conservation*, *63*(6), 533–541.

Rostamian, R., Jaleh, A., Afyuni, M., Mousavi, S. F., Heidarpour, M., Jalalian, A., & Abbaspour, K. C. (2008). Application of a SWAT model for estimating runoff and sediment in two mountainous basins in central Iran. *Hydrological sciences journal*, *53*(5), 977–988.

Sahoo, S. (2013). Assessing hydrological modeling of Bandu River Basin, West Bengal (India). *Int J Remote Sens Geosci*, *2*(5).

Sahu, M., Lahari, S., Gosain, A. K., & Ohri, A. (2016). Hydrological modeling of Mahi basin using SWAT. *Journal of Water Resource and Hydraulic Engineering*, *5*, 68–79.

Saleh, A., Arnold, J. G., Gassman, P. W. A., Hauck, L. M., Rosenthal, W. D., Williams, J. R., & McFarland, A. M. S. (2000). Application of SWAT for the upper North Bosque River watershed. *Transactions of the ASAE*, *43*(5), 1077–1087.

Saltelli, A., Tarantola, S., & Campolongo, F. (2000). Sensitivity analysis as an ingredient of modeling. *Statistical science*, 377–395.

Santhi, C., Arnold, J. G., Williams, J. R., Dugas, W. A., Srinivasan, R., & Hauck, L. M. (2001). Validation of the swat model on a large rwer basin with point and nonpoint sources 1. *JAWRA Journal of the American Water Resources Association*, *37*(5), 1169–1188.

Santra, P., & Das, B. S. (2013). Modeling runoff from an agricultural watershed of western catchment of Chilika lake through ArcSWAT. *Journal of hydro-environment research*, *7*(4), 261–269.

Sarkar, D., Mondal, P., Sutradhar, S., & Sarkar, P. (2020). Morphometric analysis using SRTM-DEM and GIS of Nagar river basin, Indo-Bangladesh barind tract. *Journal of the Indian Society of Remote Sensing*, *48*(4), 597–614.

Schumm, S. A. (1956). Evolution of drainage system and slopes in badlands at Perth Amboy, NEW Jessey. Geological Society of America Bulletin, 67, 597–646.

Schuol, J., Abbaspour, K. C., Srinivasan, R., & Yang, H. (2008). Estimation of freshwater availability in the West African sub-continent using the SWAT hydrologic model. *Journal of hydrology*, *352*(1-2), 30–49.

Sepehri, M., Ildoromi, A. R., Malekinezhad, H., Ghahramani, A., Ekhtesasi, M. R., Cao, C., & Kiani-Harchegani, M. (2019). Assessment of check dams' role in flood hazard mapping in a semi-arid environment. *Geomatics, Natural Hazards and Risk*, *10*(1), 2239–2256.

Servat, E., & Dezetter, A. (1991). Selection of calibration objective fonctions in the context of rainfall-ronoff modelling in a Sudanese savannah area. *Hydrological Sciences Journal*, *36*(4), 307–330.

Shamseldin, A. Y. (1997). Application of a neural network technique to rainfall-runoff modelling. *Journal of hydrology, 199*(3-4), 272–294.

Sharma, S., & Mahajan, A. K. (2020). GIS-based sub-watershed prioritization through morphometric analysis in the outer Himalayan region of India. *Applied Water Science*, *10*(7), 1–11.

Shekar, P. R., & Mathew, A. (2024). Morphometric Analysis of Watersheds: A Comprehensive Review of Data Sources, Quality, and Geospatial Techniques. *Watershed Ecology and the Environment*.

Sherman, L. K. (1932). On runoff. Transactions American Geophysical Union. 13(1):298

Shi Peng, S. P., Chen Chao, C. C., Srinivasan, R., Zhang XueSong, Z. X., Cai Tao, C. T., Fang XiuQin, F. X., ... & Li QiongFang, L. Q. (2011). Evaluating the SWAT model for hydrological modeling in the Xixian watershed and a comparison with the XAJ model.

Shivhare, V., Goel, M. K., & Singh, C. K. (2014). Simulation of surface runoff for upper Tapi subcatchment Area (Burhanpur Watershed) using swat. *The International Archives of the Photogrammetry, Remote Sensing and Spatial Information Sciences*, *40*, 391–397.

Shrestha, S., Semkuyu, D. J., & Pandey, V. P. (2016). Assessment of groundwater vulnerability and risk to pollution in Kathmandu Valley, Nepal. *Science of the Total Environment*, *556*, 23–35.

Shrimali, S. S., Aggarwal, S. P., & Samra, J. S. (2001). Prioritizing erosion-prone areas in hills using remote sensing and GIS—a case study of the Sukhna Lake catchment, Northern India. *International Journal of Applied Earth Observation and Geoinformation*, *3*(1), 54–60.

Shrivastava, P. K., Tripathi, M. P., & Das, S. N. (2004). Hydrological modelling of a small watershed using satellite data and gis technique. *Journal of the Indian Society of Remote Sensing*, *32*, 145–157.

Simić, Z., Milivojević, N., Prodanović, D., Milivojević, V., & Perović, N. (2009). SWAT-based runoff modeling in complex catchment areas: Theoretical background and numerical procedures. *Journal of Serbian Society for Computational Mechanics*, *3*(1), 38–63.

Singh, J., Knapp, H. V., Arnold, J. G., & Demissie, M. (2005). Hydrological modeling of the Iroquois river watershed using HSPF and SWAT 1. *JAWRA Journal of the American Water Resources Association*, *41*(2), 343–360.

Singh, P., Gupta, A., & Singh, M. (2014). Hydrological inferences from watershed analysis for water resource management using remote sensing and GIS techniques. *The Egyptian Journal of Remote Sensing and Space Science*, *17*(2), 111–121.

Singh, V. P., & Frevert, D. K. (Eds.). (2002). *Mathematical models of large watershed hydrology*. Water Resources Publication.

Singh, V. P., & Woolhiser, D. A. (2002). Mathematical modeling of watershed hydrology. *Journal of hydrologic engineering*, *7*(4), 270–292.

Singh, V., Bankar, N., Salunkhe, S. S., Bera, A. K., & Sharma, J. R. (2013). Hydrological stream flow modelling on Tungabhadra catchment:

parameterization and uncertainty analysis using SWAT CUP. *Current science*, 1187–1199.

Singh, W. R., Barman, S., & Tirkey, G. (2021). Morphometric analysis and watershed prioritization in relation to soil erosion in Dudhnai Watershed. *Applied Water Science*, *11*(9), 151.

Smith, K. G. (1950). Standards for grading texture of erosional topography. *American journal of Science*, *248*(9), 655–668.

Soni, S. (2017). Assessment of morphometric characteristics of Chakrar watershed in Madhya Pradesh India using geospatial technique. *Applied Water Science*, *7*, 2089–2102.

Sreedevi, P. D., Owais, S., Khan, H. H. & Ahmed, S. (2009) Morphometric analysis of a watershed of south India using SRTM data and GIS, J. Geol. Soc. India, 73, 543–552.

Sreedevi, P. D., Subrahmanyam, K., & Ahmed, S. (2005). Integrated approach for delineating potential zones to explore for groundwater in the Pageru River basin, Kuddapah District, Andhra Pradesh, India. *Hydrogeology Journal*, 13, pp. 534–545.

Srinivasan, R., Ramanarayanan, T. S., Arnold, J. G., & Bednarz, S. T. (1998). Large area hydrologic modeling and assessment part II: model application 1. *JAWRA Journal of the American Water Resources Association*, *34*(1), 91–101.

Steven L. Neitsch, Arnold, J. G., Kiniry, J. R., & Williams, J. R. (2005). *Soil and Water Assessment Tool Theoretical Documentation Version 2005*. Texas A&M University and USDA-ARS.

Strahler A.N. (1952). Hypsometric (area-altitude) analysis of erosional topography. *Bull Geol Soc Am,* 63(11), 1117–1142.

Strahler, A. N. (1957). Quantitative analysis of watershed geomorphology. *Eos, Transactions American Geophysical Union*, *38*(6), 913–920.

Strahler, A. N. (1964). Quantitative geomorphology of drainage basin and channel networks. In V. T. Chow (Ed.), *Handbook of applied hydrology*, New York: McGraw Hill Book Company, 4–76

Sujatha, E. R., Selvakumar, R., Rajasimman, U. A. B., & Victor, R. G. (2015). Morphometric analysis of sub-watershed in parts of Western Ghats, South India using ASTER DEM. *Geomatics, Natural Hazards and Risk*, *6*(4), 326–341.

Tang, J., Yang, W., Zy, L., Jm, B., & Liu, C. (2012). Simulation on the inflow of agricultural non-point sources pollution in Dahuofang reservoir catchment of Liao river. *J Jilin Univ*, *42*, 1462–1468.

Tavosi, M., Vafakhah, M., Sadeghi, S. H., & Bateni, S. M. (2024). Sub-watershed prioritization based on watershed hydrological security using different multi-criteria decision-making methods. *Water Resources Management,* 1–26.

Thakur, J. K., Singh, S. K., & Ekanthalu, V. S. (2017). Integrating remote sensing, geographic information systems and global positioning system techniques with hydrological modeling. *Applied Water Science*, *7*(4), 1595–1608.

Tibebe, D., & Bewket, W. (2011). Surface runoff and soil erosion estimation using the SWAT model in the Keleta watershed, Ethiopia. *Land Degradation & Development*, *22*(6), 551–564.

Tibebe, M., Melesse, A. M., & Zemadim, B. (2015). Runoff estimation and water demand analysis for Holetta River, Awash Subbasin, Ethiopia using SWAT and CropWat Models. *Landscape dynamics, soils and hydrological processes in varied climates*, 113–140.

Tim, U. S. (1995). The application of GIS in environmental health sciences: opportunities and limitations. *Environmental Research*, *71*(2), 75–88.

Tokar, A. S., & Johnson, P. A. (1999). Rainfall-runoff modeling using artificial neural networks. *Journal of Hydrologic Engineering*, *4*(3), 232–239.

Tripathi, M. P., Panda, R. K., & Raghuwanshi, N. S. (2003). Identification and prioritisation of critical sub-watersheds for soil conservation management using the SWAT model. *Biosystems Engineering*, *85*(3), 365–379.

Tripathi, M. P., Panda, R. K., Raghuwanshi, N. S., & Singh, R. (2004). Hydrological modelling of a small watershed using generated rainfall in the soil and water assessment tool model. *Hydrological processes*, *18*(10), 1811–1821.

Tripathi, M. P., Raghuwanshi, N. S., & Rao, G. P. (2006). Effect of watershed subdivision on simulation of water balance components. *Hydrological Processes: An International Journal*, *20*(5), 1137–1156.

Turconi, L., Faccini, F., Marchese, A., Paliaga, G., Casazza, M., Vojinovic, Z., & Luino, F. (2020). Implementation of nature-based solutions for hydro-meteorological risk reduction in small mediterranean catchments: The case of Portofino Natural Regional Park, Italy. *Sustainability*, *12*(3), 1240.

USDA, S. (1972). National engineering handbook, section 4: Hydrology. *Washington, DC*, *127*.

van Griensven, A., & Meixner, T. (2006). Methods to quantify and identify the sources of uncertainty for river basin water quality models. *Water Science and Technology*, *53*(1), 51–59.

Van Liew, M. W., Arnold, J. G., & Garbrecht, J. D. (2007). Hydrologic simulation on agricultural watersheds: Choosing between two models. *Transactions of the ASAE*, *46*(6), 1539–1551.

Vanrolleghem, P. A., Insel, G., Petersen, B., Sin, G., De Pauw, D., Nopens, I., ... & Gernaey, K. (2003, January). A comprehensive model calibration procedure for activated sludge models. In *WEFTEC 2003* (pp. 210-237). Water Environment Federation.

Vilaysane, B., Takara, K., Luo, P., Akkharath, I., & Duan, W. (2015). Hydrological stream flow modelling for calibration and uncertainty analysis using SWAT model in the Xedone river basin, Lao PDR. *Procedia Environmental Sciences*, *28*, 380–390.

Vittala, S. S., Govindaiah, S. & Gowda, H. H. (2004). Morphometric analysis of sub-watersheds in the Pavagada area of Tumkar district, south India using remote sensing and GIS techniques, J. Indian Soc. Remote Sens., 32 (4), 351–362.

Vittala, S. S., Govindaiah, S., & Gowda, H. H. (2008). Prioritization of sub-watersheds for sustainable development and management of natural resources: An integrated approach using remote sensing, GIS and socio-economic data. *Current Science*, 345–354.

Vrugt, J. A., Gupta, H. V., Bouten, W., & Sorooshian, S. (2003). A Shuffled Complex Evolution Metropolis algorithm for optimization and uncertainty assessment of hydrologic model parameters. *Water resources research*, *39*(8).

Vrugt, J. A., Ter Braak, C. J., Clark, M. P., Hyman, J. M., & Robinson, B. A. (2008). Treatment of input uncertainty in hydrologic modeling: Doing hydrology backward with Markov chain Monte Carlo simulation. *Water Resources Research*, *44*(12).

Wagener, T., & Gupta, H. V. (2005). Model identification for hydrological forecasting under uncertainty. *Stochastic Environmental Research and Risk Assessment*, *19*, 378–387.

Wagener, T., Boyle, D. P., Lees, M. J., Wheater, H. S., Gupta, H. V., & Sorooshian, S. (2001). A framework for development and application of hydrological models. *Hydrology and Earth System Sciences*, *5*(1), 13–26.

White, K. L., & Chaubey, I. (2005). Sensitivity analysis, calibration, and validations for a multisite and multivariable SWAT model 1. *JAWRA Journal of the American Water Resources Association*, *41*(5), 1077–1089.

Wu, K., & Johnston, C. A. (2007). Hydrologic response to climatic variability in a Great Lakes Watershed: A case study with the SWAT model. *Journal of hydrology*, *337*(1-2), 187–199.

Yadav, V., Dey, S. & Pan, S. (2024) Regional planning framework for addressing flood vulnerability: a comprehensive case study of South 24 Parganas, West Bengal, India. In: Biswas, B. & Ghute, B. B. (eds) Flood Risk Management: Assessment and Strategy, Singapore: Springer Nature, 425–456.

Yang, J., Reichert, P., Abbaspour, K. C., Xia, J., & Yang, H. (2008). Comparing uncertainty analysis techniques for a SWAT application to the Chaohe Basin in China. *Journal of hydrology*, *358*(1-2), 1–23.

Yesuf, H. M., Assen, M., Alamirew, T., & Melesse, A. M. (2015). Modeling of sediment yield in Maybar gauged watershed using SWAT, northeast Ethiopia. *Catena*, *127*, 191–205.

Yu MeiYan, Y. M., Chen Xi, C. X., Li LanHai, L. L., Bao AnMing, B. A., & Paix, M. D. L. (2011). Streamflow simulation by SWAT using different precipitation sources in large arid basins with scarce raingauges.

Zhang, X. (2008). *Evaluating and developing parameter optimization and uncertainty analysis methods for a computationally intensive distributed hydrological model*. Texas A&M University.

Zhao, J., Zhang, N., Liu, Z., Zhang, Q., & Shang, C. (2024). SWAT model applications: From hydrological processes to ecosystem services. *Science of The Total Environment*, *931*, 172605.

Zhu, Y., Tian, D., & Yan, F. (2020). Effectiveness of entropy weight method in decision-making. *Mathematical problems in Engineering*, *2020*(1), 3564835.

APPENDICES

The following appendices present supplementary materials that support and validate the analyses discussed in the preceding chapters. They include datasets, methodological details, model configurations, and calibration results, providing transparency and reproducibility to the research. Each appendix corresponds to a specific component of the study, ranging from data sources, model setup, and sensitivity analysis to climate projections. Collectively, these materials ensure comprehensive documentation of the GIS- and SWAT-based assessment of the Dzuza, Dhansiri, and Khova watersheds in Nagaland.

APPENDIX I

Data Sources and Input Datasets

All spatial and non-spatial datasets used for this research were obtained from reliable national and international agencies. These datasets formed the foundation for morphometric, hydrological, and climatic analyses.

Data Type	Source / Agency	Resolution / Scale	Period	Purpose
Digital Elevation Model (DEM)	USGS Earth Explorer (SRTM)	30 m	2021	Watershed delineation and morphometric extraction
Land Use / Land Cover (LULC)	Living Atlas / ESRI Database	30 m	2021	HRU generation in SWAT
Soil Map	FAO Digital Soil Map of the World	1: 5,000,000	2021	Soil classification and HRU definition
Meteorological Data	Department of Water Resources, Nagaland	Daily	2012 – 2021	Rainfall, temperature,

Data Type	Source / Agency	Resolution / Scale	Period	Purpose
				humidity, and wind speed inputs
Streamflow Data	Department of Soil and Water Conservation, Nagaland	Daily	2012 – 2021	Calibration / validation of SWAT model
CMIP6 Climate Projections	CanESM5 & MRI-ESM2-0	~25 km grid	2032 – 2040	Future flow and rainfall simulations

APPENDIX II

SWAT Model Setup and Parameterization

- **Model version:** ArcSWAT 2012 integrated in ArcGIS 10.5
- **HRU thresholds:** LULC = 5 %, Soil = 10 %, Slope = 5 %
- **Slope classes:** 0–5 %, 5–15 %, 15–30 %, > 30 %
- **Key parameters used in calibration:** CN2, ALPHA_BF, SOL_K, GWQMN, GW_DELAY, CH_N2, ESCO, EPCO
- **Optimization algorithm:** SUFI-2 (SWAT-CUP 2012)
- **Performance criteria:** NSE, R^2, PBIAS, RSR, p-factor, r-factor

Tables of final parameter ranges, fitted values, and sensitivity rankings are provided in Appendix 3

APPENDIX III

Model Performance and Sensitivity Results

Basin	Period	NSE	R^2	PBIAS (%)	RSR	Remarks
Dzuza	Calibration (2014-2018)	0.87	0.89	+12.8	0.37	Strong performance
	Validation (2019-2021)	0.51	0.79	+33.3	0.7	Satisfactory
Dhansiri	Calibration	0.82	0.88	+12.6	0.42	Excellent
	Validation	0.85	0.86	+2.7	0.38	Reliable
Khova	Calibration	0.76	0.78	-18.2	0.49	Acceptable
	Validation	0.7	0.7	+3	0.55	Satisfactory

Most sensitive parameters (SUFI-2 ranking):

1. CN2 (curve number)
2. SOL_K (soil hydraulic conductivity)
3. GWQMN (minimum water table depth)
4. GW_DELAY
5. ALPHA_BF

APPENDIX IV

Climate Projection Analysis

- **Models used:** CanESM5 and MRI-ESM2-0 under CMIP6.
- **Scenario period:** 2032 – 2040.
- **Projected trends:**
    - *MRI-ESM2-0*: Higher early-monsoon rainfall (+12 %) and sharper JJAS peaks.
    - *CanESM5*: Reduced monsoon intensity (–7 %) but enhanced post-monsoon recharge (+9 %).
- **Temperature rise:** +1.4 °C to +1.8 °C above baseline (2012-2021).

APPENDIX V

High-Resolution Maps and Figures

1. Location Map of Nagaland showing Dzuza, Dhansiri, and Khova watersheds. (*See Chapter 3 Figure 3.1)*
2. DEM maps and derived slope and aspect maps. (*See Chapter 3 Figure 3.2, 3.8 (a & b), 3.9 (a & b), and 3.10 (a & b))*
3. Drainage network and stream order maps. (*See Chapter 4 Figure 4.4 (a), (b), and (c))*
4. LULC and Soil maps used for HRU generation. (*See Chapter 4 Figure 4.6 (a), (b), and (c))*
5. Sub-watershed prioritization map (classified as High, Medium, Low priority). (*See Chapter 4 Figure 4.35, 4.39 & 4.43*)

All maps include legend, north arrow, and coordinate system (WGS 84 UTM Zone 46 N).

LIST OF PUBLICATIONS AND CONFERENCES

Paper Publications

1) Soil and water conservation in Dhansiri River Basin using a Sub-Watershed Prioritization Tool approach. *International Journal of River Basin Management*. 1-11 (2025).

2) Morphometric Characterization and Hydrological Dynamics of the Dzuza, Dhansiri and Khova Watersheds in Nagaland, India: Implications for Sustainable Management. A*gricultural Science Digest*, *1*-9 (2025).

Conferences

1) 6th International Conference on Strategies Challenges in Agricultural and Life Science for Food Security and Sustainable Environment (SCALFE-2023) held at Himachal Pradesh University Summer Hill, Shimla, HP, India during April, 28-30, 2023. "Study of morphometric parameters for planning and management of Dzuza watershed, Nagaland, India"

2) 7th International Conference on Global Approaches in Agricultural, Biological, Environment and Life Sciences For Sustainable Future (GABELS-2024) held at Buddha Hall, DAV College (Tribhuvan University) Kathmandu Nepal during June 08-10, 2024. "Quantitative Morphometric Analysis of Khova River Basin in Nagaland, India".

Certificate No. 3862 SCALFE-2023

ATDS SOCIETY
GHAZIABAD, UP, INDIA

DEPARTMENT OF ENVIRONMENTAL SCIENCE
HP UNIVERSITY, SUMMER HILL, SHIMLA, HP, INDIA

Shobhit
Institute of Engineering & Technology
Deemed to-be-Univesity
EDUCATION EMPOWERS

SHOBHIT DEEMED TO-BE- UNIVERSITY
MEERUT, UP, INDIA

DEPT. OF HORTICULTURE
JVC, BARAUT, UP, INDIA

6th International Conference

Strategies and Challenges in Agricultural and Life Science for Food Security and Sustainable Environment (SCALFE - 2023)

Certificate

This is to certify that Prof./ Dr./ Mr./ Ms. Imyanglula

of School of Engineering and Technology, Nagaland University.

actively participated as Delegates / Research Scholar / Student to Delivered Lecture / Presented a Paper (Oral / Poster / Participation)

entitled Study of Morphometric Parameters for Planning and Management of Dzuza Watershed, Nagaland, India.

in the 6th International Conference on "Strategies and Challenges in Agricultural and Life Science for Food Security and Sustainable Environment (SCALFE - 2023)" held at Himachal Pradesh University Summer Hill, Shimla, H.P., India during April, 28-30, 2023.

Prof. Amar P. Garg
(Organizing Chairman)

Prof Duni Chand
(Dean Faculty of Life Sciences)

Dr. Mahender Singh Thakur
(Managing Chairman)

Dr. Joginder Singh
(Organizing Secretary)

CROWN UNIV, ARGENTINA | HORT. DEPT. CCSU, MRT | FOH. SKUAST-K, J& K | UNIV. OF LIMPOPO, SA | CDB, PATNA, BIHAR | HORT. DEPT. RVSKVV, MP | SNRM, CPGSAS, CAU | AIA, ITALYENEA, TRIS

Certificate No. :...2066.......GABELS - 2024

THE NEOTIA UNIVERSITY

D.A.V. COLLGE

7th INTERNATIONAL CONFERENCE

Global Approaches in Agricultural, Biological, Environment and Life Sciences for Sustainable Future (GABELS - 2024)

CERTIFICATE

This is to certify that Prof./Dr./Mr./Ms. Imyanglula

of School of Engineering and Technology, Nagaland University

actively participated as Delegates / Research Scholar / Student to Delivered Lecture / Presented a Paper (Oral / Poster /Participation)

entitled Quantitative Morphometric Analysis of Khova River Basin in Nagaland, India

in the 7th International Conference on "Global Approaches in Agricultural Biological, Environment and Life Sciences for Sustainable Future (GABELS-2024)" held at Buddha Hall, D.A.V. College (Tribhuvan University) Kathmandu, Nepal during June 08 - 10, 2024.

Mr. Anil Kedia	Prof. Amar P. Garg	Dr. S.P. Vista	Dr. Joginder Singh
(Chairman, DAV College, Nepal)	(Organizing Chairman, India)	(Managing Chairman, Nepal)	(Organizing Secretary, India)